DESIGN AND FEM ANALYSIS OF PERMANENT MAGNET SYNCHRONOUS MOTOR FOR ELECTRIC VEHICLE APPLICATIONS

A thesis submitted
in fulfillment of the requirements of the degree of
Doctor of Philosophy

Submitted by

MONIKA VERMA
(2K17/PhD/EE/01)

Under the Supervision of

Prof. Mini Sreejeth
Professor
Department of Electrical Engineering
Delhi Technological University

and

Prof. Madhusudan Singh
Professor
Department of Electrical Engineering
Delhi Technological University

Department of Electrical Engineering
Delhi Technological University
Delhi-110042, India
August 2022CERTIFICATE

This is to certify that the thesis entitled "**Design and FEM Analysis of Permanent Magnet Synchronous Motor for Electric Vehicle Applications**" which is being submitted by **Ms. Monika Verma** for the award of degree of **Doctor of Philosophy** in **Department of Electrical Engineering**, Delhi Technological University, Delhi, is a record of scholar's own work carried out by her under our supervision and guidance. The matter embodied in this thesis has not been submitted in part or in full to any other university or institute for award of any degree or diploma.

Prof. Madhusudan Singh
Professor
Department of Electrical Engineering
Delhi Technological University
Delhi-110042, India

Prof. Mini Sreejeth
Professor
Department of Electrical Engineering
Delhi Technological University
Delhi-110042, India

ACKNOWLEDGEMENT

It has been a pleasure for me to work on this thesis. First and foremost, I would like to express my sense of gratitude and indebtedness to my supervisors Prof. Mini Sreejeth and Prof. Madhusudan Singh, Electrical Engineering Department, Delhi Technological University for their inspiring guidance, valuable suggestions, encouragement, untiring effort throughout the course of this work and help in providing necessary facilities and resources during the entire period of my research work. Their wide knowledge and logical way of thinking have helped me to complete my research work. They always made themselves available for me despite of their busy schedules. It provided me a great opportunity to carry out my research work under their guidance and to learn from their research expertise.

I am indebted to my husband Mr. Nitin Verma, daughter Nairiti Verma, and mother-in-law Mrs. Kusum Verma for their unconditional support, patience throughout my study period. They encouraged me all the time, no matter what difficulties I encountered. I would like to express my deepest regards and gratitude to my parents for their unmitigated love. I would like to express my greatest admiration to all my family members and relatives for their positive encouragement that they showered on me throughout this research work. I extend my personal thanks to my friends and colleagues for their valuable support and reminding me to complete my work at the earliest. Sincere thanks to Delhi Technological University faculties and authorities for providing me necessary facilities for the smooth completion of my work.

Above all, I would like to thank The Almighty Lord Krishna, who has blessed me strength and support throughout my life and always provides me with a path to acquire knowledge and learning.

MONIKA VERMA
(2K17/PhD/EE/01)

ABSTRACT

The depletion of fossil fuels and growing concerns relating to environmental pollution have triggered extensive research for improving the performance of electric vehicle powertrain. High performance electric vehicles are replacing conventional Internal Combustion Engine based vehicles leading to reduction in consumption of fossil fuel. This is a big breakthrough for the vehicle industry. Even though, preservation of fossil fuel can be achieved through adoption of electric vehicles, additional complexity and challenges faced in developing an efficient electric vehicle powertrain with high performance and low maintenance needs to be addressed. In this context, design of an efficient electric vehicle power train is essential. Selection of high-performance traction motor, with simple and accurate control schemes, is crucial for different electric vehicle applications. Among the various kinds of electric motors that are being researched for use in electric vehicle applications, Permanent Magnet Synchronous Motor has prominent advantages such as fast response, compact size, light weight, high efficiency, brushless configuration and good dynamic performance.

In this research work, conventional internal combustion engine and electric powertrain are modelled in MATLAB/Simulink for analysing the performance of these two distinct propulsion configurations. The conventional powertrain using spark ignition type of generic engine is modelled in Simulink and the information obtained from the dynamic analysis of conventional powertrain is set as the *benchmark parameters* for evaluating the performance of electric powertrain. The electric powertrain is modelled and simulation studies are carried out through the implementation of Space Vector Pulse Width Modulation and Field Oriented Control based control strategies. The dynamic performance of traction motor is analysed, for both traction and braking modes of operation, under different operating conditions. The modelled electric motors proposed for electric vehicle powertrain are found to be robust, with fast dynamic response in achieving the required torque and speed demand and their perturbations. The results obtained from the proposed electric vehicle powertrain models are in agreement with their suitability for EV application.

The permanent magnet synchronous motor for the power train is designed using Finite Element analysis to improve the electromagnetic performance for different electric vehicle applications. Simplification of the structure of the electric motor used in electric vehicles can result in enhanced and improved performance. Accordingly, structural optimization of the motor

for electric vehicle application is carried out to enhance performance, through reduction in losses and increase in efficiency. This is achieved by designing a surface inset type permanent magnet synchronous motor and improving its performance parameters through finite element analysis, surrogate modelling technique and metaheuristic algorithms.

Since the electromagnetic performance of the motor shows high dependence on the variation of its design parameters, the response surface models for various performance factors of motor are developed in terms of the specific design parameters. For this, metamodeling technique is implemented in MATLAB. The obtained meta-models are utilized as objective functions in the implementation of metaheuristics techniques to achieve improvement in the electromagnetic performance of the motor.

A novel optimization technique called Integrated Taguchi method assisted polynomial Metamodeling & Genetic Algorithm is developed to optimize the motor geometry for electric compressor application, like environment control, in electric vehicles. The optimal results obtained from proposed approach are compared with those obtained from the traditional design optimization technique and found to be giving better response of the motor.

In addition, a novel design optimization algorithm called Aquila Grasshopper Optimization is developed to achieve minimum core losses through improved motor geometry of the traction motor. Trench cuts are introduced in this optimized geometry to obtain light-weight and high-power density. Sensitivity analysis of the motor design parameters is also carried out to predict the effect of variation in geometrical parameters on its electromagnetic performance. Further, thermal modelling of permanent magnet synchronous motor is performed via Lumped Parameter Thermal Network. The change in the temperature in different parts of the motor under different operating conditions are observed and used to detect thermal faults in the motor. To identify which part of the motor is faulty, statistical approach of Linear Discriminant Analysis method is used. Different nodes in Lumped Parameter Thermal Network are treated as differentiable classes (or groups). Finite Element analysis is used for evaluating the loss information in motor parts (nodes). The change in temperature is computed for specific operating conditions and the corresponding discriminant functions are obtained for each class feature. For particular change in temperature at any operating condition, the specific classes are identified to diagnose the faulty part in the motor.

TABLE OF CONTENTS

Certificate---------- *i*
Acknowledgement---------- *ii*
Abstract---------- *iii*
Table of Contents---------- *v*
List of Abbreviations---------- *viii*
List of Symbols---------- *xi*
List of Figures---------- *xvi*
List of Tables---------- *xix*

Chapter - I: INTRODUCTION 1
1.1 General 1
1.2 Electric Motors used in EV application 2
1.2.1 Permanent Magnet Synchronous Motor (PMSM) 2
1.2.2 Brushless Direct Current Motor 3
1.2.3 Synchronous Reluctance Motor 4
1.3 Simulation Tool 4
1.4 Research Objective 6
1.5 Organization of Thesis 7
1.6 Conclusion 9

CHAPTER – II: LITERATURE REVIEW **11**
2.1 General 11
2.2 Conventional Power Train and Electric Power Train 12
2.2.1 Architecture of Powertrain 12
2.2.2 Process Level of Electrification of Vehicles 13
2.2.3 Architectures of P-EV Powertrain 14
2.2.3.1 Type A: P-EV with Single Motor and no Transmission 14
2.2.3.2 Type B: P-EV with Single Motor and Multi-Gear Transmission 15
2.2.3.3 Type C: P-EV with Multiple Motors 15
2.2.4 Architectures of HEV Powertrain 16
2.2.4.1 Series Configuration 16
2.2.4.2 Parallel Configuration 17
2.2.4.3 Power-split Configuration 18
2.3 Control and Design Strategies of PMSM 19
2.3.1 Control of PMSM 19
2.3.2 Design of PMSM 20
2.4 Meta-modelling 22
2.4.1 Approximation of Model 23
2.4.2 Exploration of Design Space 23
2.4.3 Formulation of Problem 24
2.4.4 Support for Optimization 25
2.5 Metaheuristic Algorithms for Design Optimization 27
2.5.1 MH based on Metaphor 28
2.5.1.1 Biology and Swarm Influenced MH 28
2.5.1.2 Chemistry and Music Influenced MH 29
2.5.1.3 Mathematics Influenced MH 30
2.5.1.4 Physics Influenced MH 31
2.5.1.5 Sport and Social Influenced MH 31

2.5.2 MH based on non-Metaphor 33
2.5.3 MH Variants 34
2.5.3.1 Upgradation of MH 34
2.5.3.2 Hybridization 35
2.5.4 Limitations and New Trends 37
2.6 Thermal Modelling of PMSM 37
2.7 Research Gaps Identified 38
2.8 Conclusion 38

CHAPTER – III: ANALYSIS OF ELECTRIC VEHICLE POWER TRAIN WITH PMSM AS TRACTION DEVICE **39**
3.1 General 39
3.2 Modelling and Analysis of Conventional Powertrain 40
3.2.1 Physical Model of Conventional Powertrain 40
3.2.2 Simulink Model of Conventional Powertrain 41
3.2.3 Results and Discussions 43
3.3 Modelling and Analysis of Electric Powertrain using SVPWM 45
3.3.1 Physical Model of Electric Powertrain 45
3.3.2 Space Vector Pulse Width Modulation (SVPWM) 46
3.3.3 Simulink Model of EVPT 49
3.3.4 Results and Discussions 50
3.4 Field Oriented Control of EVPT system 52
3.4.1 Dynamic Modelling of PMSM 52
3.4.2 Simulink Model of PMSM 54
3.4.3 Results and Discussions 54
3.4.4 Laboratory Testing of EVPT System using Test Bench Emulator 61
3.5 Conclusion 59

CHAPTER – IV: DESIGN, FEM ANALYSIS AND META-MODELLING OF PMSM **60**
4.1 General 60
4.2 Analytical Design of PMSM-1 61
4.2.1 Geometrical Parameters and Material Properties: Preliminary Design of PMSM-1 61
4.2.2 FEM analysis: Preliminary Model of PMSM-1 63
4.3 Analytical Design of PMSM-2 65
4.3.1 Geometrical Parameters and Material Properties: Preliminary Design of PMSM-2 65
4.3.2 FEM analysis: Preliminary Model of PMSM-2 65
4.4 Mesh Analysis 66
4.5 Surrogate Modelling Technique for Optimization of Motor Geometry 67
4.5.1 Establishment of Design of Experiments 69
4.5.2 Computation of Coefficients using Least Square Method 73
4.5.3 MATLAB Implementation 75
4.6 Root Mean Square Error Test Analysis 76
4.7 Conclusion 77

CHAPTER – V: DESIGN OPTIMIZATION OF PMSM-1 USING INTEGRATED TAGUCHI METHOD ASSISTED POLYNOMIAL METAMODELING AND GENETIC ALGORITHM TECHNIQUE **79**
5.1 General 79
5.2 ITM&GA Optimization Mechanism 80
5.3 Formulation of Experiment 80
5.4 Implementation of ITM&GA Technique 82
5.4.1 Experiments using Taguchi Method 82

5.4.2 Metamodeling 86
5.4.3 Phase II – GA 89
5.5 Analysis of Initial and Optimal Model Performance 91
5.5.1 Analysis at No Load Condition 91
5.5.2 Analysis at Rated Condition 93
5.6 Conclusion 96

CHAPTER – VI: DESIGN OPTIMIZATION OF PMSM-2 USING AQUILA-GRASSHOPPER-OPTIMIZATION TECHNIQUE **98**
6.1 General 98
6.2 Formulation of Optimization Problem 99
6.2.1 Motivation 100
6.2.2 Core Material Properties 100
6.2.3 Topologies of Designed Models 101
6.2.4 FEM Analysis and Surrogate Modelling Analysis 102
6.3 Proposed AGO Mechanism 105
6.4 Implementation of AGO Technique 108
6.4.1 Testing of AGO Algorithm on Benchmark Functions 108
6.4.2 Implementation of AGO Algorithm on Formulated Problem 115
6.5 Performance Analysis of Designed Models 116
6.5.1 Comparative Analysis of Initial and Optimal Models; Model I and Model II 116
6.5.2 Comparative Analysis of Electromagnetic Performance of Models 117
6.5.3 Sensitivity Analysis of Optimized Models 122
6.6 Conclusion 123

CHAPTER – VII: THERMAL MODELLING OF PMSM FOR FAULT DIAGNOSIS **125**
7.1 General 125
7.2 LPTN Structure 125
7.2.1 Node Configuration 126
7.2.2 Computation of Conductance Matrices 129
7.3 Fault Diagnosis using LPTN 133
7.3.1 LDA Classification w.r.t. Temperature Change 133
7.3.2 Results and Discussions 134
7.4 Conclusion 136

CHAPTER – VIII: CONCLUSION AND FUTURE SCOPE OF WORKS **138**
8.1 General 138
8.2 Conclusions 138
8.3 Scope of Future Work 141

Appendix A: Laboratory Testing of EVPT System using Test Bench Emulator **142**
Appendix B: Advantages of Motor Geometry Selection **157**
References **158**
Publications **174**

LIST OF ABBREVIATIONS

The list of principal abbreviations, that are used in this thesis, is given below. The abbreviations which are not included in this list are locally defined in the text.

ABC	: Ant Bee Colony
AC	: Alternating Current
ACO	: Ant Colony Optimization
AGO	: Aquila Grasshopper Optimization
ANSYS	: Analysis System
AO	: Aquila Optimizer
AOM	: Analysis of Means
AOVA	: Analysis of Variance
AS	: Ant System
AW	: Automatic Wheel
BLDC	: Brush-Less Direct Current motor
BO	: Base Optimization
CR	: Chemical Reaction
CS	: Clonal Selection
DC	: Direct Current
DE	: Differential Evolution
DOE	: Design of Experiments
EM	: Electric Motor
ER-EV	: Extended Range Electric Vehicle
EV	: Electric Vehicle
EVPT	: Electric Vehicle Power Train
FA	: Firefly Algorithm
FAS	: Fast Ant System
FC-EV	: Fuel Cell Electric Vehicle
FEM	: Finite Element Method
FER	: Factor Effect Ratio
FFV	: Flexible Fuel Vehicle
FOC	: Field Oriented Control
FP	: Flower Pollination

FW : Front Wheel
GA : Genetic Algorithm
GBM : Gases Brownian Motion
GOA : Grasshopper Optimization Algorithm
GP : Geometrical Parameter
GRASP : Greedy Randomized Adaptive Search Procedure
GS : Gravitational Search
HCSA : Hill Climbing Search Algorithm
HEV : Hybrid Electric Vehicle
HSA : Harmony Search Algorithm
ICE : Internal Combustion Engine
IGBT : Insulated Gate Bipolar Transistor
IM : Induction Motor
ISA : Improved Simulated Annealing
ITM&GA : Integrated Taguchi method assisted Metamodeling & Genetic Algorithm
LC : League Championship
LDA : Linear Discriminant Analysis
LPTN : Lumped Parameter Thermal Network
LSI : Large Scale Integrated
LSM : Least Square Method
MATLAB : Matrix Laboratory
MC : Musical Composition
MH : Meta-Heuristic
MKF : Multiple Kernel Fuzzy
OA : Orthogonal Array
P-EV : Pure Electric Vehicle
PGS : Planetary Gear System
PH-EV : Plug-in Hybrid Electric Vehicle
PM : Permanent Magnet
PMSM : Permanent Magnet Synchronous Motor
POMSIC : Partial Optimization Metaheuristic under Special Intensification Conditions
PSD : Power Split Device
PSO : Particle Swarm Optimization

PWM : Pulse Width Modulation

RMSE : Root Mean Square Error

RSM : Response Surface Method

RW : Rear Wheel

SA : Simulated Annealing

SC : Sine Cosine

SI-PMSM : Surface Inset Permanent Magnet Synchronous Motor

SRM : Switched Reluctance Motor

SVPWM : Space Vector Pulse Width Modulation

SWOT : Strength Weakness Opportunities Threats

SynRM : Synchronous Reluctance Motor

THD : Total Harmonic Distortion

TLBO : Teaching Learning Based Optimization

TSM : Tabu Search Method

TTM : Traditional Taguchi Method

VNDA : Variable Neighbourhood Descent Algorithm

VNSA : Variable Neighbourhood Search Algorithm

VSI : Voltage Source Inverter

LIST OF SYMBOLS

The list of principal symbols, that are used in this thesis, is given below. The symbols, which are not included in this list, are locally defined in the text.

V_D	: Battery voltage in VSI
V_A , V_B , V_C	: Three phase voltages at output of VSI
U_r	: Reference voltage vector in SVPWM
θ	: Angle of rotation of reference vector U_r in SVPWM
T_s	: Sampling time in SVPWM
V_d, V_q	: dq stator voltage
I_d, I_q	: dq stator current
λ_d, λ_q	: dq flux linkage
R_s	: Stator resistance
ω_r	: rotor speed
I_{kd}, I_{kq}	: d-axis and q-axis equivalent currents of damper
L_d, L_q	: d-axis and q-axis synchronizing inductance
L_{md}, L_{mq}	: d-axis and q-axis mutual form of inductance
I_m	: Magnetization currents due to PMs
λ_m	: PM flux linkage
T_{em}	: Electromagnetic torque
P	: Number of pole pairs
J_m	: Moment of inertia of motor
B_m	: Damping coefficient of motor
T_l	: Load torque
K_p	: Proportional controller constant
K_I	: Integral controller constant
t	: Torque Angle
Y	: Response of interest in RSM
$f(p)$	: Second order response surface function
ρ	: Number of input variables in RSM
p_n	: n^{th} input predictor variable in RSM
β_0, β_k	: Individual Coefficients of variables in RSM

β_{kl}, β_{kk} : Associative Coefficients of variables in RSM

P_1 : Magnetic pole eccentricity in PMSM-1

P_2 : Stator slot opening in PMSM-1

P_3 : Magnet thickness in PMSM-1

P_4 : Length of air gap in PMSM-1

T_c : Cogging torque in PMSM-1

T_r : Ripple torque in PMSM-1

T_a : Average torque in PMSM-1

A : Magnet width in PMSM-2

B : Pole embrace in PMSM-2

C : Stack length in PMSM-2

$\boldsymbol{y}$: Output response matrix in RSM

$\boldsymbol{X}$: Matrix formed by regression in RSM

$\boldsymbol{\beta}$: Beta coefficient matrix in RSM

$\boldsymbol{\epsilon}$: Error term matrix in RSM

L : Least square estimator in LSM

SS_E : Squared sum of residuals in LSM

SS_T : Total sum of squares in LSM

SS_R : Regression sum of squares in LSM

R^2 : Coefficient of multiple determination in LSM

R^2_{adj} : Adjusted coefficient of multiple determination in LSM

$RMSE$: Root Mean Square Error

n : Number of experiments performed in RSM

i : Level of design parameters of PMSM-1 in ITM&GA

j : The number of iteration in FEM experiments

μ : Mean value of torque response in AOM

μ_{P_i} : Mean value of torque response for i^{th} level of design parameters

Var_{P_i} : Variance of parameter in AOVA

$\widehat{Y_1}$: Meta-model of cogging torque in PMSM-1

$\widehat{Y_2}$: Meta-model of ripple torque in PMSM-1

$\widehat{Y_3}$: Meta-model of average torque in PMSM-1

ϵ : Error term in Meta-modelling

L_1 : Lower bound of design variables in ITM&GA

U_1 : Upper bound of design variables in ITM&GA

$Parent_1$, $Parent_2$: Parent agents in Binary Tournament scheme of ITM&GA

Off_1, Off_2 : Offspring agents in Simulated Binary Crossover of ITM&GA

cf : Crossover SBX controlling factor

r_1, r_2 : Random numbers in ITM&GA

η_c : Distribution index for crossover in ITM&GA

Off_m : Mutated offspring in ITM&GA

Δ : Mutation control factor in ITM&GA

η_m : Distribution index for mutation in ITM&GA

k : Variable number in meta-modelling

l : Variable number other than k^{th} variable in meta-modeling

$\hat{y}_1$: Meta-model of core loss for model I of PMSM-2

$\hat{y}_2$: Meta-model of core loss for model II of PMSM-2

X^P : Population of solutions in AGO

a : The solution number in X^P in AGO

g : The variable number in X^P in AGO

X_{ag} : Candidate solution in X^P in AGO

N : Total number of solutions in X^P in AGO

dim : Total dimension of problem (number of variables) in X^P in AGO

$x_{N,dim}$: Value of dim^{th} variable at N^{th}solution in AGO

$rand_1, rand_2, rand_3, rand_4, rand_5$: Random numbers in range of [0,1] in AGO at different stages using uniform distribution

it : The iteration number in AGO

IT : Total number of iterations in AGO

$X_b(it)$: Best updated solution at it^{th} iteration in AGO

$X_m(it)$: Mean of the solutions at it^{th} iteration in AGO

$X_r(it)$: Random solution at it^{th} iteration in AGO

$levy(dim)$: Levy flight function of Aquila in AGO

σ, y, x : Control factors of Levy function in AGO

$s, \beta, r_c, p, \omega, \theta_1$: Constants of Levy function in AGO

u, v : Random numbers in AGO

d_1 : Vector of integers containing elements from 1 to dim in AGO

α, δ : Exploitation control parameters in AGO

$QF(\mathrm{it})$: Quality function calculated at it^{th} iteration in AGO

g_1, g_2 : Control parameters in AGO

c : Control Coefficient in AGO

sf : Social force strength among grasshoppers in AGO

af : Attraction intensity factor in AGO

lf : Length scale factor of attraction in AGO

d_{ag} : Distance between a^{th} grasshopper and g^{th} grasshopper in AGO

c_{max}, c_{min} : Maximum and minimum value of Control Coefficient (c) in AGO

$\hat{T}_{dim}$: Target position of grasshopper (best solution found so far) in AGO

F1, F2, …, F23 : Names of Benchmark functions

f_{min} : Minimum value of Benchmark functions

m : Parameters of PMSM-2 for sensitivity analysis

m_z : z^{th} independent variable for sensitivity analysis

df : Data function whose sensitivity is to be computed

S_z^{df} : Sensitivity of data function w.r.t. variation in z^{th} independent variable

i_t : The node number in LPTN model

n_t : Total nodes in LPTN model

$\boldsymbol{G}$: Conductance matrix in LPTN

$\boldsymbol{Pl}$: Loss vector in LPTN

$\boldsymbol{\vartheta}$: Temperature vector in LPTN

R : Thermal resistance between nodes in LPTN

λ : Thermal conductivity

R_r : Thermal resistance of a rectangular object in LPTN

A_r : Surface area of rectangular object in LPTN

L_r : Length of rectangular object in LPTN

R_h : Thermal resistance of a hexahedron in LPTN

y_t : Thickness of hexahedron in LPTN

y_l : Length of hexahedron in LPTN

x_i : Inner width of hexahedron in LPTN

x_o : Outer width of hexahedron in LPTN

R_{hd} : Thermal resistance of a disk-shaped hollow cylinder in LPTN

r_i : Inner radius of disk-shaped hollow cylinder in LPTN

r_o : Outer radius of disk-shaped hollow cylinder in LPTN

l_d : Thickness of disk-shaped hollow cylinder in LPTN

R_{hs} : Thermal resistance of a hollow cylinder for a segment of angle ϕ

l_s : Thickness of hollow cylinder for a segment of angle ϕ in LPTN

sm : Symmetry factor in LPTN

q : The class (or group) number in LDA

t_q : Class vector in LDA

t_q^o : Mean corrected vector in LDA

μ_g : Global mean vector in LDA

c_q : Covariance matrix for each class in LDA

S_q : Total samples in q^{th} class of LDA

C_v : Overall covariance matrix in LDA

f_q^{LD} : Discriminant function of q^{th} class of LDA

μ_q : Mean vector of each class in LDA

t_γ : γ^{th} object to be identified through LDA

pr_q : The prior probability vector for each class in LDA

LIST OF FIGURES

1.1	Traction Motor Characteristics during Different Drive Cycles of Vehicle……..	1
2.1	Schematic Representation of Type A P-EV Architecture…….	13
2.2	Schematic Representation of Type B P-EV Architecture…….	14
2.3	Schematic Representation of possible Type C P-EV Architecture……...	15
2.4	Series HEV Architecture……...	15
2.5	Parallel HEV Architecture……	16
2.6	Power-split HEV Architecture……..	17
2.7	Generalized Process Flow for Designing PMSM…….	19
2.8	General View of Meta-Modelling Support for Optimization……...	25
2.9	Meta-Modelling based Process of Design Optimization……..	26
3.1	Physical Model of Conventional Vehicle Powertrain……...	41
3.2	Simulink Model of Conventional Vehicle Powertrain……..	42
3.3	Characteristic Plots of Conventional Powertrain for Three Conditions of Throttle.	45
3.4	Schematic Diagram of EVPT system……...	46
3.5	Space Vector Representation ……...	48
3.6	SVPWM Switching Pattern for Sector 1……..	48
3.7	Simulink Model of EVPT System with SVPWM Control……...	48
3.8	Characteristic Plots of Electric Powertrain……...	51
3.9	Output Response of VSI……...	52
3.10	Schematic Diagram for FOC of EVPT System……	53
3.11	Simulink Model of EVPT System (PMSM with FOC)……	54
3.12	Dynamic Response under Load Disturbance for Constant Speed Operation……...	56
3.13	Dynamic Response under Load Disturbance for Variable Speed Operation……	57
3.14	Dynamic Response under Load Disturbance for Ramped Speed Operation……	57
3.15	Dynamic Response under Load Disturbance for Breaking Mode Operations……..	58
4.1	Flow Chart for Development of the Preliminary Model Design……..	61
4.2	PMSM-1: (a) Quarter-Sectional Model (b) Location of PMs in Rotor……	62
4.3	BH Curves: (a) Stator & Rotor Core (b) Shaft Core…….	63
4.4	FEM Analysis of PMSM-1……...	64
4.5	PMSM-2: (a) Half-Cross-Sectional Model (b) Location of PMs in Rotor……...	65
4.6	FEM Analysis of PMSM-2……...	66
4.7	SI-PMSM Geometries using ANSYS Maxwell's Meshing Proficiency……..	67

4.8	Process Flow for Formation of RS models……..	69
4.9	Cross Section of One pole of Preliminary Design of PMSM-1……	71
4.10	Cross Section of PMSM-2 to Present Variable Design Parameters…….	72
4.11	Pseudo Code for Surrogate Modelling using LSM……...	76
4.12	RMSE Test Results for Responses of Interest……..	77
5.1	Process Flow for Novel ITM&GA Technique……..	80
5.2	Electric Compressor System of EV …….	81
5.3	Cross Section of a pole of Preliminary Model of PMSM-1……..	82
5.4	Plots for AOM results of Taguchi Method……...	84
5.5	Graphical Representation of FER values using AOVA……	86
5.6	Contour and Surface Plots for Variations in Design Parameters of PMSM-1……..	89
5.7	Implementation of Phase II of ITM&GA…….	91
5.8	Induced Voltage Waveforms of Preliminary and Optimal Models of PMSM-1 under No Load Conditions……	92
5.9	Comparison of Cogging Torque Characteristics……...	93
5.10	Rated Torque Characteristics of Preliminary and Optimal Models of PMSM-1…..	94
5.11	Constructional Features of Preliminary and Optimal Models of PMSM-1……..	94
5.12	(a) Flux Distribution and (b) Magnetic Flux Density of Preliminary and Optimal Models of PMSM-1……..	95
5.13	Torque and Power Variation at Different Temperatures……..	96
6.1	Characteristics of Core Materials……..	101
6.2	Model Designs of PMSM-2……..	102
6.3	Cross Section of PMSM-2……	103
6.4	Process Flow Chart of the Proposed AGO Algorithm……..	106
6.5	Pseudo Code of the Proposed AGO Algorithm……	108
6.6	Convergence Characteristics of AGO for various Benchmark Functions……	114
6.7	Comparative Analysis for Convergence Test of Different Algorithms……	115
6.8	Comparison of Electromagnetic performance of Preliminary and Optimised Models……...	118
6.9	Performance Comparison of six Models……...	119
6.10	Comparison of Weight and Power Density of six Models……...	119
6.11	Magnetic Flux Densities for Model II and Model IV……...	121
6.12	Sensitivity of Core Loss to Variation in Magnet Thickness (A), Pole Embrace (B) and Stack Length (C)……	122
7.1	Important Angles and Radii……..	128

7.2 Node Placement for designing LPTN Models…….. 129
7.3 Segmentation Performed in PMSM Models for Computation of Thermal Resistance…….. 130
7.4 (a) Rectangular object (b) Hexahedron (c) A Segment or Disk-shape of a Hollow Cylinder……. 130
7.5 LPTN based Thermal Modelling…….. 132

LIST OF TABLES

1.1	Major Advantages, Disadvantages and Applications of PMSM……..	3
1.2	Major Advantages, Disadvantages and Applications of BLDC……	3
1.3	Major Advantages, Disadvantages and Applications of SynRM……..	4
2.1	Comparison of Level of Electrification of EVs…….	12
2.2	Generally Utilized Approximation Methods…….	22
3.1	Vehicle Body Parameters……..	42
3.2	Generic Engine Parameters……	43
3.3	Load Variation Analysis……	43
3.4	Phase Voltages at Different Switching States……...	47
3.5	PMSM Parameter Specification……	49
3.6	Benchmarked EVPT Performance Parameters……..	49
3.7	Comparison of Benchmarked EVPT Performance Parameters…….	58
4.1	Specifications of Preliminary Model of PMSM-1…….	62
4.2	Specifications of Preliminary Model of PMSM-2…….	65
4.3	Electromagnetic Performance for Various FEM Experiments on PMSM-1…….	71
4.4	FEM Experiment Results for PMSM-2…….	72
4.5	Coefficients of RSM Models of PMSM-1…….	75
4.6	Coefficients of RSM models of PMSM-2…….	75
4.7	Coefficients of Determination for Fitted Regression Models……	77
5.1	Levels Of Design Variables……...	83
5.2	Motor Performance for Various Taguchi Experiments…….	83
5.3	AOM Results For All Levels of Parameters……..	84
5.4	Effects Of Various Parameters on Motor Performance…….	85
5.5	GA Parameters……...	90
5.6	Performance of Preliminary and Optimal Models of PMSM-1…….	93
6.1	Core Material Properties……	101
6.2	Specification of Designed Models…….	102
6.3	FEM Simulation Responses for Model I and Model II…….	103
6.4	Individual and Associative Coefficients of RSM……..	104
6.5	Values of Computational Parameters of Different Algorithms…….	109
6.6	Definitions of Benchmark Functions and Comparative Analysis Results……	109
6.7	Performance Analysis of Algorithms for Core Loss Models $\hat{y}_1$ and $\hat{y}_2$……	116

6.8 Parameters and Performance Analysis of Preliminary and Optimal Models I and II…… 117
6.9 Sensitivity Values of Key Design Parameters…….. 122
7.1 Machine Dimensions……. 126
7.2 Material Used in the Motor and their Thermal Conductivities……. 127
7.3 Change in Temperature Vector for Corresponding Speed Variation of PMSM-1… 135
7.4 Change in Temperature Vector for Corresponding Speed Variation of PMSM-2… 135
7.5 Analysis of LDA Classification w.r.t. Temperature Change in PMSM-1……. 136
7.6 Analysis of LDA Classification w.r.t. Temperature Change in PMSM-2……. 136

Chapter 1

INTRODUCTION

1.1 General

The major motivation for the Electric Vehicle (EV) industry is to deliver state of the art mobility solutions, which do not consume fossil fuel and produces minimal pollution at higher overall efficiency and minimum mean time between failures. The overall cost, reliability and fidelity of the traction device of EV are the key result areas during the development of an EV system [1-3]. The use of different types of electric motors (EM) have been explored for their employment in EVs in terms of their maximum operating speed, output power, manufacturing and maintenance cost, durability and efficiency [4-5].

The requirements of an ideal traction motor in an EV during different drive cycle modes is shown in Fig. 1.1. The acceleration attained by the vehicle at low speed and its hill climbing potential determines the maximum torque of traction motor. Maximum vehicle speed required determines the maximum speed of the motor. The acceleration of the vehicle from base speed to maximum speed determines the power of the traction motor. The grey portions indicate the operating areas of the vehicle generally used during urban or highway drive cycles.

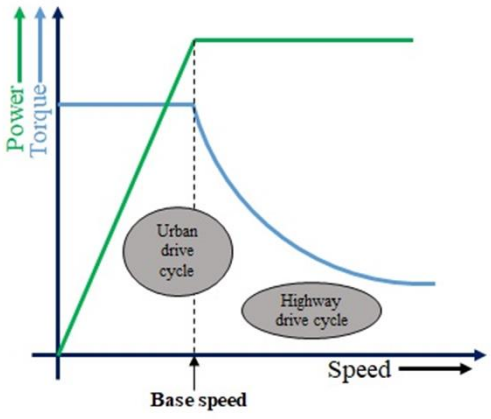

Fig. 1.1 Traction Motor Characteristics during Different Drive Cycles of Vehicle

In Internal Combustion Engine (ICE) vehicles, the broad area of constant power is achieved by using multi-gear system of transmission which results in additional vehicle weight and space. In the urban drive cycle the traction system of ICE vehicles has low operating efficiency [6]. In comparison, efficient operation of traction EM can be achieved using a single gear transmission system for urban drive cycle to meet the requirements of the vehicle [7]. One of the possible options for enhancing the performance of the EM used in EV is to simplify its structure [8-10].

The motivation for this research work stems from the possibilities of exploring structural optimisation and reducing losses of the EMs that can be suitably used for EV applications.

1.2 Electric Motors used in EV Application

Use of various EMs, like Induction motors (IM), Direct Current (DC) motors, Switched Reluctance Motors (SRM), Permanent Magnet Synchronous Motors (PMSM), Brushless DC (BLDC) motors and Synchronous Reluctance Motors (SynRM), have been explored for use in EVs. Out of these, DC motors suffer from high maintenance cost and fault problems related to its operation during commutation. IMs suffer high losses due to presence of winding in the stator and rotor. The control of SynRMs is complex. Over the past few years BLDC motors, PMSMs and SynRMs have gained popularity as they have competitive capabilities for EV applications [11-13].

1.2.1 Permanent Magnet Synchronous Motor

The PMSMs are fast, compact, safe, efficient, brushless, less bulky and provide good dynamic performance [14]. It works on the principles similar to that of three phase alternating current (AC) synchronous motor. Three phase windings are installed in the stator and unlike conventional motors, permanent magnets (PMs) are mounted on the rotor in order to produce the rotating magnetic field. Due to the absence of magnetising coils in the rotor, these motors are simple in construction and costs less. Based on the rotor position, the stator windings are suitably energised to produce unidirectional torque.

PMSM are broadly classified into: (1) Surface PMSM; having the magnets mounted on the surface of rotor, (2) Interior PMSM; having the magnets embedded into the rotor and (3) Surface Inset PMSM (SI-PMSM); having inset surface mounted magnets in the rotor. The major advantages, disadvantages and applications of PMSM are tabulated in Table 1.1.

Table 1.1: Major Advantages, Disadvantages and Applications of PMSM

Advantages	Disadvantages	Application
• High efficiency at higher speeds • Easy to install and maintain as compared to IM • Available in compact size • Provides smooth dynamic performance • Can deliver full torque at low speeds • Provide low torque ripples at rated conditions	• Higher cost compared to IM. • Since they are not self-starting motors, it is quite difficult to start up the motor.	• AC compressors • Refrigerators • Data storage units • Air conditioners • Washing machines • Machine tools • Electrical power steering system in automotive industry • Power factor improvement in large power systems • Traction control • Electric Vehicles and Hybrid Electric Vehicles • Robotics applications • Aerospace applications • Servo drives • Industrial applications • Large medical instruments

1.2.2 Brushless Direct Current Motor

The BLDC motor has similar working principle as that of a typical DC motor that is based on Lorentz force law. The stator of BLDC motor consists of current carrying conductor while the rotor has PMs. BLDC motor does not need any commutator or brush. Instead, it requires control circuitry and hall sensors or encoders for rotor position sensing. It is a kind of synchronous motor in which the stator and rotor magnetic fields rotates at the same frequency [15]. The major advantages, disadvantages and applications of BLDC motor are tabulated in Table 1.2.

Table 1.2: Major Advantages, Disadvantages and Applications of BLDC Motor

Advantages	Disadvantages	Application
• Less maintenance cost • High speed operation • Reduced size • Light weight • High dynamic response • Low noise since brushes are not present	• High manufacturing cost since it requires complicated power electronic controller • Needs additional sensors for detecting rotor position • Requires complex control circuitry	• Electric Vehicles and Hybrid Electric Vehicles • Computer hard drives • Industrial robots • Belt driven systems • Washing machines, dryers and compressors • Fan, blowers • Pumps

1.2.3 Synchronous Reluctance Motor

It is a class of synchronous motor in which there is a difference of permeance in direct and quadrature axes of the rotor due to which torque is produced at the shaft of the motor. The rotor has no field windings or PMs. The stator has a core with a winding which may be concentrated or distributed. The rotating magnetic field is created in the air gap by AC passing through the stator winding. For minimizing the reluctance in the magnetic circuit, the rotor seeks to enact its direct axis with the applied field in order to develop the torque. Since the torque is proportional to the difference between direct and quadrature axis inductances, the higher this difference the greater is the developed torque [16]. The major advantages, disadvantages and applications of SynRM are tabulated in Table 1.3

Table 1.3

Major Advantages, Disadvantages and Applications of SynRM

Advantages	Disadvantages	Application
• Robust rotor construction • Low heat variations • Low cost due to absence of magnets • Low inertia of motor • Speed control over wide range	• Require variable frequency control drive • Low power factor • Require power correction devices	• Electric Vehicle applications

Based on the comparison of above three candidate motors for EV applications, PMSM has low overload capacity and high manufacturing cost. However, it has – lower torque ripples, lower noise, higher power density, wider speed range, higher efficiency, lesser maintenance cost, more robustness, more ruggedness and is easier to control. The dominance of more favourable characteristics of PMSM make it the most eligible candidate for EV applications [17-19]. The preliminary motor design can be optimized for better electromagnetic performance. SI-PMSM exhibits lesser flux leakage, has better efficiency and robust mechanical structure [20]. It is therefore selected for design optimization using Finite Element Method (FEM) analysis in this research work. The selected motor design with different pole/slot combinations along with different winding configurations are optimized using different novel optimization algorithms as explained in the upcoming chapters.

1.3 Simulation Tool

Differential equation representations are generally used in all domains of physical sciences for solving complex problems. One of the numerical methodology tools used to solve partial as well

as ordinary differential equations is FEM analysis. FEM analysis can be used for solving complex problems, which are representable in the form of differential equations. There are limitless applications of FEM analysis with reference to the real-world design problems [21].

It is possible to model different phenomena of magnetic field like microwaves propagation or torque produced in EM. The true observation or insight towards the nature of response around the specified structure or passing through that structure is provided by analysing the magnetic fields or electrostatic fields around it. This assists the user to obtain precise responses in order to regulate such fields.

The analysis of behaviour of devices with respect to their linear electromagnetic nature can also be performed using FEM analysis, which involves the electric, magnetic and/or thermal field assessment.

The FEM has its application roots in many disciplines. It can be used in civil, mechanical, electrical and structural engineering etc. In the field of engineering design, this tool has endless importance [22]. The major areas of applications in the field of designing include analysis of:

- Rotating electrical machines like DC machines, induction machines, synchronous machines, brushless motors, coupling devices, stepper motors, PM motors, switched reluctance motors or generators etc.
- Energy conversion and transfer modules like cables, transformers, high voltage devices, connectors, insulators or fuses etc.
- Electric actuator devices like electromagnetic brakes, linear motors, contactors, fuel injectors, magnetic bearings or electromagnetic launchers etc.
- Sensor devices like eddy current devices, speed sensor devices, resolvers, non-destructive testing sensor devices or electric meters
- Field generator modules like magnetic recorders, mass spectrometers, magnetization devices or polarization devices etc.

The mathematical modelling, simulation studies and analysis in this research work has been carried out through FEM Analysis using ANSYS Maxwell Software v.2019. This tool has two modes of simulation analysis, which are:

- Transient/time stepping mode
- Magneto-static mode

The transient mode is more helpful for the design models having rotational operations. It produces reliable results by providing the potential to control the level of precision through the selection of the steps per unit time period. The magneto-static mode of calculation does not include the motion of rotor and parasitic loss constituents. A parametric (Opti-metric) interface tool is available for facilitating the utilization of above-mentioned modes. It provides the opportunity to customize parameters to refine the profile and select different options to enhance simulation flexibility [23].

The computational mathematics involved in this work is performed using the language of technical computing – MATLAB/Simulink (R2016a). The Simulink tool helps to analyse model-based design and enables the user to incorporate multiple algorithms into design models and export the results to MATLAB for further analysis [24].

1.4 Research Objective

The proposed research work focuses on improvement in performance of SI-PMSM using design optimization techniques. The objectives of this research work include:

(1) Modelling and Simulation of SI-PMSM Drivetrain

The conventional ICE and electric powertrain are modelled in MATLAB/Simulink for analysing the performance of these two distinct propulsion configurations. The conventional powertrain using spark ignition type of generic engine is modelled in Simulink and the information obtained from the dynamic analysis of ICE powertrain is set as the benchmark parameters for evaluating the performance of electric powertrain. The electric powertrain is modelled and simulation studies are carried out through the implementation of space vector pulse width modulation (SVPWM) and field oriented control (FOC) based control strategies. The dynamic performance of traction motor is analysed, for both traction and braking modes of operation, under different operating conditions.

(2) Study of Design Features of SI-PMSM for EV applications

The necessary aspects involved in designing the SI-PMSM for EV application are studied and explained. The analytical computation of stator and rotor dimensions are carried out for different models. Preliminary mesh analysis of designed models is carried out to ensure accuracy of model designs. The effects of variation in designing features on electromagnetic performance of PMSM is studied and analysed. To save computation time, the meta-models of

various output characteristic parameters are developed using Response Surface Method scheme with the help of FEM analysis.

(3) Implementation of Algorithms for obtaining the Optimized Machine Model

A novel design optimization methodology - Integrated Taguchi Method Assisted Polynomial Metamodeling and Genetic Algorithm (ITM&GA) is designed and implemented for optimizing the motor geometry. The comparative analysis of initial and optimized models using conventional design algorithm and proposed novel technique is presented for electric compressor application in EVs.

(4) Efficiency Improvement in the Design of SI-PMSM through FEM Analysis

A novel metaheuristic (MH) Aquila Grasshopper Optimization (AGO) technique is developed by hybridizing the excellence of natural hunting-based Aquila Optimizer (AO) and natural hoping based Grasshopper Optimization Algorithm (GOA). At exploration as well as at exploitation stages of AO, distance between different swarms (or solutions) is normalized so as to maintain the balance between both the stages. This proposed novel AGO technique is validated by testing its potential on various predefined benchmark functions and then applied to solve the designed real-world problem to reduce core losses in the developed preliminary SI-PMSM design. The torque performance and efficiency performance of the initial and optimized models are compared.

(5) Comparative Analysis of different PMSM Models on the basis of Design Aspects

The FEM models of the six structurally different models having two different core materials are designed and analysed based on the geometrical alterations. Appropriate trench cuts are provided in the core of motor to reduce the core losses in different models at rated conditions. The introduction of trench cuts results in lightweight motor structure. Sensitivity analysis is carried out to analyse the impact of small deviation in parameters on the core loss and efficiency of the models. The thermal modelling of the designed PMSM is carried out for fault detection using Linear Discriminant Analysis.

1.5 Organization of Thesis

The organization of thesis has been done in the form of different chapters, which is described below:

Chapter 1 gives a brief introduction of the advantages of EVs over conventional ICE vehicles. It discusses operating principles, advantages and disadvantages of different motors used in EV application. In addition, the summarised specifications of simulation tools are presented. Research objectives and the work performed to fulfil them are described. The organization of this dissertation thesis in the form of different chapters is also listed.

Chapter 2 enlists the relevant literature review related to the conventional and electric powertrain, different topologies of PMSM, control, design strategies and performance measures of PMSM. An overview of reported design strategies, surrogate modelling and metaheuristic techniques for design optimization are presented, along with the thermal modelling of PMSM.

Chapter 3 elucidates the analysis of key mechanical and electrical aspects of the vehicle powertrain. The conventional powertrain using spark ignition type of generic engine is modelled and the information obtained from the dynamic analysis of ICE powertrain is set as the benchmark parameters for evaluating the performance of Electric Vehicle Power Train (EVPT) through implementation of FOC and SVPWM control strategy for SI-PMSM.

Chapter 4 describes the analytical design, geometric parameters and material properties of the developed preliminary models of SI-PMSMs for compressor and traction application in e-vehicles. The basic designs are analysed for different operating conditions and the electromagnetic performance of the designed motors is validated using Mesh Analysis. In addition, optimization of the motor geometry for the two developed preliminary models is carried out using Surrogate Modelling Technique and the models of the motor are validated using Root Mean Square Error (RMSE) analysis.

Chapter 5 presents a novel ITM&GA optimization technique developed and implemented for design optimization of the preliminary model of the SI-PMSM, used for environment conditioning application in EVs. The comparison between performances of optimized model by conventional Taguchi method and proposed ITM&GA method is investigated and presented.

Chapter 6 enumerates a novel hybrid metaheuristic AGO technique and its application to address a real-world problem of optimizing the preliminary design of SI-PMSM, designed for traction application in EV, through reduction in core losses. The proposed novel AGO technique is tested against various Benchmark Functions. The performance of the preliminary and optimized SI-PMSM models are compared and presented.

Chapter 7 describes the thermal analysis of the designed models of SI-PMSM using Lumped Parameter Thermal Network (LPTN) technique. The node selection in motor geometry, thermal

resistance calculation, node temperature calculation, etc. involved in investigating the thermal behaviour of the models is presented. This technique is useful in diagnosing the faulty part of the motor under different operating conditions.

Chapter 8 gives the summarized conclusions and achievements of this research work. The possible future scope of work in this area of research is also listed.

1.6 Conclusion

This chapter presents the motivation behind this research work, gives a glimpse of the comparison between conventional and electric powertrain and an overview of the different types of motors that can be used for EV application. The pros and cons of using PMSMs, BLDC motors and SynRMs are outlined along with their various application areas. The benefits of FEM analysis and the simulation tools used for analytical and computational analysis are described briefly. In addition, the major objectives of this research and the corresponding work done to fulfil them is summarized.

Chapter 2

LITERATURE REVIEW

2.1 General

Earlier in the last decade, DC motors were found suitable for propulsion of EV or HEV systems since it works directly with DC provided by the batteries and does not require conversion to AC for its operation. However, its low efficiency and frequent demand of maintenance made it unattractive for EV applications. With the swift evolution in power switching equipment like insulated gated bipolar transistor (IGBT) and large scale integrated circuits; IMs, PMSMs, BLDC motors and SynRMs have become popular in running traction system of EVs [25].

IMs are used in applications where high-speed variation and rigorous speed control is necessary. Its torque control is performed using pulse width modulation (PWM) of current. Above base speed, its current control along with constant power can be performed using flux weakening operation. However, maintaining constant power above base speed is difficult in IMs. Generally, if appropriate designed, IMs can work up to a maximum of two or three times the base speed with higher breakdown torque; such IMs are bulky in size [26].

In PMSM, due to the magnetic field produced by PMs, many advantages are observed as compared to an IM. The rare earth PMs possess abundant magnetizing energy which empower the PMSM operation and helps in obtaining compact size of the motor. Besides, it has superior torque characteristics and power density. It has better power factor and efficiency due to the absence of windings in rotor. PMSMs show very high efficiency even at low speed, which makes it the most suitable motor for EVs in urban areas where the vehicle encounters frequent switchover between start and stop operation [27]. However, it faces limitations of operating in constant power zone since field weakening operation in the air gap can only be achieved by producing the component of stator field which is opposing the field produced by PM in rotor. According to the recent research for enhancing the constant power region of PMSM operation, a supplementary field winding is added for the field current control and hence constant power zone is increased up to four times the base speed [28].

In SynRMs, the absence of PMs can cut down its manufacturing cost. Since there is no magnetic flux, the restriction on maximum speed along with the constant power operation is eliminated.

However, the burden of producing the magnetic field by only stator windings and the controller due to lack of excitation of PMs is increased. This gives rise to higher copper losses, material deterioration and reduced efficiency. Also, the air gap architecture in SynRMs is non-uniform which causes acoustic noise and high ripples in torque [29].

2.2 Conventional Power Train and Electric Power Train

The exploration of climate-friendly, adaptive, economical and sustainable transportation solutions is pushed by the governments, automotive industries and researchers to address environmental issues, energy security and fuel efficiency. As transportation industry is facing environmental and energy crisis, researchers are putting their efforts in developing new strategies to work towards cutting the fuel emissions by reducing the use of fossil fuel. One forthright approach to reduce fuel consumption is to enhance the efficiency of electric powertrain by reducing resistive forces of vehicle. The second strategy is to replace fossil fuel with alternate energy source. Among these sources, the dominant solutions comprise of flexible fuel vehicle (FFV) or EV. Despite the appreciable market penetration done by FFV, the task to produce EV is the most reasonable and significant preference for the following reasons: (1) Electrical energy is one of the critical element to diversify the energy sources which is advantageous for energy preservation, (2) since on-road vehicles will continue to use fossil fuel, primarily in upcoming decades, by hybridizing the energy sources in vehicles, its efficiency can be improved and tailpipe emissions can be decreased, (3) EV provides numerous technical solutions like energy management, regenerative braking, smooth and noise-free propulsion system, etc. [30].

2.2.1 Architecture of Powertrain

The architecture of powertrain identifies the energy flow and topological connection among its various components. A conventional powertrain consists of engine and drivetrain components. A drivetrain is composed of a group of elements that are responsible of delivering power to the wheel system. The major elements of a conventional drivetrain are flywheel, clutch system, gearbox, propeller shaft, rear axle consisting of differential system. In electric powertrain, unlike conventional one, the architecture consists of electric motor, coupling device and transmission system along with the topological connection of elements. Also, the architecture of powertrain communicates with distinct management schemes, which makes the selection of proper architecture even more complicated. Broadly, the architecture of powertrain is categorized as series, parallel and power-split types on the basis of electric motors, modelling or power

electronics. Although with rapid development and variations in these basic types, conventional schemes have to be updated and more divided to match the pace of current development. The process level of electrifying a vehicle has a great influence on selection and design of architecture, based on this EVs are classified into five grades; Hybrid EV (micro, mild and strong Hybrid EV(HEV)), Plug-in Hybrid EV (PH-EV), Pure EV (P-EV), Extended Range EV (ER-EV), Fuel Cell EV (FC-EV) [31].

2.2.2 Process Level of Electrification of Vehicles

The process level of electrification governs the ability of electric path, which inhibits the energy preserving tools of EVs. It is generally expressed by the voltage of the battery, energy storage system and power. Different EVs based on the process level of electrification are compared in Table 2.1, which gives the dominant characteristics of different EVs based on the level of electrification. Micro and mild HEVs have full capacity to cut off the supply of fuel during 'idle-stop'. Mild HEV has more 'voltage level' than micro HEV. It possesses partial capacity of 'power-assist' and 'regenerative braking'. Strong HEV has partial capacity of running like P-EV ('P-EV driving') at lower speed and can exhibit 'power-assist' and 'regenerative braking' excellently. When the three HEVs without 'charger' are compared to PH-EV, ER-EV and P-EV, over 300 V of 'voltage level' battery pack is used to store energy from grid. PH-EV supports low range of 'P-EV driving' level. ER-EV has got ICE as back up energy storage system. P-EV exclusively runs on electrical motors powered by the battery stored energy.

Table 2.1

Comparison of Level of Electrification of EVs (FC=Full Capacity, PC=Partial Capacity)

EVs	Power assist	Idle stop	Regenerative Braking	P-EV Driving	Charger	Voltage level (V)
Micro HEV	-	FC	-	-	-	12
Mild HEV	PC	FC	PC	-	-	48
Strong HEV	FC	-	FC	PC	-	300
PH-EV	FC	-	FC	FC	FC	300+
ER-EV	FC	-	FC	FC	FC	300+
P-EV	-	-	FC	FC	FC	300+

2.2.3 Architectures of P-EV Powertrain

The types of P-EV powertrain architectures are classified on the basis of numbers and locations of electric motor, transmission system and gears etc. Three broad categories of P-EV architectures are discussed here.

2.2.3.1 Type-A: P-EV with Single Motor and no Transmission

This powertrain has similar architecture to conventional one less the transmission system. The motor is powered by the battery to produce shaft torque which is delivered to the differential system via one-step reduction speed gear. In this configuration, motor, gear and differential system are coalesced into a single compact entity so as to obtain reduced weight of vehicle. The Schematic representation of Type A P-EV architecture is shown in Fig. 2.1.

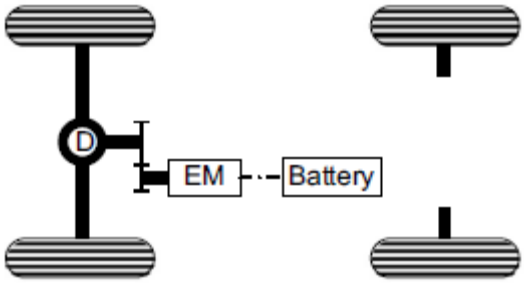

Fig. 2.1 Schematic Representation of Type A P-EV Architecture

Advantages of Type A architecture are:

- Simple constructional layout
- Less installation space
- Less driveline losses
- No control of gear shift is required

Disadvantages of Type A architecture are:

- Probable efficiency drop
- Can only produce its maximum power partially at low speed
- Large motor size requirement for overall operation
- High manufacturing cost due to large size of motor

2.2.3.2 Type-B: P-EV with Single Motor and Multi-Gear Transmission

By introducing multi-gear transmission system between motor and differential system in Type A architecture, the formation of Type B P-EV architecture is achieved. Hence Type B architecture is similar to the conventional one minus the coupling devices. Usually, the upper limit of number of gears is four in this configuration which helps in the improvement of fuel economy by 2-5 %. Schematic representation of Type B P-EV architecture is given in Fig. 2.2. Advantages of Type B architecture are:

- Gearbox can have different realizations for obtaining variable operational speeds
- Fuel saving is increased as compared to that obtained from type A configuration
- Smooth shift of speed using planetary gear set

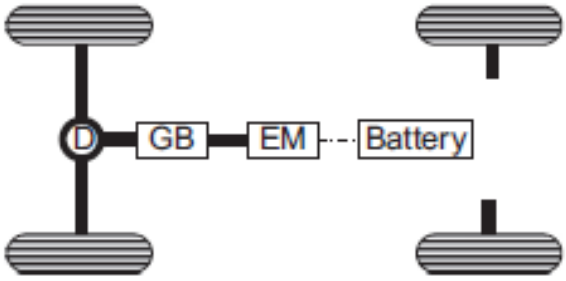

Fig. 2.2 Schematic Representation of Type B P-EV Architecture

Disadvantages of Type B architecture are:

- Limited gear numbers
- Torque gap during gear transition
- Probable vehicle jerk production

2.2.3.3 Type-C: P-EV with Multiple Motors

This type of P-EV architecture contains configurations having more than one electric motor along with the battery and differential system. The major categories of this architecture type are shown in the form of schematic diagram in Fig. 2.3. Front wheel (FW), rear wheel (RW) or automatic wheel (AW) drive systems can be operated depending upon the location of the motor in the drivetrain.

Advantages of type C architecture are:

- Packaging space can be spared

- Space for cargo, passenger and battery can be saved
- Flexible operation of FW, RW or AW drive can be obtained

Disadvantages of type C architecture are:

- Additional clutch system can reduce degree of freedom of planetary gear set
- Coupling of multiple motors may be complex

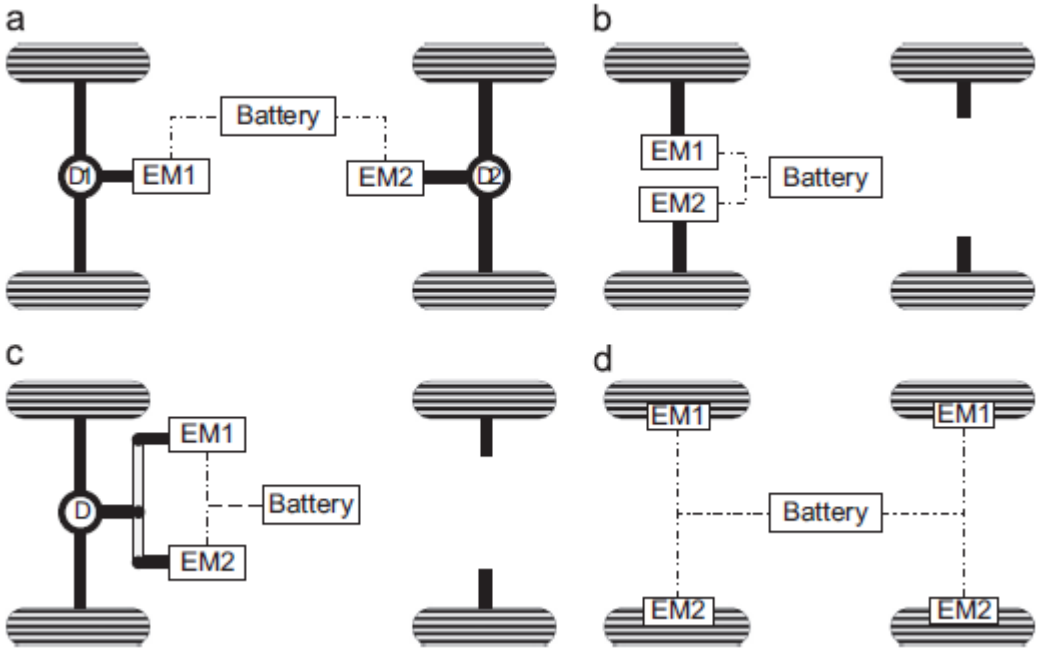

Fig. 2.3 Schematic Representation of possible Type C P-EV Architecture

2.2.4 Architectures of HEV Powertrain

The architecture of HEV becomes complex when compared to that of P-EV powertrain. HEV powertrain architecture are classified based on the presence of ICE, electric motor(s), transmission system(s), coupling system(s) with respect to the location. Three major categories are described here.

2.2.4.1 Series Configuration

A series HEV architecture consists of a combustion engine, electric motor(s), battery storage system and controller(s) etc. It can be realized in different designs as (a) Front-engine-rear-drive (FE-RD), (b) Rear-engine-rear-drive (RE-RD) and (c) Front-engine-front-drive (FE-FD), as shown in Fig. 2.4.

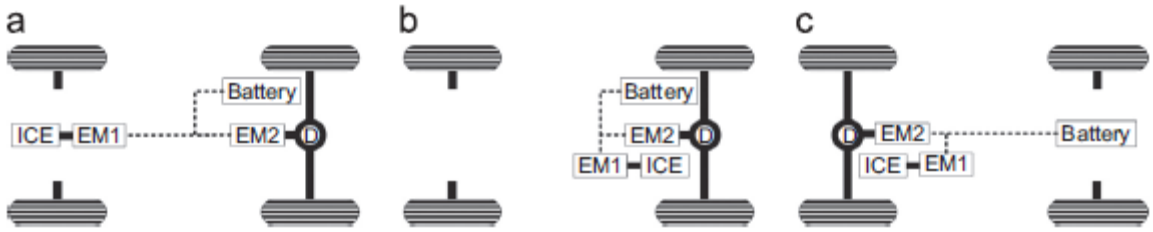

Fig. 2.4 Series HEV Architecture

The engine generator system produces electrical energy by converting chemical energy of fuel. This electrical energy is transferred to the traction device to produce the output mechanical power.

Advantages of series configuration are:

- ICE operates at full efficiency since the mechanical path is absent between wheel and engine
- Fuel consumption is reduced
- Excellent dragging capacity of motor at lower speed
- Simple procedure to control the schematic

Disadvantages of series configurations are:

- Burden of peak power demand from electronic controllers is increased
- Increased cost and weight.
- Multiple stage of energy conversion decreases overall efficiency

2.2.4.2 Parallel Configuration

In parallel configuration of HEV architecture, the connection of electric motor and engine has fixed value of speed ratio so that driving toque can be provided to the wheel system separately or together. The location of electric motor varies with respect to the other components. Fig. 2.5 presents the various possible layouts of parallel HEV architectures (Trans means clutch).

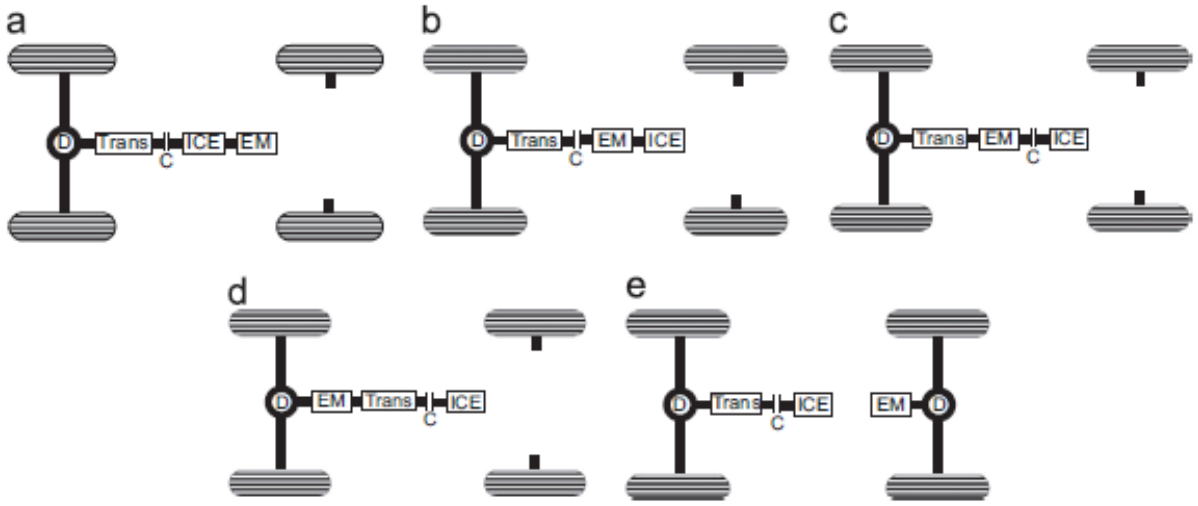

Fig. 2.5 Parallel HEV Architecture (a) Type A (b) Type B (c) Type C (d) Type D (e) Type E

Type A can be used in both mild and micro HEVs. The motor is needed to be placed between the flywheel engine and coupling device in Type B. Because of the position of motor between clutch and coupling system, type C can perform well in mild, micro, strong HEVs, PH-EV and ER-EV applications. The transmission system is absent between motor and wheel system in type D due to which steady output power flow is obtained. Type E is one of the AW drive version of parallel HEV architecture. This type of configuration permits the increase in installation space in the vehicle.

2.2.4.3 Power-split Configuration

It consists of a power-split-device (PSD), ICE, motor(s), battery storage system and controller(s). Power-split HEV architecture is a composition of series-parallel configurations of HEV architecture. The various architectures of power-split HEVs are shown in Fig. 2.6. Two electrical machines are employed in it out of which one act as motor and one act as generator addressed as machine 1 and machine 2. The dotted box shows the PSD device containing one or more planetary gear system (PGS). Fig. 2.6(a) shows the input split type of power-split HEV. It contains a PGS having three ports (sun, ring and carrier gear) to which an ICE, machine 1 and machine 2 are connected. The output shaft is coupled to one of the machines. Fig. 2.6(b) presents output split type of power split HEV. In this configuration, one machine is firmly connected to ICE and PGS contains an ICE, machine 2 and output shaft connected to its three ports. Fig. 2.6(c) shows the compound split type of power-split HEV.

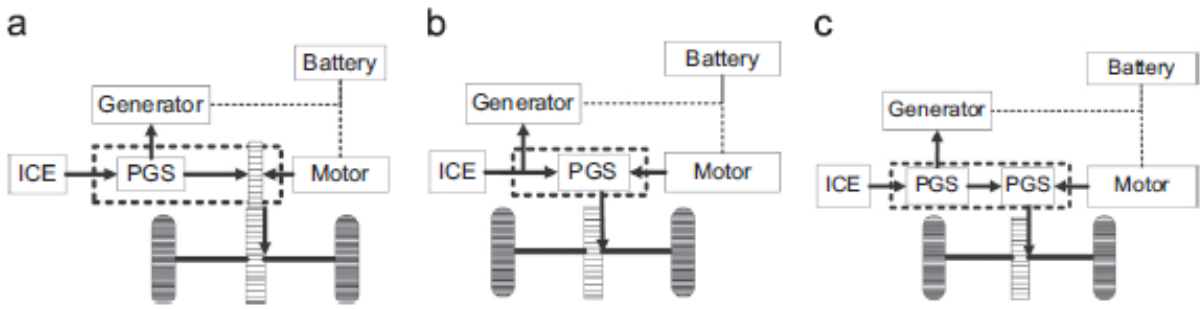

Fig. 2.6 Power-split HEV Architecture:

(a) Input Split Type (b) Output Split Type (c) Compound Split Type

It requires a PSD containing two interlinked PGS systems having two single and two compound ports. An ICE, machine 1, machine 2 and output shaft are coupled to these four ports.

Study of the configurations and architectures of electric powertrains helps to yield a vision to select and design the appropriate powertrain architecture as per the requirement of the end user.

2.3 Control and Design Strategies of PMSM

Electrical traction motors provide the impellent power to a vast and still expanding sector of our current industrial economy. The scope of types and sizes of electrical motors has become large and the count and variety of applications keeps on increasing. A review of control and design strategies of PMSM applied for various utility sectors is presented in this section.

2.3.1 Control of PMSM

The control mechanisms of AC motors can be divided into two types: scalar control methods and vector control methods. The method of implementing scalar control and obtaining a respective steady-state response is comparatively easier. However, to obtain dynamic response via scalar control methods is moderately difficult. Hence, for improving dynamics and precision along with the steady-space, the mechanism of vector control is being extensively engaged having feedback of closed loop type [32-33]. Four different control schemes, are mainly used on the basis of vector control: (1) FOC, (2) Non-linear Control, (3) Direct Torque Control, and (4) Predictive Control. The implementation of control method on PMSM drive is comparatively easier than that on an IM drive. In PMSM, decoupling of flux and torque is carried out so that these two parameters can be separately controlled. The PMs produce rotor flux and when rotor position is known, the information about rotor flux is also known. In this fashion, there is no strict requirement of its corresponding flux model. It is a well-known fact that the flux and torque control of DC motor are decoupled. PMSM can be controlled like a DC motor using

FOC. The stator windings in PMSM are exploited for applying control over PMSM drive. There is still eloquent research going on in area related to FOC through the implementation of progressive characteristics to obtain high accuracy as well as precision, especially for sensor-less control operation. In sensor-less controlled drives, variation in motor parameters has a great impact on the performance of FOC, which is being addressed by researchers through use of artificial intelligent (AI) [34-42].

For controlling PMSM through vector control or FOC, to gain accuracy in speed regulation, swiftness in dynamic performance and increment in efficiency, the knowledge of rotor position must be well established. In general, optical encoders, Hall sensors or resolver mounted on a shaft provides the information about position of rotor. But, elimination of sensing devices from PMSM can result in benefits such as, reduction in overall cost of system, decrement in the complexity of hardware system, increase in reliability and robustness of mechanical structure, reduction in frequent maintenance, guaranteed undisturbed inertia of the system and improvement in immunity against noise. Due to these advantages, sensor-less type of control of PMSM drive has been researched on recently [43]. Various categories of this type of control are: (1) Estimators on the basis of inductance variation because of saturation effects [44-45], (2) flux estimators on the basis of PMSM voltage models [46-47], (3) Extended Kalman filters [48-49], (4) State observers [50-52], (5) Sliding mode observers [53], (6) Fuzzy logic, AI based estimators [54-55] and (7) Model-reference-adaptive-schemes (MRAS) [56-58].

2.3.2 Design of PMSM

The design engineering of any electrical machine is an interdisciplinary area. This process needs to include various studies like electromagnetic, mechanical and thermal analysis. The generalized process flow for designing PMSM is shown in Fig. 2.7.

The motor design procedure starts with the consideration of necessary specifications, for instance, speed rating, power output, voltage rating, weight, geometrical dimensions and efficiency. By means of prior insight using basic equations related to machine sizing, various basic parameters of motor design can be determined. Thereby, the rough estimation of geometrical dimensions of motor can thus be carried out with the help of motor sizing mathematical statements or trade-offs. Then the simulation of the designed model is performed to study its electromagnetic performance. Concurrently, dynamic test of rotor performance and stress test of rotor along with the thermal test are performed to ensure the fulfilment of fundamental design prerequisites [59]. In case of PMs, it is necessary to consider its appropriate

operating point so that its unwanted demagnetization can be avoided during several load conditions. Demagnetization can also occur due to application of magnetic field externally at an elevated temperature. The effective magnetic and thermal properties of PMs have to be monitored during the best, as well as the worst operating conditions [60]. The steps of the design procedure of an electric motor includes repetitive analysis of their electromagnetic, structural, dynamical and thermal behaviour. Consideration of the aforesaid criteria is necessary to make the design optimal.

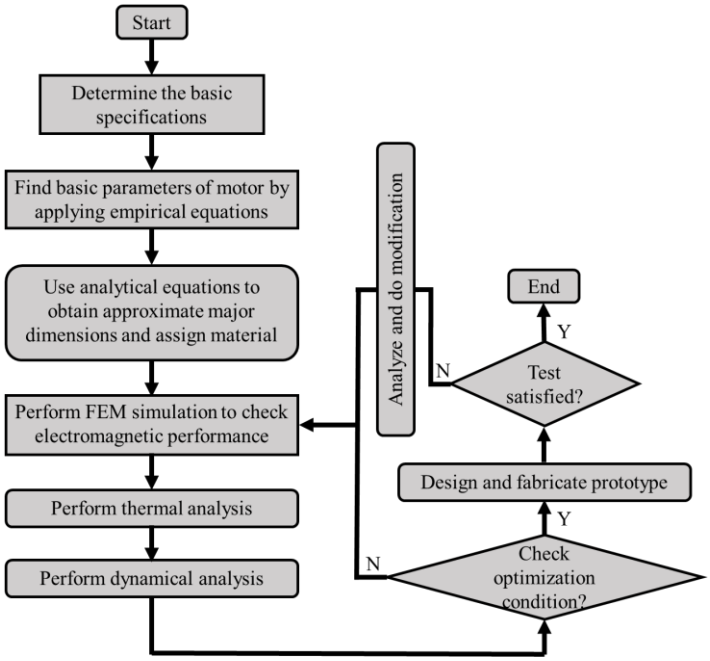

Fig. 2.7 Generalized Process Flow for designing PMSM

An electromagnetic approach makes use of both analytical as well as FEM calculations. Analytical methodology works on the principle of PMSM theory providing rapid initial measure of motor parameters. FEM analysis facilitates the optimization process by accurately providing simulation results related to motor performance like back EMF curve, flux density curve in air gap and loss curve etc. The goal of thermal approach is to safeguard the operating temperature of each element under different surrounding conditions for robust reliable design. Maintaining rotor temperature becomes a critical aspect in low power rating motors, as no supplementary cooling strategy is applied in small sized rotors. Hence, on the basis of desired norms, optimization is one of the most essential steps to achieve the best performance of motor. When the desired requirements are met via simulation, the building and testing of prototype can be

accomplished. If not so, the previous steps are repeated until the specified condition is satisfied [61-62].

2.4 Meta-modelling

The motor manufacturing industries aim to develop more competitive and economical product with a rapid pace to address worldwide competitive environment. For motor design, the procedure includes inherently exhausting task of optimization that involves diverse objectives, diverse disciplines and computation based comprehensive operations for overall simulation of final product. For example, with respect to the computation operation, it is proclaimed that to run a simulation of single crash, almost 36-160 hours were taken by Ford Motors [63]. For an optimization problem having 2 variables, say the task needs 50 iterations on an average and if say every iteration requires single crash simulation, then the overall estimation time will be 2-11 months which is clearly impractical. In spite of persistent improvements in power computation, complications in various analyses like computational fluid dynamics (CFD) and finite element analysis (FEA) implies to hold on with advancing solutions [64].

Lately, design methods and optimization methods based on approximation have gained radical attention. This approach basically approximates the computation based comprehensive operations to appropriate simple models analytically. These models are termed as 'Meta-models' and the construction procedure of meta-models is termed as 'meta-modelling'. Using a meta-model, optimization can be performed to seek the optimum. Haftka *et. al.* has conferred about the relationship between optimization and experiments [65-66] i.e., to design the experiments through the optimization process and to support optimization through the usage of experiments. The process of meta-modelling has following benefits:

- To establish connection between proprietary and other costly codes of simulation is easier. Since it runs the similar simulation for various design bits, it is simpler to implement the equivalent computation.
- It is better to perform filtration of numerical noise through meta-modelling methods rather than methods based on gradient computations.
- The meta-models portray a wide view of the whole design space. Thus, to identify simulation errors becomes simpler.

A wide centralized review has been pointed out by Simpson *et. al* about meta-models by exploring various sampling methodologies, meta-modelling techniques, approximating models,

experimental methodologies and its applications [67]. The necessary protocols and guidelines are also provided. As per the panel discussion during 9th AIAA/USAF/NASA/ISSMO Symposium, 2002, on the multidisciplinary optimization and analysis, the possible directions for research on this topic were identified as: (1) sampling methodologies for computerized experiments (2) capture of unpredictability using approximation methodologies (3) acuteness of empirical results (4) problems related to high dimensions. On the basis of intense research for design engineering in the literature [68], the act of meta-modelling may play crucial role in following areas:

1) Approximation of model: It helps in reducing the cost of computation.
2) Exploration of design space: It enhances the knowledge of design engineers about the problem by introducing reasonable meta-models.
3) Formulation of problem: Using the obtained knowledge, the design variables with respect to their count and range of values may be easily reduced. Also, certain insignificant constraints may be eliminated and one-to many or many-to-one objective function may be converted. Thus, its assistance can be utilized to formulate a problem of optimization which is straightforward and highly accurate to solve.
4) Support for optimization: Meta-modelling process is applicable or can be integrated to fulfil many optimization requirements of industries, like, global, multidisciplinary, multi-objective or probabilistic optimization etc., by overcoming the particular challenges of each kind of optimization need.

2.4.1 Approximation of Model

In general, approximation aims to realize an accurate global meta-model at moderate cost. The categorization of various approximation techniques based on sampling, selection and curve fitting is shown in Table 2.2.

Table 2.2

Generally Utilized Approximation Methods [67]

Sampling	Meta-model selection	Curve fitting
Classic techniques • Factorial/fractional • Box - Behnken	Polynomial • Linear • Quadratic	Least square regression (weighted)

Sampling	Meta-model selection	Curve fitting
• Plackett - Burman • Central composite • Alphabetical optimum	• Higher order • Least interpolating polynomial	
Space-filling techniques • Simple grids • Orthogonal arrays • Latin hypercube • Hammersley sequence • Minimax and maximin • Uniform designs	Splines • Linear • Cubic • Non uniform Rational B splines (NURBS) • Multi-variate adaptive regression splines (MARS)	Best linear predictor
Hybrid techniques	Gaussian process	Best linear unbiased predictor (BLUP)
Human or random selection	Kriging model	Multipoint approximation (MPA)
Based on importance	Radial basis function (RBF)	Log likelihood
Directional simulation	Hybrid model	Back propagation (in ANN)
Sequential methods	Artificial neural network (ANN)	Sequential or adaptive meta-modelling
Adaptive methods	Support vector machine (SVM)	Entropy (for inductive learning on decision tree
Based on discrimination	Knowledge based or decision tree	

The classic sampling techniques like factorial/fractional, Box-Behnken, Plackett-Burman, Central composite and alphabetical optimum originates from the provision of Design of Experiments (DOE). The main focus of such methods is preparing the experiments in order to have least influence of arbitrary errors in physical tests in validating or invalidating any hypothesis. Owen and Koehler reported various space filling methods [69] out of which the most commonly used sampling technique is orthogonal array technique [70-72], Hamersley sequential technique [73-74], homogenous designs [75] and Latin hypercube techniques [75-80]. The other methods used for sampling may be employed based on the accuracy to be reported in approximation. For meta-modelling, Sacks et al. introduced the usage of stochastic Kriging model [81] to deal with the deterministic mainframe reaction in the form of formulation of a

stochastic function analogous to substantial scheme reaction. The approximation is also carried out using Neural networks [82], RBFs [83,84], MARS [85] and least interpolating polynomial [86]. Every meta-model selection type is correlated to its corresponding fitting technique. Such as, the BLUP search is utilized for fitting of Kriging model and the weighted least square regression is utilized to fit polynomial functions etc. A comprehensive review on the models and their corresponding fitting techniques is reported by Simpson et. al in [67].

2.4.2 Exploration of Design Space

To clearly understand the problem, it is necessary to appropriately explore the design region for a particular meta-model so that better formulation of optimization problem can be carried out. Today the design tools like CAD are already embedded with the relational functions of design parameters and the corresponding performance indices which are difficult to grasp. So, engineers interpret design problems through investigation of sensitiveness. However, such analysis generally depends on a steady situation with respect to variation in one parameter. In case of change in this situation, the information of sensitiveness changes too. The meta-modelling technique serves the engineers in providing deep insight of the problem via two different approaches. First, through meta-model curve fitting approach, where its various intrinsic properties can be studied. For example, for a meta-model of quadratic polynomial, by normalizing all design parameters to the range [-1,1], the sensitiveness of a particular term in the meta-model is indicated by the measure of the corresponding coefficient in the model [87]. This approach is useful in evaluation of design parameters. Second, the interpretation of design problems is obtained through the visualization approach. For this, several methodologies have been introduced in the last decades [88-89]. Such as, a virtual design steering technique on the principle of morphing of graph is developed by Bloebaum and Winer [90-91]. Similarly, Kemper and Eddy introduced cloud visualization [92]. Ligetti et al. have shown that the design effectiveness and efficiency both can be enhanced using the meta-model curve fitting approach in interfacing of graphical design [93].

2.4.3 Formulation of Problem

One of the most critical steps in design field is the construction of optimization model. Its quality has direct influence over effectiveness, feasibility and cost of the problem. The formulation of optimization problem aims to take several decisions, like objective (or goal), constrains (or limitations), design parameters and the feasible region for parameter search space. The curve fitting and exploration of design region provide the major guidance for deciding a reasonable

objective or goal and appropriate constraints. Further, the use of meta-modelling provides assistance in eliminating or modifying or combining few objectives or corresponding constraints. Thus, the significant decrement in dimensionality or the search area has direct influence over the sample cost. Draper et al. proposed a methodology for the reduction of total count of design parameters by gradually refining the corresponding response surface through the act of screening out the insignificant parameters for capturing the function [94]. A systematic way for performing the screening of parameters is introduced by Welch et al. [95]. The response surface methodology, involving variable-complexity, adopted the investigation of varying allegiance in order to decrease the design area to the appropriate space of interest [96]. The designers often lack enough knowledge of properties of a particular function and the relationship between the objectives and limit functions or constraints at initial stage of optimization due to which the steady bounds of lower limit and upper limit are fixed during the phase of formulation of problem. A heuristic approach is reported by Chen for leading the refinement of surface to some narrower design region [97]. The usage of new sequence-based meta-modelling technique though limit movements or locating region of interests is upheld by few researchers [98-100]. For example, the process of concurrent sub-region optimization adopted the raw data produced during the process execution for developing the required response surface fitted curve of the given design region, that established the foundation of formulation of sub-region coordination [101]. An adaptive response surface (ARS) technique is proposed by Wang to discard segments of design space corresponding to those objective values which are higher than a specified threshold parameter for each execution of optimization process in order to decrease the design region size [102].

2.4.4 Support for Optimization

There are various requirements in optimization problems like global optimization to locate global optima, multi-objective problems to satisfy various objectives of design, multi-disciplinary problems having coupling of the functions, or probabilistic problems having uncertainties of parameters, as can be seen in Fig. 2.8.

Generally, the classical optimization techniques, which are gradient based, show certain constraints that hamper the direct implementation of such methodologies in state-of-the-art designs. Following are the hindrance points offered by such methods differentiable from the present-day scenario for designers:

- Gradient based methods demand reasonable models which are formulated explicitly while the design engineering comprises implicitly comprehensive models like FEA or CFD or others providing inaccurate and upscale gradient data.
- Gradient based methods provide a lone optimal design value while the engineers seek multiple alternatives for design.
- Since gradient-based methods have non-transparent sequential execution, it does not provide clarity of the corresponding problem to engineers.
- The need of high expertise over the concept of efficient optimization is also required for engineers. This information is lacked by gradient-based techniques.

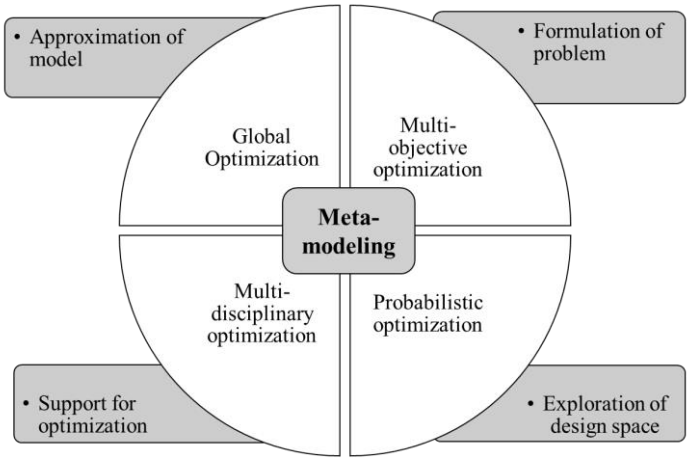

Fig. 2.8 General view of Meta-modelling support for Optimization

Thus, application of the concept of meta-modelling provides various benefits such as:

- Improvement in the efficiency of design optimization.
- Independent and parallel estimation of sample data points is sustained which reduces the computation time.
- Support of sensitivity analysis of parameters, which provides clear understanding of the problem
- Both continuous as well as discrete variables can be handled.

The various types of meta-modelling-based process of design optimization techniques are shown in Fig. 2.9.

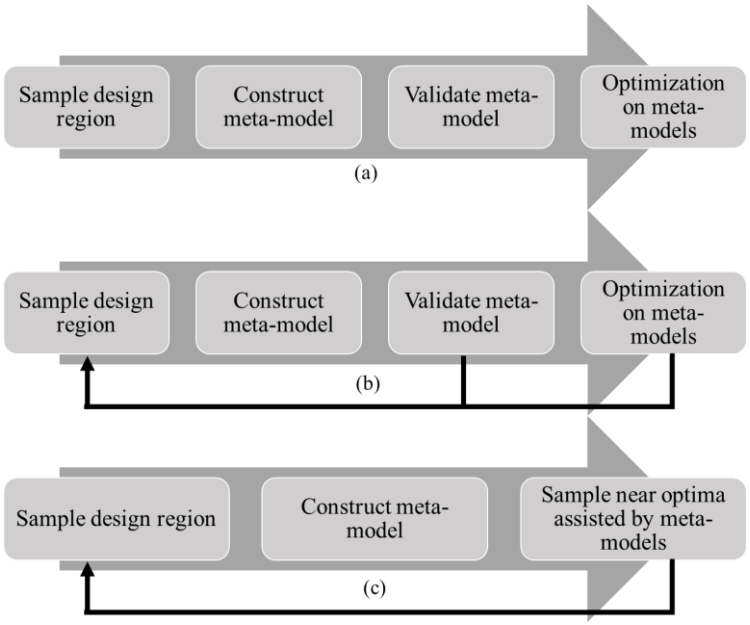

Fig. 2.9 Meta-modelling-based process of Design Optimization; (a) Sequential Method, (b) Adaptive Method, (c) Direct Method

1) The first one is a conventional sequential technique to fit a global meta-model and considering it as surrogate of the considered function. A large count of sample data points is needed for this kind of process flow. There may or may not be a stage of model validation present in this process. If present, the cross validation has to be done for the model [103].
2) The second one includes optimization and (or) validation in a loop to make the decision of applying re-sampling strategy. Osio proposed a multi-stage strategy involving Kriging technique so as to sequentially improve and update the approximate model with respect to accuracy by the addition of extra sample data points [104]. Schonlau et al. explained about the need of balancing the search efficiency for local as well as global optima through a sequential technique for constraint optimization problem [105]. A streak of adaptive sample data points and meta-modelling techniques is proposed by Wang for design optimization, where the loop of optimizing and validating processes formed the extra required sample points [106-107].
3) The third one produces the new required sample data points near the optima through the assistance of meta-models directly [108]. Unlike first and second type of approaches, the third one does not use meta-model as surrogate in execution of optimization procedure. The realization of optimization is done by adaptive sampling only. There is no formal calling of optimization procedure involved. Such approach is needed to be tested further for large dimensional problems.

2.5 Metaheuristic Algorithms for Design Optimization

With fast advancements in information technology, a large number of problems related to optimization have been addressed in different fields like engineering, operational research, geophysics and bioinformatics etc. In order to find satisfactory solution to such problems in rational time, researchers used mathematical programming tools/methods. Such methods have been classified into two broad kinds: heuristics and metaheuristics. Heuristic techniques are specific to a particular problem and they are efficient to solve them, while they may become inefficient to solve other problems. Whereas generically designed MH techniques are problem independent and can be employed to achieve all types of optimization goals. The word 'metaheuristic' was invented in 1986 by Fred Glover for manifesting heuristic techniques with characteristic of being problem independent [109]. MH techniques have robust scheme of searching capabilities due to the presence of compatibility between two mechanisms: exploration, also called diversification and exploitation, also called intensification [110]. Exploration mechanism performs the job of searching in the finest solution encompassed region. Exploitation mechanism contributes to penetrate new search regions. Despite the prosperous characteristics of MH, it lacks the capability to solve all classes of optimization problems like unconstraint, continuous, discrete or multi-objective types of problems. This sought encouragement for the development of colossal count of metaheuristics for its adaptation with various types of optimization goals.

Metaheuristics are algorithm frameworks applied to various optimization problems by incorporating few alterations so as to make it adaptable with the given goal. The key characteristics of MHs are outlined below:

- It is not problem specific. Customarily, they are approximate.
- It scouts the search region to acquire 'finest' solution.
- It is typically illustrated by abstraction status.
- Generally, they allow a smooth parallel operation.
- The basic level of search can be extended to advanced learning methods using MHs.
- It can incorporate various schemes to escape premature confluence.
- It can use memory as a guidance to preserve search participation.

As mentioned earlier, the appropriate resolution of exploration with exploitation is the crucial aspect for finding better efficiency of the search procedure. As per the literature review, various categorizations of MHs have been reported in systematic way by M. Abdel Basset et al. [111]. The broad two categories are named as: (1) MHs based on metaphor (2) MHs based on non-metaphor.

2.5.1 MH based on Metaphor

There are eight major classes namely; swarm influenced, social influenced, physics influenced, chemistry influenced, biology influenced, music influenced, mathematics influenced and sport influenced, found in the literature which fall in this category. These are briefly explained in the upcoming subsections.

2.5.1.1 Biology and Swarm Influenced MH

On the basis of principle of biological evolution, this class of MH techniques is involved with imitating metaphors of biology and swarm differing in type of their portrayal strategy. The paradigms are mainly based on: evolution, immune system and swarm. First, the theory of evolutionary estimation; involving progressive stages of selection of population, parent crossover, offspring mutation and offspring reproduction; consists of historical criterions of evolutionary strategies [112], evolutionary programming [113], genetic programming [114] and genetic algorithms (GA) [115]. Second, artificial immune systems are influenced by immunology theory, functions, fundamentals and versions [116]. When they are implemented in optimization, the objective function is represented as antigen, candidates are represented as antibodies, the evolution is performed by repetitive cloning, selection and mutation. Third, evolution based on swarm mimics the cumulative nature of community agents like that of insects or birds etc. The principle of decentralization that updates the solution through the individual as well as associative interaction with natural resources. Ant colony optimization (ACO) [117] and particle swarm optimization (PSO) [118] are the most famous among all such methods.

These biology-based concepts have inter-relation with respect to the adopted operators while they differ with respect to the manner in which the exploration stage and exploitation stage are executed [119-120].

2.5.1.2 Chemistry and Music Influenced MH

Li and Lam introduced Chemical Reaction (CR) optimization in which the behaviour of molecules interaction is simulated for obtaining stable condition having low energy [121]. The two types of energies are possessed by a molecule out of which the first is potential energy

which represents objective function and second one is kinetic energy that represents the constraints of transforming to the worst form. The chemical reaction phases like decomposition, impotent collision on wall, synthesis and impotent collision interactively are used for molecular upgradation by implementing the corresponding condition check. The efficacy test of such chemical reaction-based optimization method is performed using twenty-three examples of problems associated with quadratic assignment. When compared with the conventional techniques already applied over such problems like Improved Simulated Annealing (ISA) [122], Tabu search Method (TSM) [123] and fast ant system (FAS) [124], it was found that CR method needed modifications to reach considerable potential.

The Gases Brownian Motion (GBM) optimization technique was designed by taking the inspiration from the suspended fluid particles motion involving Brownian motion and rotational motion [125]. The specifications of candidate solution are influenced by the molecular properties of positioning, turbulent radius, velocity and mass. The candidates or molecules approach the target in accordance with Brownian motion. The temperature of surrounding environment plays a major role in the resolution of diversification and stage of intensification along with the turbulence in the rotational motion of molecule. The eighteen examples of satisfiability problems, seven benchmark functions and two problems related to real world are used to test the adaptability of GBM based method [126-127].

In [128], Geem et al. introduced a harmony search algorithm (HSA) that replicates improvisation mechanism with respect to music. For this, each musician plays some tone in the feasible range which creates a vector of harmony. A candidate solution is represented by a vector in HSA. when an elegant harmony is made by the tones, it is stored in the memory of each musician and betterment of harmony is enhanced at every next step. The corresponding harmony memory is stored in the form of augmented matrix having decision variables along with their fitness. The rates of harmony search considering or pitch adjusting are stored in the form of vector in order to compute the new candidate solution through comparison with the worst generated vector. The older vector is replaced with the new one if its new fitness is better [129-130].

R. A. Mora introduced a method of musical composition (MC) in which the social interaction of musicians with respect to their musical compositions is carried out via exchange of information among their society [131-132]. The main inspiration is to create a network of musical tunes of various composers. MC method is not a HSA variant since it adopts the method of learning and information exchange with respect to the rules of interaction. This rule states

that the information exchange can only take place if first musician's worst tune is found to be better than the second musician's worst tune.

There are two sub-phases of such condition; updating the links and exchange of information. First sub-phase involves the change of artificial community network in accordance with the previous one. Second sub-phase involves the knowledge vector upgradation with respect to the information about the neighbourhood by updating score vector and environment-based information. Thirteen benchmark functions were used to test method of MC. The analysis results were compared with those produced by HSA [133], global check HSA [134] and self-adjusting HSA [135]. The better performance of MC method is shown for multi-modal benchmark functions.

2.5.1.3 Mathematics Influenced MH

The algorithm of base optimization (BO) was introduced by Salem [136] which works on the principle of using basic operators related to arithmetic i.e., $+, -, \times, \div$. After generating the random population and defining the displacement factor Δ, the solution is updated using four base operators. Out of four possible updated solutions, the best solution is chosen as the new candidate solution. By testing this method for two unimodal and six multi-modal benchmarks and comparing the corresponding performance with GA and Ant Systems (AS) [137], BO algorithm was found to have commendable rate of success and quality search capabilities.

The sine-cosine (SC) algorithm was proposed by Mirjalili in which random population is generated initially and the best solution currently available is kept aside in order to update the solution at each iteration [138]. The range of sine and cosine functions are changed for carrying out balance between the phase of exploration and the phase of exploitation. The popular functions of benchmarks were employed for efficacy test of SC algorithm and when its performance is compared with GA, PSO, firefly algorithm (FA) and flower pollination (FP) algorithm, it is found that SC algorithm has been efficient enough to produce better results for complex problems by extending its ability to lend enhancement to high dimensions [139-140].

2.5.1.4 Physics Influenced MH

Metropolis et al. introduced physics based simulated annealing (SA) MH method for simulating the cooling of a particular material inside a heated bath [141]. This idea was implemented to optimization problems by Kirkpatrick et al. [142]. The SA algorithm is lenient at initial state just like annealing and it could converge to poor solution. This algorithm starts at generating random initial solution. At high temperature, by considering another nearby solution, the

computation of difference between their corresponding function values is done. In case this difference is smaller, the search continues by updating the current solution. Otherwise, the considered temperature is reduced after accepting the probability of that point. Various case studies on the performance test of SA algorithm were reported in [143-146].

Another physics influenced MH method is gravitational search (GS) method which has been designed on the basis of Newton's law of gravitational force and Newton's law of motion [147]. Various physical characteristics of an object like its position, gravitational mass and inertial mass etc. are taken into consideration. Position of object represent the candidate solution and its mass represents its fitness. The object with superior performance having large gravitational mass possess huge range and better strength of adequate attraction. In this way, the best solution is approached by the object. Nezamabadi-Pour reported discussion about GS method [148].

2.5.1.5 Sport and Social Influenced MH

The league championship (LC) algorithm mimics sport tournament in which various teams participate in pairs in the league for numerous seasons. The candidate solutions are denoted by number of participant teams and population is denoted by the league. The strength-weakness-opportunities-threats (SWOT) scrutiny is performed for all the matches. The fitness is judged on the basis of players' strength. The reformulation of teams' players helps to improve the performance (better solution). Until end of the season, the championship resumes for a couple of weeks. By considering following six appropriate assumptions,

- Strength of the player determines the winning team.
- There cannot be a definite forecasting of the player strength through one match result.
- Any two team can compete with similar probability.
- Only result of win or lose is to be considered. The result of Tie is ignored.
- If the wining of one team is supported by a strength, the loss of other competing team is caused by a relative weakness.
- A particular team only has the focus on upcoming match without knowing the consecutive matches. Only on the basis of prior weak accomplishment, the players are reformulated.

For validation of LC algorithm, the tests were performed using thirty-six benchmarks. The performance comparison with Particle Swarm Optimization (PSO), GA, Artificial Bee Colony

(ABC) and Differential Evolution (DE) showed the better effectiveness of LC method. The research studies on LC algorithm have been reported in [149].

Apart from this, the teaching-learning-based optimization (TLBO) method was introduced [150] in which the social conduct of learning procedure of students by the teachers' influence is considered for the development of optimization methodology. The knowledge is shared by the teacher, which depicts the best solution, with students, depicting population of solution. The teaching quality has the direct effect on grades of the students, depicting the fitness value. The learning procedure is categorized into two sub-phases: teacher and learner sub-phases. In teacher sub-phase, the best solution is chosen to be the teacher and mean of positions of students is computed and relocated near the position of teacher. After calculation of new position of student, in learner sub-phase, the knowledge of student is enhanced by his random interaction with another student. The comparison between two students is done as per the rules mentioned below:

- If both are feasible solutions, the one with higher fitness is chosen.
- If one of the two is infeasible, the feasible one is chosen.
- If both are infeasible solutions, the one with minimum violation of feasibility is chosen.

In case, the chosen candidate has better knowledge (fitness), the knowledge of the previous candidate is modified. This algorithm is parameter-less. It only requires the standard controlling parameters like count of generations and size of the population. Its performance is compared with evolutionary strategy having multiple members [151], cultural differential evolution [152], evolutionary PSO [153] and co-evolutionary DE [154] to solve benchmark functions having constraints and to solve few design problems. The TLBO method is found to be efficient as compared with its competitors.

2.5.2 MH based on non-Metaphor

Glover et al. proposed Tabu search method (TSM) [155] which mainly works on the principle of applying taboo over pre-searched areas from searching again in order to boost diversification by exploring the region of solution and avoiding the convergence towards the local optimum. The two main characteristics of TSM are flexible memory and susceptible exploration. In the first one, the previously executed actions during search operation are stored as history in order to barricade within loops. The second characteristic targets the advantageous area and the finest solution to intensify and explore promising new search areas [156-160].

The method of variable neighbourhood search algorithm (VNSA) is one of the advanced stochastic MH methods as compared to method of variable neighbourhood descent algorithm (VNDA) which is an extended version of hill climbing search algorithm (HCSA) [161]. The basic facts that build the groundwork of VNSA are:

- If one local optimum point for a particular neighbourhood is located, it is not necessarily the same for another one.
- The local optimum point concerned with every feasible neighbourhood may be a global optimum.
- Every local optimum point is relatively near to another optimum for numerous problems.

The final basic fact works on observations performed empirically. The local optimum points imply the possibility of containing effective knowledge about the global optimum. Two types of updating processes are applied in VNSA. First, the 'shaking' process is carried out to leave the analogous valley by simply applying local exploration to locate the local optimum from neighbourhoods. Then, the 'neighbourhood altering' process involves the exploitation of remote neighbourhoods around the current point and then shifting to new neighbourhood if the condition of updating is satisfied [162].

Voss and Taillard proposed a non-metaphor based partial optimization metaheuristic under special intensification conditions (POMSIC) [163]. POMSIC can solve combinational type of optimization problems by breaking down it into sub-problems. The formulation of sub-problems is performed by involving the selected seed and its neighbour with respect to the pre-set distance. Then the formulated sub-problem is solved through the use of MH or a precise algorithm. This process is repeated until all sub-problems are improved. POMSIC provides a generic structure that consists of mechanisms like large neighbourhood exploration [164], and modified randomized decomposition [165] etc. The conventional aspects for applying POMSIC structure are:

- The characterization of solution sub-parts
- The criteria for selecting process of sub-part to prevent recurrence of improvement
- The linking function between sub-parts
- The optimization algorithm for formulated sub-problem

The POMSIC method has been applied to solve applications like maintenance of mechanical part balance and clustering of centroid. The efficiency of POMSIC was found to be more than VNSA method. For mechanical part balancing problem, TSM was utilized in POMSIC. This combination was found to be more effective than the conventional TSM for huge examples of such problems.

2.5.3 MH Variants

In order to enhance the quality of the solution and the convergence ability of MH algorithm, additional improvements and transformations have been researched every once in a while. To produce variants of MH techniques, modifications can be performed with respect to randomized operant or parameters. Few examples of this are discussed in upcoming sub-sections.

2.5.3.1 Upgradation of MH

The previously iterative solution is upgraded using stochastic exploration. The methodologies are:

- **Chaotic MH**

There are evolution functions which produces a predetermined bounded series of randomized numbers on the basis of primary condition having either continuous or discrete time domain. Such functions are chaos maps like tent map, logistic map or Chebyshev map etc. These maps can reinstate randomized series producer since they are non-periodic, random and diverging for variable modification. Since such chaotic variants possess higher randomness and convergence pace, they have been proposed in literature as chaotic HS [166], chaotic LC algorithm [167], chaotic PSO [168] and chaotic GA [169] etc.

- **Adaptive MH**

In adaptive MH variation technique, the randomized step size or range of search can be consequently modified in accordance to advancement of the algorithm so as to escape the local convergence. Few examples include adaptive PSO [170], modified cuckoo search [171], adaptive SA [172], mam-min ant system [173] and modified grey wolf algorithm [174] etc.

- **Acceleration based MH**

The purpose of this variation in MH is to omit the redundant variables or add new useful variable for speeding up the algorithm execution. In accelerated PSO, the modified solution is computed on the basis of best global solution while the best individual solution is ignored [175]. Other

variants are accelerated bio-geography based optimization [176], accelerated mine blast algorithm [177] and accelerated ABC [178] etc.

- **Gaussian based MH**

The Gaussian based variation is implemented as a calibrating process. Additionally, the general solutions are replaced by new ones through the upgradation with sampling inspired by Gaussian distribution. Examples of such variations are Gaussian bare-bones DE [179], Gaussian firefly algorithm [180], bare-bones PSO [181] and bare-bones TLBO [182] etc.

2.5.3.2 Hybridization

As stated earlier, no MH can solve every type of problem. Hence the process of hybridization has been adopted to gain advantages of each individual algorithm. The degree of interference in the components of both MHs decides the level of hybridization being high or low. If there is an interference in the internal process of algorithms, it is called hybridization of high-level while if only an MH function is consigned with another MH, it is termed as hybridization of low-level. The collaborative information exchange or integration with master MH may occur in hybridized search procedure. The sequence of execution must be reckoned. The four main characteristics considered to be the basis of hybridization are: (1) The strategy of hybridization, (2) The execution order of MHs, (3) The strategy of control and (4) The level of hybridization. Few examples of variants of MH hybridization are discussed in [183-186].

- **Interleaved and Sequential**

Binu et al. merged the benefits of cuckoo search method with multiple kernel fuzzy (MKF) method to propose MKF-Cuckoo method [187-189]. The main aim of this method is that the search of centroid in the search region should be the best of all. The encoding of candidate solution is done by selecting centroid randomly from the dataset of input vector. Additionally, the fuzzy membership function is introduced in order to compute the kernel based minimum distance of data points from its cluster centroid of closest neighbour. Then, Cuckoo search MH is executed to reach the target solution.

The combination of ACO and GA along with a local search MH is introduced as ANGEL hybrid algorithm [190]. ACO performs the job of generating the initial population effectively. GA performs the job of processing the data. Additionally, a feedback scheme is introduced between ACO and GA. The execution of local search MH occurs when GA provides feedback to ACO by updating the entire pheromone throughout the search procedure.

The hybridization of clonal selection (CS) method with FP method is proposed in [191]. It combines the exploitation capabilities of FP algorithm with approach of clonal selection which simulates the principles of immunology. In case the specified condition for switching is satisfied, the best solution (of antibodies) to form a new population is chosen from the present population. The cloning of the antibodies with larger affinities is done to produce additional antibodies contrary to the antigen i.e., the objective function. Local pollination is applied to the non-cloned antibodies. In literature, the binary variant of this algorithm is also reported [192].

- **Parallel Mechanisms**

The concept of parallelism was encouraged in order to solve dynamic or large-dimensional class of optimization problems [193]. It promotes time saving and produces quality solutions. Examples are: parallel ABC [194], parallel GA [195] and parallel greedy-randomized-adaptive-search-procedure (GRASP) [196] etc. The essential components like multi-core processors, data storage and networks etc. are needed for the implementation of parallel mechanisms. There are trajectory-based models and population-based models in parallel schemes.

In trajectory based parallel models, the three fundamental models are utilized; (1) parallel moves, in which the present solution of master MH is first duplicated and then distributed to parallel MHs at each execution and the final solution are reciprocated to the master, (2) parallel multi-start, in which various trajectories are launched for the similar problems and (3) move acceleration models, in which parallel computation of fitness for each solution is done.

In population based parallel models, three basic models are introduced: (1) master-slave models, in which the selection job is done by the master MH while improvement job is done by slave MH, (2) distributed models, in which the division of entire population is done into sub-populations and then MH is applied to each sub-population. Additionally, the exchange of solutions is also done among all sub-populations in order to promote diversification and (3) cellular models, in which the feature of interaction with closest neighbour is used to update the corresponding solution to increase exploration capability.

2.5.4 Limitations and New Trends

The goal of processing optimization task is to find the fittest solution for a specified problem. The way of dealing with the specified problem concocts the limitations over the usage of MHs.

The decision of getting best characterization of controlling parameters with respect to the nature and magnitude of the problem raises the biggest question while applying MHs. Moreover, selection a relevant MH algorithm is a critical task. To conquer such concerns, recent drift is to prefer liberalization of MH techniques from possessing prototypes and having restricted control parameters. Hyper-heuristics techniques offer speculative characteristics for selection of heuristic [197-198]. Banzhaf and de Melo proposed drone squadron optimization which produces the real code through the cloud hyper-heuristic on the fly [199]. A library having open access source, termed as 'LibOPT', is introduced by Papa et al. in order to implement and prototype the MH which are nature inspired [200].

2.6 Thermal Modelling of PMSM

Geometrical and electrical disturbances develop undesired behaviour in the motor like fault occurrence and unaligned eccentricity of rotor. Sensitivity analysis proposes an interesting approach to further analyse the motor performance and develop robust and reliable motor designs [201-203]. Thermal supervision is an important feature of electric machine at design stage because it is one of the essential factors which defines the operating range and overloading capacity of the machine [204-206]. Particularly, in PM machines, the performance is influenced by the component temperature as a result of thermal related losses and thermal conditions of working PMs [207-209]. Thermal behaviour of electric motors has been reported by many researchers. Many research papers have addressed the thermal analysis of electric machines [210-212]. A generic review of thermal management of electric motors for transportation application is presented in [213]. It includes cooling methodologies, thermal properties and design aspects of the motor materials. An overview of frequently implemented thermal investigations are presented in [214].

2.7 Research Gaps Identified

Based on the extensive literature survey to understand the state of art in the field of EV power train, challenges and issues related to design optimization, the following research gaps are identified:

1) The effect of rolling resistance, aerodynamics resistance and climbing forces on the dynamic behaviour and performance of traction motor of the electric powertrain needs to be analysed and addressed.

2) The poor dynamic performance of EV with respect to optimum performance solutions rises the opportunities for investigation of PMSM at system design level.

3) Analysis of design, control and optimization techniques for efficient performance of EV powertrain system.

4) Explore the possibility of exploiting the advantages of FEM to improve the electromagnetic and thermal performance of motor compatible for EV applications

5) Use of surrogate modelling technique for design optimization methods for EV applications.

2.8 Conclusion

A thorough literature survey has been reported that is beneficial for implementing design, control and optimization techniques to obtain efficient PMSM model. The conventional powertrain components are compared with those of various electrical powertrain configurations. A detailed study about the meta-modelling technique and its support for optimization problems is also reported. In addition, the possible research gaps have been identified.

Chapter 3

Analysis of Electric Vehicle Power Train with PMSM as Traction Device

3.1 General

The global EV industry is striving to provide mobility technology which consumes less fuel, produces minimal pollution and has high overall efficiency. The strategic initiatives of the Indian Government of launching the National Electric Mobility Plan, announcing and providing financial support to alleviate vehicular pollution, promote automobile manufacturers' proficiencies and ensure nation's energy sustainability [215], [216] have borne appreciable outcomes. The governments green initiatives have resulted in India EV Industry rapidly maturing over the last few decades.

The vehicle powertrain employs the components that perform the task of transforming the stored form of energy (chemical, mechanical, solar or potential energy) into kinetic energy to provide the necessary force and power to the vehicle. The conventional vehicle powertrain consists of ICE, torque converter, gearbox, transmission and battery. Adverse environmental issues attributable to the conventional powertrain include - automobile related pollution, greenhouse gas emissions, dependency on fossil fuel-based economy, noise pollution etc. These drastic issues can be overcome through adoption of clean mobility, which is effectively addressed by the use of EVPT system. An electric powertrain uses electric motor and controllers rather than ICE in propulsion system of the vehicle [217].

ICE and EM have different principles of operation. The understanding of their operating principles is essential to get the idea of working of conventional and electric powertrain. The main criterion used for motor selection in EV application is its acceleration characteristics. It also helps to determine drivability performance of the EV which is an important concept for powertrain analysis. Drivability issues include starting, idle, pedal, braking, engine response, damping of torque oscillations etc.

In conventional powertrain, there are starting, cranking and idle modes while there is no such mode of operation in EV. ICE has high oscillations, discontinuities and ripples in torque produced. These issues can be addressed in electric powertrain by the implementation of suitable control strategies such as space vector pulse width modulation (SVPWM), field-oriented control (FOC) or direct torque control (DTC) control method. The overall optimal efficiency of combustion engine is around 30-40 % while electric motor is capable of running in motor as

well as in regenerative mode which not only helps in recovering the extra kinetic energy from the vehicle and recharging the batteries during braking operation but also improves overall efficiency up to 90% and above. Despite showing various advantages like null emission and high efficiency, there is limitation over battery capacity in electrical powertrains when compared with the conventional ones.

The design and integration of EVPT system is an inter-disciplinary area. Modelling of electric powertrain is essential for detailed analysis and evaluation of EV dynamics. This chapter elucidates the key mechanical and electrical aspects of the vehicle powertrain, which are studied, simulated and analysed. The conventional powertrain using spark ignition type of generic engine is modelled in Simulink and the information obtained from the dynamic analysis of ICE powertrain is set as the *benchmark* parameters for evaluating the performance of electric powertrain. Key vehicle performance variables like maximum speed attained and acceleration achieved using conventional ICE have been considered for setting the benchmark. In addition, parameters relating to driving comfort like torque ripples is also considered while analysing the EVPT system.

3.2 Modelling and Analysis of Conventional Powertrain

In this subsection, the physical model of conventional powertrain is discussed and the Simulink model has been developed to analyse the vehicle performance. This analysis helps to understand the dynamic performance of conventional powertrain.

3.2.1 Physical Model of Conventional Powertrain

The physical model of conventional vehicle powertrain has an engine connected to a torque converter. The torque converter is connected to a gear transmission which is further connected to a differential. This differential splits the torque between two wheels on the rear axle of the vehicle body [218] (Fig. 3.1).

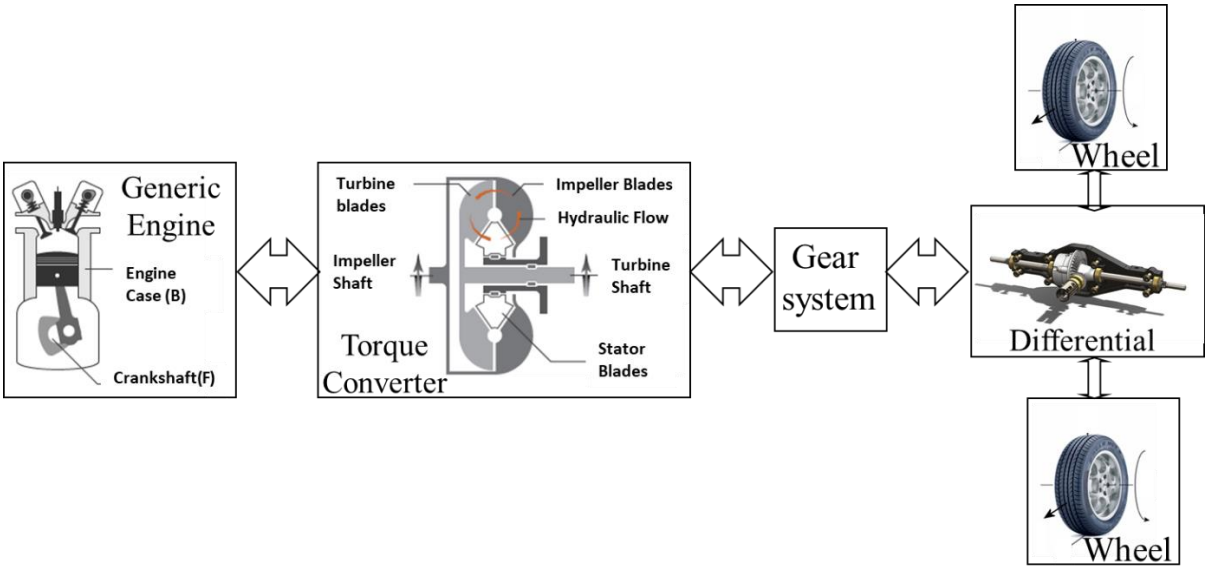

Fig. 3.1 Physical Model of Conventional Vehicle Powertrain

3.2.2 Simulink Model of Conventional Powertrain

The MATLAB Simulink model of conventional powertrain is shown in Fig. 3.2. For the research study, the Jaguar Land Rover AJ133 naturally aspirated V8 spark-ignition type of generic engine is taken as propulsion system [219]. In this generic engine, the throttle input signal, whose value lies between 0 and 1, is provided at input terminal (T). This specifies the torque demanded from the engine as a fraction of maximum possible torque. Terminals F and B are mechanical conservative ports imitating crankshaft and engine block respectively. The engine power and fuel consumption are obtained from physical signal output port terminals P and FC respectively.

The crankshaft of the engine is connected to impeller port (I) of torque converter. The torque converter couples the two drivelines and transfers angular motion and torque through hydrodynamic action of a viscous fluid. It is different from a frictional clutch in the sense that it is incapable of locking the axes of two drivelines together. The turbine port (T) of the torque converter is connected to the base (B) port of the gear system of the powertrain.

The follower (F) port of the fixed ratio gear system is connected to the mechanical rotational conservative driveshaft port (D) of differential system, which is arranged as a planetary gear train. The sun gear ports (S1 and S2) of differential system transmit the power to two highway tires through mechanical rotational ports (A). The simulation study is carried out on a vehicle having basic parameters presented in Table 3.1. The parameters of generic engine used in conventional vehicle powertrain are listed in Table 3.2.

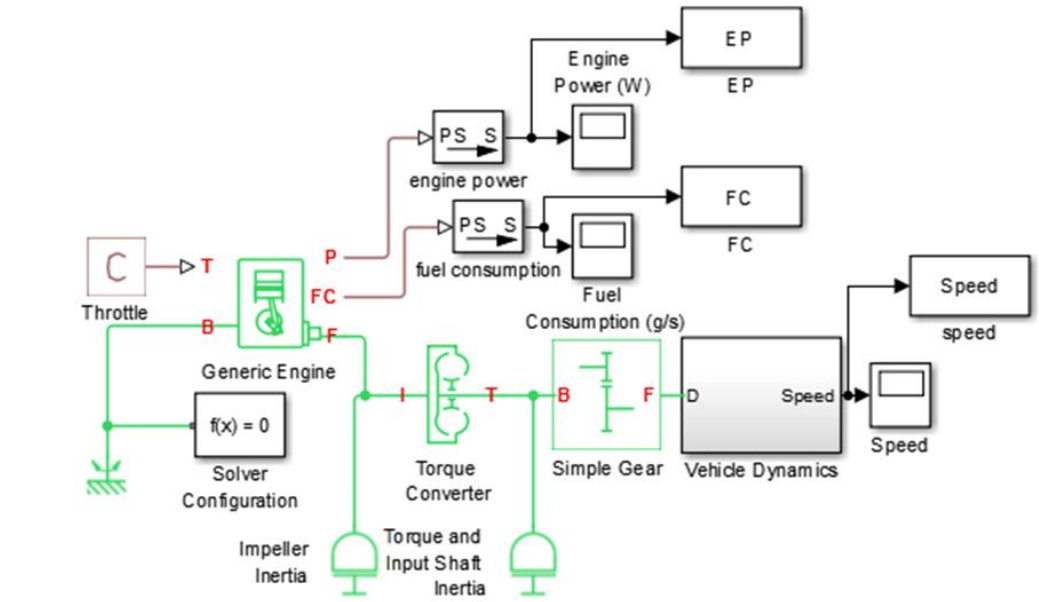

(a)

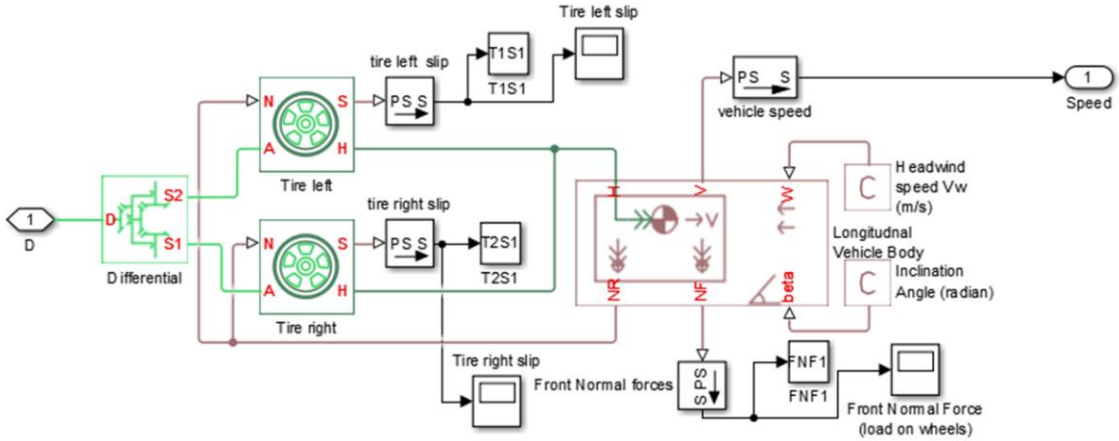

(b)

Fig. 3.2 Simulink Model of Conventional Vehicle Powertrain;

(a) Overall Model (b) Vehicle Dynamics Subsystem

Table 3.1

Vehicle Body Parameters

Parameter	Value	Unit	Parameter	Value	Unit
Mass	2000	Kg	Vertical load on wheels	3000	N
Frontal area	2.4	m^2	Peak longitudinal force	3500	N
Drag coefficient	0.24	-	Slip at peak load	10	%
Rolling radius	0.3	M	Carrier to driveshaft teeth ratio	4	-
Wheel velocity threshold	0.1	m/s	Follower to base teeth ratio (F/B)	2	-

Table 3.2

Generic Engine Parameters

Parameter	Value	Unit	Parameter	Value	Unit
Type	Spark-ignition	-	Maximum speed	9000	rpm
Maximum power	283	kW	Stall speed	1000	rpm
Speed at maximum power	6500	rpm	Inertia	0.2	kg m^2
Fuel consumption per revolution	25	mg/rev	Speed threshold	1000	rpm

3.2.3 Results and Discussions

The conventional powertrain model is analysed on the basis of vehicle and engine ratings given in Table I and Table II respectively. In the spark ignition type of generic engine, the spark plug initiates the ignition process. It ignites the mixture of fuel and air which is compressed in combustion chamber. In Simulink model, the analysis of engine performance is carried out by providing throttle physical signal which specifies normalized engine torque. The instantaneous engine power in Watts, the fuel consumption rate in grams per second, longitudinal vehicle speed (kilometres per hour) and the corresponding acceleration (meter per seconds squared) attained by vehicle body are the basic performance parameters which are recorded for following three conditions:

(i) Condition I: No load (engine throttle level = 0),

(ii) Condition II: 50% of full load (engine throttle level = 0.5)

(iii) Condition III: Full load (engine throttle level = 1).

The plots of instantaneous engine power, fuel consumption rate, vehicle longitudinal speed and acceleration for three conditions mentioned above are shown in Fig. 3.3. The peak values of all performance parameters are recorded in Table 3.3.

Table 3.3

Load Variation Analysis (Peak Value)

Parameters	Condition I	Condition II	Condition III
Engine Power (kW)	0	141	281.7
Fuel Consumption rate (g/s)	0.41	2.74	3.74
Vehicle Speed (km/h)	1.02	89	122.2
Acceleration (m/s^2)	1.4	4.65	6.03

The following observations are recorded from simulation studies:

- Condition I: The system model is started from rest. Under no load condition, there is no utilization of engine power. However, by consuming fuel at the rate of 0.41 g/s, the vehicle attains longitudinal speed up to 1.02 km/h. The initial acceleration is 1.4 m/s^2. By the time, the speed of vehicle settles down at peak threshold speed, the acceleration is reduced to zero and fuel consumption rate decreases to 0.01 g/s.
- Condition II: For 50 % of load condition, initial acceleration of vehicle is 4.65 m/s^2. By utilizing up to 141 kW peak power of engine at fuel consumption rate of 2.74 g/s, the powertrain attains longitudinal speed of 89 km/h in 10 s. After this, the fuel consumption increases in proportion to the increase in speed.
- Condition III: At full throttle, up to 99% of full engine power is being utilized by the powertrain. The initial acceleration of vehicle is 6.03 m/s^2. The powertrain cruises for nearly 6.7 s increasing speed up to 93 km/h and consumes peak fuel of 3.27 g/s. At 6.8 s, the engine power of 276.1 kW is again consumed by powertrain by producing acceleration of 5.9 m/s^2. At 10 s, the vehicle speed increases up to 122.2 km/h, the rate of fuel consumption increases up to 3.74 g/s, thereby decreasing the fuel economy.

From the above analysis, it is observed that at full throttle, the maximum speed attained by the conventional powertrain is 122 km/h. While attaining this speed, the engine power is utilized up to its full potential. The efficiency and output power capacity of generic engine highly depends upon compression ratio as well as research octane number of available gasoline and there are various widespread methods which are being researched to improve fuel economy in conventional powertrain [219]. However, in this research work, the computational analysis has been restricted to the understanding of dynamic performance of conventional powertrain using fundamental features of vehicle dynamics.

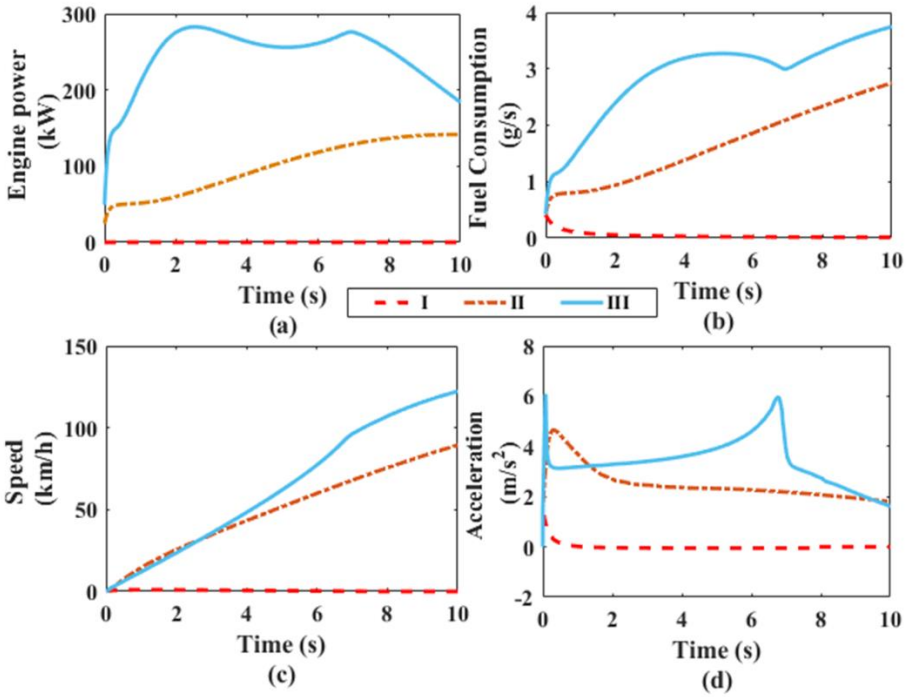

Fig. 3.3 Characteristic Plots of Conventional Powertrain for three Conditions of Throttle: (a) Engine Power (kW), (b) Fuel Consumption (g/s), (c) Vehicle Longitudinal Speed (km/h), (d) Vehicle Acceleration (m/s^2)

3.3 Modelling and Analysis of Electric Powertrain using SVPWM

Modelling of electric powertrain is required for thorough study of electric vehicle dynamics. The major components of electric powertrain are electric motor acting as traction device, inverter and controller for deciding the operational region of the motor and the load demand. For this research study, out of the existing choices available for EV application, PMSM is chosen as the traction motor. It is because its advantages, like fast response, reduced losses, better power factor, high power density and higher efficiency, overpowers its disadvantages like high cost of the rare earth magnets which replaces the rotor coils in the machine.

The mathematical equations describing the PMSM are necessary to understand the control of motor in electric powertrain applications [220]. The motor is powered by a Voltage Source Inverter (VSI). The controller in EV is developed on the principle of SVPWM [221]. The proposed system is validated for different torque demands.

3.3.1 Physical Model of Electric Powertrain

Unlike conventional ICE based power train, in EVPT, the electrical energy from a battery is supplied to the traction motor via three phase inverter system. The mechanical energy developed

at the shaft of electric motor is transferred to the electric car wheel system through transmission unit and the gear system. Fig. 3.4 shows the physical model of EVPT system in the form of block diagram.

Three phase two level VSI is connected to three phase load which is the traction motor in EV application while simulating complete electric powertrain.

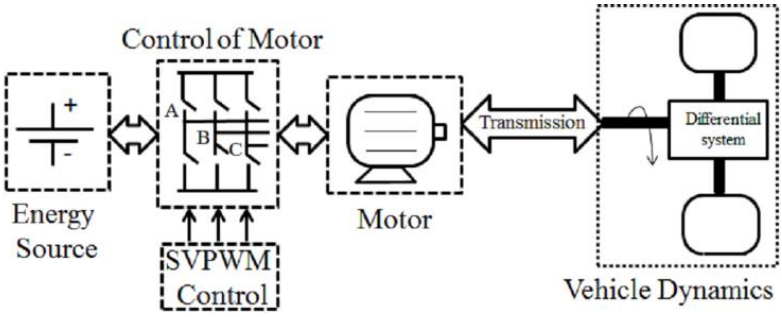

Fig. 3.4 Schematic Diagram of EVPT system

In VSI, if the battery voltage is V_D, the three phase voltages, V_A , V_B , V_C are given by:

$$[V_A \quad V_B \quad V_C]' = (V_D/3)\begin{bmatrix} 2 & -1 & -1 \\ -1 & 2 & -1 \\ -1 & -1 & 2 \end{bmatrix}\begin{bmatrix} A \\ B \\ C \end{bmatrix} \tag{3.1}$$

where A, B and C are the states of switches of the three legs of VSI. If either of them is 1 it means that the upper switch of the leg is on and if value is 0 it means that the lower switch of the leg is on.

3.3.2 Space Vector Pulse Width Modulation (SVPWM)

There are 8 possible states for a three-phase VSI. These possible states are given in Table 3.4. When these eight switching states are represented collectively on phasor diagram, a hexagon is obtained and radius of the hexagon depicts the voltage space vector structure, given in Fig.3.5(a) as $U_n;\ n = 0,1, \ldots 7$. From the table, it can be observed that there are six states which are supplying non zero voltage values, such states are known as active voltage states. Also, there are two states which provide zero voltage; such states are called zero voltage states. The states of switches are in accordance with (3.1).

For two-level inverter, each pole has either positive or negative level of voltages. All the six active voltage vectors are along the radii of the hexagon. So, for one cycle of operation, active vectors switch between these six states or steps. Therefore, a two-level inverter is also known as six-step inverter. Active vectors take six steps to complete one revolution. This hexagon has

six sectors with 60° span. A reference voltage vector having magnitude of U_r and angle θ, is given as input to the control unit. This voltage is generated by the inverter.

In SVPWM technique, the sector containing the reference voltage vector is first recognized via the angle measurement. Then this reference vector is sampled at high frequency so that sinusoidal variation of the average voltage value is obtained through the inverter.

Table 3.4

Phase Voltages at Different Switching States

Voltage Vectors	**Switch States**			**Phase Voltages as a factor of V_D**		
	A	**B**	**C**	V_A	V_B	V_C
U_0	0	0	0	0	0	0
U_1	1	0	0	2/3	-1/3	-1/3
U_2	1	1	0	1/3	1/3	-2/3
U_3	0	1	0	-1/3	2/3	-1/3
U_4	0	1	1	-2/3	1/3	1/3
U_5	0	0	1	-1/3	-1/3	2/3
U_6	1	0	1	1/3	-2/3	1/3
U_7	1	1	1	0	0	0

In one sampling period of T_s, it is assumed that the amplitude and angle of reference voltage are stationary and hence the average reference voltage is generated by switching between two active states and two zero states. The volt-sec balance concept gives the average reference voltage value given by (3.2):

$$U_r T_s = U_0 T_0 + U_1 T_1 + U_2 T_2 + U_7 T_0 \tag{3.2}$$

Here, T_0 is the period of zero voltage states, T_1 and T_2 are switching periods of two active voltage states. By splitting this equation into two orthogonal axes and solving, the time periods for each state is calculated using equation (3.3)-(3.5):

$$T_1 = T_s \times (U_r/V_D) \times \frac{\sin(60^0 - \theta)}{\sin 60^0} \tag{3.3}$$

$$T_2 = T_s \times (U_r/V_D) \times \frac{\sin\theta}{\sin 60^0} \tag{3.4}$$

$$T_0 = T_s - (T_1 + T_2) \tag{3.5}$$

Fig. 3.5(b) represents one sampling period T_s for switching states of Sector 1. The states are reversed in the next sampling period. During one sampling period, minimum switching transitions are required to avoid transition losses.

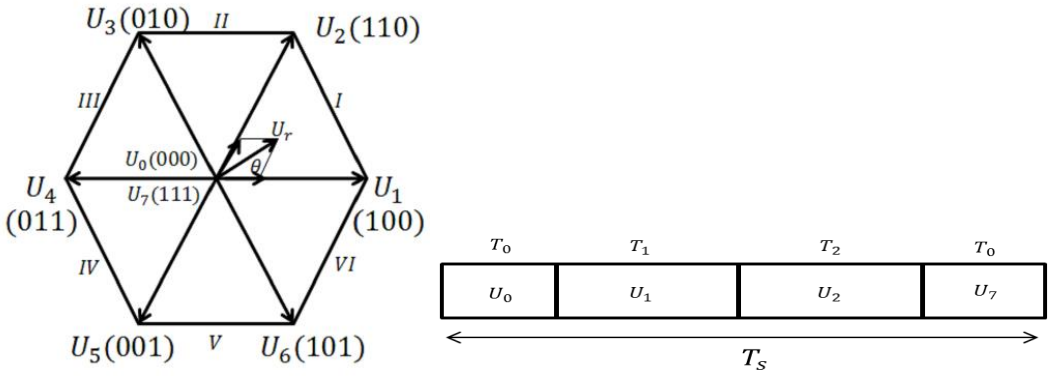

(a) (b)

Fig. 3.5 Space Vector Representation; (a) Sector Representation (b) One Sampling Period for 3-Phase 2-Level VSI

Fig. 3.6 shows the switching pattern for sector 1. The same is followed by any sector in which the location of the reference vector is identified. During one sampling period, only one phase switching is there, even though the voltage space vectors are changing. Hence using Fig. 3.6, the average values of the phase voltage calculations show that there is no contribution in voltage by zero voltage vectors. The vector pattern during one sampling period as depicted in Fig. 3.5(b) is U_0, U_1, U_2, U_7. For next sampling period, the vector pattern is followed in reverse, i.e., U_7, U_2, U_1, U_0.

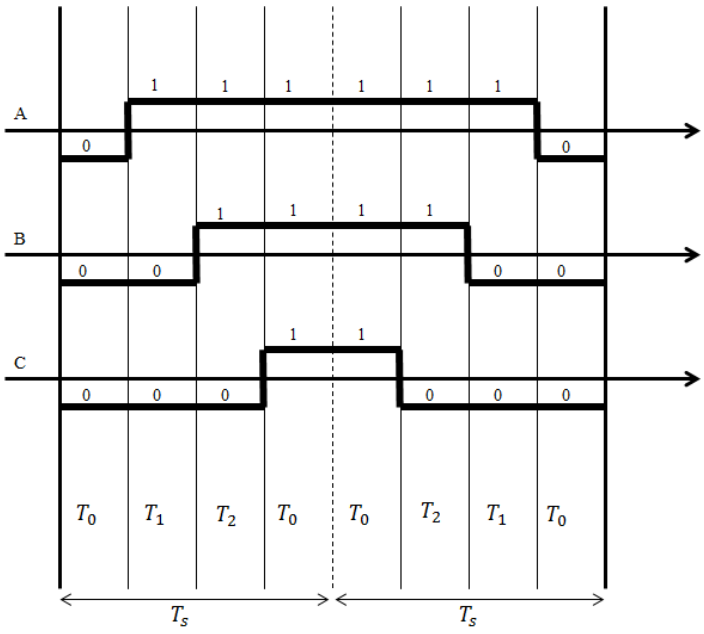

Fig. 3.6 SVPWM Switching Pattern for Sector 1

Using the SVPWM method, 2 adjacent effective vectors and the null vector are selected to form the space voltage vector U_r needed according to their respective response time [222]. The dynamic behaviour of EVPT is studied, simulated and analysed in the subsequent sections.

3.3.3 Simulink Model of EVPT

The base electric motor used in EVPT model is a four-pole inset type PMSM having basic parameters in accordance with high performance highway EVs [223-224] shown in Table 3.5. The system is analysed for various torque levels commanded to the SVPWM controlled EVPT model. In order to achieve the performance requirements obtained using generic engine and presented in Section 3.2.3, the electric powertrain system should satisfy the *benchmarked* specifications presented in Table 3.6.

The designed Simulink model is presented in Fig. 3.7. The motor shaft is coupled to the gear box taken under consideration for electrical powertrain simulation. A Three Phase VSI is used along with the pulse control implemented via SVPWM with 50 kHz switching frequency. The DC supply source of 400 V is used as a battery source in the model [223].

Table 3.5

PMSM Parameter Specification

Parameter	**Value**	**Units**
Rated Power	220	kW
Rated Torque	380	Nm
Rated Voltage	400	V
Phase	3	-
Phase resistance	10.52	mΩ
d axis inductance	306.3	mH
q axis inductance	559.3	mH
Magnetic flux	0.12	Vs

Table 3.6

Benchmarked EVPT Performance Parameters

Parameter	**Value**	**Units**
Torque	In accordance to load	-
Vehicle Speed	≥ 122.2	km/h
Acceleration	≥ 6.03	m/s^2

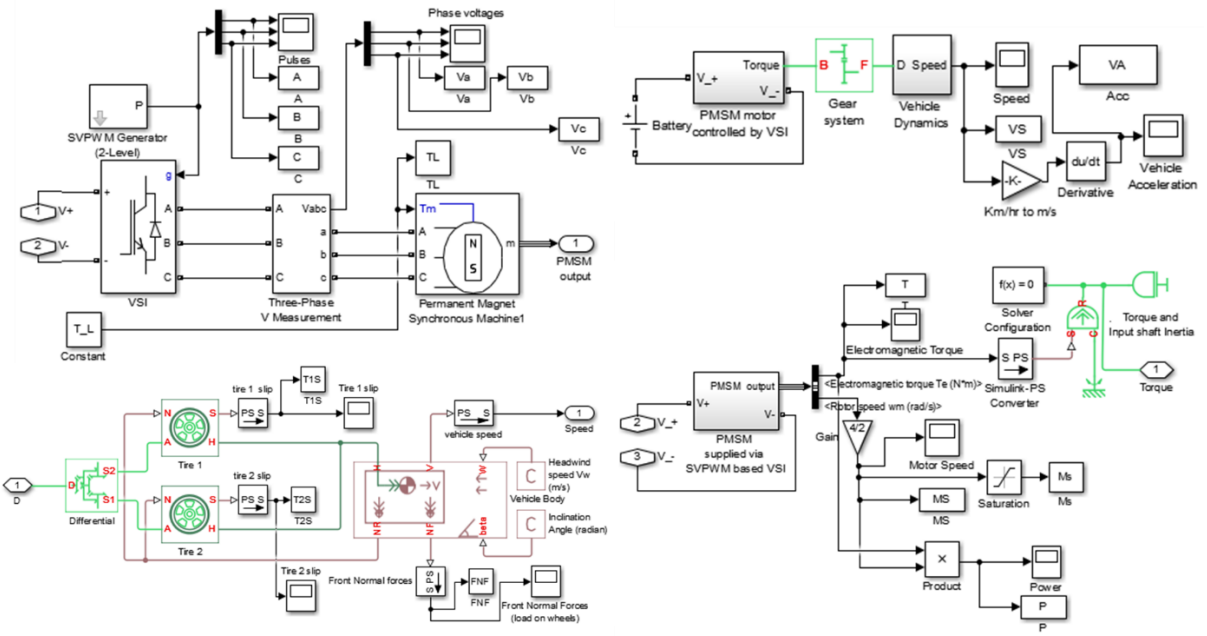

Fig. 3.7 Simulink Model of EVPT System with SVPWM Control

3.3.4 Results and Discussions

The analysis of electric powertrain is performed using variations of torque at different instants of time. It is to be duly noted that this analysis is restricted for studying the vehicle performance as per the torque produced at shaft due to given load commands to the motor in the powertrain.

The load variation application [225], applied to the EVPT system, having a set speed, actually refers to the addition of torsional resistance to a running powertrain. The way the powertrain reacts to such variation shows its ability to overcome the extra force needed to run the powertrain. At a fixed speed, EVPT system will be producing a fixed torque at the shaft. When a load disturbance is applied to the powertrain, its effect shows noticeable variation in the performance of EVPT system. In case of low load disturbance, the force produced by EVPT should overcome easily with little deviation in acceleration of powertrain while in case of large load variation, the EVPT system will react by demanding extra power from the traction motor. Hence, for analysing effects of such variation in load, the designed EVPT system is analysed for low and high values of load disturbances in order to check the reaction of powertrain to such condition.

Thus, the vehicle longitudinal speed is recorded at 0%, 10%, 80% and 100% load torque. The corresponding d and q axes currents are controlled by the controller in order to produce the necessary acceleration in the vehicle in accordance with the load demand.

The motor torque profile, vehicle longitudinal speed, acceleration, d-q axes currents of electric powertrain are shown in Fig. 3.8. At 0.08 s, for 37.5 Nm load torque, the initial acceleration of 6 m/s^2 rises up to 12.8 m/s^2 due to which vehicle attains 94 km/h. At 0.24 s, load torque is reduced to zero. The vehicle cruises with steady speed of 98 km/h. At 0.4 s, for 300 Nm load torque, the vehicle accelerates at the rate of 1.9 m/s^2 and attains up to 120 km/h longitudinal speed. When at 0.72 s, full load command is given to the powertrain, it attains the speed of up to 150 km/h with an acceleration of 2.1 m/s^2. The maximum speed attained by the electric powertrain is observed to be 22.7 % more than 122.2 km/h (generated by conventional powertrain). Also, the peak acceleration in EVPT system is almost 2 times that in conventional powertrain. This ensures the better performance of electric powertrain. The controlled switching and triggering pattern using pulse width modulation of generated space vector and three phase voltage obtained from VSI during load variation in EVPT powertrain is presented in Figs. 3.9(a) and 3.9(b) respectively.

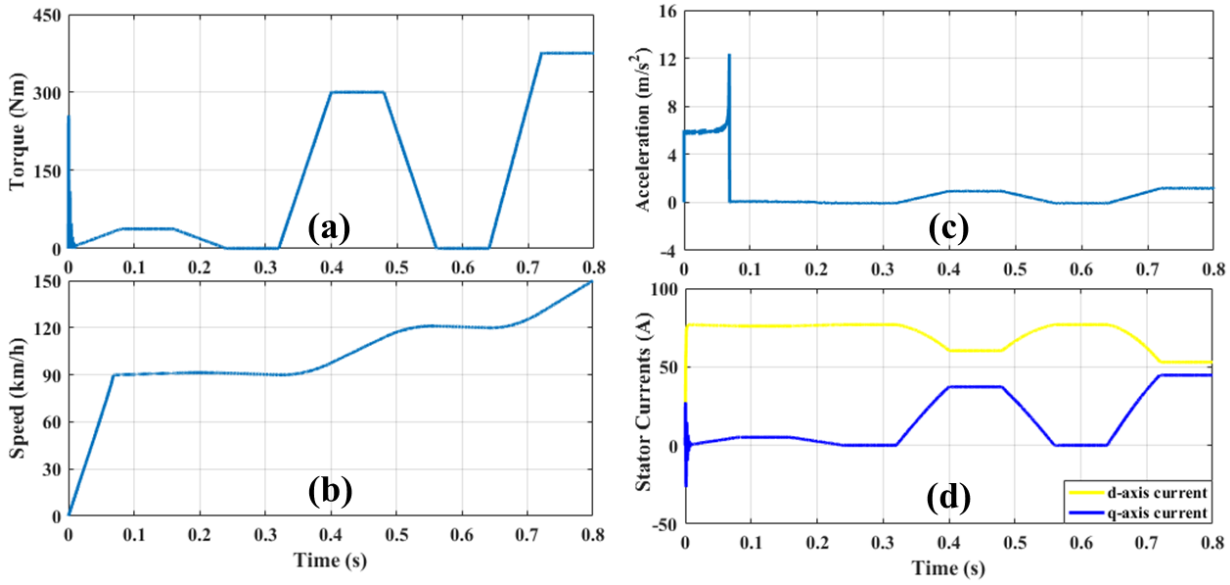

Fig. 3.8 Characteristic Plots of Electric Powertrain: (a) Shaft Torque, (b) Longitudinal Speed, (c) Acceleration and (d) dq axes Stator Currents

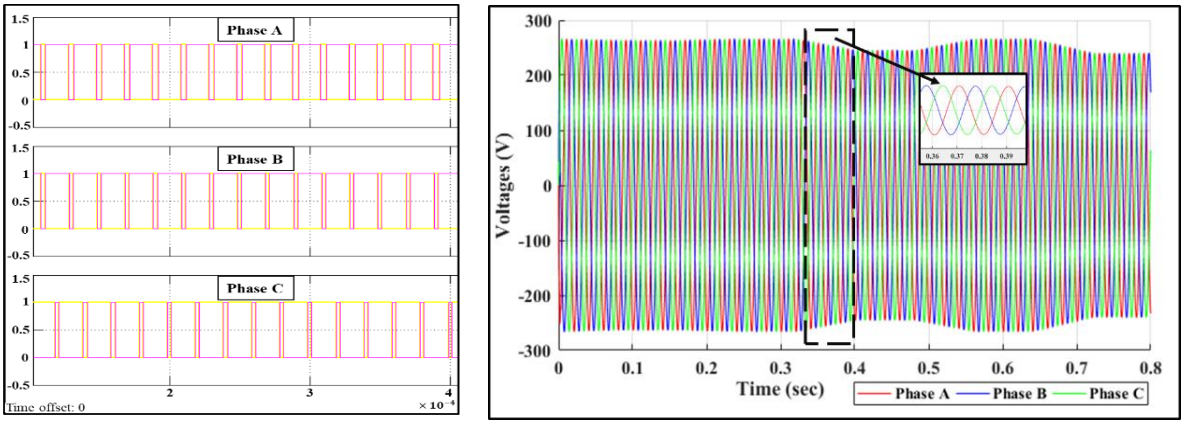

(a) (b)

Fig. 3.9 Output Response of VSI; (a) Controlled Triggering Pattern Generated using SVPWM (b) Three Phase Voltage Waveform Generated from VSI during Load Variation in EVPT.

3.4 Field Oriented Control of EVPT system

The Field Oriented Control (FOC) is an effective control technique employed in AC drives. This strategy decouples the flux and torque components by transformation from three phase quantities to two phase quantities. The dynamic modelling necessary to implement FOC for EVPT system is briefly described in this section. Thereafter, the Simulink model and its analysis results are presented. The detailed block diagram of implemented FOC strategy for EVPT system is shown in Fig. 3.10.

3.4.1 Dynamic Modelling of PMSM

The traction motor is modelled in synchronously rotating frame to avoid the difficulty in calculation of quantities due to variations in the machine parameters [226]. Three-phase to two-phase transformation is carried out using Park's transformation. The stator voltages in direct and quadrature axes are given by.

$$V_q = R_s I_q + \frac{d}{dt}(\lambda_q) + \omega_r \lambda_d \tag{3.6}$$

$$V_d = R_s I_d + \frac{d}{dt}(\lambda_d) - \omega_r \lambda_q \tag{3.7}$$

Stator fluxes in two axes are:

$$\lambda_q = L_q I_q + L_{mq} I_{kq} \tag{3.8}$$

$$\lambda_d = L_d I_d + L_{md} I_{kd} + L_{md} I_m \tag{3.9}$$

The electromagnetic torque developed by PMSM is given by:

$$T_{em} = \frac{3}{2}P\left(\lambda_d I_q - \lambda_q I_d\right) = \frac{3}{2}P\left(\lambda_m I_q + (L_d - L_q) I_q I_d\right) \quad (3.10)$$

Where R_s is stator resistance; ω_r is the rotor speed; L_q, L_d, I_q, I_d are quadrature and direct axes inductances and currents respectively.

The mechanical equation of torque for motor having load torque T_l is:

$$T_{em} = \frac{J_m}{P}\frac{d}{dt}(\omega_r) + \frac{B_m}{P}\omega_r + T_l \quad (3.11)$$

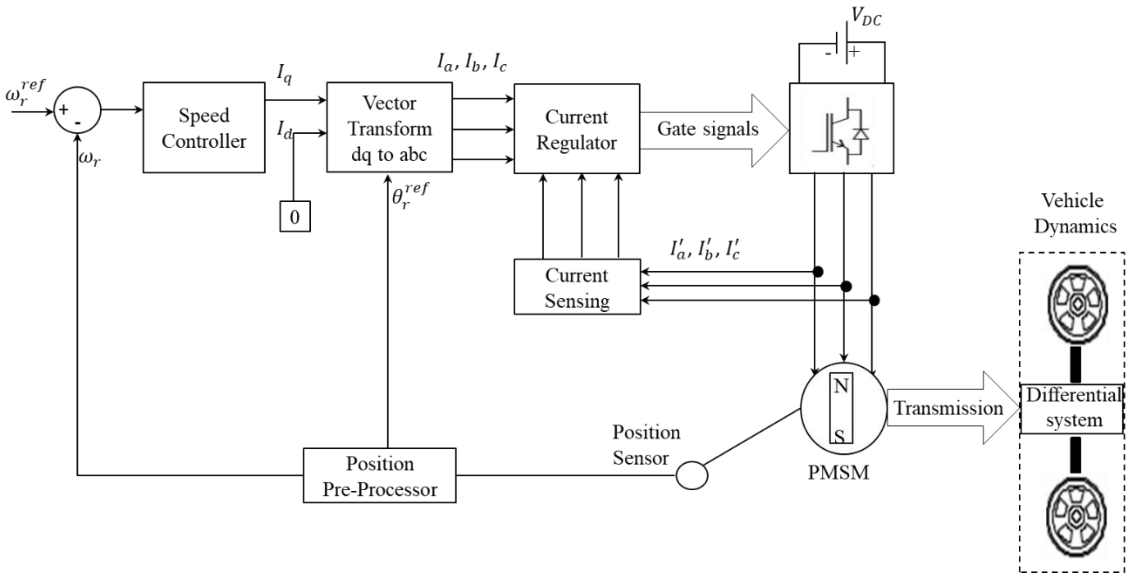

Fig. 3.10 Schematic Diagram for FOC of EVPT System

There are two different terms in the electromagnetic torque equation (3.10)- (a) one is due to permanent magnet λ_m and q axis current component I_q , known as magnetic torque and (b) the second due to difference in direct and quadrature axes interaction, known as reluctance torque. By maintaining I_d equal to zero and controlling I_q component of stator current, the speed control strategy can be applied for the PT system by utilizing magnetic torque component up to base speed. Reluctance torque component is utilized for flux weakening operation beyond base speed. However, it is not a sufficient condition for a motor to operate above rated speed at specified voltage and current ratings of motor and inverter configuration because the d axis flux linkage is dependent only on the permanent magnet. So, for high-speed operations and flux weakening regions, the I_d component is maintained at non-zero value [227].

Equation (3.12) gives analogous torque equation of DC machine, where the direct axis current component is zero. Rotor flux due to permanent magnet λ_m is constant in this motor.

$$T_{em} = \frac{3}{2}P\lambda_m I_q \quad (3.12)$$

3.4.2 Simulink Model of PMSM

The dynamic model of traction motor drive with FOC is implemented, simulated and tested under varying load and speed conditions using technical specifications given in Table – 3.5. The developed Simulink model of EVPT system with FOC is shown in Fig. 3.11. FOC is implemented for both modes of operation: traction and braking mode.

3.4.3 Results and Discussions

In order to validate the performance of the controller, simulations are performed for four different cases. The controller gains are taken as: K_p =1000 and K_I = 5 respectively. The initial conditions of all the estimated parameters are assumed to be zero in order to monitor exact vehicle performance. The below mentioned scenarios (a) to (c) cover the performance analysis for traction mode of PT system while (d) shows the braking mode operation of EVPT system.

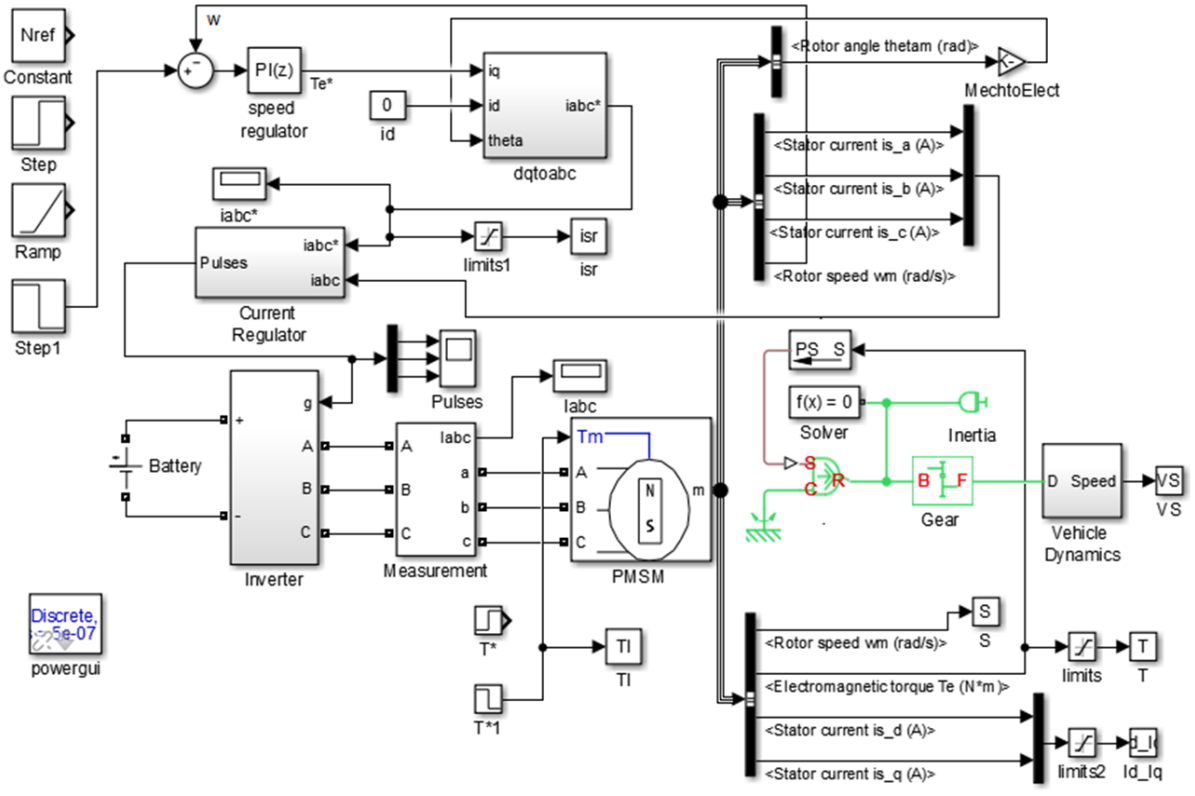

Fig. 3.11 Simulink Model of EVPT System (PMSM with FOC)

a) Constant Speed Operation:

For constant speed operation, the reference value of 200 rad/s (1909 rpm) is given to the system and at 1 s, a load disturbance of 16 % is applied. The system response plots of the actual shaft

torque and reference load torque, motor and vehicle speed, stator three phase and d-q phase currents and vehicle acceleration are presented in Fig. 3.12. As soon as the load demand from the motor increases, the controller generates the required quadrature axis current i_q in order to control the motor speed. The vehicle accelerates at the peak rate of 7.3 m/s^2 to reach peak speed of 86 km/h. Thus, the EVPT system tracks the variation in the load torque for constant speed command.

b) Step Varied Speed Operation:

The motor is started at a commanded speed of 150 rad/s. At 0.5 s, a step variation of speed from 150 rad/s (1432 rpm) to 300 rad/s (2864 rpm) is applied. Before speed disturbance, the vehicle attains longitudinal speed of 68 km/h with peak acceleration of 6.5 m/s^2. After speed disturbance is applied to motor, vehicle reaches up to 80 km/h. Moreover, at 2 s, when a step variation from 0 % to 50 % load torque is applied, vehicle attains peak speed of 110 km/h with acceleration of 2 m/s^2. As the load fluctuates, the necessary q axis current i_q is generated by the controller for providing the required acceleration to EVPT system. The system response plots for speeds, torques and currents are shown in Fig. 3.13.

c) Ramped Speed Operation:

The motor is started with a ramp input where the speed is increasing at the rate of 10 rad/s (95 rpm per second). At 1 s, when load condition is changed from 50 % to 100 %, the controller produces the required quadrature current for regulating motor and vehicle speed. The vehicle speed attains peak value of 143 km/h. The peak value of vehicle acceleration is 11 m/s^2. The performance plots of EVPT system model under this category of speed operation is shown in Fig. 3.14.

d) Braking Mode of Operation:

For braking mode of operation, the system is tested with load torque varied from 50 % to 0 % load at 0.5 s and speed profile varied from 480 rad/s (4583 rpm) to 0 rad/s at 1 s. At 50 % load and 90 % of rated speed, the vehicle attains peak longitudinal speed of 187 km/h with peak acceleration of 11 m/s^2.

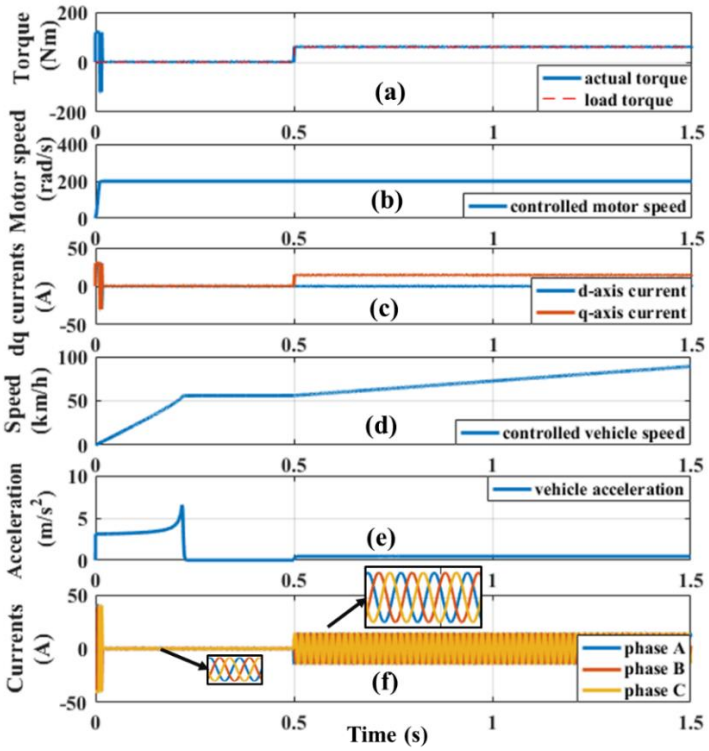

Fig. 3.12 Dynamic Response under Load Disturbance for Constant Speed Operation: (a) Shaft Torque, (b) Motor Speed, (c) d-q axes Stator Currents, (d) Vehicle Longitudinal Speed, (e) Vehicle Acceleration, (f) Three Phase Stator Currents

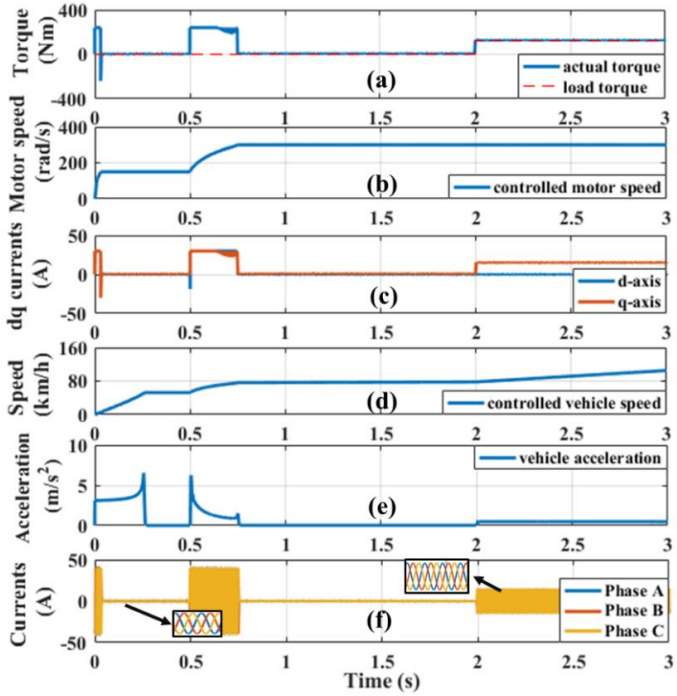

Fig. 3.13 Dynamic Response under Load Disturbance for Variable Speed Operation: (a) Shaft Torque, (b) Motor Speed, (c) d-q axes Stator Currents, (d) Vehicle Longitudinal Speed (km/h), (e) Vehicle Acceleration, (f) Three Phase Stator Currents

At 1 s, vehicle speed starts decreasing by experiencing negative peak acceleration of 7.3 m/s^2 and stops at 1.2 s. The controlled motor and vehicle speeds, acceleration, torques and stator dq and abc currents are shown in Fig. 3.15. It is observed that the system responds in accordance with the load variations and the field control is easier and advantageous to maintain the required vehicle speed. The performance of designed EVPT system with two types of control strategies, i.e., SVPWM and FOC, are thus compared with the specifications obtained from the conventional powertrain in Table 3.7 It is thus observed that, the traction motor meets the essential specifications for providing satisfactory performance for overall movement of the vehicle body [228].

.

Table 3.7

Comparison of Benchmarked EVPT Performance Parameters

Parameter	**Conventional Powertrain**	**EVPT System with SVPWM Control**	**EVPT System with FOC**
Torque	In accordance to load	In accordance to load	In accordance to load
Peak Vehicle Speed	122.2 km/h	150 km/h	187 km/h
Peak Acceleration	6.03 m/s^2	12.8 m/s^2	11 m/s^2

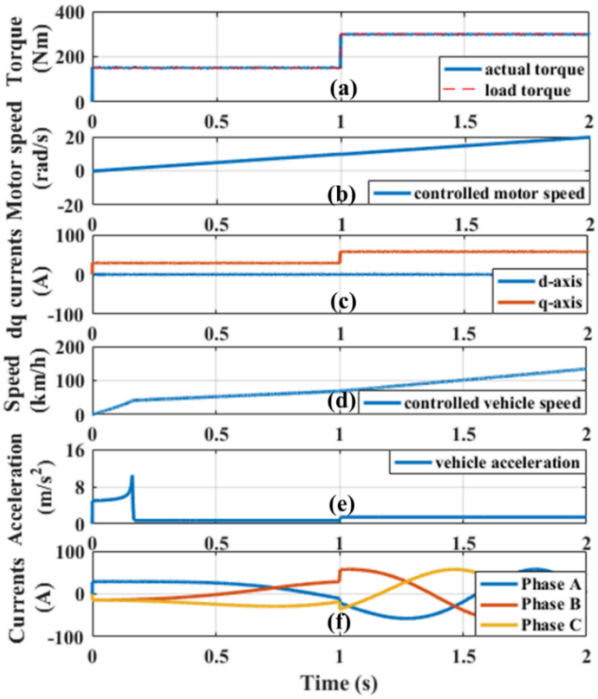

Fig. 3.14 Dynamic Response under Load Disturbance for Ramped Speed Operation: (a) Shaft Torque, (b) Motor Speed, (c) d-q axes Stator Currents, (d) Vehicle Longitudinal Speed, (e) Vehicle Acceleration, (f) Three Phase Stator Currents

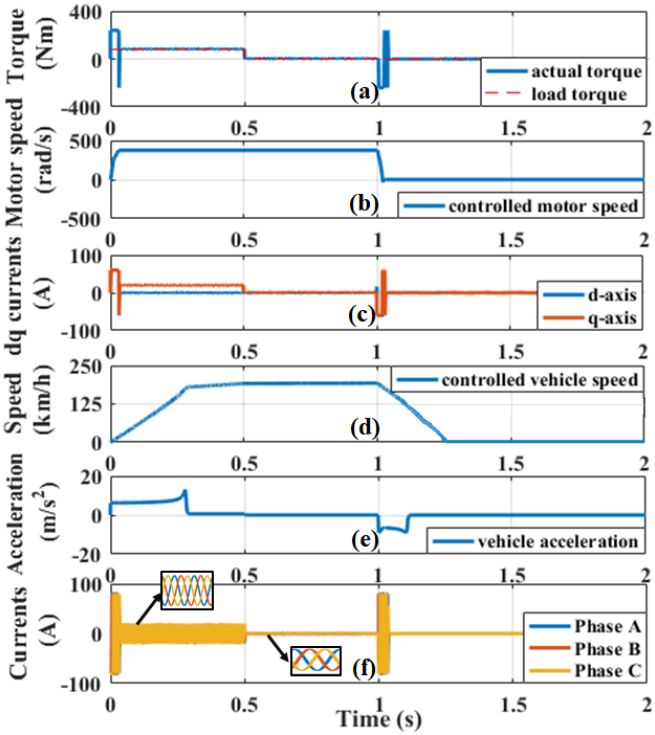

Fig. 3.15 Dynamic Response under Load Disturbance for Breaking Mode Operations: (a) Shaft Torque, (b) Motor Speed, (c) d-q axes Stator Currents, (d) Vehicle Longitudinal Speed, (e) Vehicle Acceleration, (f) Three Phase Stator Currents

3.4.4 Laboratory Testing of EVPT System using Test Bench Emulator

FOC based control of EVPT system was implemented in a laboratory prototype using a test bench emulator. The details along with the test results are given at **Appendix A.**

3.5 Conclusion

In this chapter, vehicle powertrains using two different propulsion configurations are modelled, analysed and presented. The conventional powertrain using spark ignition type of generic engine is modelled in Simulink and the information obtained from the dynamic analysis of ICE powertrain is set as the benchmark parameters for evaluating the performance of electric powertrain. Key vehicle performance variables like maximum speed attained and acceleration achieved using conventional ICE have been considered for setting the benchmark.

Thereafter, the simulation model of electric powertrain is developed. To control electric powertrain, SVPWM strategy is implemented. The developed simulation model of the EVPT is tested and analysed under various operating conditions. The proposed powertrain model is found suitable for the electrical vehicle application. This model can be further investigated using various factors affecting the operation of electrical vehicle to have a closer look over the dynamics of automobile.

In addition, the implementation of FOC based control of EVPT system is presented. The dynamic performance of traction motor is analysed. Both traction and braking modes of operation of vehicle are tested under different operating conditions. For achieving the necessary power, torque and speed requirements by the traction motor employable by different Original Equipment Manufacturers (OEMs), the electric motor used by the proposed EVPT system is found to be robust and dynamically fast in response. The designed controller shows fast response to the load and speed perturbations. This analysis can be further extended for investigating the system for different drive cycles considering various environmental and mechanical factors.

Chapter 4

Design, FEM Analysis and Meta-modelling of PMSM

4.1 General

While the performance analysis of PMSM as traction device in electric drivetrain, carried out in the previous chapter helped to analyse the dynamic behaviour of the motor during controlled electric drive operation, this chapter elucidates the design features of PMSM for EV applications. This includes the evaluation of the material properties along with the motor design parameters and development of the preliminary PMSM model. This designed and developed preliminary PMSM model is refined through design optimization of models; the design optimization aspect is covered in detail in the subsequent chapters. The objective is to select appropriate geometrical parameters (GPs) of the motor at design stage to optimize motor torque and minimize losses.

The stator and rotor of the PMSM are conventionally fabricated using laminated electrical steel core material and PMs are embedded in the rotor [229]. Use of PM increases the efficiency and the torque density of the motor. Optimization of controllable GPs of PMSM at design stage results in improvement of torque density, power density and efficiency, in addition to other benefits of PM motor design, such as lesser harmonic distortion in back emf, low ripple, low cogging torque and high flux linkage. The optimization entails accurate assessment of the impact of variations in GP on the performance factors of PMSM model [230] at the design stage. This is achieved through FEM analysis, in which initially an elementary model is developed and analysed by setting up the preliminary simulation and the corresponding results are utilized for design optimization. FEM analysis helps to reduce high computation time for such complex structural studies. It offers virtual visualization of various properties of models which are user-friendly and helpful to spot flexibility and sensitivity of the design [231]. The current research work is focused on the design and development of two PMSMs, viz – a smaller sized compressor motor used in the environment conditioning system and a larger traction motor used in the drive system of e-vehicles. For ease of comprehension, the smaller sized PMSM is christened PMSM-1 and the larger traction motor is called PMSM-2.

This chapter elucidated the analytical design, GPs and material properties of the developed preliminary models of SI-PMSMs for compressor and traction application in e-vehicles. The

basic designs are analysed for different operating conditions and the electromagnetic performance of the designed motors is validated using Mesh Analysis. In addition, the optimization of the motor geometry for PMSM-1 and PMSM-2 is carried out using Surrogate Modelling Technique and the model is validated using RMSE analysis. The process flow chart for development of the preliminary model design is shown in Fig. 4.1.

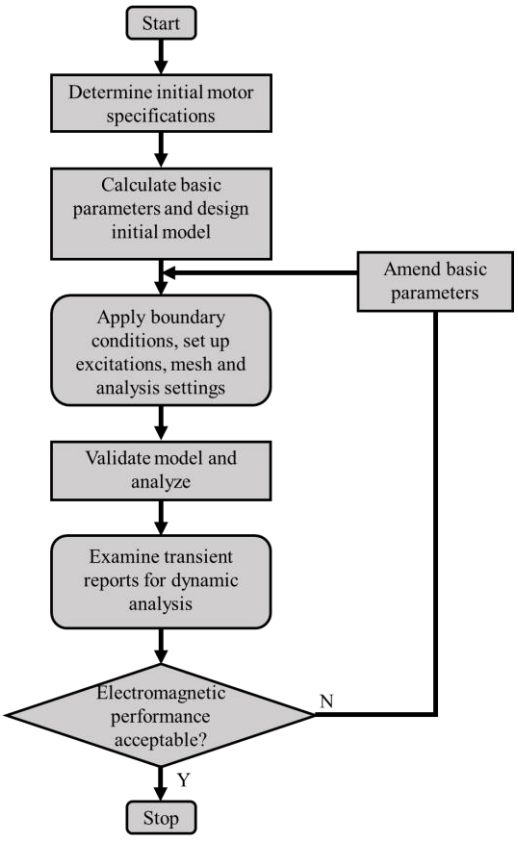

Fig. 4.1 Flow Chart for Development of the Preliminary Model Design

4.2 Analytical Design of PMSM-1

This section describes the preliminary design of PMSM-1, which has a concentrated winding configuration, lesser number of slots and pole combination with low power rating. This design is intended for utilization electric compressor of the environmental conditioning system of an EV. The material properties, model specifications, corresponding simulation results and discussions are described in upcoming subsections.

4.2.1 Geometrical Parameters and Material Properties: Preliminary Design of PMSM-1

The quarter-sectional view of initially designed PMSM-1 is presented in Fig. 4.2(a). The stator, PM and rotor dimensions are shown in Table 4.1. It has a six pole and nine slot three phase SI-

PMSM structure having fractional slots per pole per phase = 1/2. The stator slots ~~consist of~~ have double layer concentrated winding configuration. The location of PM in rotor of PMSM-1 is shown in Fig. 4.2(b). The non-linear magnetic B-H characteristics for the stator / rotor core and the shaft materials is shown in Fig. 4.3.

Table 4.1

Specifications of Preliminary Model of PMSM-1

	Parameter	Specification		Parameter	Specification
Motor Geometry	Rated Output Power	3 HP	Motor Geometry	Cogging Torque	0.80 Nm
	Rated Speed	3000 rpm		Torque (@rated speed)	7.12 Nm
	Operation Frequency	150 Hz		Input Current (@rated speed)	5.45 A
	Stator Inner Diameter	67.6 mm		Slot height	14.2 mm
	Stator Outer Diameter	110 mm		Stator yoke thickness	6 mm
	Rotor Outer Diameter	66.6 mm	Permanent Magnet	Permanent Magnet material	NdFeB
	Shaft Diameter	24 mm		Remanence Flux Density, B_r	1.2 T
	Stack Length	50 mm		Relative Permeability, μ_r	1.099
	Air gap Length	2.5 mm		Coercive Magnetic Field Intensity, H_c	890000 A/m
	Coil Turns	30		Bulk Conductivity	625000 Siemens/m
	Electrical Steel	M400-50A		Mass Density	7400 kg/m^3
	Shaft Material	Mild Steel		Young's Modulus	147e9 N/m^2
	RMS Back-emf (@500rpm)	25 V			

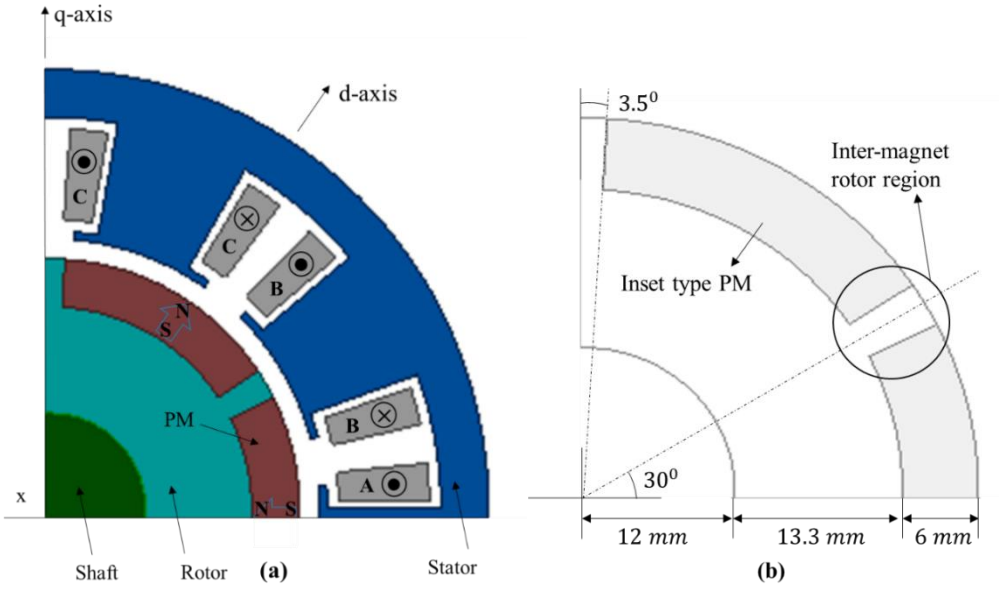

Fig. 4.2 PMSM-1: (a) Quarter-Sectional-Model (b) Location of PMs in Rotor

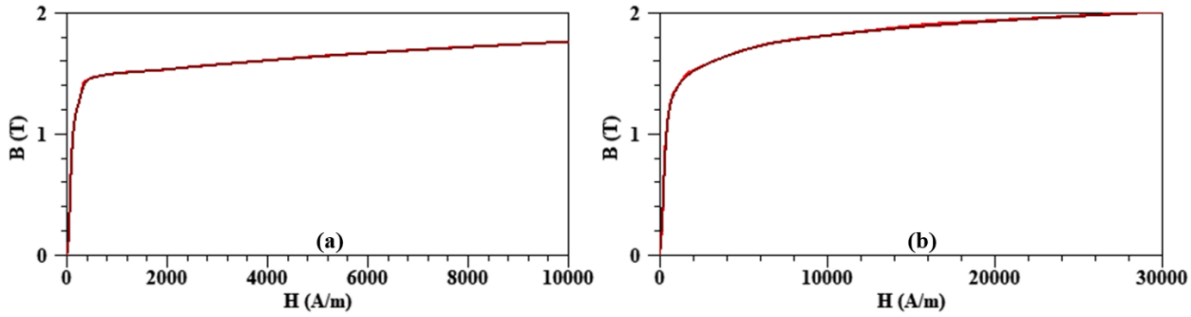

Fig. 4.3 BH Curves: (a) Stator & Rotor Core (b) Shaft Core

4.2.2 FEM Analysis: Preliminary Model of PMSM-1

For PMSM, the electromagnetic torque in rotating d-q reference frame is given as:

$$T_{em} = \frac{3}{2}P\left(\lambda_m I_q \sin t + (L_d - L_q) I_q I_d \sin 2t\right) \quad (4.1)$$

Where, t is the torque angle. The electromagnetic torque comprises of two components: magnetic and reluctance torque. To compute these torque components, the method of frozen permeability is used, in which total torque from machine is obtained using FEM analysis. The magnetic material is replaced by air and consequent FEM analysis is carried out to obtain the reluctance torque component. The difference of the reluctance torque and total torque yields the magnetic torque [232-233].

Since SI-PMSM has magnets embedded in the surface of the rotor, there is a reluctance difference observed between d-q axes. Because of this difference in reluctance, the machine produces maximum torque at a torque angle that is higher than 90^0. The method of shifting in reluctance torque can be used to enhance the utilization of both components of torque [234]. For this, an additional air gap is introduced beside the magnet in the rotor of inset type PMSM, which increases overall torque performance of the motor. However, the air gap flux density gets higher distortion in such design and torque ripples also remain un-improved due to which the motor becomes noisy. Therefore, in this research, without introducing additional air gap beside the magnets, the torque angle corresponding to peak torque is extracted from the torque versus torque angle characteristics to address the above issues.

From the analysis of the relationship between rotor position estimation error and magnetic saliency ratio in PMSMs, it is found that if magnetic saliency ratio falls below 1.65, the error in estimating rotor position increases manifold due to which it becomes impractical to estimate position of rotor in PMSMs [235]. A high saliency ratio results in the production of higher value of reluctance torque than magnetic torque in inset type PMSMs [236]. This way these

motors are capable of producing high output torque by the cause of utilizing its harmonic components. However, the rise in torque ripples becomes a disadvantage. This issue is also resolved in this research work by design optimization of models in the upcoming chapters.

Through the FEM analysis of PMSM-1, it is found that the reluctance torque to magnetic torque ratio is 1.74. It is also observed that maximum torque of 5.82 Nm is obtained at phase angle of 220° as shown in Fig. 4.4 (a)(i). Since the motor is operated for producing maximum torque for EV application, the phase angle of 220° is fixed for further considerations. The motor performance is further analysed at this obtained torque angle of 220°. When the motor is run at rated speed of 3000 rpm (with 5.45 A operating current), output torque of 5.8 Nm with ripples of 0.38 per unit (pu) is obtained for the initial model as shown in Fig. 4.4 (a)(ii). The flux linkage and induced back emf for the three phases when the motor is run at one-sixth of the rated speed are shown in Figs. 4.4(b)(i) and 4.4(b)(ii) respectively.

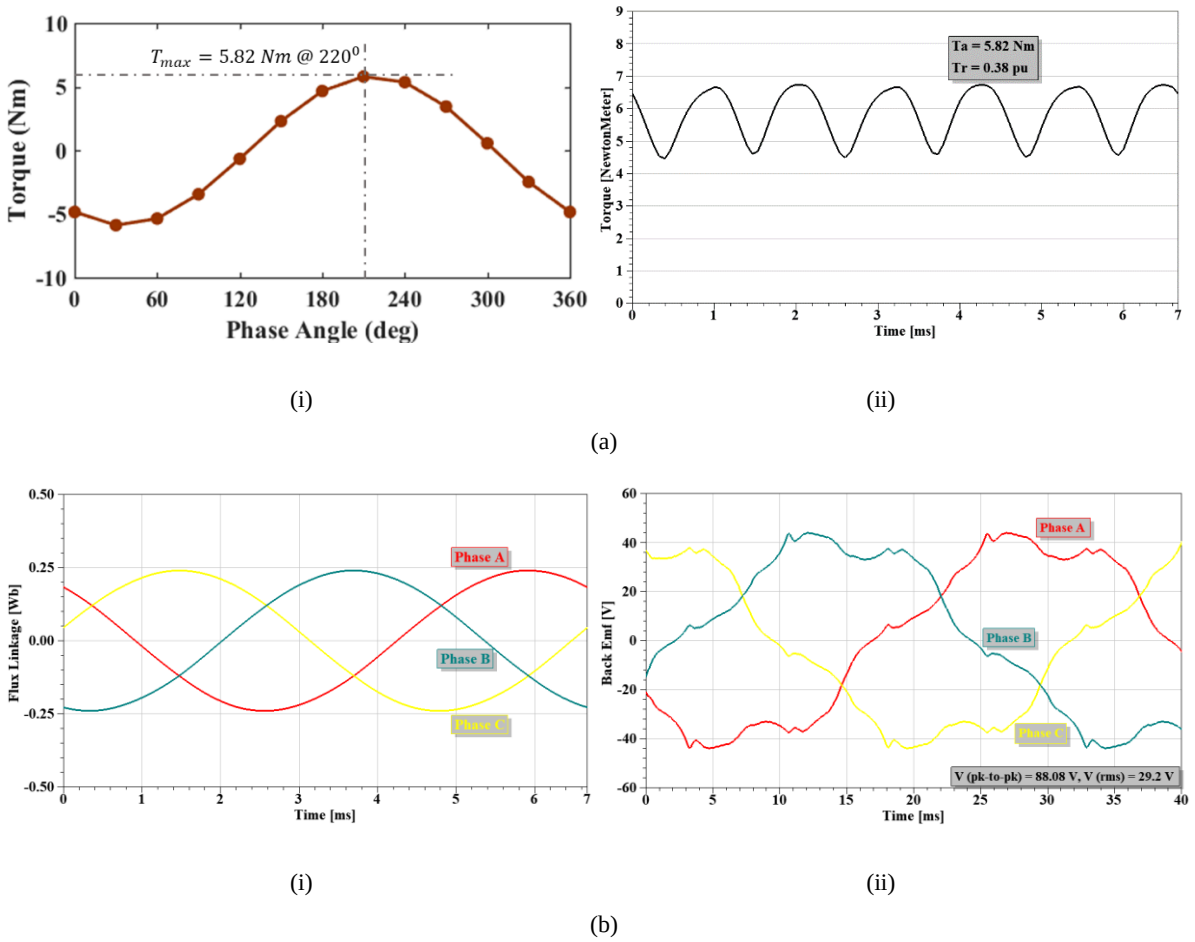

Fig. 4.4 FEM Analysis of PMSM-1: (a) (i) Torque vs Phase Angle (ii) Torque Characteristics at 3000 rpm, (b) (i) Flux Linkage (ii) Induced Back Emf

The induced back emf is observed to have total harmonic distortion (THD) of 28%. The shortcomings of this preliminary model are improved by optimizing its design parameters, which is discussed in the upcoming chapters.

4.3 Analytical Design of PMSM-2

This section describes the preliminary design of PMSM-2, which has a distributed winding configuration, high number of pole and slot combination with high power rating. This design is intended for utilization as traction motor of EV. The material properties, model specifications, corresponding simulation results and discussions are described in upcoming subsections.

4.3.1 Geometrical Parameters and Material Properties: Preliminary Design of PMSM-2

The half-cross-sectional view of initially designed PMSM-2 is shown in Fig. 4.5(a). The stator, PM and rotor dimensions are presented in Table 4.2. It has a fourteen pole and thirty-six slot three phase SI-PMSM structure having fractional slots per pole per phase = 6/7. The stator slots have single layer distributed winding configuration. The PM in the rotor of PMSM-2 is located as shown in Fig. 4.5(b). The non-linear magnetic B-H characteristics for the stator / rotor core and the shaft materials are already presented in Fig. 4.3.

Table 4.2

Specifications of Preliminary Model of PMSM-2

	Parameters	**Specification**		**Parameters**	**Specification**
Motor Geometry	Power	125 kW	Motor Geometry	Cogging Torque	70 mNm
	Base Speed	3000 rpm		Torque (@rated speed)	351 Nm
	Frequency	350 Hz		Input Current (@rated speed)	17 A
	Stator Inner Diameter	121 mm		Slot height	16.74 mm
	Stator outer diameter	172 mm		Stator yoke thickness	8.7 mm
	Rotor diameter	120 mm	Permanent Magnet	Permanent Magnet material	NdFeB
	Shaft Diameter	28 mm		Relative Permeability	1.09
	Stack Length	150 mm		Bulk Conductivity	625000 Siemens/m
	Air gap length	0.5 mm		Remanence Flux Density	1.2 T
	Coil Turns	300		Magnetic Coercivity	890000 A/m
	Electrical Steel	M400-50A		Mass Density	7400 kg/m3
	Shaft Material	Mild steel		Young's Modulus	147 Giga Pascal (GPa)
	RMS Back-emf (@500 rpm)	8.9 kV			

4.3.2 FEM Analysis: Preliminary Model of PMSM-2

In order to produce high torque, the motor having higher power rating and lower speed capacity is chosen for evaluating its ability for EV application. The preliminary model is tested to check and ensure the appropriateness of the model configuration. As already discussed in Section 4.2.2, it is observed that for initial model of PMSM-2, peak torque of 351 Nm is obtained at phase angle of 220^0 which is fixed for further investigations. The flux linkage and torque characteristics of PMSM-2 are presented in Figs. 4.6(a) and 4.6(b) respectively. At rated operating speed of 3000 rpm, approximately 30 Wb of rms flux linkage is obtained, which generates approximately 351 Nm of torque with 0.29 pu of ripples.

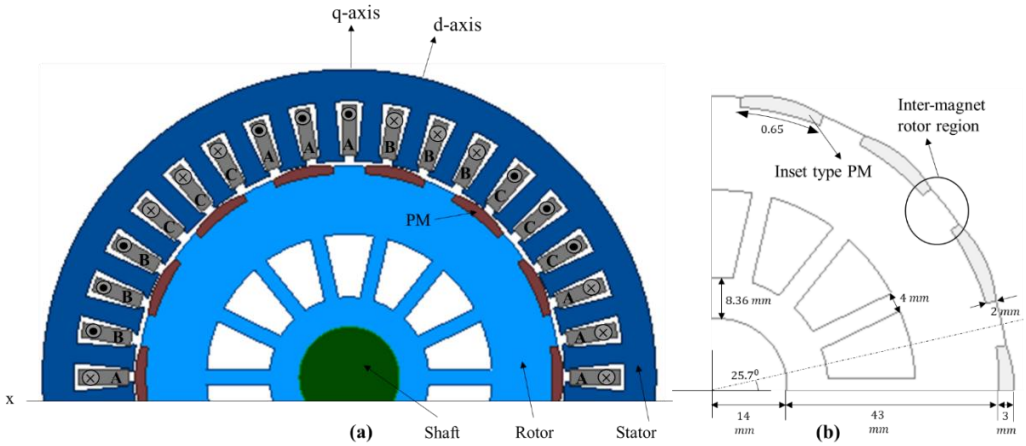

Fig. 4.5 PMSM-2: (a) Half-Cross-Sectional Model (b) Location of PMs in Rotor

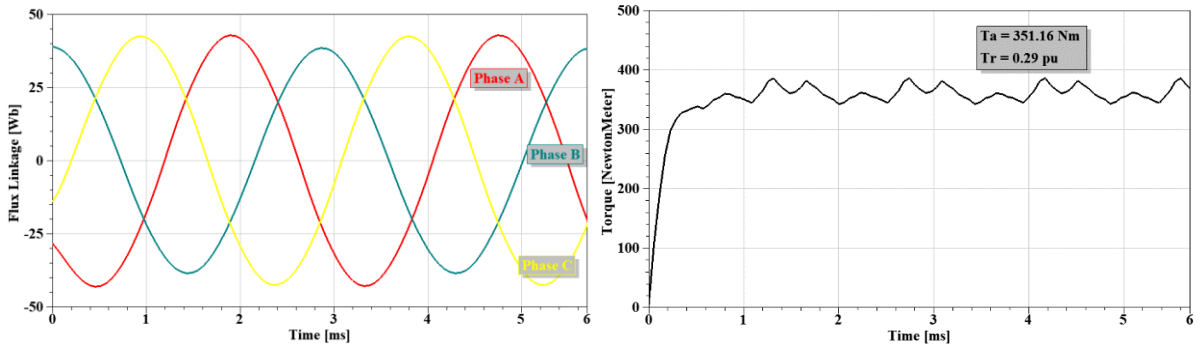

(a) (b)

Fig. 4.6 FEM Analysis of PMSM-2 (a) Flux linkage (b) Torque Characteristics at 3000 rpm

4.4 Mesh Analysis

The preliminary models of SI-PMSM having two different configurations are analysed by creating meshes in which the domain is split into various discrete elements to calculate the solution. PMSM-1 is designed with double-layer concentrated winding since this configuration

is suitable for compressor application in electric transportation system and is further needed to be tested and refined for the same purpose [237]. PMSM-2 is designed with single layer distributed winding. Such structure is found to be relevant for light weight EVs [238]. The mesh plots of PMSM-1 in the air gap bands and in overall geometry is investigated in this section. It is observed that the air gap bands mesh into 1526 elements. The overall geometry meshes into 14584 elements in order to obtain the residual of 4.45×10^{-7} of mean elemental area to ensure adequate output performance of PMSM-1.

By analysing mesh plots of PMSM-2 by setting of maximum elemental length to 0.35 mm, the number of elements in air gap band are found to be 4735. The mesh plots signify that satisfactory electromagnetic performance has been produced by the motor by resolving the motor complex geometry into total 17883 recognizable elements [239]. The Mesh plots of PMSM-1 and PMSM-2 are presented in Figs. 4.7(a) and 4.7(b) respectively.

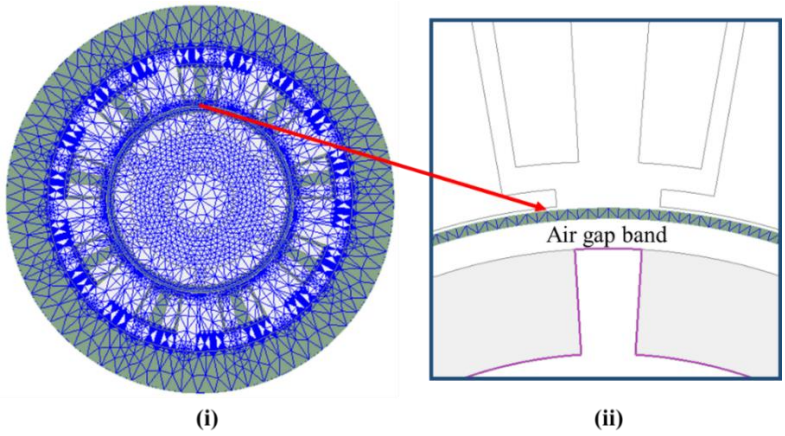

(a) Mesh Plot of PMSM-1

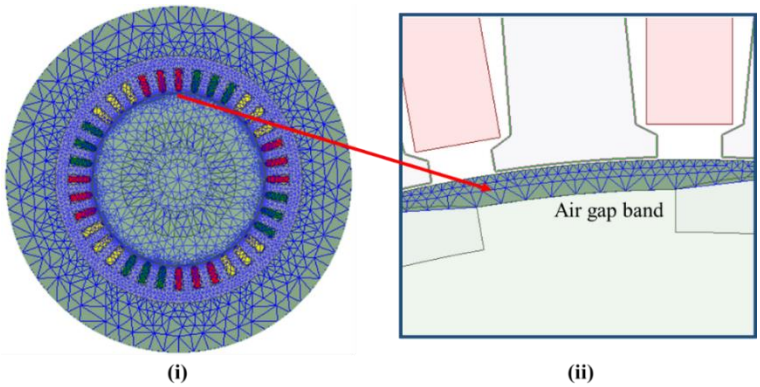

(b) Mesh Plot of PMSM-2

Fig. 4.7 SI-PMSM Geometries using ANSYS Maxwell's Meshing Proficiency

4.5 Surrogate Modelling Technique for Optimization of Motor Geometry

This section brings out the implementation of surrogate modelling technique to the designed models. When different GP dimensions are altered with minute variation in values, the task of re-designing the model and thereby performing FEM simulation becomes time consuming. It becomes impractical to examine the design region earnestly by computing huge aggregate of samples directly. The main goal of metamodeling is to estimate an approximate function, which is also termed as 'surrogate model', that impersonates the behaviour of the original system. This results in faster evaluation.

The construction of such function is carried out by performing numerous simulations, also termed as 'samples', at essential points in design area of region. The outcomes are then analysed and the necessary parameters of the selected surrogate models are computed. Thus, the designed surrogate model approximates these sample points as well as overall behaviour of the complete system effectively [240]. After the model is framed, the model optimization as well as sensitivity investigation can be performed to acquire accurate and deep understanding of function behaviour and the overall global structure [241]. Thus, the aim of metamodeling process is to conquer the time-consuming computations by implementing definite approximation using one-time authentic modelling attempt.

The objective challenge in this task is the generation of design space which is highly accurate. Among the widely available approximation methods expressed in Section 2.4.2 (Chapter 2), the Response Surface Method (RSM) is one of the classical forms of surrogate modelling scheme. It generates accurate and efficient performance [242]. Hence, the surrogate models in this research work are designed using RSM scheme.

In this scheme, the input parameters are varied and corresponding output responses are recorded to form Design of Experiments (DOEs). For computation of coefficients of Response Surface (RS) models, the Least Square Method (LSM) is implemented in the simulation studies using MATLAB. The validation of RS models is carried out using RMSE test for different output quantities. The process flow of RSM is shown in Fig. 4.8.

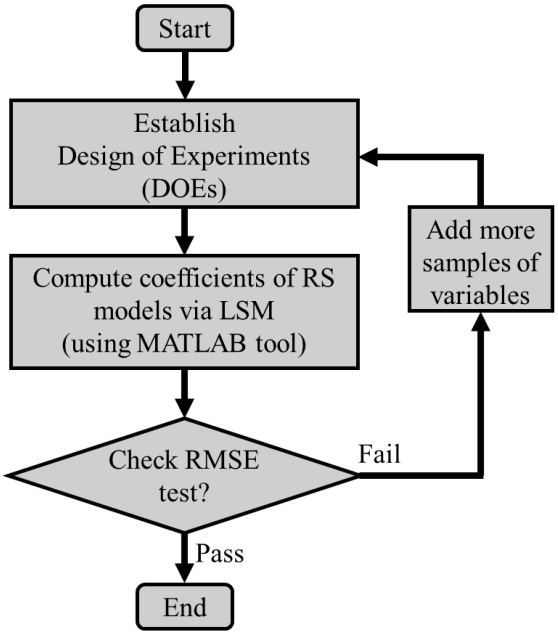

Fig. 4.8 Process Flow for Formation of RS Models

4.5.1 Establishment of Design of Experiments

Meta-models or surrogate models are designed to study relationship between machine design input parameters and output characteristics quantities. The RSM procedure incorporates the entirety of techniques when it is applied to the numerical statistics, obtained from a real-world phenomenon, representing a mathematical surface that is 'best fit'.

RSM is one of the approximation methods to determine mathematical relationship between response of interest and a set of input predictor variables, the relationship is given by:

$$Y = f(p_1, p_2, p_3, \dots, p_\rho) + \epsilon \tag{4.2}$$

Where Y denotes the required response; ϵ is the error between the approximate response and the experimental (true) response, $p_1, p_2, p_3, \dots p_\rho$ denote ρ variables and $f(p)$ is a second order polynomial function which is called response surface (RS). The polynomial function including the interaction terms of variables is given by:

$$f(p_1, p_2, p_3, \dots p_\rho) = \beta_0 + \sum_{k=1}^{\rho} \beta_k p_k + \sum_{k=1}^{\rho} \sum_{l=k+1}^{n} \beta_{kl} p_k p_l + \sum_{k=1}^{\rho} \beta_{kk} p_k^2 \tag{4.3}$$

Where β_0, β_k, β_{kl} and β_{kk} are coefficients, which are calculated by regression from the observations of the corresponding response. If $\beta_{kn} = 0$ for $k \leq \rho$ in Eq. 4.3, an approximate model of first order is obtained that fits planar surface. Since the true relation between $f(p)$ and vector of predictor variables is not known, the typical practice in such situations is to accomplish experimental objective, that is, to select an experimental design which consists of $u = 1,2, \dots j$

units of predictor variable settings $p_u = (p_{1u}, p_{2u}, \dots p_{\rho u})'$ and record the corresponding responses Y_u. Then the recorded data are employed to compute numerical values of coefficient vector β by implementing the LSM.

Generally, the '*experimental factors*' or '*conditions*' may include n number of predictor variables. They are combined to form the vector $p = (p_1, p_2, p_3, \dots p_\rho)'$. The domain of the experiment in which the vector p may vary while performing the experiment is expressed as χ which is a subset of Euclidean space of dimension ρ. A distinct vector $p = (p_1, p_2, p_3, \dots p_\rho)'$ in χ characterizes a setting for ρ predictor variables for which the specific response is being examined. Thus, experimental design is defined to perform ρ executions which involves ρ operating conditions or in other words, ρ empirical combinations of predictor variables for which ρ responses are observed and recorded.

In surrogate modelling technique, the number of experiments is decided on the basis of the closeness of values of determination factors R^2 and R^2_{adj}. (The mathematical expressions for R^2 and R^2_{adj} are explained in Section 4.5.2.) If the difference between these factors is not below 10^{-3}, then extra samples of design variables are added. This practice ensures that the meta-model obtained for a particular response of interest is accurate.

As mentioned earlier, PMSM-1 is intended to be used for compressor application in EVs. This requires high and steady torque output from the motor along with reduced unwanted cogging torque and ripple torque. Therefore, in PMSM-1, four GPs i.e., P_1 = magnetic pole eccentricity (distance between O_1 and O_2), P_2 = stator slot opening, P_3 = magnet thickness, P_4 = air gap length are varied because they effect the torque performance of the motor more than other parameters. The variable GPs are shown in Fig. 4.9. The values of determination factors are found to be close with an error of 0.0001 after performing 18 experiments. Therefore, FEM responses are computed for $d = 18$ experiments. The corresponding values of cogging torque T_c, ripple torque T_r and average torque T_a are computed for various set of variables $[\{P_1, P_2, P_3, P_4\}_j]_{1:d}$ which is referred to DOEs. The corresponding electromagnetic response of the motor with respect to the variation in considered GP dimensions are recorded in Table 4.3. These experiments aim to predict the outcome or response by the introduction of change in preconditions that is depicted in the form of design variables in this research exploration.

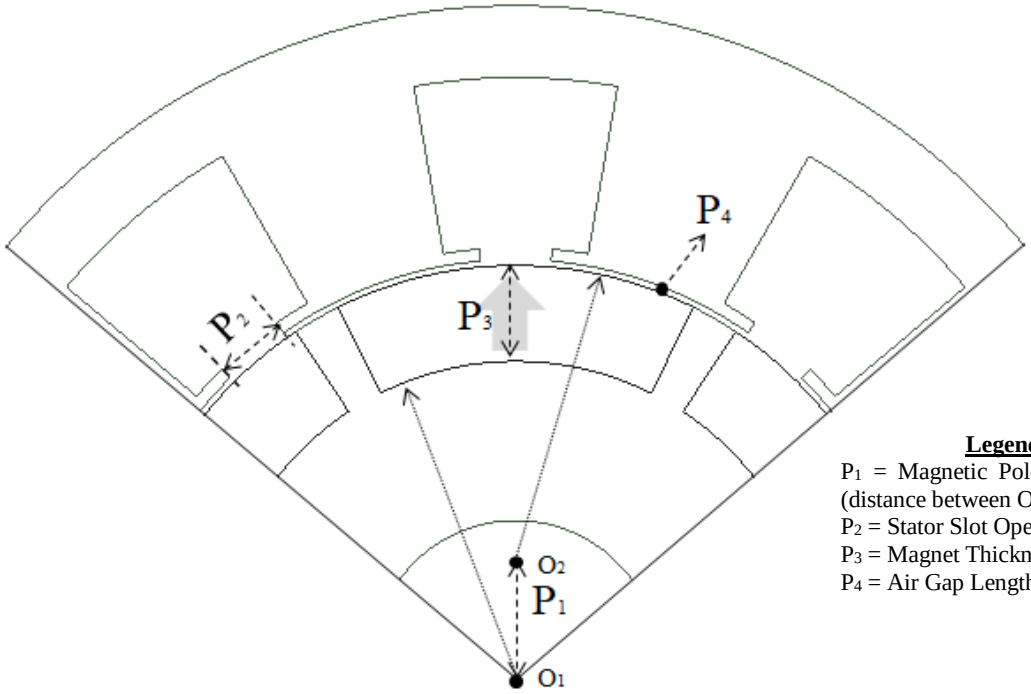

Fig. 4.9 Cross Section of one Pole of Preliminary design of PMSM-1

Table 4.3

Electromagnetic Performance for various FEM Experiments on PMSM-1

Iteration j	{P_1, P_2, P_3, P_4} (mm)	T_c (Nm)	T_r (pu)	T_a (Nm)
1	{0,6,6,2.5}	0.80	0.378	5.84
2	{0,6,2,0.5}	1.92	1.560	6.45
3	{0,3,4,1.5}	0.58	0.305	6.45
4	{0,3,2,0.5}	1.38	0.796	6.69
5	{0,1.5,2,2.5}	0.07	0.090	4.05
6	{0,1.5,6,1.5}	0.48	0.158	7.21
7	{2,6,4,0.5}	1.71	0.937	6.19
8	{2,6,6,2.5}	1.46	0.824	5.19
9	{2,3,6,0.5}	0.35	0.186	6.95
10	{2,3,4,1.5}	0.05	0.044	5.20
11	{2,1.5,6,1.5}	0.92	0.384	6.79
12	{2,1.5,4,2.5}	0.21	0.105	5.28
13	{4,6,6,1.5}	0.25	0.137	6.85
14	{4,6,4,2.5}	0.20	0.126	4.50
15	{4,3,2,0.5}	0.42	0.249	5.93
16	{4,3,2,1.5}	0.43	0.235	5.24
17	{4,1.5,4,0.5}	0.18	0.140	6.51
18	{4,1.5,2,2.5}	0.01	0.036	3.27

As specified earlier, PMSM-2 is designed for obtaining least core losses with improved torque performance in EV applications. The design parameters such as A = magnet width, B = pole embrace and C = stack length affect the torque performance and weight of the motor directly or

indirectly. But, the question of 'how stochastically do these parameters effect core loss in the motor' remained unanswered. Hence, to understand core loss response in PMSM-2 core loss RS model is designed by varying these design parameters. The design variables which are altered to establish the required DOE are shown in Fig. 4.10. In PMSM-2, the values of determination factors are found to be nearly equal (with error ≈ 0) after performing 36 experiments. Therefore, FEM responses are computed for 36 experiments to record the core loss in the motor. The FEM experiments and the corresponding core-losses are tabulated in Table 4.4.

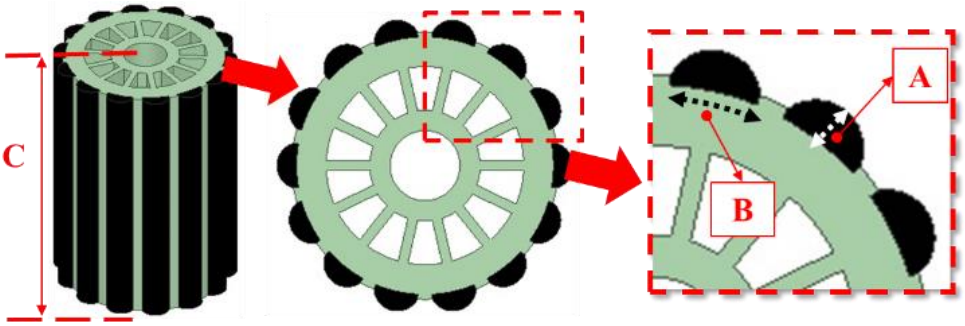

Fig. 4.10 Cross Section of PMSM-2 to Present Variable Design Parameters
(A = Radial Magnet Thickness, B = Pole Embrace and C = Stack Length)

Table 4.4

FEM Experiment Results for PMSM-2

(Units of A and C parameters are mm, B is unit-less)

Experiment	A	B	C	Core loss (mW)	Experiment	A	B	C	Core loss (mW)
1	3	0.65	150	123.4	19	6	0.65	150	87.7
2	3	0.75	150	119.5	20	6	0.75	150	85.4
3	3	0.65	160	131.6	21	6	0.65	160	93.6
4	3	0.85	160	123.0	22	6	0.85	160	88.1
5	3	0.75	170	135.4	23	6	0.75	170	96.8
6	3	0.85	170	130.7	24	6	0.85	170	93.6
7	4	0.65	150	108.2	25	7	0.65	150	80.3
8	4	0.75	150	104.7	26	7	0.75	150	78.3
9	4	0.65	160	115.4	27	7	0.65	160	85.7
10	4	0.85	160	108.2	28	7	0.85	160	81.1
11	4	0.75	170	118.7	29	7	0.75	170	88.7
12	4	0.85	170	114.9	30	7	0.85	170	86.2
13	5	0.65	150	96.9	31	8	0.65	150	74.2
14	5	0.75	150	93.9	32	8	0.75	150	72.3
15	5	0.65	160	103.4	33	8	0.65	160	79.2
16	5	0.85	160	97.1	34	8	0.85	160	75.2
17	5	0.75	170	106.4	35	8	0.75	170	82.0
18	5	0.85	170	103.2	36	8	0.85	170	79.9

Once the DOE is established, the β coefficients of RS models as expressed in (4.2) are computed using LSM. The details of LSM for estimating β coefficients are explained in next subsection.

4.5.2 Computation of Coefficients using Least Square Method

Polynomial models are used in regression analysis when the response variable is non-linear in nature. That is, for a given set of data, $(x_i, y_i); i = 1,2, \dots n$, first approach is to get the scatter plot. The scatter plot indicates the relationship between the response variable and the regression variable respectively. In general, k^{th} order polynomial in one variable is $y = \beta_0 + \beta_1 x + \beta_2 x^2 + \cdots + \beta_k x^k + \epsilon$. By setting, $x_j = x^j$, k^{th} order polynomial model in one variable becomes a Multiple Linear Regression (MLR) model with k regressors $x_1, x_2, \dots, x_k$, given as $y = \beta_0 + \beta_1 x_1 + \beta_2 x_2 + \cdots + \beta_k x_k + \epsilon$. So, fitting a k^{th} order polynomial is same as fitting a MLR model involving k regressors. There are several considerations while fitting an MLR, such as: what would be the order of the polynomial. It is suggested that the order of polynomial should be as low as possible. When the response variable is non-linear, i.e., when the scatter plot indicates non-linear relationship between response and the regressors, first some transformations are practiced to make the model linear. If it fails, then second order model should be considered. The polynomial fitting of model of very high degree is not recommended. Usually, the order of polynomial model is taken as less than or equal to 2. The next consideration is model building strategy. The first strategy suggests to start with fitting of a linear model, i.e., to start with $y = \beta_0 + \beta_1 x + \epsilon$. Then fitting of second order model, i.e., $y = \beta_0 + \beta_1 x + \beta_2 x^2 + \epsilon$ is carried out. Then the significance of the highest order term is tested. That is, in second order polynomial, the significance of β_2 is tested and if β_2 is found to be significant, then fitting of third order model, i.e., $y = \beta_0 + \beta_1 x + \beta_2 x^2 + \beta_3 x^3 + \epsilon$ is performed. But if β_2 is found to be non-significant, then the increment in the order of polynomial can be stopped at second order or polynomial model can be fixed to be of second order. So, model building strategy ensures the successive fit model of increasing order until the t test for the highest order term is non-significant [243]. The next consideration is the ill conditioning. It states that as the order of the polynomial increases, the $X'X$ matrix becomes ill conditioned. This simply means that the $X'X$ matrix becomes nearly singular, i.e., $(X'X)^{-1}$ calculation becomes inaccurate. If the values of x are limited to a narrow range, there can be significant ill conditioning problem in columns of X. This problem can be removed by centering the data. The model is fitted as $y = \beta_0 + \beta_1 (x - \bar{x}) + \beta_2 (x - \bar{x})^2 + \epsilon$, instead of $y = \beta_0 + \beta_1 x + \beta_2 x^2 + \epsilon$.

The RSM involves a collection of statistical and mathematical techniques having the response of interest being influenced by certain variables. Usually, the graphical representation of RS is plotted with respect to the variations in considered design variables. To aid the visualization of RS, the contours of RS are plotted as well. The contour plots consist of constant response lines drawn in the plane of variables. Re-writing equation (4.2) in matrix form in (4.4) yields:

$$\boldsymbol{y} = \boldsymbol{X\beta} + \boldsymbol{\epsilon} \tag{4.4}$$

Where, $\boldsymbol{y} = \begin{bmatrix} y_1 \\ y_2 \\ \vdots \\ y_n \end{bmatrix}$, $\boldsymbol{\beta} = \begin{bmatrix} \beta_1 \\ \beta_2 \\ \vdots \\ \beta_n \end{bmatrix}$, $\boldsymbol{\epsilon} = \begin{bmatrix} \epsilon_1 \\ \epsilon_2 \\ \vdots \\ \epsilon_n \end{bmatrix}$ and

$$\boldsymbol{X} = \begin{bmatrix} (1)_1 & (x_1)_1 & \dots & (x_k)_1 & (x_1x_2)_1 & \dots & (x_{k-1}x_k)_1 & (x_1^2)_1 & \cdots & (x_k^2)_1 \\ (1)_2 & (x_1)_2 & \dots & (x_k)_2 & (x_1x_2)_2 & \dots & (x_{k-1}x_k)_2 & (x_1^2)_2 & \cdots & (x_k^2)_2 \\ \vdots & \vdots & \vdots & \vdots & \vdots & \vdots & \vdots & \vdots & \vdots & \vdots \\ (1)_n & (x_1)_n & \dots & (x_k)_n & (x_1x_2)_n & \dots & (x_{k-1}x_k)_n & (x_1^2)_n & \cdots & (x_k^2)_n \end{bmatrix}.$$

The least square estimator, *L*, is aimed to be minimized, which is expressed as shown in (4.5). It is noticeable that *L* may also be solved as shown in (4.6).

$$L = \sum_{i=1}^{n} \epsilon_i^2 = \boldsymbol{\epsilon'\epsilon} = (\boldsymbol{y} - \boldsymbol{X\beta})'(\boldsymbol{y} - \boldsymbol{X\beta}) \tag{4.5}$$

$$L = \boldsymbol{y'y} - \boldsymbol{\beta'X'y} - \boldsymbol{y'X\beta} + \boldsymbol{\beta'X'X\beta} = \boldsymbol{y'y} - 2\boldsymbol{\beta'X'y} + \boldsymbol{\beta'X'X\beta} \tag{4.6}$$

The operator, *L*, is then minimized by differentiating it with respect to parameters of model and equating it to zero as given in (4.7) to (4.9).

$$\frac{\boldsymbol{\partial L}}{\boldsymbol{\partial \beta}}|_{\widehat{\boldsymbol{\beta}}} = -2\boldsymbol{X'y} + 2\boldsymbol{X'X\widehat{\beta}} = 0 \tag{4.7}$$

$$\boldsymbol{X'X\widehat{\beta}} = \boldsymbol{X'y} \tag{4.8}$$

$$\boldsymbol{\widehat{\beta}} = (\boldsymbol{X'X})^{-1}\boldsymbol{X'y} \tag{4.9}$$

The fitted regression model is given by:

$$\boldsymbol{\widehat{y}} = \boldsymbol{X\widehat{\beta}} \tag{4.10}$$

which is written in scalar notation given:

$$\hat{y}_i = \hat{\beta}_0 + \sum_{j=1}^{k} \hat{\beta}_j \, x_{ij} \tag{4.11}$$

The residual, $\boldsymbol{e}$, is computed by:

$$\boldsymbol{e} = \boldsymbol{y} - \boldsymbol{\widehat{y}} \tag{4.12}$$

The squared sum of residuals, SS_E, is calculated using:

$$SS_E = \sum_{i=1}^{n}(e_i)^2 = \sum_{i=1}^{n}(y_i - \hat{y}_i)^2 = \boldsymbol{e'e} = \boldsymbol{y'y} - \boldsymbol{\hat{\beta}'X'y} \quad (4.13)$$

The validation of regression model is carried out mathematically using the calculation of total (SS_T) and regression (SS_R) sum of squares as given in equations (4.14) and (4.15).

$$SS_T = \boldsymbol{y'y} - \frac{(\sum_{i=1}^{n} \boldsymbol{y_i})^2}{\boldsymbol{n}} \quad (4.14)$$

$$SS_R = SS_T - SS_E \quad (4.15)$$

The coefficient of multiple determination, R^2, is computed using :

$$R^2 = \frac{SS_R}{SS_T} = 1 - \frac{SS_E}{SS_T} \quad (4.16)$$

The adjusted coefficient of multiple determination, R^2_{adj}, is computed using:

$$R^2_{adj} = 1 - \frac{SS_E/(n-k)}{SS_T/(n-1)} \quad (4.17)$$

If the difference between R^2 and R^2_{adj} is found out to be relatively high, it indicates that insignificant terms have been included in the meta-models computations. Using the LSM implementation, the corresponding coefficient matrices are computed. The coefficient matrix analysis results are shown in Table 4.5 for PMSM-1 and in Table 4.6 for PMSM-2 respectively.

Table 4.5

Coefficients of RSM Models of PMSM-1

Coefficient	T_c(Nm)	T_r(pu)	T_a(Nm)	Coefficient	T_c(Nm)	T_r(pu)	T_a(Nm)
β_0	0.5694	0.6597	9.7675	β_{23}	-0.0344	-0.0338	-0.0562
β_1	0.3162	0.0094	-0.1547	β_{24}	-0.0378	-0.0378	0.0942
β_2	0.1073	0.2927	0.8645	β_{34}	-0.0179	0.0263	0.2523
β_3	-0.2140	-0.2850	-1.7086	β_{11}	-0.0461	-0.0054	-0.0427
β_4	0.2983	-0.2455	-1.7912	β_{22}	0.0423	0.0066	-0.1284
β_{12}	-0.0106	-0.0173	0.0533	β_{33}	0.0291	0.0299	0.1971
β_{13}	-0.0253	0.0089	0.0572	β_{44}	-0.0488	0.0621	0.0126
β_{14}	-0.0925	-0.0191	-0.0816				

Table 4.6

Coefficients of RSM Models of PMSM-2

Coefficient	y_2	Coefficient	y_2
β0	400.4877	β13	0.1171
β1	-37.9300	β23	-3.3156
β2	247.6950	β11	1.8694
β3	-4.0040	β22	203.5722
β12	-13.3768	β33	0.0208

4.5.3 MATLAB Implementation

The computation of corresponding $\boldsymbol{\beta}$ coefficient matrices, squared sum of residuals, SS_E, total sum of squares (SS_T) and regression sum of squares (SS_R), coefficient of multiple determination, R^2, and adjusted coefficient of multiple determination, R^2_{adj}, has been carried out via LSM (as explained in section 4.5.2) with the assistance of MATLAB R2016a tool. The basic outline of pseudo code is shown in Fig. 4.11. The response vector is fed into the code (line 4) along with the input parameter vectors (line 1). The code thus evaluates the regression model parameters (line 5 – line 6) and the corresponding parameters used for validation of regression models (line 7- line 13).

1 Input the k parameter vector(s) $\boldsymbol{x_1}, \boldsymbol{x_2}, \dots, \boldsymbol{x_k}$
2 Specify n (no. of experiments)
% Compute matrix **X**:
3 **for** j=1:termination value
for i=1:n
if j==1
X(i,j)=1;
end
if j==2
X(i,j)=$\boldsymbol{x_1}$(i,1);
end
:
if j==termination value
X(i,j)=$\boldsymbol{x_n}$(i,1)^2;
end
end
end
4 Input response vector(s) $\boldsymbol{y_1}, \boldsymbol{y_2}, \dots, \boldsymbol{y_m}$
% Compute coefficient vector(s) using Eq. (4.9):
5 **beta_hat**$_{\boldsymbol{m}} = inv(\boldsymbol{X}.'\boldsymbol{X}) * \boldsymbol{X}' * \boldsymbol{y_m}$
…**continued
…**continued
% Compute fitted model vector(s) using Eq. (4.3):
6 $\widehat{\boldsymbol{y}}_{\boldsymbol{1}}, \widehat{\boldsymbol{y}}_{\boldsymbol{2}}, \dots, \widehat{\boldsymbol{y}}_{\boldsymbol{m}}$
% Compute residual SS using Eq. (4.13):
7 **for** i=1:n
$SS_1 = \text{sum}(\boldsymbol{y_1}(\boldsymbol{i},\boldsymbol{1}) - \widehat{\boldsymbol{y}}_{\boldsymbol{1}}(\boldsymbol{i},\boldsymbol{1}))^2$;
:
$SS_m = \text{sum}(\boldsymbol{y_m}(\boldsymbol{i},\boldsymbol{1}) - \widehat{\boldsymbol{y}}_{\boldsymbol{m}}(\boldsymbol{i},\boldsymbol{1}))^2$;
8 **end**
% Compute RMSE values using Eq. (4.18)
9 rmse$_{\boldsymbol{m}} = sqrt(SS_m/n)$
% Compute total SS using Eq. (4.14):
10 $SS_m^T = (\boldsymbol{y_m}.'\boldsymbol{y_m}) - (\boldsymbol{sum}(\boldsymbol{y_m})^2/\boldsymbol{n})$
% Compute regression SS using Eq. (4.15):
11 $SS_m^R = SS_m^T - SS_m$
% Compute R^2 using Eq. (4.16):
12 $R\_sq_m = 1 - (SS_m/SS_m^T)$
% ComputeR^2_{adj}using Eq. (4.17):
13 $R\_ad\_sq_m = 1 - ((SS_m * (n-k))/(SS_m^T * (n-1)))$

Fig. 4.11 Pseudo Code for Surrogate Modelling using LSM

4.6 Root Mean Square Error Test Analysis

RMSE is defined as the square root of mean of squares of errors. The practice of computing RMSE is quite ubiquitous. It is considered an outstanding universal error criterion for predictions in numerical analysis. The mathematical representation of RMSE calculation is given by (4.18).

$$RMSE = \sqrt{\frac{1}{n}\sum_{i=1}^{n}(\boldsymbol{y} - \widehat{\boldsymbol{y}})^2} \tag{4.18}$$

Where $\boldsymbol{y}$ represents observed values of response, $\widehat{\boldsymbol{y}}$ represents predicted value of response and n represents number of experiments performed for analysis. RMSE gives an adequate estimation of accuracy. It is utilized to compare errors of predicted and original model or various configurations with respect to specific variables.

Once a surrogate model is designed, it is important to inspect the validity of that model. At initial stage of diagnosis, various values of model with respect to the DOE points are studied. This is a study that involves adjustment. For this, there are various criteria that are used to examine the fitted model between predicted and observed value of the data for accurate model construction. This particular role is fulfilled by coefficients of determination R^2 and R^2_{adj} along with the analysis of residuals and so on, explained by (4.15) and (4.16) respectively.

The corresponding results for coefficient of determination values obtained for T_c, T_r, T_a for PMSM-1 and core loss, P_c, for PMSM-2 are presented in Table 4.7. The corresponding RMSE results are presented in Fig. 4.12 for all response of interests. It is observed that RMSE values for all responses are lower (<1), which indicates the better predictive performance of surrogate models.

Table 4.7

Coefficients of Determination for Fitted Regression Models

Response	R^2	R_{adj}^2
T_c	0.9997	0.9998
T_r	0.9999	1.0000
T_a	0.9995	0.9996
P_c	0.9999	1.0000

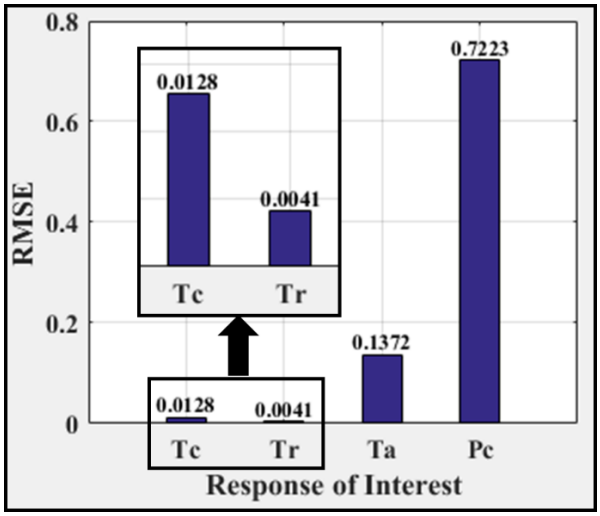

Fig. 4.11 RMSE Test Results for Responses of Interest

4.7 Conclusion

The design and development of two SI-PMSMs, one a smaller sized compressor motor used in the environment conditioning system and the second a larger traction motor used in the drive system of e-vehicles, having different ratings and configurations are discussed. The motor configurations, GP dimensions and material properties for initial designs are discussed. The

FEM analysis of preliminary designs is carried out to verify the appropriateness of the designed models. The torque performance, back-emf at low speed operation, flux linkage and mesh plots show the accurate electromagnetic behaviour of the models.

To obtain better electromagnetic performance of the models, the variation in GP dimensions is carried out. It is found that even the small change of nearly 1 mm in various design parameters shows noticeable variation in electromagnetic performance of the motor. However, if GP dimensions of models are repeatedly changed, the task of redesigning and re-analysing the altered models becomes time consuming.

Therefore, the meta-models of various output characteristic parameters are designed using RSM scheme. Various experiments are performed to obtain FEM results with respect to variations of design parameters. Hence, using the DOEs, the necessary β coefficients of RSM are obtained for corresponding output parameters via LSM. The verification of meta-models is carried out using RMSE test. The test result shows the meta-models obtained do not contain any unwanted parameter.

Chapter 5

Design Optimization of PMSM-1 using Integrated Taguchi Method Assisted Polynomial Metamodeling and Genetic Algorithm Technique

5.1 General

The previous chapter covered the design and development of the preliminary model of PMSM-1 and its FEM analysis, in addition to development of the meta-models of different performance parameters such as cogging torque, ripple torque and average torque. PMSM-1 is the smaller motor designed for use as compressor in EVs for environment conditioning. This chapter presents the design optimization of the developed preliminary model of PMSM-1 using a novel Integrated Taguchi Method assisted Polynomial Metamodeling and Genetic Algorithm (ITM&GA) optimization Technique.

Taguchi Method is a statistical design optimization method, which facilitates the determination of optimum settings for multiple design variables, thus aiding the design process. It enables the user to extract the advantageous working points of design variables at which the model has the possibility of obtaining optimal values of the objectives [244]. However, there is uncertainty in obtaining the accurate or best optimal values of design parameters since the determination of optimum objective value is not clear in the vicinity of these working points and objective value may converge to local optima. In other words, it involves ambiguity in obtaining the convergence of the solution in between these working points of the variables. For addressing this issue, an intelligent optimization technique called ITM&GA is designed to obtain the accurate optimum solutions.

For reducing time and effort of redesigning the time-consuming FEM models, the surrogate models are computed, as given in Chapter 4. The experiments conducted by Taguchi Method plays the role of assistant to obtain the required response of interest by RSM. The optimum values of design parameters are thus obtained by applying Genetic Algorithm, which utilizes the meta-models as fitness functions of the parent/offspring generations.

ITM&GA technique is successfully used for improvement of torque performance of PMSM-1 in addition to reduction of unwanted ripples in torque and cogging torque.

5.2 ITM&GA Optimization Mechanism

The ITM&GA procedure has two phases: Phase I and Phase II, details of which are given in the subsequent paragraphs. Execution of Phase I assists Phase II mechanism outflow.

In Phase I, the DOEs are obtained by setting the levels of design variables using conventional Taguchi Method. The corresponding performance parameters are recorded using FEM analysis. The surrogate models are then designed using LSM technique. In other words, by taking rows of Orthogonal Array (OA) as input and corresponding FEM analysis results as output, meta-models are designed for all the objectives in Phase I. The surrogate models are assigned as fitness functions.

In Phase II, the conventional Genetic Algorithm (GA) is implemented. The new generations of initial population and their fitness are computed by setting various GA parameters via selection, crossover and mutation processes until termination criteria is satisfied. The proposed novel ITM&GA optimization process follows these two phases as shown in Fig. 5.1.

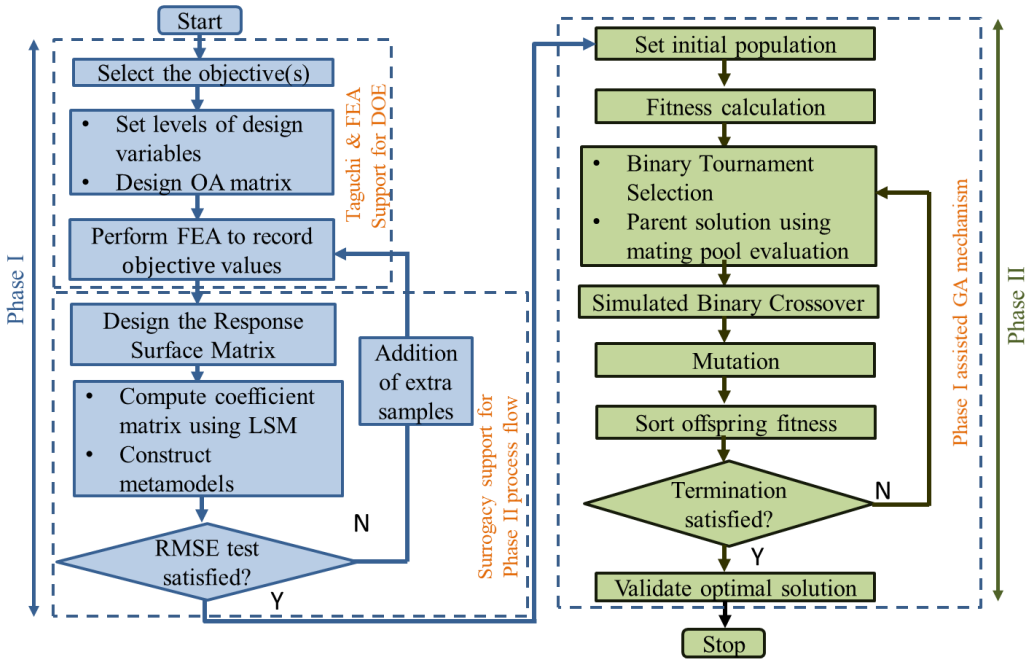

Fig. 5.1 Process Flow for Novel ITM&GA Technique

5.3 Formulation of Experiment

The main function of compressor in the environment conditioning system in EVs is to inject the refrigerant under high pressure into the condenser. An elliptical disc, tilted at an angle to the central axis, called '*swash plate*' moves the internal pistons up and down parallel to the drive

shaft. In conventional ICE based vehicles, the engine force rotates these internal parts of the compressor, which results in increased fuel consumption and poor economy. To eliminate this problem, electric compressor is employed in EVs. It operates even during the idling stop condition accruing better fuel efficiency and a better environment controlled air-conditioned cabin of the vehicle.

Figs. 5.2(a) and 5.2(b) show the schematic layout of electric compressor system employed in EV and image of a typical PMSM used in electric compressor, respectively. PMSM-1 used in this research study is 6 poles, 9 slots SI-PMSM, designed with concentrated winding arrangement in stator. The specifications of the preliminary model are given in Table 4.1.

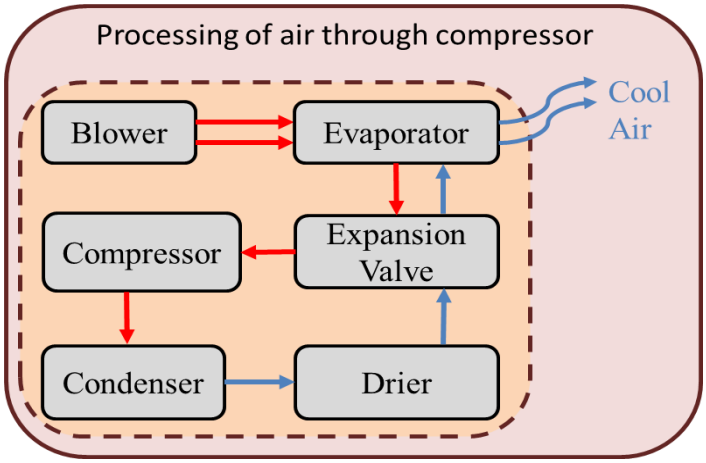

(a)

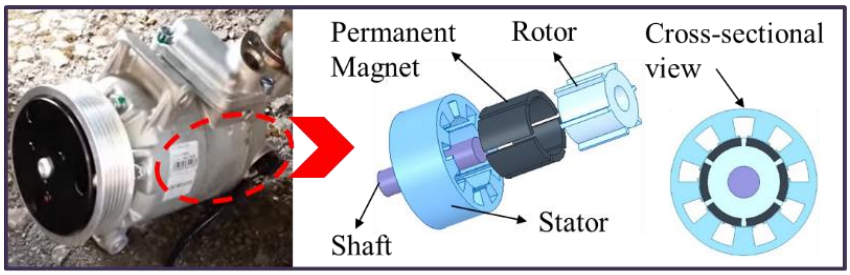

(b)

Fig. 5.2 Electric Compressor System of EV; (a) Working Principle (b) Typical PMSM used in Electric Compressor

Considering reference temperature to be $20^0\ C$, the initial dimensions of model design are selected to satisfy the given environmental conditioning application conditions. This application needs smooth torque operation of electric motor with least torque ripple and cogging torque. The objective functions for this study are defined by (5.1). The GP dimensions used as constraints to optimize the model are depicted in Fig. 5.3.

- Objective functions:
  - Maximize the torque, T_a
  - Minimize the torque ripple, T_r
  - Minimize the cogging torque, T_c (5.1)
- Constraints:
  - $0\ mm \leq P_1 \leq 4\ mm$
  - $1.5\ mm \leq P_2 \leq 6\ mm$
  - $2\ mm \leq P_3 \leq 6\ mm$
  - $0.5\ mm \leq P_4 \leq 2.5\ mm$

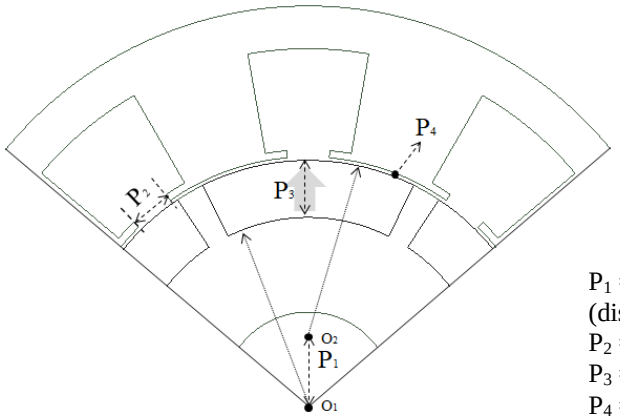

Legend
P_1 = Magnetic Pole Eccentricity (distance between O_1 and O_2)
P_2 = Stator Slot Opening
P_3 = Magnet Thickness
P_4 = Air Gap Length

Fig. 5.3 Cross Section of a Pole of Preliminary Model of PMSM-1

5.4 Implementation of ITM&GA Technique

This section elucidates the phase-wise implementation of the ITM&GA optimization technique for PMSM-1. The subsequent subsections present the analysis results and discussions.

5.4.1 Experiments using Taguchi Method

Taguchi method is a competent statistical design technique. In Phase I of ITM&GA technique, it facilitates to employ the Design of Experiments (DOEs) by systematically setting the levels of controlling factors, i.e., design variables to form the OA. For the generated OA, FEM simulations are carried out using ANSYS Maxwell 9.0 to record the response of the motor for various objective parameters.

Table 5.1 presents the level setting of design parameters and their feasible ranges. In Table 5.2, OA of parameters and corresponding values of T_c, T_r and T_a obtained by FEM analysis are reported.

Table 5.1

Levels of Design Variables

(all units in mm)

Parameters	Feasible Range	Level 1	Level 2	Level 3
P_1	[0,4]	0	2	4
P_2	[1.5,6]	6	3	1.5
P_3	[2,6]	6	4	2
P_4	[0.5,2.5]	0.5	1.5	2.5

Table 5.2

Motor Performance for various Taguchi Experiments

Experiment	{P_1, P_2, P_3, P_4} (mm)	Tc (Nm)	Tr (pu)	Ta (Nm)
1	{0,6,6,2.5}	0.80	0.378	5.84
2	{0,6,2,0.5}	1.92	1.560	6.45
3	{0,3,4,1.5}	0.58	0.305	6.45
4	{0,3,2,0.5}	1.38	0.796	6.69
5	{0,1.5,2,2.5}	0.07	0.090	4.05
6	{0,1.5,6,1.5}	0.48	0.158	7.21
7	{2,6,4,0.5}	1.71	0.937	6.19
8	{2,6,6,2.5}	1.46	0.824	5.19
9	{2,3,6,0.5}	0.35	0.186	6.95
10	{2,3,4,1.5}	0.05	0.044	5.20
11	{2,1.5,6,1.5}	0.92	0.384	6.79
12	{2,1.5,4,2.5}	0.21	0.105	5.28
13	{4,6,6,1.5}	0.25	0.137	6.85
14	{4,6,4,2.5}	0.20	0.126	4.50
15	{4,3,2,0.5}	0.42	0.249	5.93
16	{4,3,2,1.5}	0.43	0.235	5.24
17	{4,1.5,4,0.5}	0.18	0.140	6.51
18	{4,1.5,2,2.5}	0.01	0.036	3.27

By conducting 18 FEM experiments, the recorded results are analysed through Analysis of Means (AOM) and Analysis of Variance (AOVA). The mean of data is calculated using (5.2) for all the quantities under observation; where $T(j)$ denotes T_c, T_r and T_a characteristics of the motor for j^{th} iteration. In this analysis, to calculate the average effect of design parameters P_i on T_c, T_r and T_a, the mean values of $T(j)$ for i^{th} level is computed using (5.3).

$$\mu = \frac{1}{18}\sum_{j=1}^{18} T(j) \tag{5.2}$$

$$\mu_{P_i} = \frac{1}{6}\sum_{j=1}^{6} T(j) \tag{5.3}$$

For example, to calculate effect of magnet thickness on cogging torque, for level of $P_3 = 4\ mm$, which appears in 3^{rd}, 7^{th}, 10^{th}, 12^{th}, 14^{th} and 17^{th} experiment, the mean is calculated using (5.4). AOM values for cogging torque, torque ripple and average torque for all levels of set values are presented in Table 5.3. The pictorial representation of AOM results is shown in Fig. 5.4.

$$\mu_{P_3} = \frac{1}{6}(T_{c_3} + T_{c_7} + T_{c_{10}} + T_{c_{12}} + T_{c_{14}} + T_{c_{17}}) \tag{5.4}$$

Table 5.3

AOM Results for all Levels of Parameters

Cogging Torque (Nm)				
Level *i*	**P_1**	**P_2**	**P_3**	**P_4**
1	0.87	1.06	0.71	0.99
2	0.78	0.53	0.49	0.45
3	0.25	0.31	0.70	0.46
Torque Ripple (pu)				
1	0.55	0.66	0.34	0.64
2	0.41	0.30	0.28	0.21
3	0.15	0.15	0.49	0.26
Torque (Nm)				
1	6.11	5.84	6.47	6.45
2	5.93	6.08	5.69	6.29
3	5.38	5.52	5.27	4.69

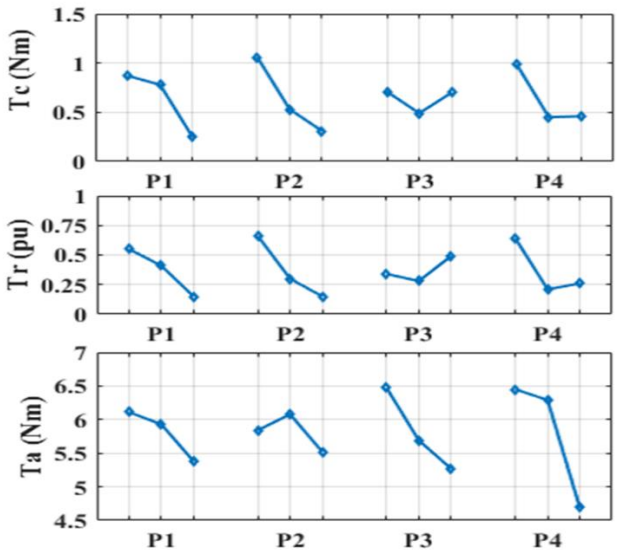

Fig. 5.4 Plots for AOM results of Taguchi Method

It is observed that value of cogging torque decreases up to 0.25 Nm with increase in P_1, P_2 and P_4 levels and with increase in P_3 level values, it decreases up to 0.49 Nm and then increases to 0.7 Nm. Torque ripple also decreases up to 0.15 pu with increase in the levels of parameters. The value of torque also decreases up to 4.69 Nm with increase in levels of parameters P_1, P_2, P_3 and P_4.

Further, AOVA is performed to obtain a clear vision of effects of parameters on different output quantities. The Factor Effect Ratio (FER) is computed using variance (Var), to check the effect of particular parameter over the calculation of the output quantity under observation. Variance gives the measurement of spread out of experiments with respect to their mean value. For i^{th} level, the variance, Var_{P_i} of parameter present at j^{th} iteration is calculated using (5.5). where μ and μ_{P_i} are calculated using (5.2) and (5.3) respectively. Use of variance in AOVA makes the calculation simpler and less time consuming. Thus, more accurate results are obtained. Table 5.4 shows the various calculated FER with respect to the variance of each quantity for all levels of parameters.

$$Var_{P_i} = \frac{1}{va-1}\sum_{j=1}^{va}\left(\mu_{P_i} - \mu\right)^2 \qquad ; va = 3 \tag{5.5}$$

Fig. 5.5 shows FER as a graphical representation for T_c, T_r and T_a, where the bars represent value of FER of corresponding torque. It is observed that P_1 has more effect on T_c (30.2%) whereas P_2 has nearly similar effect on T_c and T_r (approximately 40%). Both P_3 and P_4 have major effects on T_a (25.6% and 68.4% respectively). Thus, out of possible combinations of design parameters, the best combination is chosen. For this, the need to re-design the model with possible optimum dimensions can be eliminated. This is done by establishing a relationship between the response of interest (that represents torques here) and a set of input design variables. This methodology is implemented in the next section.

Table 5.4

Effects of Various Parameters on Motor Performance

Parameters	**T_c**		**T_r**		**T_a**	
	Var	**FER**	**Var**	**FER**	**Var**	**FER**
P_1	0.11225	30.2%	0.0412	23.3%	0.14465	3.8%
P_2	0.14865	40.0%	0.0687	38.8%	0.07895	2.1%
P_3	0.01545	4.1%	0.0117	6.6%	0.9602	25.6%
P_4	0.09545	25.7%	0.0553	31.3%	2.5672	68.4%
Total	0.3718	100%	0.1769	100%	3.751	100%

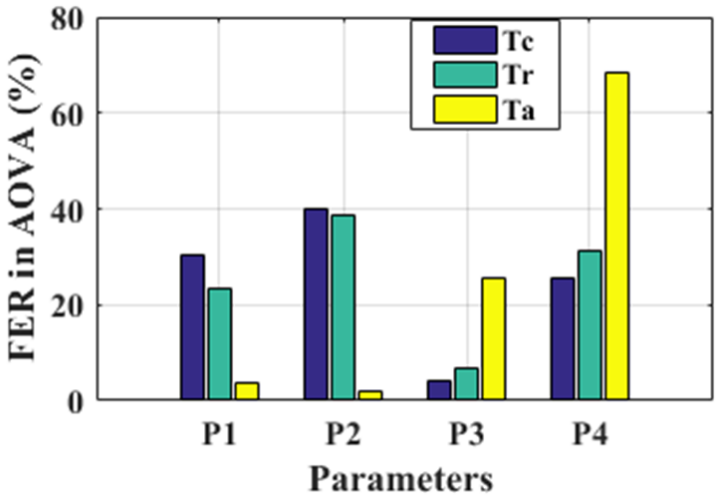

Fig. 5.5 Graphical Representation of FER values using AOVA

5.4.2 Metamodeling

Meta-models or surrogate models are designed to study relationship between machine design input parameters and output characteristics quantities. RSM is one of the approximation methods used to determine the mathematical relationship between response of interest and a set of input variables, the relationship is given as:

$$Y = f(p_1, p_2, p_3, p_4) + \epsilon \tag{5.6}$$

Where Y denotes T_c, T_r and T_a; ϵ is the error term, p_1, p_2, p_3, p_4 denote four design variables and $f(p)$ is a second order polynomial function which is called response surface. The polynomial function including the interaction terms is given by:

$$f(p_1, p_2, p_3, p_4) = \beta_0 + \sum_{k=1}^{4} \beta_k p_k + \sum_{k=1}^{4} \sum_{l=k+1}^{4} \beta_{kl} p_k p_l + \sum_{k=1}^{4} \beta_{kk} p_k^2 \tag{5.7}$$

Where β_0, β_k, β_{kk} and β_{kl} are coefficients, which are calculated by regression from the observations of the response. For developing meta-models of output responses in PMSM-1, FEM results were computed for $n = 18$ experiments to calculate T_c, T_r and T_a for various set of variables $[\{p_1, p_2, p_3, p_4\}_j]_{1:n}$, referred as DOEs. The coefficient matrix is typically computed using LSM. The coefficients of response surface models of motor parameters estimated from regression are shown in Table 4.5.

The meta-models for all the responses of interest are given by (5.8), (5.9) and (5.10) respectively. Here, $\widehat{Y_1}$, $\widehat{Y_2}$ and $\widehat{Y_3}$ corresponds to cogging torque, ripple torque and average torque respectively. On comparison with Fig.4.11, it is observed that the RMSE values for three responses of interest are lower after implementation of the optimization technique as given here

in. Lower values of RMSE signifies that the residual data are not spread out. The data are more concentrated around the best fit line. So, it indicates the appropriate performance of the surrogate models.

$$\widehat{Y_1} = 0.5694 + 0.3162P_1 + 0.1073P_2 - 0.214P_3 + 0.2983P_4 - 0.0106P_1P_2 - 0.0253P_1P_3 - 0.0925P_1P_4 - 0.0344P_2P_3 - 0.0378P_2P_4 - 0.0179P_3P_4 - 0.0461P_1^2 + 0.0423P_2^2 + 0.0291P_3^2 - 0.0488P_4^2 \quad (5.8)$$

$$\widehat{Y_2} = 0.6597 + 0.0094P_1 + 0.2927P_2 - 0.285P_3 - 0.2455P_4 - 0.0173P_1P_2 + 0.0089P_1P_3 - 0.0191P_1P_4 - 0.0338P_2P_3 - 0.0378P_2P_4 + 0.0263P_3P_4 - 0.0054P_1^2 + 0.0066P_2^2 + 0.0299P_3^2 + 0.0621P_4^2 \quad (5.9)$$

$$\widehat{Y_3} = 9.7675 - 0.1547P_1 + 0.8645P_2 - 1.7086P_3 - 1.7912P_4 + 0.0533P_1P_2 + 0.0572P_1P_3 - 0.0816P_1P_4 - 0.0562P_2P_3 + 0.0942P_2P_4 + 0.2523P_3P_4 - 0.0427P_1^2 - 0.1284P_2^2 + 0.1971P_3^2 + 0.0126P_4^2 \quad (5.10)$$

The various torque contour and surface plots are presented in Fig. 5.6, where regions of maximum torque, minimum ripple and minimum cogging torque are identified. In conventional Taguchi method, out of possible combinations of design parameters, their best combination is estimated. Whereas, in ITM&GA, the meta-models of output parameters, computed in Phase I, are utilized as fitness functions for obtaining their best optimum values in the feasible range of design parameters.

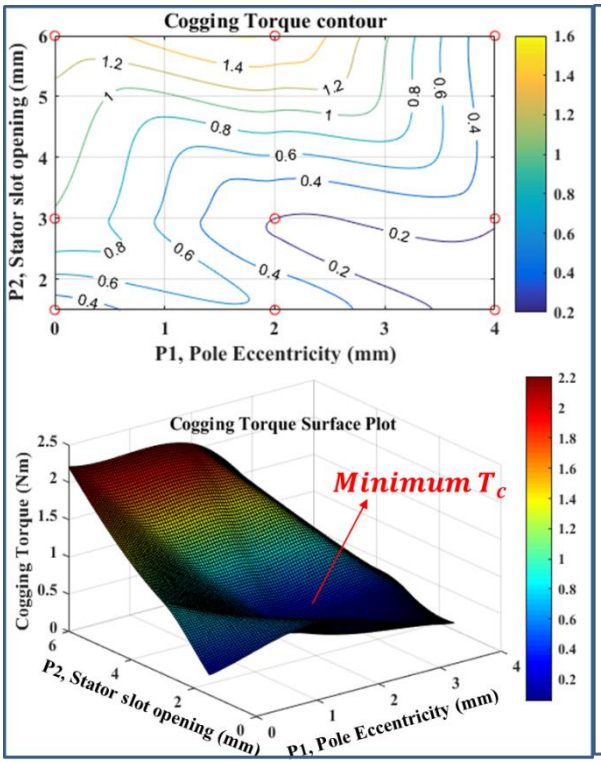
Cogging Torque contour
P2, Stator slot opening (mm)
P1, Pole Eccentricity (mm)
Cogging Torque Surface Plot
Minimum T_c
Cogging Torque (Nm)
P2, Stator slot opening (mm)
P1, Pole Eccentricity (mm)

(a)

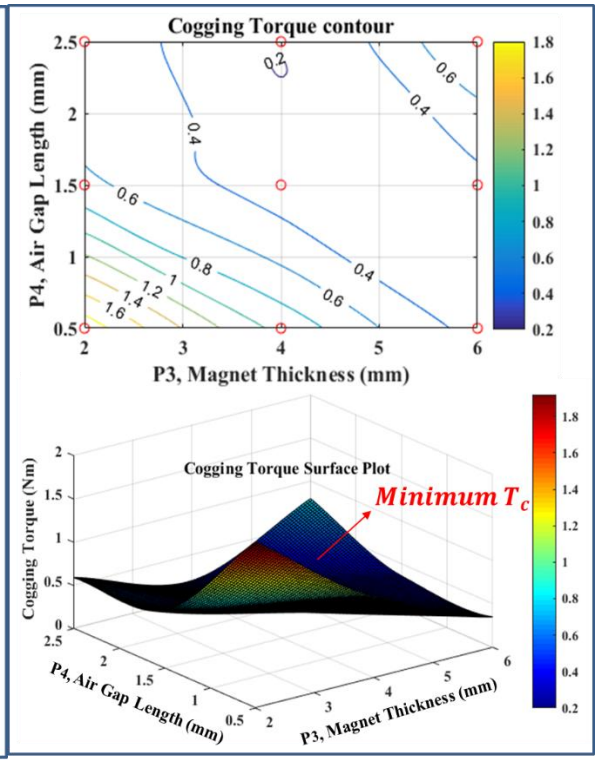
Cogging Torque contour
P4, Air Gap Length (mm)
P3, Magnet Thickness (mm)
Cogging Torque Surface Plot
Minimum T_c
Cogging Torque (Nm)
P4, Air Gap Length (mm)
P3, Magnet Thickness (mm)

(b)

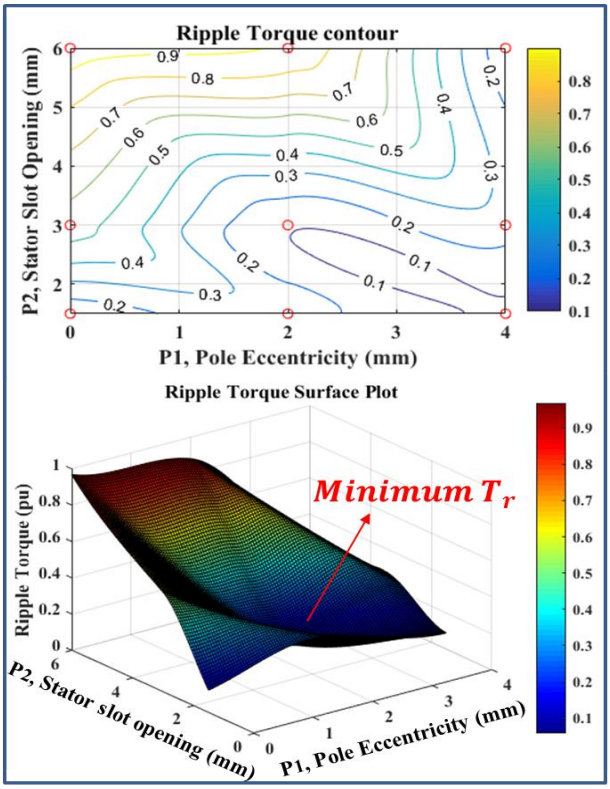
Ripple Torque contour
P2, Stator Slot Opening (mm)
P1, Pole Eccentricity (mm)
Ripple Torque Surface Plot
Minimum T_r
Ripple Torque (pu)
P2, Stator slot opening (mm)
P1, Pole Eccentricity (mm)

(c)

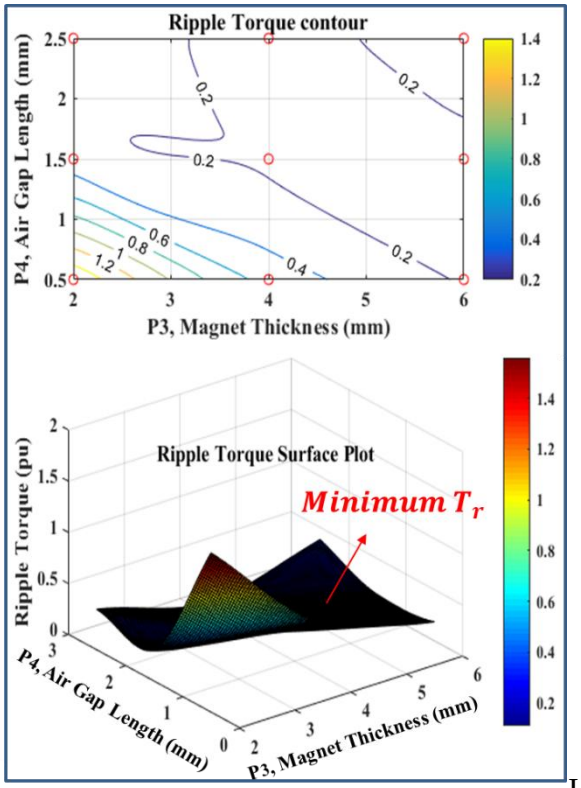
Ripple Torque contour
P4, Air Gap Length (mm)
P3, Magnet Thickness (mm)
Ripple Torque Surface Plot
Minimum T_r
Ripple Torque (pu)
P4, Air Gap Length (mm)
P3, Magnet Thickness (mm)

I

(d)

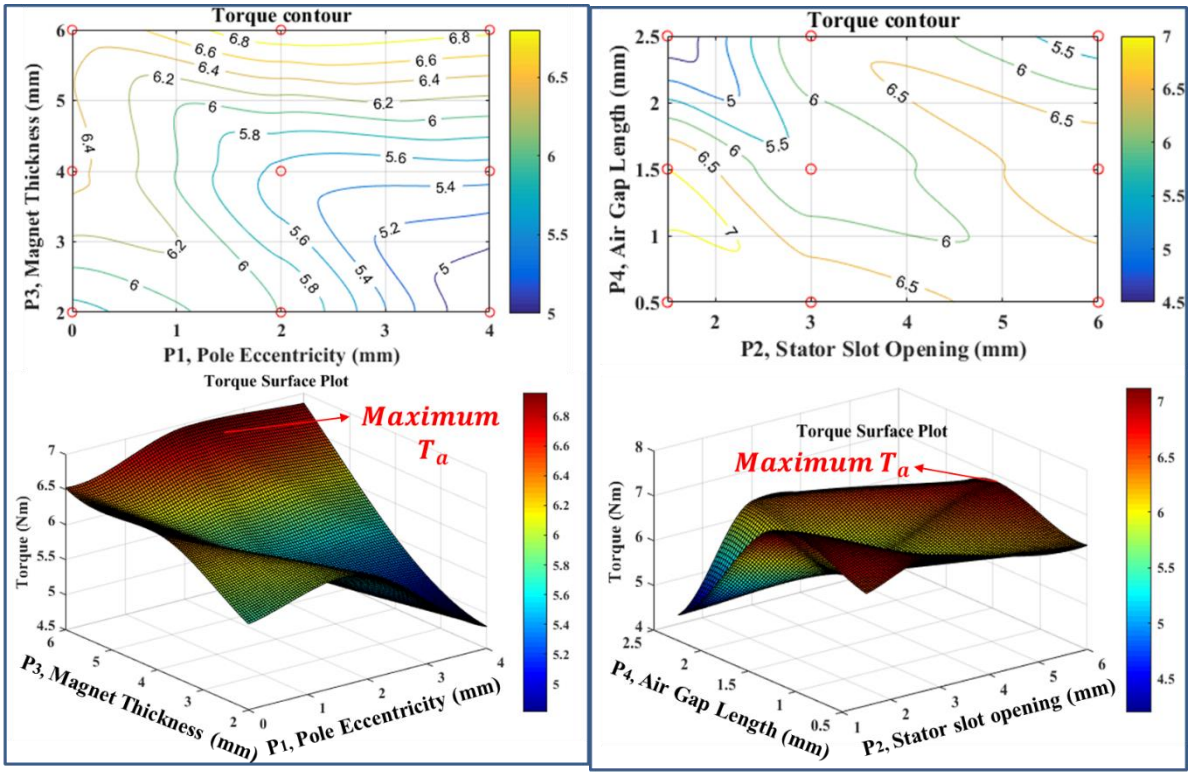

(e) (f)

Fig. 5.6 Contour and Surface plots for Variations in Design Parameters of PMSM-1: (a) Cogging Torque Plots for Variation in P1 & P2 (b) Cogging Torque Plots for Variation in P3 & P4 (c) Ripple Torque Plots for Variation in P1 & P2 (d) Ripple Torque Plots for Variation in P3 & P4, I Torque Plots for Variation in P1 & P3 (f) Torque Plots for Variation in P2 & P4

5.4.3 Phase II – GA

In Phase II, the formation of initial population matrix, consisting of values of design variables, is done stochastically within the specified lower (L_1) and upper (U_1) bounds. Each row of this matrix is assigned as a sequential chromosome, which corresponds to a string of variable parameters. Thereafter, the fitness values of these chromosomes are computed using the fitness functions obtained using the support of Taguchi assisted polynomial Meta-models (Phase I).

Binary Tournament scheme is employed for the 'Selection' stage to retrieve the mating pool. Once the parent solution is obtained, the 'Simulated Binary Crossover' (SBX) occurs to generate offspring.

For this, two parent agents $Parent_1 = [Parent_{1,1}, Parent_{1,2}, Parent_{1,3}, Parent_{1,4}]$ and $Parent_2 = [Parent_{2,1}, Parent_{2,2}, Parent_{2,3}, P_{2,4}]$ are picked randomly by SBX. The generation of each element of offspring Off_1 and Off_2 is performed using (5.11).

$$Off_1 = 0.5 \times [(1 + cf) \times Parent_1 + (1 - cf) \times Parent_2]$$

$$Off_2 = 0.5 \times [(1 - cf) \times Parent_1 + (1 + cf) \times Parent_2] \quad (5.11)$$

Where cf is the crossover SBX controlling factor, computed by (5.12).

$$cf = \begin{cases} (2r_1)^{\frac{1}{(\eta_c+1)}} & ; if\ r_1 \leq 0.5 \\ (\frac{1}{2(1-r_1)})^{\frac{1}{(\eta_c+1)}} & ; otherwise \end{cases} \quad (5.12)$$

where r_1 is random number, η_c is the distribution index for crossover. Then the offspring undergo 'Mutation' stage. The mutation population should ensure the new offspring to be different from parents for comprising diverse population for the betterment of the convergence [29]. Each offspring agent is mutated to produce mutated offspring Off_m from offspring vector $Off = [Off_1, Off_2]$ using (5.13).

$$Off_m = Off + (U_1 - L_1) \times \Delta \quad (5.13)$$

Where Δ is the mutation control factor, calculated as:

$$\Delta = \begin{cases} (2r_2)^{\frac{1}{(\eta_m+1)}} - 1 & ; if\ r_2 < 0.5 \\ 1 - [2(1 - r_2)]^{\frac{1}{(\eta_m+1)}} & ; if\ r_2 \geq 0.5 \end{cases} \quad (5.14)$$

Where r_2 is random number, η_m is the distribution index for mutation. The combined population is obtained and is sorted non-dominantly. Thus, the best solution vector is updated. Various operational parameters of GA are shown in Table 5.5. The Pseudo code for Phase II of ITM&GA is shown in Fig. 5.7.

Table 5.5

GA Parameters

Parameters	**Values**
Population size	50
Fitness Function	Meta-models
Number of generations	100
Crossover probability	0.8
Distribution index for crossover, η_c	20
Mutation probability	0.2
Distribution index for mutation, η_m	20
Selection scheme	Binary tournament selection

Pseudo code of Phase II

Input: f_{obj}, x (initial population),
n (size of population), T(number of generations)
Output: x_b (best solution), f_b (best fitness)
Generate x randomly
Initialize parameters
Compute fitness
While (termination criteria ← not satisfied)
  Compute parent solution, x
  (using binary tournament selection)
  Generate offspring solution, x
  (using Eq. (5.11))
  Compute mutated offspring solution, x_m
  (using Eq. (5.13))
  $x \leftarrow x \cup x_m$
  Compute fitness of offspring x
  sort fitness of new x
  select n solutions from new x
  examine and renew fitness
  $t = t + 1$
end while
Return x_b and f_b

Fig. 5.7 Implementation of Phase II of ITM&GA

5.5 Analysis of Initial and Optimal Model Performance

This section presents the comparative analysis of initial and optimized models of PMSM-1. The optimization is carried out by both Traditional Taguchi Method (TTM) and ITM&GA techniques for fair comparison. The corresponding results are presented for no load as well as rated torque conditions.

Electromagnetic field simulation software ANSYS Maxwell (v9.0, Canonsburg, USA) is used to generate the characteristics of the motor with two-dimensional FEM analysis to validate the analytical and optimized model. Analytical accuracy is ensured by including high quality meshes with 14,996 elements.

5.5.1 Analysis at No Load Condition

The shape of back emf waveform is an important factor, which influences the torque characteristics [245]. When back emf waveform has lesser distortion and is closer to sinusoidal shape, the ripples in torque gets reduced. The preliminary model of PMSM-1 had back-emf with peak-to-peak value (V_{pk2pk}) of 97.6 V with THD = 28 % while optimal model obtained by TTM has V_{pk2pk} = 89.7 V with THD = 8.9 % and optimal model obtained by ITM&GA has V_{pk2pk} = 91.9 V with THD = 5%. Fig. 5.8 (a) and (b) show the waveform of back-emf and back emf distribution ratio for each harmonic order on the basis of THD analysis of the waveforms.

The comparison of cogging torque characteristics is shown in Fig. 5.9. The optimal models have cogging torque of 0.23 Nm (by TTM) and 0.2 Nm (by ITM&GA) which is less than 0.79 Nm, i.e., cogging torque of initial model. Cogging torque of initial model is reduced by 74.7 % using ITM&GA and by 70.8 % using TTM.

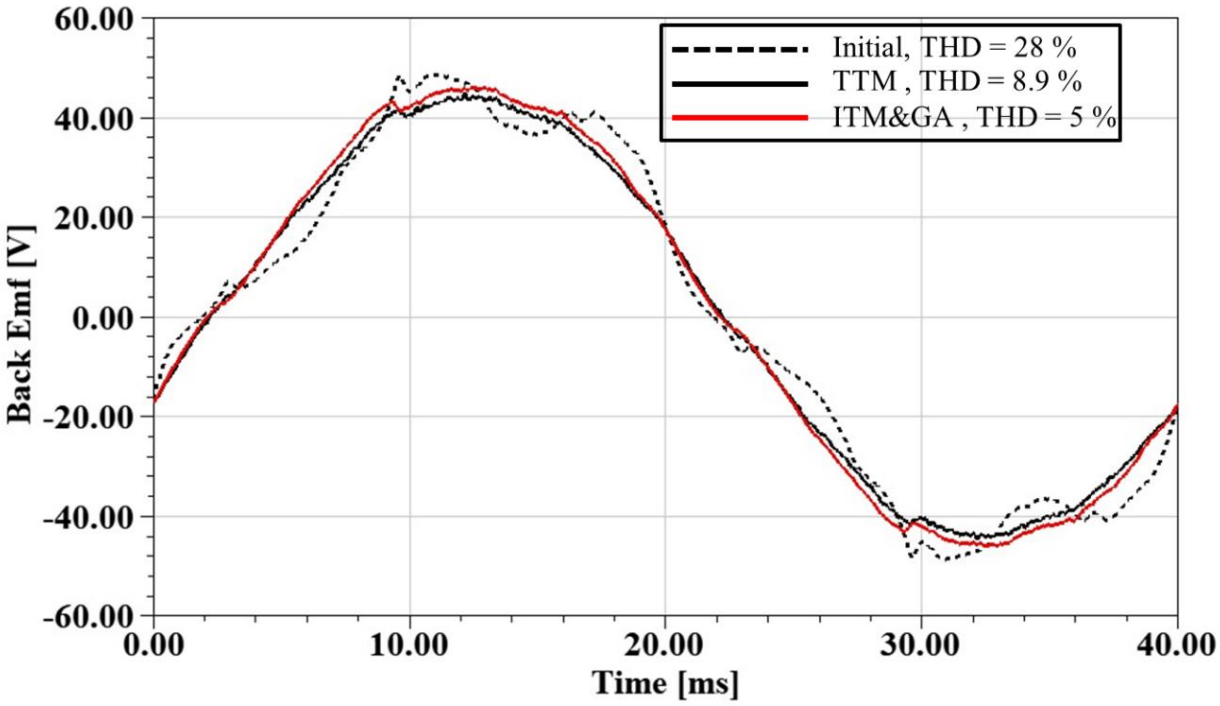

(a)

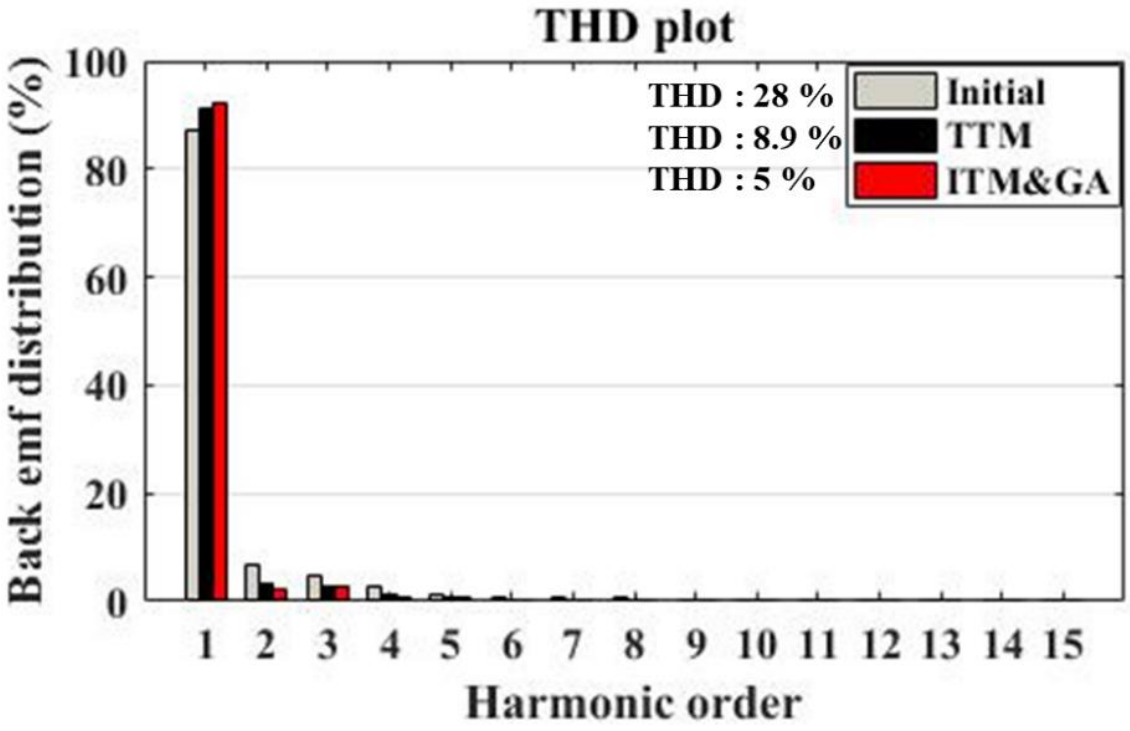

(b)

Fig. 5.8 Induced Voltage Waveforms of Preliminary and Optimal Models of PMSM-1 under No Load Conditions (rotational speed = 500 rpm) (a) Waveforms (b) THD plots

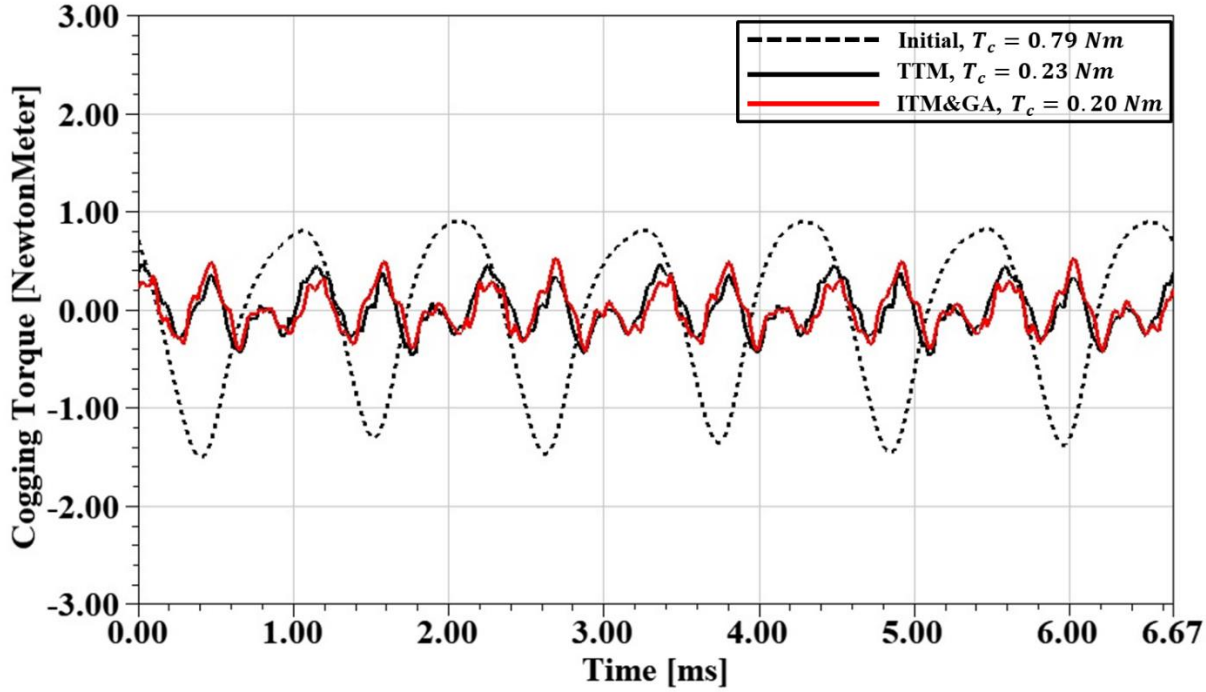

Fig. 5.9 Comparison of Cogging Torque Characteristics

5.5.2 Analysis at Rated Condition

For compressor application in EVs, the characteristics of load is constant torque in nature with least ripples [246]. Owing to this requirement, the motor is run at rated speed. The comparison of torque characteristics of optimal and initial models is shown in Fig. 5.10. It is observed that torque is improved by 27.8% by TTM and 31% by ITM&GA. The ripples in torque are reduced by 85.7% by TTM and 92.8% when compared with the initial model. The parameters and objective values from initial and optimized models obtained by TTM and ITM&GA are compared in Table 5.6. It is observed that using the proposed ITM&GA technique results in better torque performance of the motor. The constructional features of the preliminary and optimised models of PMSM-1are presented in Fig. 5.11.

Table 5.6

Performance of Preliminary and Optimised Models of PMSM-1

Parameters/ Response	Initial model	Optimal models	
		TTM	ITM&GA
$\{P_1,P_2,P_3,P_4\}$	{0,6,6,2.5}	{4,1.5,6,0.5}	{3.8,2.3,5.7,0.8}
T_c	0.80	0.23	0.20
T_r	0.38	0.14	0.12
T_a	5.82	7.44	7.62

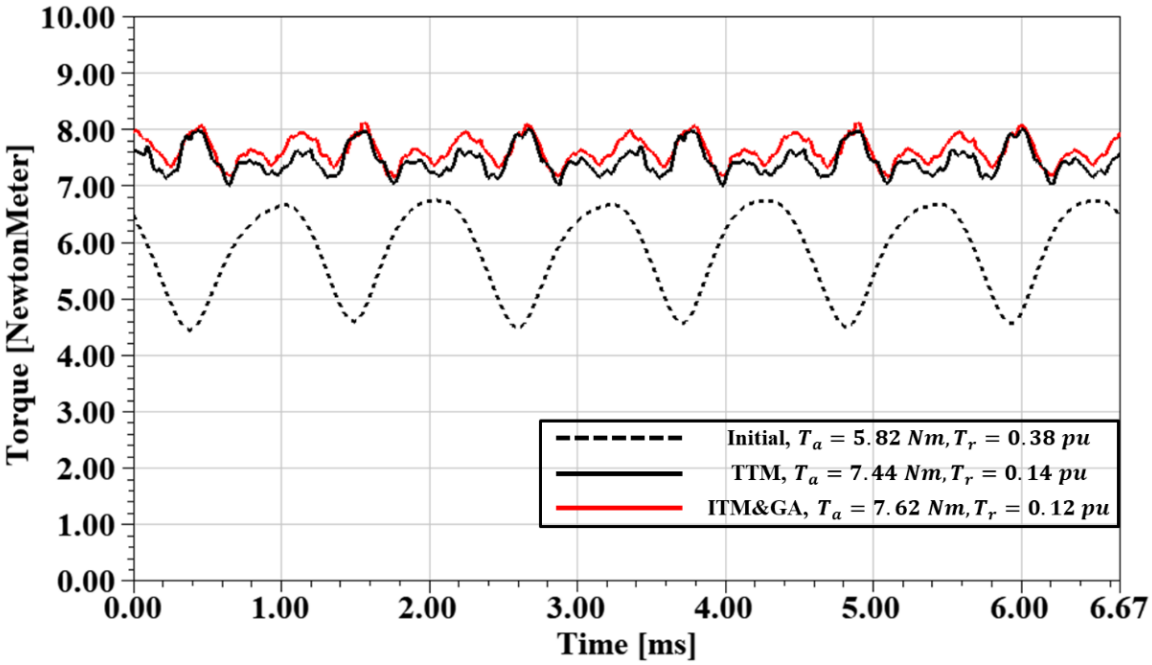

Fig. 5.10 Rated Torque Characteristics of Preliminary and Optimised Models of PMSM-1

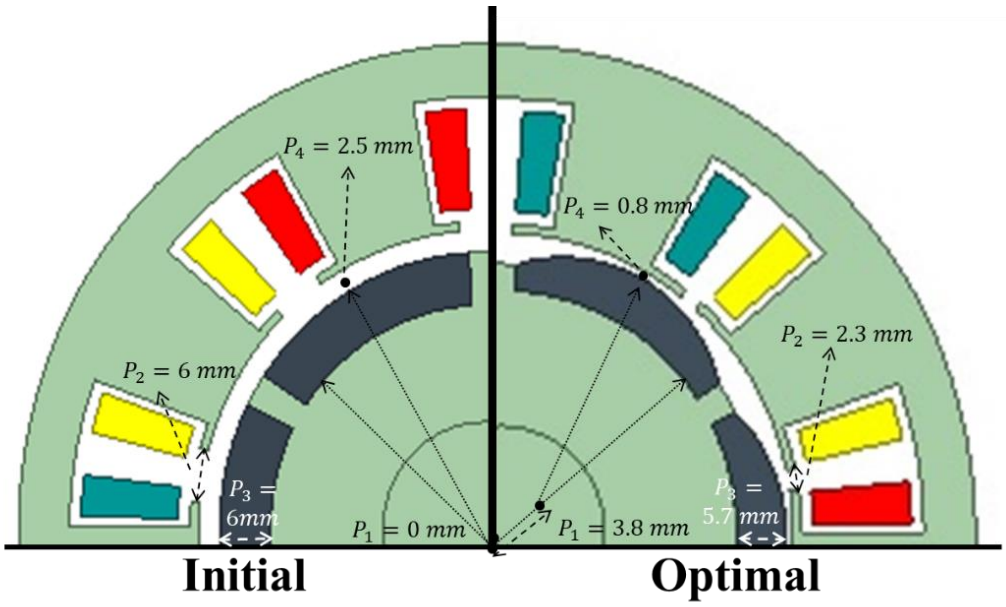

Fig. 5.11 Constructional Features of Preliminary and Optimised Models of PMSM-1

The flux distribution and magnetic flux density of initial and optimal model at the instant $time = 20\,ms$ and rated speed of 3000 rpm are shown in Figs. 5.12(a) and 5.12(b) respectively. It is observed that the motor design optimization results in the increase of magnetic flux flow. This helps in improving back emf profiles during operation under loaded conditions. Magnetic flux density in stator is 1.9 T (it is not saturated) near the teeth shoe in both the models. This concludes that model is accurately designed.

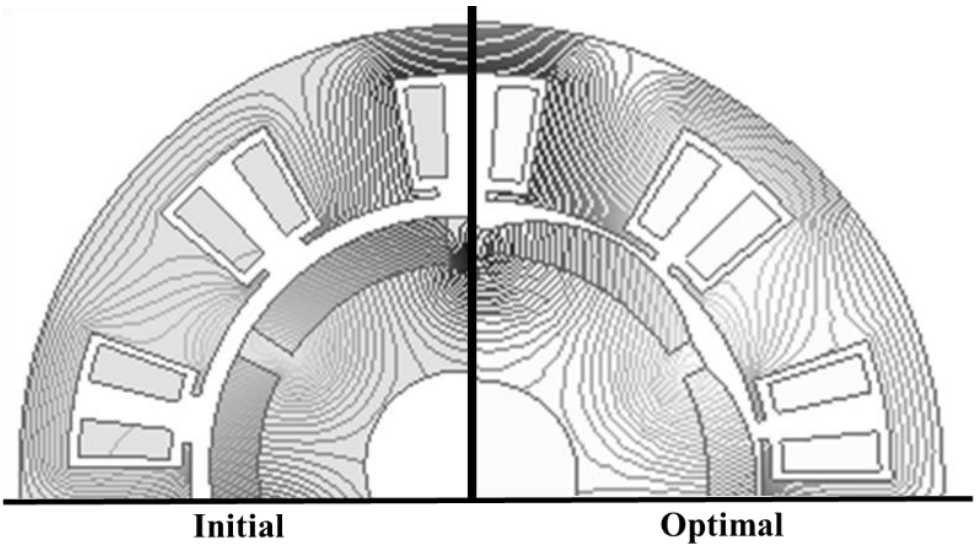

(a)

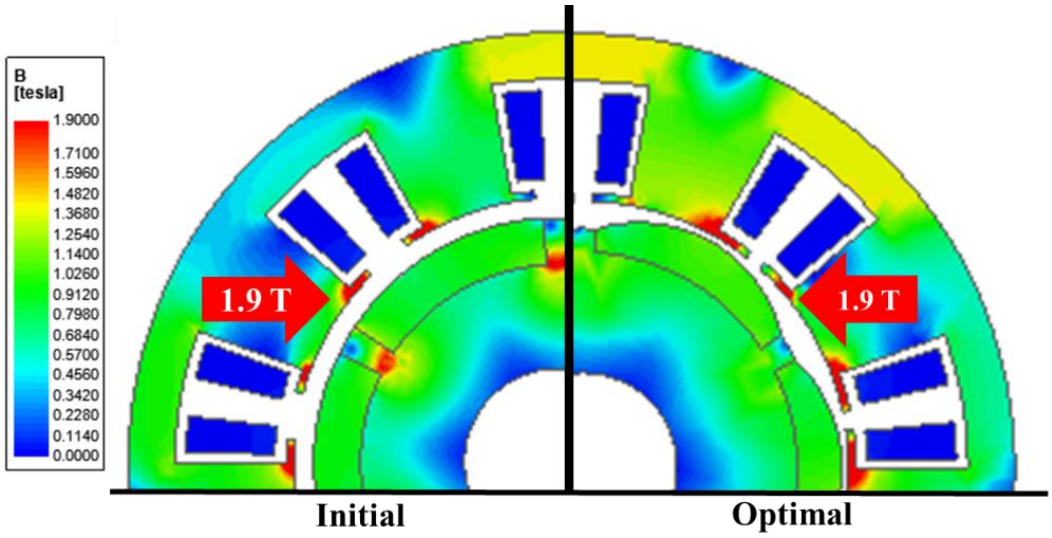

(b)

Fig. 5.12 (a) Flux Distribution and (b) Magnetic Flux Density of Preliminary and Optimised Models of PMSM-1

When temperature varies in EV, variation in the electromagnetic properties of the electrical and mechanical subparts of compressor is observed [247]. So it is necessary that motor performance should not deteriorated with variation in temperature. The model obtained from the proposed ITM&GA technique is further tested for variation in temperature. The torque and power variation at different temperatures is given in Fig. 5.13. It is observed that that even with increase in temperature, there is no substantial change in torque (~0.1 Nm with every 5^{o}C rise) as well as in output power (~0.03 kW for each 5^{o}C rise). This ensures lesser fuel consumption [248] to run electric compressor for removing heat from the vehicle cabin using the proposed method.

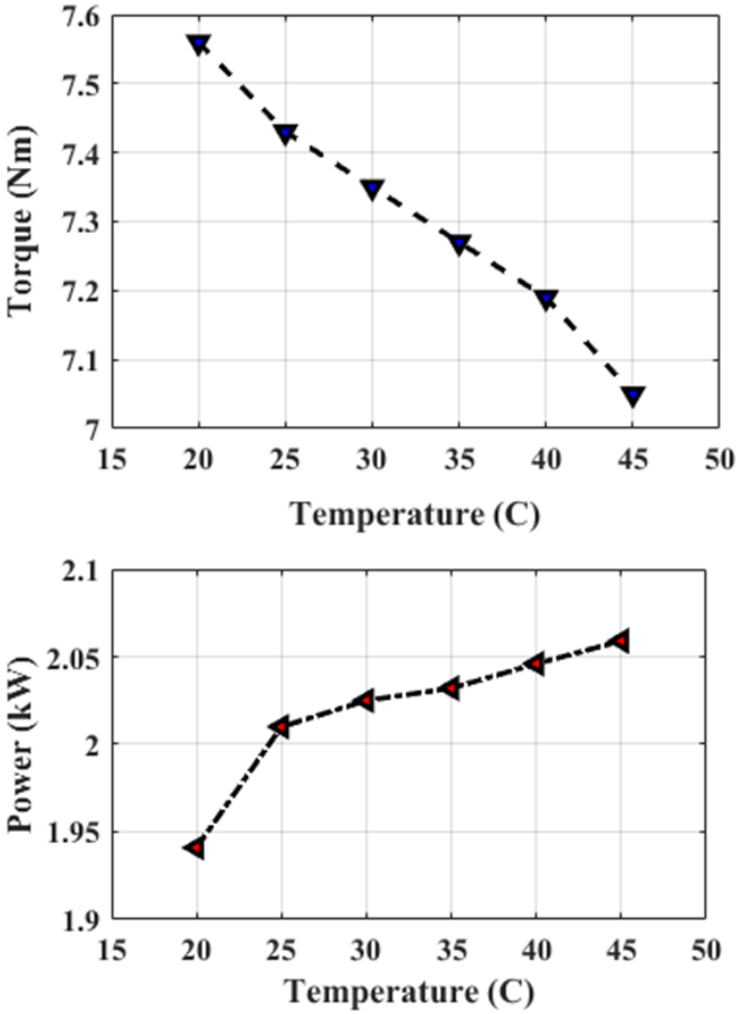

Fig. 5.13 Torque and Power variation at different temperatures

5.6 Conclusion

This chapter enumerates the implementation of a novel ITM&GA mechanism for the development and performance analysis of an optimized model of PMSM-1. The improvement in torque characteristic of the motor helps in better compression and suction operations of the refrigerant in electric compressors of air conditioning systems of EVs. With increase in vehicle speed, electric compressors have to produce the steady output power with lesser consumed fuel energy to maintain a good coefficient of performance (COP). For this prognosis, the motor geometry is optimized by performing 18 experiments in Phase I and then undergoing the surrogacy stage which further assists 100 experiments (generations) in genetic algorithms in Phase II of the proposed optimization mechanism. The performance of initial model of PMSM-1 is compared with the model obtained by TTM and proposed ITM&GA techniques.

It is observed that using traditional method TTM, the cogging torque is reduced by 70.8 % while using proposed ITM&GA, it is reduced by 74.7 %. The THD are reduced by 8.9 % using TTM and by 5 % using ITM&GA. The torque produced by the motor at rated speed has increased by 27.8 % using TTM and by 31 % using ITM&GA. Also, the ripples in torque are decreased by 85.7 % using TTM and 92.8 % using proposed ITM&GA. Comparing the optimal model performance using TTM and ITM&GA, it is thus concluded that ITM&GA method improves motor performance of PMSM-1 substantially as compared to that obtained by TTM.

Chapter 6

Design Optimization of PMSM-2 using Aquila-Grasshopper-Optimization Technique

6.1 General

The performance factors of electric motors employed at the energy conversion stage of EVPT systems can be easily scaled up or down at design stage. Various research attempts for improving the performance of electrical machines using different fabrication techniques with appropriate core material have been reported in literature [249] - [255].

This chapter dwells on the investigation of core losses in the motor of PMSM-2 through FEM analysis using two different core materials. Core loss is a major component of losses in motors. Hence, due consideration has to be given to this at the design stage of the motor as reduction in this loss increases the efficiency. The flux density and operating frequency have a major role in altering the values of core losses (hysteresis loss, eddy current loss and excess loss) [256]. Core loss is also sensitive to variation in motor GPs.

Owing to the typical drawbacks of the traditional optimization methods, the MH techniques are gaining attention of researchers in various engineering applications. The incorporation of hybridization in the basic methodology enhances the performance of basic MH techniques by adopting the advantages of each individual algorithm.

This portion of the research work addresses a real-world problem of optimizing PMSM-2 to obtain reduced core losses under specified constraints, by introducing a novel hybrid MH technique called Aquila-Grasshopper-Optimization (AGO). It blends the merits of Aquila optimizer (AO) and Grasshopper Optimization Algorithm (GOA).

The two main phases of MH techniques are (a) Exploration (also called diversification); which explores search zonal areas, and (b) Exploitation (also called intensification); which attempts to locate the optimum value from search zonal area. If the search area is not thoroughly analysed from the entire population or the optimum point is not tested properly in the explored search area, there is a good chance that the overall solution may converge to local optima by missing out the global optimum. Hence, there is a need for maintaining appropriate balance between the two phases so that the probability of skipping global optima is eliminated.

Aquila, Latin for '*eagle*', is believed to be the bird that carried Zeus/Jupiter's thunderbolts in Greek/Roman mythology. Aquila is a wise and proficient hunter. AO method is designed on the basis of its hunting methods; viz. (1) high ascend with vertical sag called expanded exploration, (2) silhouette navigation with shortened slide called narrowed exploration, (3) low navigation with steady drop called expanded exploitation, and (4) stretch and snatch prey called narrowed exploitation. It ensures that the optimization process invent the search area efficiently with wide as well as narrow vision. However, it has few limitations such as imbalance between exploration and exploitation phases, possibility of convergence to local optima and disproportion in convergence pace in both phases [257].

Grasshoppers, on the other hand, come under the insect category that hop and fly like rolling cylinders forming a swarm. GOA is designed on the basis of social interactions of grasshopper swarms in search of the food source. This method is effective, robust, accurate and simple to implement. However, GOA has some disadvantages like slow speed to reach global optimum and wastage of iterations while converging to the new optimum (time consuming) [258].

In the proposed novel hybrid AGO technique, in both expanded and narrowed exploration phase, first the solutions are updated using AO. Then in the updated current solution, the concept of normalizing the distance between solutions is applied by using GOA. Similarly, in both expanded and narrowed exploitation phase, first the solutions are updated using AO and then solutions are updated by normalizing the distance between the solution sets by using GOA. Also, greedy selection is performed to update better fitness value of the solution at each step of AGO to obtain the global optima.

Using proposed AGO technique, the design optimization of PMSM-2 is carried out in order to obtain reduction in core losses. In addition, sensitivity analysis is carried out on optimized PMSM-2 model to analyse the effect of variation in design parameters on its core loss and efficiency. The corresponding simulation studies, its analysis and results are presented and discussed herein.

6.2 Formulation of the Optimization Problem

In this section, the properties of core materials used in PMSM-2 model are enumerated. The core loss reduction and efficiency optimization strategy is formulated using FEM analysis and Surrogate Modelling techniques.

6.2.1 Motivation

In this section, the formulation of core loss reduction problem is carried out. As higher power density of PMSM is required in high performance EV applications, core loss is among the most critical components that influence motor's performance. The major dependence of the motor performance on core material property provides the impetus for research study in efficiency optimization of PMSM-2 for enhancing the employability of this motor in EVPT systems.

Core materials have different electro-magnetic properties and core loss depends on these properties of core materials. Also, it exhibits high dependence on the motor GP. Core loss modelling is established in terms of motor design parameters so that investigation can be carried out to minimize core losses at the design stage. The PMSM-2 model, with 36 slots and 14 poles, is designed with distributed winding configuration. The design specifications of the preliminary model of PMSM-2 are given in Table 4.1.

6.2.2 Core Material Properties

The electrical steel normally used in PM machines is an iron alloy forged to exhibit certain magnetic properties. It is designed with small hysteresis area and high permeability, which results in low power loss per cycle. Two types of core materials have been used in analysis of PMSM-2: a low carbon silicon sheet (M19-29G) and a non-grain oriented electrical steel (M400-50A). The magnetization curves and the core loss curves of the two materials at different frequencies are presented in Figs. 6.2(a) and 6.2 (b) respectively. It is observed that the core losses of M400-50A are lesser than that of M19-29G at the same frequency. This loss difference becomes more significant with rise in frequency. This aspect of M400-50A ensures that it is more suitable for applications in which high value of power density is required. The core material properties and advantages of the two core materials are shown in Table 6.1. In this research work, performance of the motor is analysed at rated operating conditions of 3000 rpm and 350 Hz. The core losses can also be reduced by shaping appropriate domain structure of the core material [259].

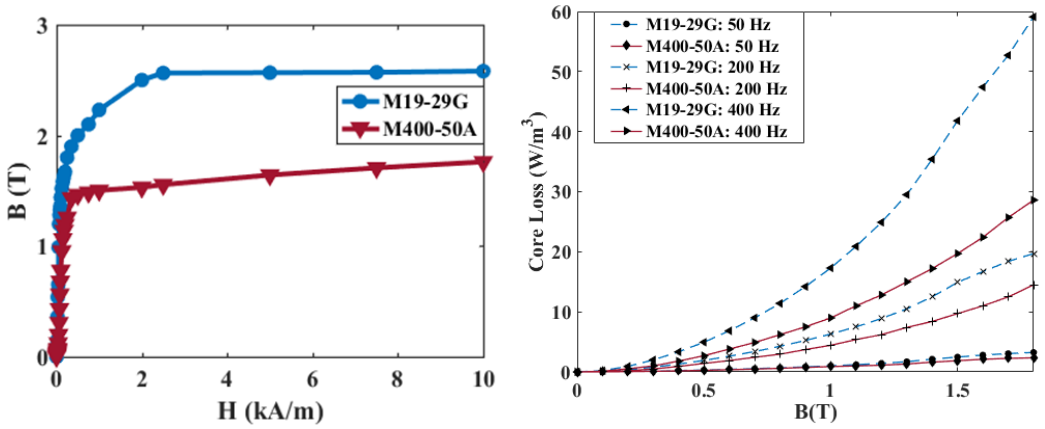

(a) (b)

Fig. 6.1 Characteristics of Core Materials (a) B-H curves at Working Frequency of 350 Hz; (b) Core losses

Table 6.1

Core Material Properties

Property	**M19-29G**	**M400-50A**
Mass Density	7872 kg/m³	7650 kg/m³
Thickness	0.35 mm	0.50 mm
Composition	Fe-C (C<~0.1%)	Fe-Si (2-3.5%Si)
Anisotropy of Loss	±17%	±10%
Resistivity	0.52 μΩ.m	0.42 μΩ.m
Hysteresis Loss Coefficient, k_h	2.05e-2 W/m³	9.59e-3 W/m³
Eddy Current Loss Coefficient, k_e	3.46e-5 W/m³	3.78e-5 W/m³
Excess Loss Coefficient, k_{exc}	5.96e-4 W/m³	2.01e-5 W/m³
B (5000 A/m)	2.57 T	1.64 T
Saturation Flux Density	2.58 T	1.7 T
Advantages	No rust, high malleability, high ductility	High alloy content, low energy loss, high corrosion resistance

6.2.3 Topologies of Designed Models

In PMSM-2 model, trench cuts are provided in the stator and rotor periphery to obtain reduced weight and to study its effect on the electromagnetic performance of the motor. Three topologies of the proposed designs are studied by employing two core materials, whose properties are explained in the previous section. The three topologies of designs of motor models are shown

in Fig. 6.2, which illustrates – 1) stator and rotor without trench cuts, 2) stator and rotor with trench cuts and 3) stator with trench cuts and rotor without trench cuts. These models are analysed for two different core materials to form 6 models listed in Table 6.2. The six model designs are given labels as: Model I, Model II, Model III, Model IV, Model V, Model VI; so that they can be separately addressed during analysis.

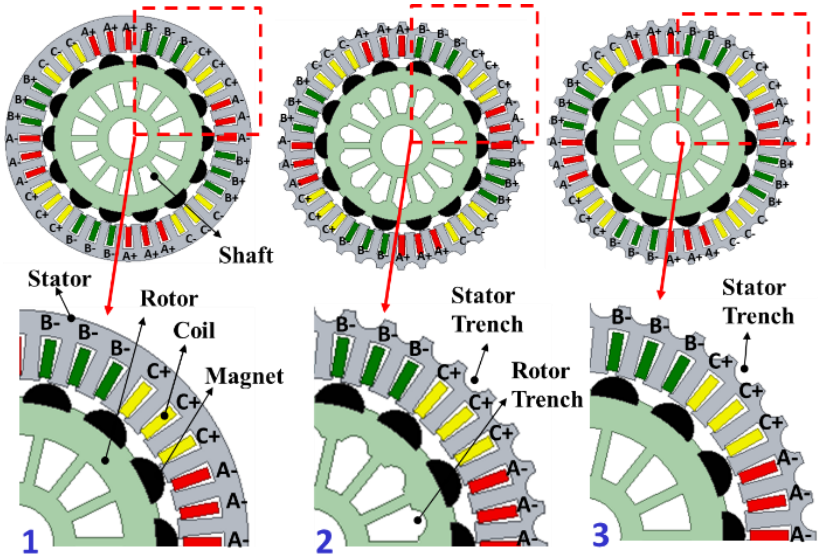

Fig. 6.2 Model Designs of PMSM-2

Table 6.2

Specification of Designed Models

Model Name	Core Material used in the Model	Presence of Trench Cuts in stator/rotor geometry Yes (Y) / No (N)
I	M19-29G	N
II	M400-50A	N
III	M19-29G	Y (in both stator and rotor)
IV	M400-50A	Y (in both stator and rotor)
V	M19-29G	Y (in stator), N (in rotor)
VI	M400-50A	Y (in stator), N (in rotor)

6.2.4 FEM Analysis and Surrogate Modelling Analysis

For reducing the analysis complexity, the GP of Model I and Model II are first optimized to obtain minimal core loss since they do not have trench cuts. In the later sections, the trench cuts

are added in the other four topologies of optimized models. The electromagnetic performance of six optimized models are then discussed and analysed.

The key design parameters that are varied to compute the core loss model in PMSM-2 are magnet thickness (A), pole embrace (B) and stack length (C). The meta-models of core loss, in terms of motor GP, are developed using FEM analysis and surrogate modelling technique. The design variables which are altered to establish the required DOE are shown pictorially in Fig. 6.3.

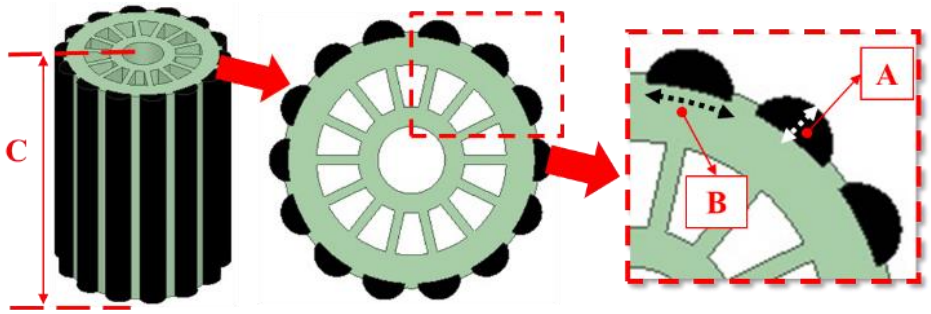

Fig. 6.3 Cross Section of PMSM-2 (A = radial magnet thickness, B = pole embrace and C = stack length)

For implementing surrogate modelling, the response of interest is considered as a polynomial function $f(p)$ which includes all associative terms given by:

$$f(p_1,\ p_2, p_3) = \beta_0 + \sum_{k=1}^{3} \beta_k p_k + \sum_{k=1}^{3} \sum_{l=k+1}^{3} \beta_{kl} p_k p_l + \sum_{k=1}^{3} \beta_{kk} p_k^2 \qquad (6.1)$$

Where, terms β_0, β_k are individual coefficients and β_{kl}, β_{kk} are associative coefficients. These coefficients are computed by regression method. The n = 36 FEM experiments are conducted for calculating core loss for set of variables$[\{p_1, p_2, p_3\}_j]_{1:n}$, referred as DOE, where j indicates j^{th} experiment. For DOEs, various combinations of design parameters are tabulated and the corresponding FEM simulation responses are recorded in Table 6.3.

Table 6.3

FEM Simulation Responses for Model I and Model II

(Units of A and C parameters are mm, B is unit-less)

Exp.	Parameters			Core loss (mW)		Exp.	Parameters			Core loss (mW)	
	A	B	C	Model I	Model II		A	B	C	Model I	Model II
1	3	0.65	150	178.7	123.4	**19**	6	0.65	150	152.0	87.7
2	3	0.75	150	175.5	119.5	**20**	6	0.75	150	149.9	85.4
3	3	0.65	160	190.6	131.6	**21**	6	0.65	160	162.2	93.6
4	3	0.85	160	183.7	123.0	**22**	6	0.85	160	157.2	88.1

Exp.	Parameters			Core loss (mW)		Exp.	Parameters			Core loss (mW)	
	A	B	C	Model I	Model II		A	B	C	Model I	Model II
5	3	0.75	170	199.0	135.4	**23**	6	0.75	170	169.9	96.8
6	3	0.85	170	195.2	130.7	**24**	6	0.85	170	167.1	93.6
7	4	0.65	150	167.9	108.2	**25**	7	0.65	150	146.1	80.3
8	4	0.75	150	165.3	104.7	**26**	7	0.75	150	144.0	78.3
9	4	0.65	160	179.1	115.4	**27**	7	0.65	160	155.8	85.7
10	4	0.85	160	172.9	108.2	**28**	7	0.85	160	151.1	81.1
11	4	0.75	170	187.3	118.7	**29**	7	0.75	170	163.2	88.7
12	4	0.85	170	183.7	114.9	**30**	7	0.85	170	160.6	86.2
13	5	0.65	150	159.3	96.9	**31**	8	0.65	150	137.2	74.2
14	5	0.75	150	156.7	93.9	**32**	8	0.75	150	138.7	72.3
15	5	0.65	160	169.9	103.4	**33**	8	0.65	160	149.8	79.2
16	5	0.85	160	164.4	97.1	**34**	8	0.85	160	145.7	75.2
17	5	0.75	170	177.6	106.4	**35**	8	0.75	170	157.2	82.0
18	5	0.85	170	174.6	103.2	**36**	8	0.85	170	154.8	79.9

The coefficients in (6.1) are computed using LSM as given in Section 4.5.3. The coefficients of RS models, obtained for two core loss models, $\hat{y}_1$, for Model I and $\hat{y}_2$, for Model II, respectively, are shown in Table 6.4. The advantages of motor geometry selection are presented in **Appendix B**.

Table 6.4

Individual and Associative Coefficients of RSM

Coefficient	$\widehat{y}_1$	$\widehat{y}_2$	Coefficient	$\widehat{y}_1$	$\widehat{y}_2$
β_0	-16.0281	400.4877	β_{23}	-0.3057	-3.3156
β_1	-11.0124	-37.9300	β_{11}	0.6420	1.8694
β_2	39.5326	247.6950	β_{22}	-24.0917	203.5722
β_3	1.7875	-4.0040	β_{33}	-0.0009	0.0208
β_{12}	3.5295	-13.3768	**RMSE**	0.0331	0.7223
β_{13}	-0.0407	0.1171			

It is observed from Table 6.4 that RMSE values for two responses of interest are lower. Lower values of RMSE signify that the residual data are more concentrated around the best fit line. So, it indicates the appropriate performance of the surrogate models. The meta-models for two responses of interest are given by (6.2) and (6.3) respectively.

$$\hat{y}_1 = -16.0281 - 11.0124A + 39.5326B + 1.7875C + 3.5295A.B - 0.0407A.C - 0.3057B.C + 0.642A^2 - 24.0917B^2 - 0.0009C^2 \quad (6.2)$$

$$\hat{y}_2 = 400.4877 - 37.93A + 247.695B - 4.004C - 13.3768A.B + 0.1171A.C - 3.3156B.C + 1.8694A^2 + 203.5722B^2 + 0.0208C^2 \quad (6.3)$$

The obtained meta-models are utilized as objective functions, in the upcoming Sections, under the constraints of 3mm ≤ A ≤ 8 mm, 0.65 ≤ B ≤ 0.85 and 150mm ≤ C ≤ 170mm.

6.3 Proposed AGO Mechanism

The Process Flow Chart of the proposed novel AGO Algorithm is presented in Fig. 6.4. The proposed AGO algorithm begins with the stochastic generation of initial population, X^P, given by (6.4), of capable candidate solutions (X_{ag}) between lower and upper bounds of the input parameters of the optimization problem.

$$X^P = \begin{bmatrix} x_{1,1} & \cdots & x_{1,dim} \\ \vdots & \ddots & \vdots \\ x_{N,1} & \cdots & x_{N,dim} \end{bmatrix} \quad (6.4)$$

Where each element of X^P matrix is generated using (6.5):

$$X_{ag} = lb_g + rand_1 \times (ub_g - lb_g) \qquad \begin{cases} a = 1,2,\ldots.N \\ g = 1,2,\ldots dim \end{cases} \quad (6.5)$$

Where N denotes the size of population and dim denotes the dimension of the problem, $rand$ is random number, lb_g and ub_g are lower and upper bounds of g_{th} variable.

This method takes into account the mathematical modelling of the hunting behaviour of Aquila into four discrete steps. In each step, the travelling in search space is further carried out by including the swarming behaviour of grasshoppers to reach the target food source with better fitness. The mathematical modelling of four hunting methods of Aquila is described below:

A) High Ascend with a Vertical Sag:

Initially, Aquila explores search space area from high ascend and chooses the best area for hunting the prey with a vertical sag. This behaviour is modelled mathematically as (6.6):

$$X_1(it+1) = X_b(it) \times \left(1 - \frac{it}{IT}\right) + (X_m(it) - X_b(it)) \times rand_2 \quad (6.6)$$

Where $X_1(it+1)$ is the updated solution at $(it+1)^{th}$ iteration, updated at step 1, $X_b(it)$ is the best updated solution up to current iteration, $\left(1 - \frac{it}{IT}\right)$ factor controls the exploration stage with respect to the change in iteration, IT denotes maximum number of iterations, $X_m(it)$ is the mean of the solutions at it^{th} iteration calculated using (6.7):

$$X_m(it) = \frac{1}{N}\sum_a^N x_{a,g}(t) \qquad \{ g = 1,2,..,dim \quad (6.7)$$

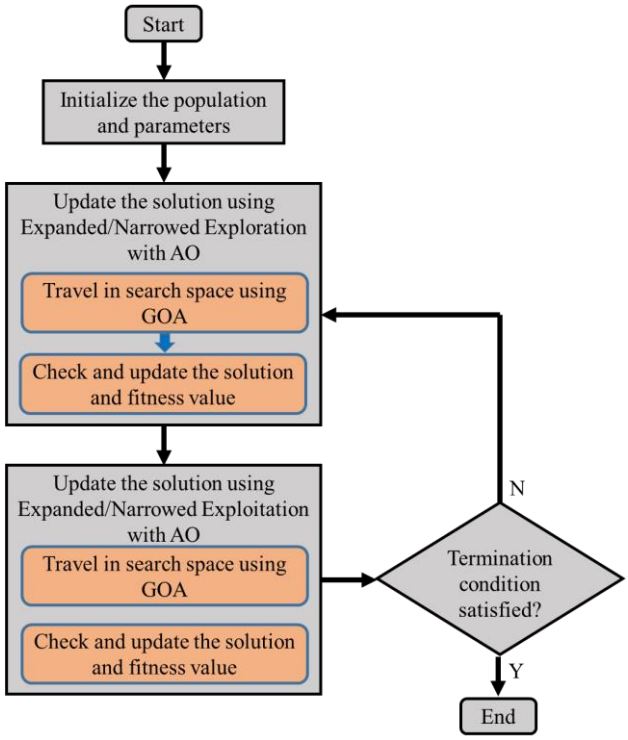

Fig. 6.4 Process Flow Chart of the Proposed AGO Algorithm

B) Silhouette Navigation with Shortened Slide:

Then Aquila forms a circle above the prey food source, narrows the search area to attack. The method is termed as silhouette navigation with shortened slide, for which mathematical model is represented by (6.8):

$$X_2(it+1) = X_b(it) \times levy(dim) + X_r(it) + (y - x) \times rand_3 \quad (6.8)$$

Where $X_2(it+1)$ is the updated solution at $(it+1)^{th}$ iteration updated at step 2, dim is the dimension value of the problem, $X_r(it)$ is the random solution selected from $[1, N]$ at

it^{th} iteration. The levy flight function is denoted by $levy(dim)$ which is computed as: $levy(dim) = \frac{s \times u \times \sigma}{|v|^{1/\beta}}$, where $\sigma = \frac{\Gamma(1+\beta) \times \sin\frac{\pi\beta}{2}}{\Gamma(\frac{1+\beta}{2}) \times \beta \times 2^{\frac{\beta-1}{2}}}$

Variables y and x represent contour spiral shape during the search. All the respective parameters are computed using (6.9) through (6.12).

$$y = r \times cos\theta_2 \tag{6.9}$$

$$x = r \times sin\theta_2 \tag{6.10}$$

$$r = r_c + p \times d_1 \tag{6.11}$$

$$\theta_2 = -\omega \times d_1 + \theta_1 \tag{6.12}$$

The parameters s, β, r_c, p, ω and θ_1 are constants; u and v are random numbers in [0,1] and d_1 is a vector of integers containing elements from 1 to dim.

C) Low Navigation with Steady Drop:

As the area of the prey is stated, Aquila navigates a bit low with steady drop. Here, prey area is being exploited with a wide vision, which is mathematically represented by (6.13):

$$X_3(it+1) = (X_b(it) - X_m(it)) \times \alpha - rand_4 + ((ub - lb) \times rand_4 + lb) \times \delta \tag{6.13}$$

Where $X_3(it+1)$ is the updated solution at $(it+1)^{th}$ iteration updated at step 3, α and δ are exploitation control parameters.

D) Stretch and Snatch Prey:

When prey is close to Aquila, it stretches and snatches the prey in accordance to the random motion of the prey, which is mathematically represented as (6.14):

$$X_4(it+1) = QF \times X_b(it) - (g_1 \times X(it) \times rand_5) - (g_2 \times levy(dim)) + rand_5 \times g_1 \tag{6.14}$$

Where $X_4(it+1)$ is the updated solution at $(it+1)^{th}$ iteration updated at step 4, QF is quality function calculated at it^{th} iteration using $QF(it) = it^{\frac{2 \times rand_5() - 1}{(1-IT)^2}}$. The control parameters g_1 and g_2 to track the prey by Aquila are given as (6.15):

$$\begin{aligned} g_1 &= 2 \times rand_5 - 1 \\ g_2 &= 2 \times \left(1 - \frac{it}{IT}\right) \end{aligned} \tag{6.15}$$

The updated solutions, using each hunting method of AO, are treated as new grasshopper positions at it^{th} iteration. The positions of grasshoppers are then updated using the mathematical model of their social swarming behaviour, represented by (6.16):

$$X_5 = c\left(\sum_{\substack{g=1 \\ g\neq a}}^{N} c\frac{ub_g - lb_g}{2} sf(|x_g - x_a|)\frac{x_g - x_a}{d_{ag}}\right) + \hat{T}_{dim} \tag{6.16}$$

Where X_5 denotes the position of a^{th} grasshopper in dim dimensional search space, given as: $X_a = (x_{a,1}, x_{a,2}, \ldots, x_{a,dim})$, c is a control coefficient calculated using (6.17):

$$c = c_{max} - it \times \frac{c_{max} - c_{min}}{IT} \tag{6.17}$$

The parameter sf calculates the social force strength using (6.18):

$$sf(|x_g - x_a|) = (af)e^{\frac{-|x_g - x_a|}{lf}} - e^{-|x_g - x_a|} \tag{6.18}$$

The distance, d_{ag}, between a^{th} grasshopper x_a and g^{th} grasshopper x_g is given as (6.19):

$$d_{ag} = |x_g - x_a| \tag{6.19}$$

The parameters af and lf are attraction intensity factor and length scale factor of attraction respectively. The variables c_{max} and c_{min} are maximum and minimum value of control coefficient, c which controls the search area based on the iterations [260]. The pseudo-code of the proposed algorithm is shown in Fig. 6.5.

```
Initialize the population X
Initialize the parameters of AO and GOA
While (end criteria not satisfied)
   store best solution X_b(t)
   calculate fitness value
   for each solution (i=1,2,...N)
      update mean value of current solution X_m(t)
      update parameters c, x, y, g_1, g_2, levy(d)
      if t ≤ (2/3) × T
         %% Step (1) Expanded exploration
           update solution using Eq. (3)
           check and update fitness
           normalize the distance between solutions
           update position using Eq. (17)
           check and update fitness
         %% Step (2) Narrowed exploration
           update solution using Eq. (5)
           check and update fitness
           normalize the distance between solutions
           update position using Eq. (17)
           check and update fitness
.....Continued
```

```
.....Continued
      else
         %% Step (3) Expanded exploitation
           update solution using Eq. (12)
           check and update fitness
           normalize the distance between solutions
           update position using Eq. (17)
           check and update fitness
         %% Step (4) Narrowed exploitation
           update solution using Eq. (13)
           check and update fitness
           normalize the distance between solutions
           update position using Eq. (17)
           check and update fitness
      end if
   end for
   t = t + 1
end while

Return the best solution and best fitness
```

Fig. 6.5 Pseudo Code of the Proposed AGO Algorithm

6.4 Implementation of AGO Technique

This section enumerates the performance analysis of the proposed novel AGO algorithm under two sub-heads; Implementation of AGO algorithm on Benchmark Functions and Implementation of AGO algorithm on a real-world problem of optimizing motor geometry to obtain reduced core loss. In addition, the performance of proposed algorithm is compared with classical MH techniques.

6.4.1 Testing of AGO Algorithm on Benchmark Functions

Simulation studies of the proposed novel AGO Algorithm is implemented using MATLAB 2016b and tested for various Benchmark Functions. Various unimodal, multimodal and fixed dimension multimodal benchmarks functions are used for the comparative analysis of the performance of proposed AGO algorithm with classical MH techniques like Artificial Bee Colony (ABC) method, Particle Swarm Optimization (PSO) method, Teaching Learning Based Optimization (TLBO) method and Differential Evolution (DE) method. In addition, the performance of proposed hybrid AGO algorithm is compared with its constituent AO and GOA techniques. The values of the computational parameters used in different algorithms are listed in Table 6.5.

Table 6.5

Values of Computational Parameters of Different Algorithms

Method	Parameter	Value	Method	Parameter	Value
ABC	permissible no. of failures	5	**DE**	Crossover probability	0.8
PSO	Inertia weight	0.5		Scaling factor	0.85
	Cognitive and social coefficients	1.5, 1.5	**AO**	Exploitation control parameters	0.1, 0.1
TLBO	Population size	20		ω	0.005
GOA	c_{max}	1		s	0.01
	c_{min}	0.00004		u	0.0265
	Attraction intensity factor	0.5		β	1.5
	Length scale factor of attraction	1.5		θ_1	$3\pi/2$

The definitions of Benchmark functions and the comparative study with other MH techniques are shown in Table 6.6. The simulations are run for 1000 iterations with 20 solutions (search agents). The exploitation tendency of AGO is tested for unimodal functions F1-F7 and the

exploration tendency of AGO is tested for multimodal functions F8-F13. Ranks are awarded to each algorithm based on the number of Benchmark Functions, for which it shows the successful least amount of fitness.

Table 6.6

Definitions of Benchmark Functions and Comparative Analysis Results

Function	Name	Description	Range	f_{min}	AGO	AO	GOA	ABC	PSO	TLBO	DE
Unimodal	F1	$f(x)=\sum_{i=1}^{n} x_i^2$	[-100, 100]	0	8.839E-35	1.770E-19	2.509E-06	4.507E-11	1.715E-25	3.854E-33	8.383E-17
	F2	$f(x)=\sum_{i=1}^{n} \lvert x_i\rvert + \prod_{i=0}^{n} \lvert x_i\rvert$	[-10, 10]	0	9.111E-23	1.554E-10	0.283E+00	2.879E-16	1.532E-12	1.020E-17	6.647E-06
	F3	$f(x)=\sum_{i=1}^{d} (\sum_{j=1}^{i} x_j)^2$	[-100, 100]	0	3.831E-53	1.044E-19	1.633E-04	2.448E-10	2.912E-24	5.817E-32	1.234E-17
	F4	$f(x)=max_i\{\lvert x_i\rvert, 1\le i\le n\}$	[-100, 100]	0	2.521E-62	9.034E-10	1.968E-04	5.199E-17	4.850E-12	4.703E-16	2.874E-07
	F5	$f(x)=\sum_{i=1}^{n-1}[100(x_i^2 - x_{i+1})^2 + (1 - x_i)^2]$	[-30, 30]	0	8.222E-04	8.306E-04	1.011E+00	0.401E+00	0.000E+00	0.000E+00	0.000E+00
	F6	$f(x)=\sum_{i=1}^{n} (\lvert x_i+0.5\rvert)^2$	[-100, 100]	0	2.152E-25	4.556E-06	1.012E-09	0.500E+00	0.000E+00	4.264E-08	1.080E-08
	F7	$f(x)=\sum_{i=0}^{n} ix_i^4 + random[0,1)$	[-128, 128]	0	5.318E-03	2.661E-03	5.812E-03	0.098E+00	3.292E-05	0.004E+00	0.011E+00
Multimodal	F8	$f(x)=\sum_{i=1}^{n} (-x_i\sin(\sqrt{\lvert x_i\rvert}))$	[-500, 500]	-418.982	-413.586	-412.784	-417.336	-402.968	-408.229	-400.868	-362.886
	F9	$f(x)=\sum_{i=1}^{n} [x_i^2 - 10\cos(2\pi x_i) + 10]$	[-5.12, 5.12]	0	1.294E-10	0.000E+00	4.682E+00	4.052E-10	0.000E+00	0.000E+00	3.979E+00
	F10	$f(x)=-20\exp\left(-0.2\sqrt{\frac{1}{n}\sum_{i=1}^{n} x_i^2}\right) - \exp\left(\frac{1}{n}\sum_{i=1}^{n}\cos(2\pi x_i)\right) + 20 + e$	[-32, 32]	0	1.764E-16	8.881E-16	4.619E-05	4.148E-16	8.881E-16	8.881E-16	6.525E-06
	F11	$f(x)=1+\frac{1}{4000}\sum_{i=1}^{n} x_i^2 - \prod_{i=1}^{n}\cos(\frac{x_i}{\sqrt{i}})$	[-600, 600]	0	1.775E-15	0.000E+00	0.096E+00	2.390E-05	0.000E+00	4.440E-15	0.012E+00

Function	Name	Description	Range	f_{min}	AGO	AO	GOA	ABC	PSO	TLBO	DE
	F12	$f(x) = \frac{\pi}{n}\{10\sin(\pi y_1)\} + \sum_{i=1}^{n-1}(y_i - 1)^2\left[1 + 10sin^2(\pi y_{i+1}) + \sum_{i=1}^{n} u(x_i,10,100,4)\right]$;whe $= 1 + \frac{x_i + 1}{4}$, $u(x_i,a,k,m)$ $= \begin{cases} K(x_i - a)^m ; for\ x_i > a \\ 0 ; for\ -a \le x_i \le a \\ K(-x_i - a)^m ; for\ x_i \le - \end{cases}$	[-50, 50]	0	1.498E-06	1.505E-05	5.519E-06	1.000 E+00	4.711E-03	4.326E-04	3.110E+00
	F13	$f(x) = 0.1(sin^2(3\pi x_1) + \sum_{i=1}^{n}(x_i - 1)^2[1 + sin^2(3\pi x_i + 1)] + (x_n - 1)^2[1 + sin^2(2\pi x_n)]) + \sum_{i=1}^{n} u(x_i,5,100,4)$	[-50, 50]	0	1.537E-07	1.353E-06	1.327E-06	1.000 E+00	1.349E-02	6.816E-03	0.019E+00
			Rank		1	2	3	7	4	5	6
Function	**Name**	**Description**	**Range**	f_{min}	**AGO**	**AO**	**GOA**	**ABC**	**PSO**	**TLBO**	**DE**
Fixed Dimensional Multimodal	F14	$f(x) = (\frac{1}{500} + \sum_{j=1}^{25}(j + (x_1 - a_{1j})^6 + (x_2 - a_{2j})^6)^{-1})^{-1}$	[-65, 65]	1	0.999	0.996	1.992	0.978	0.998	0.998	12.670
	F15	$f(x) = \sum_{i=1}^{11}[a_i - \frac{x_1(b_i^2 + b_i x_2)}{b_i^2 + b_i x_3 + x_4}]^2$	[-5, 5]	0.00030	7.730E-04	3.320E-04	7.034E-04	3.100 E-02	2.989E-03	2.972E-02	3.321E-01
	F16	$f(x) = 4x_1^2 - 2.1x_1^4 + \frac{1}{3}x_1^6 + x_1x_2 - 4x_2^2 + 4x_2^4$	[-5, 5]	-1.0316	-1.031	-1.031	-1.031	-1.019	-1.002	-1.029	-1.006
	F17	$f(x) = (x_2 - \frac{5.1}{4\pi^2}x_1^2 + \frac{5}{\pi}x_1 - 6)^2 + 10\left(1 - \frac{1}{8\pi}\right)cosx_1 + 10$	[-5, 5]	0.398	0.398	0.397	0.397	0.397	0.397	0.377	1.943

Function	Name	Description	Range	f_{min}	AGO	AO	GOA	ABC	PSO	TLBO	DE
	F18	$f(x) = [1 + (x_1 + x_2 + 1)^2(19 - 14x_1 + 3x_1^2 - 14x_2 + 6x_1x_2 + 3x_2^2)] \times [30 + (2x_1 - 3x_2)^2(18 - 32x_1 + 12x_1^2 + 48x_2 - 36x_1x_2 + 27x_2^2)]$	[-2, 2]	3	3	3.001	3	2.998	2.909	2.998	2.990
	F19	$f(x) = -\sum_{i=1}^{4} c_i \exp(-\sum_{i=1}^{3} a_{ij}(x - p_{ij})^2)$	[-1, 2]	-3.86	-3.861	-3.860	-3.857	-1.899	-1.899	-1.899	-1.899
	F20	$f(x) = -\sum_{i=1}^{4} c_i \exp(-\sum_{i=1}^{6} a_{ij}(x - p_{ij})^2)$	[0, 1]	-3.32	-3.322	-3.304	-3.322	-1.169	-1.169	-1.166	-1.169
	F21	$f(x) = -\sum_{i=1}^{5} [(X - a_i)(X - a_i)^T + c_i]^{-1}$	[0, 1]	-10.1532	-10.055	10.151	-5.055	-8.152	-10.001	-10.113	-5.101
	F22	$f(x) = -\sum_{i=1}^{7} [(X - a_i)(X - a_i)^T + c_i]^{-1}4$	[0, 1]	-10.4028	-10.402	-10.400	-10.402	-9.908	-10.376	-10.400	-5.128
	F23	$f(x) = -\sum_{i=1}^{10} [(X - a_i)(X - a_i)^T + c_i]^{-1}4$	[0, 1]	-10.5363	-10.427	-10.535	-10.536	-9.693	-10.359	-10.519	-6.529
			Rank		1	2	3	6	4	5	7

It is observed that AGO produces the fittest value with the ongoing process flow of the iterations securing rank 1. The performance of AGO is found to be better than AO and GOA, which secure ranks 2 and 3, respectively. Whereas, PSO and TLBO ranked 4 and 5 respectively. DE did not convergence for functions F7, F8, F12, F13 and secured rank 6. While ABC operates satisfactorily for few functions like F1-F5, F9, F10, F11; it failed to converge to the required minima for functions like F6, F7, F8, F12, F13 thus, securing rank 7. The performance of AGO is tested for the low dimension problems using functions F14-F23. AGO is found to be converging to the optimum value in fewer iterations in almost all the functions F14-F23 and hence secures rank 1. Similarly, other algorithms are also awarded the ranks based on their corresponding performance.

The balance between exploration and exploitation carried out by AGO is shown in Fig. 6.6 for different benchmark functions.

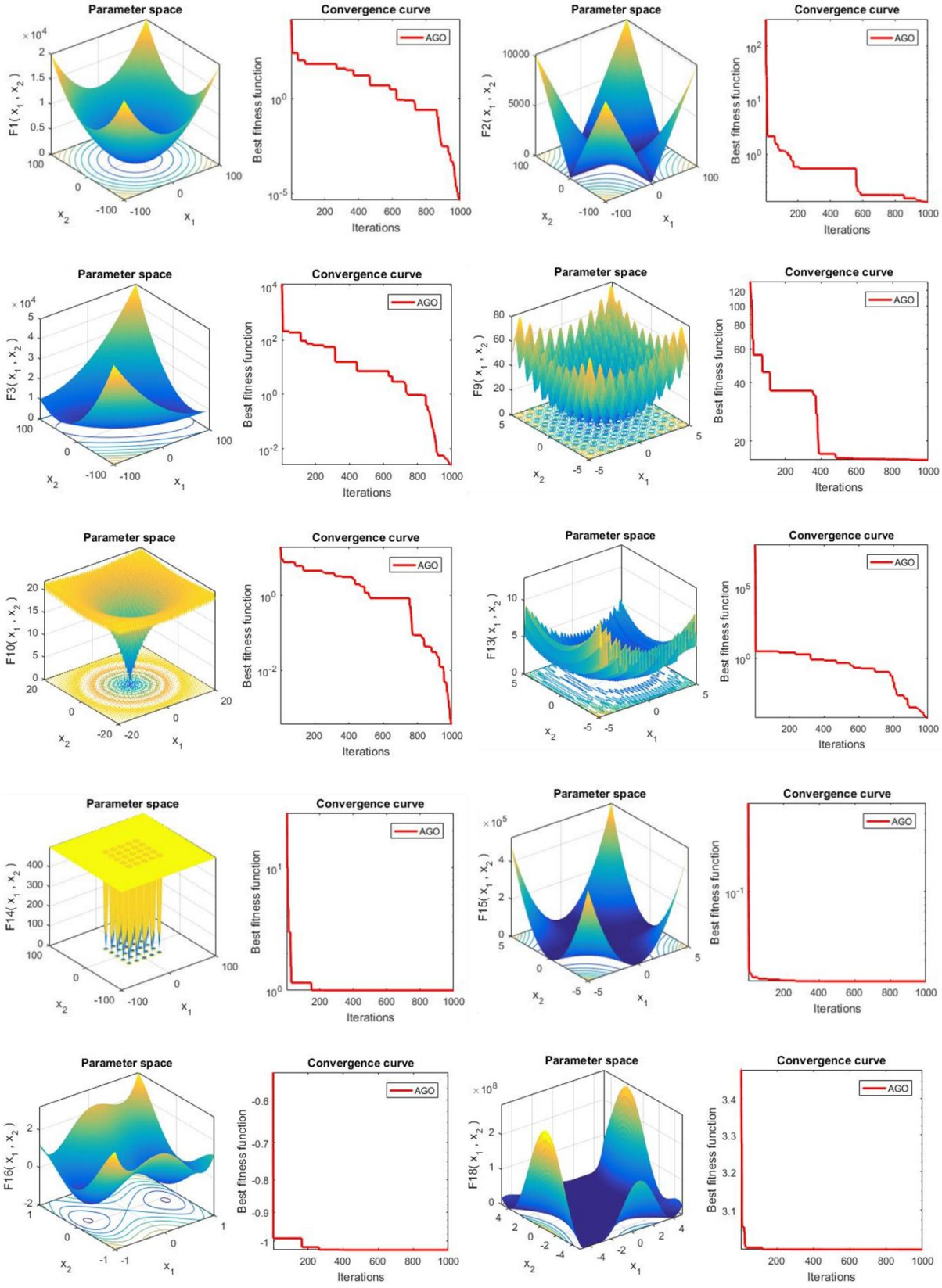

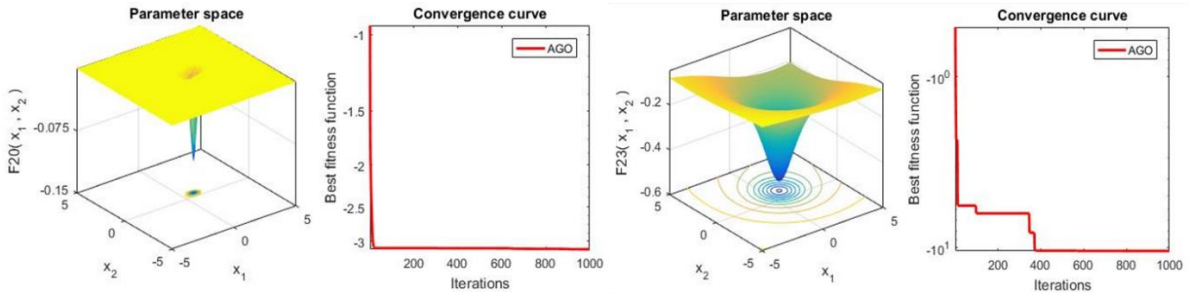

Fig. 6.6 Convergence Characteristics of AGO for various Benchmark Functions

It is evident from the convergence curve of AGO (Fig. 6.6) that the qualitative results are approaching the target by searching the population thoroughly for unimodal functions whereas the results are following step-wise exploration or exploitation based on the complexity of the multimodal functions. AGO quickly experience the transition from exploration to exploitation in case of fixed dimensional multimodal functions.

The convergence curves for different algorithms are compared in Fig. 6.7 to test the acceleration tendency of AGO. It is observed that for unimodal functions F1-F7, AGO experience a favourable drop off rate as compared to other algorithms. For multimodal functions F8-F23, AGO shows appreciable deceleration rate and hence shows rapid convergence capability. While the other algorithms show the drawback of converging to local optima in functions F1, F2, F3, F4, F9, F10, F11 and undergo sluggishness in reaching the optima in functions F7, F20, F21, F22, F23.

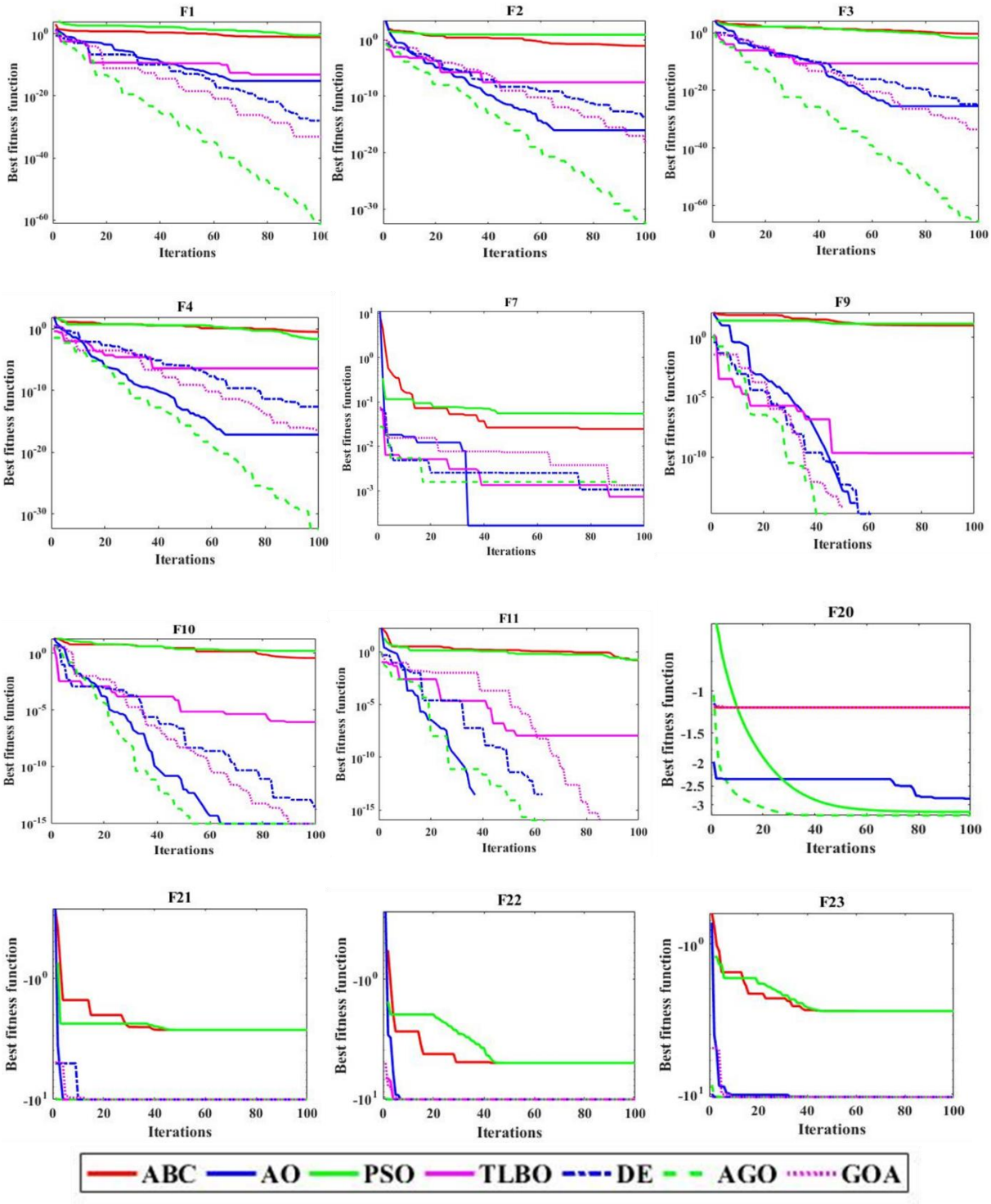

Fig. 6.7 Comparative Analysis for Convergence Test of Different Algorithms

6.4.2 Implementation of AGO Algorithm on Formulated Problem

This section describes the implementation of the proposed AGO algorithm for minimization of core losses in PMSM-2 by applying it on the formulated core loss model. The results of the analysis for the loss models are presented in Table 6.7. The algorithms are ranked based on the

fitness values of y_1 and y_2. The proposed AGO algorithm gives the least values of core loss for the surface inset PMSM-2 model as compared to other algorithms.

Table 6.7

Performance Analysis of Algorithms for Core Loss Models $\hat{y}_1$ and $\hat{y}_2$

Method	$\hat{y}_1$		Rank	$\hat{y}_2$		Rank
	(A,B,C)	$\hat{y}_{1min}$		(A,B,C)	$\hat{y}_{2min}$	
AGO	(8,0.85,150)	136.216	1	(8,0.85,150)	68.529	1
AO	(7.9,0.85,150)	137.607	3	(7.2,0.85,150)	71.251	4
GOA	(7.77,0.84,151.34)	139.523	7	(8,0.82,154.56)	71.337	5
ABC	(7.97,0.85,150)	137.297	2	(8,0.85,156.05)	71.437	6
PSO	(8,0.82,150)	137.637	4	(7.82,0.81,150)	69.583	2
TLBO	(7.93,0.75,150)	139.051	6	(7.88,0.79,150.29)	69.958	3
DE	(7.6,0.85,150)	138.836	5	(6.4,0.79,150)	76.135	7

6.5 Performance Analysis of Designed Models

This section presents the performance analysis of different topologies of PMSM-2 (mentioned in section 6.2.3). The core losses in stator, core losses in rotor, copper losses, torque, ripple in torque, weight and power densities are compared and discussed. Furthermore, sensitivity analysis is carried out for Models I and II to study the effect of variation in design parameters on the respective performance variables.

6.5.1 Comparative Analysis of Initial and Optimal Models: Model I and Model II

This Section presents the comparative analysis of the optimized Models I and II with their respective initial models after the application of proposed AGO technique. The motors are run at rated speed of 3000 rpm to obtain high electromagnetic performance of motor under steady state condition. The parameters and corresponding responses are presented in Table 6.8. It is observed that core losses in models are reduced without affecting copper losses. Also, the torque performance showed improvement along with the reduction in unwanted torque ripples.

Table 6.8

Parameters and Performance Analysis of Preliminary and Optimised Models I and II

Parameters / Response	**Initial models**		**Optimal models**	
	Model I	Model II	Model I	Model II
{A,B,C}	{3,0.65,150}		{8,0.85,150}	
Core loss	178.7 mW	123.4 mW	153.8 mW	68.5 Mw
Copper loss	244 W	216 W	243 W	217 W
Torque	275 Nm	351 Nm	318 Nm	412 Nm
Ripple torque	0.41 pu	0.29 pu	0.27 pu	0.13 pu

It is observed that the core losses in optimized Model I and Model II are reduced by 14% and 44 %, respectively. Model I and Model II have very small change, of ≈1 %, in copper losses after optimization. The torque produced by Model I and Model II have increased up to 15% and 17%, respectively. The ripples in torque produced by Model I and Model II are reduced by 34% and 55% respectively.

The analysis results are represented in the form of bar graph in Fig. 6.8. Here, the stator and rotor core losses are separately compared for initial and optimized models. The stator core loss in Model I is reduced by 9% while in Model II, it is reduced by 39%. The rotor core loss is reduced by 30% in Model I and by 60% in Model II.

It is observed that using proposed AGO technique, the obtained optimal models possess lesser core losses and better torque performance as compared to the initial models.

6.5.2 Comparative Analysis of Electromagnetic Performance of Models

In this section, the optimized geometry of all six models is analysed for comparing core loss in stator, core loss in rotor, torque and torque ripple. The corresponding comparison of six models when operated at rated speed of 3000 rpm are presented in Fig. 6.9.

It is observed that Models I and II produce average torque of 318Nm and 412Nm respectively. Core losses in stators of Models I and II are 126.4mW and 57.2mW, while core losses in rotors are 27.4mW and 11.3mW respectively. Torque ripple produced by Model II is 0.13pu which is 52% lesser than that produced by Model I. Models III and V produce equal average torque of 224Nm and torque ripple of 0.21pu. Also, Models IV and VI produce equal average torque of 320Nm and torque ripple of 0.12pu. Thus, it is inferred that the presence of trenches in rotor core does not have any significant effect on motor torque performance but this additional feature

is helpful in reducing motor weight which is presented in Fig. 6.10. Model IV and Model VI possess least torque ripple of 0.12pu and least core loss of 64mW. But they produce 45% lesser torque than Model II. Model II produces the highest average torque of 412Nm, with 7 % more ripples than Model IV and Model VI. So, it is concluded that the applications in which least core losses are preferable with compromise of lesser torque, Model IV and Model VI gives better performance. Whereas, the applications where least core loss and high torque performance are preferable, Model II exhibits the best performance. The weight and power density of the six models are compared in Fig. 6.10.

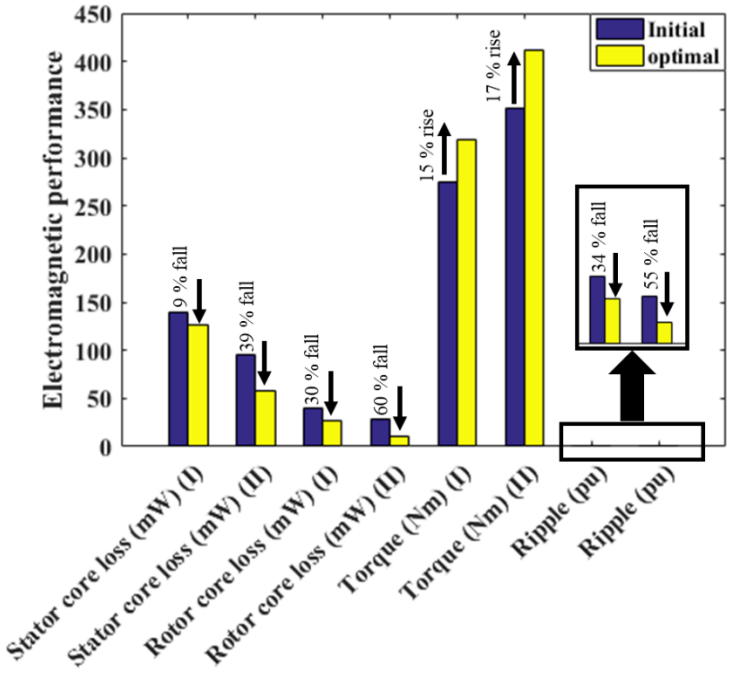

Fig. 6.8 Comparison of Electromagnetic Performance of Preliminary and Optimised Models I and II

It is observed from Fig. 6.10 that Model I has 2 % more weight than Model II. Whereas Model III and Model V are of similar weight, having 8 % lesser weight than Model II. Model IV and Model VI are of similar weights, having 13 % lesser weight than Model II. Hence, it is concluded that although the torque produced by the motor having trench cuts (Model III, Model IV, Model V, Model VI) is lesser, but these designs are beneficial for light weight EV applications. It is also observed from Fig. 6.10 that the power density of Model II is the highest among all six models since its torque producing capability is the highest. So Model II is also suitable for high power density applications.

The magnetic flux density distributions in Models II and IV at different time instants are shown in Figs. 6.11(a) and 6.11(b) respectively. On outer periphery of the stator yoke and inner

periphery of the rotor yoke, magnetic flux density is approximately 0T and 0.4T respectively at different time instants depending upon the rotor position θ. In Fig. 6.11 (c), the partial motor models are presented to examine the influence of presence of trench cuts in stator and rotor yokes with respect to magnetic flux density distribution. Points P_{s1}, P_{s2}, P_{s3}, P_{s4}, P_{s5} in stator and points P_{r1}, P_{r2} in rotor are representing the points of observation (trench cuts positions) in partial models respectively. It is observed that if in Model II, trench cuts are provided in stator and rotor yoke geometry at these points of observation, magnetic flux density gets distributed in the confined yoke geometry near to the slots. Thus, Model II exhibits least core losses of 68.5mW. In Model IV, the core material is reduced without affecting the flux density and hence light weight motor structure is achieved, which is suitable for electrical transportation applications.

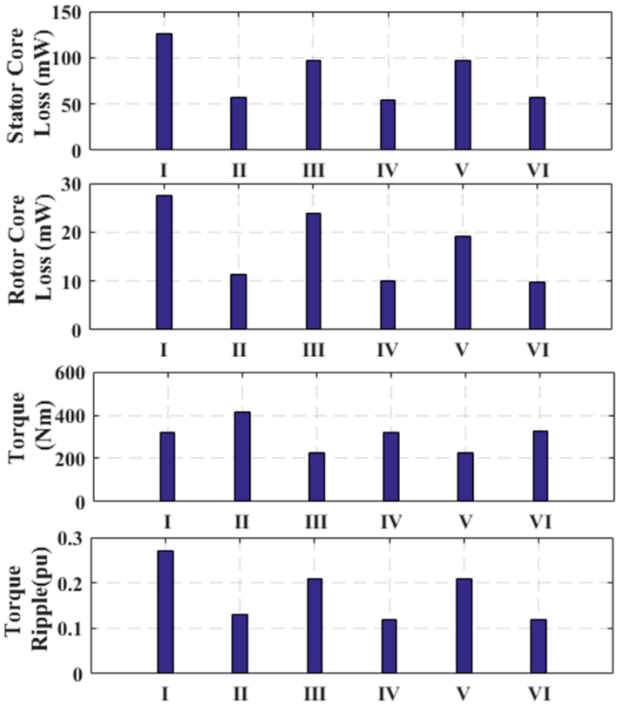

Fig. 6.9 Performance Comparison of six Models

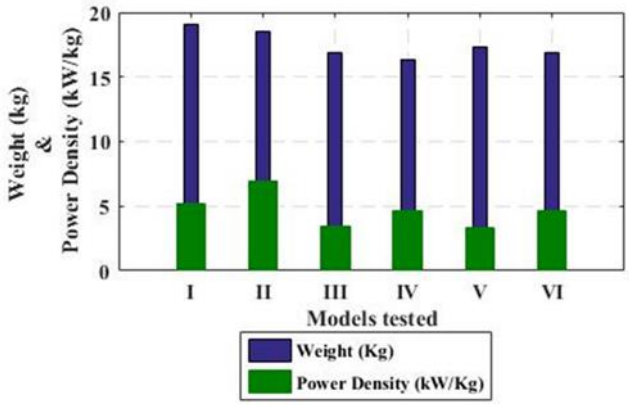

Fig. 6.10 Comparison of Weight and Power Density of six Models

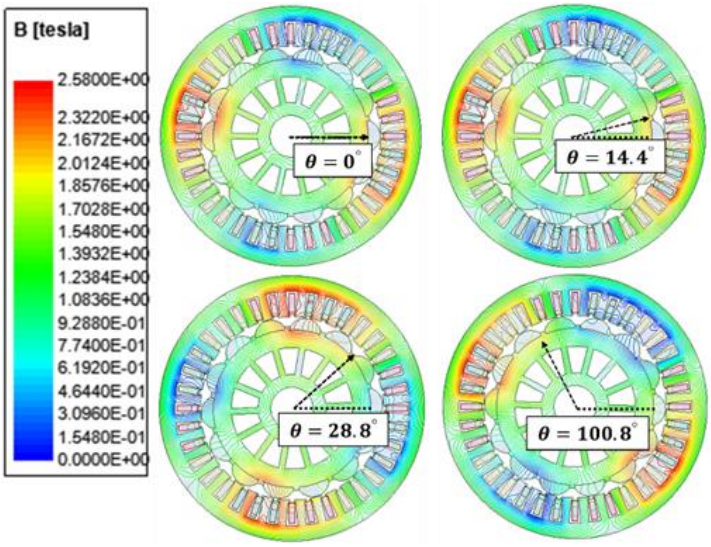

(a) Magnetic Flux Density for Model II

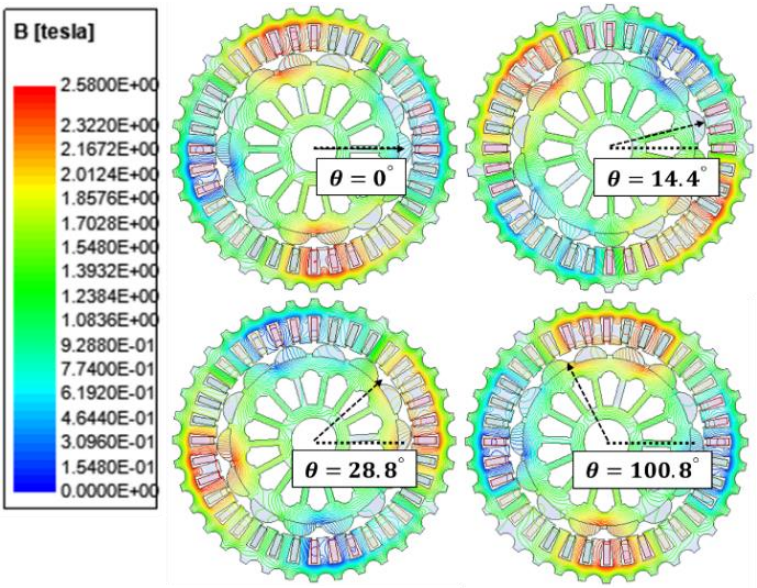

(b) Magnetic Flux Density for Model IV

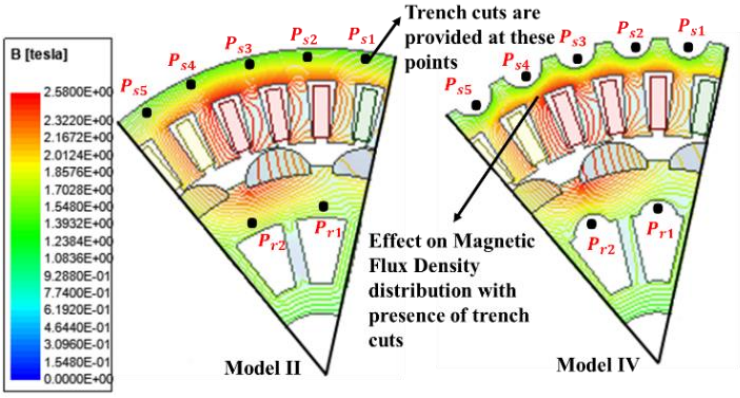

(c) Partial Motor Diagrams at t=0ms (θ=0˚)

Fig. 6.11 Magnetic Flux Densities for Model II and Model IV at t=0ms (θ=0˚), t=0.8ms (θ=14.4˚), t=1.6ms (θ=28.8˚) and t=5.6ms (θ=100.8˚).

6.5.3 Sensitivity Analysis of Optimized Models

Sensitivity analysis of core-loss and efficiency are carried out for the six designed models by introducing deviations in design parameters $m = [A, B, C]$.

The deviations are applied to one parameter at a time while keeping other variables unchanged. The parameter sensitivity is given by:

$$S_z^{df} = \frac{df(m_1, \ldots, m_z + \Delta m_z, \ldots, m_g) - df(m_z)}{\Delta m_z} \tag{6.9}$$

Where df denotes the data function; core loss or efficiency and m_z denotes the z^{th} independent variable. Fig. 6.12 shows the core loss deviation (%) as a function of parameter deviation (%). Table 6.9 presents the sensitivity values for key design parameters.

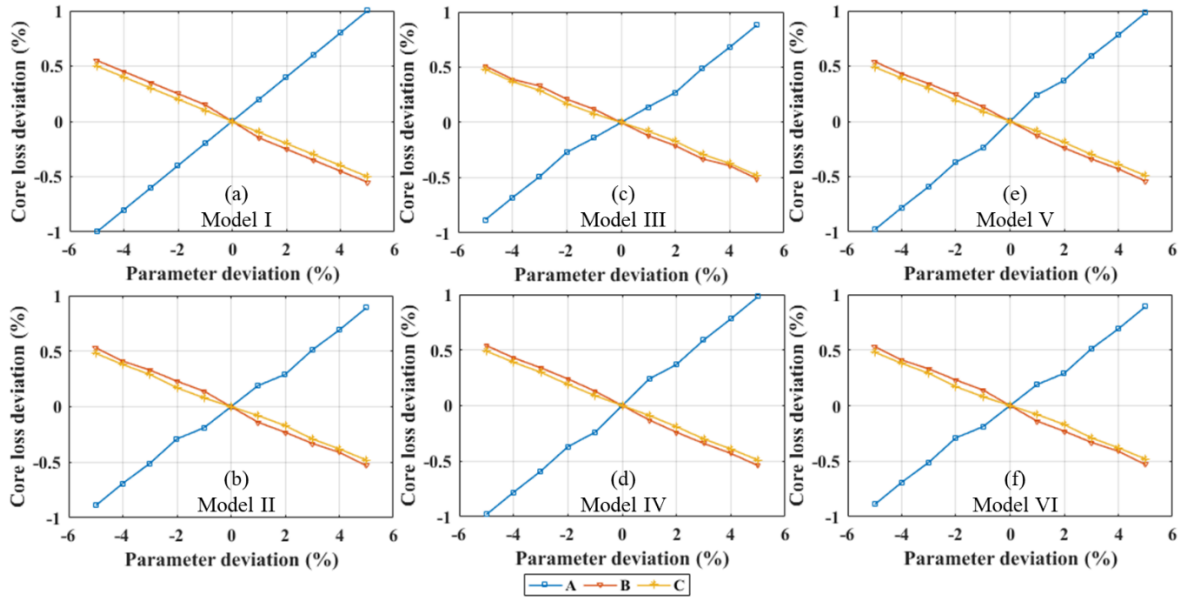

Fig. 6.12 Sensitivity of Core Loss to Variation in Magnet Thickness (A), Pole Embrace (B) and Stack Length (C): (a) Model I (b) Model II (c) Model III (d) Model IV (e) Model V (f) Model VI

Table 6.9

Sensitivity Values of Key Design Parameters

Parameters	**Core Loss**					
	Model I	**Model II**	**Model III**	**Model IV**	**Model V**	**Model VI**
A	0.80	0.68	0.72	0.70	0.72	0.70
B	0.45	0.39	0.43	0.40	0.43	0.40
C	0.40	0.37	0.40	0.39	0.40	0.39
Parameters	**Efficiency**					
	Model I	**Model II**	**Model III**	**Model IV**	**Model V**	**Model VI**
A	0.099	0.090	0.095	0.091	0.095	0.091
B	0.034	0.020	0.032	0.023	0.032	0.023
C	0.049	0.037	0.048	0.038	0.048	0.038

It is observed that for all models, core loss and efficiency are highly sensitive to deviation in magnet thickness (A), while deviation in pole embrace (B) and Stack length (C) have less effect on model performance. Also Model II is comparatively less sensitive to parameters disturbance as compared to other models. The sensitivity of Model III is similar to that of Model V and the sensitivity of Model IV is similar to that of Model VI with respect to deviations in design parameters. The geometrical and electrical disturbances also develop undesired behaviour in the motor, like fault occurrence due to unknown disturbances and unaligned eccentricity of rotor. Such sensitivity analysis proposes an interesting approach to further analyse the motor performance and develop a robust and reliable motor designs [261-262]. This can be considered as a future task to enhance knowledge of the subject with different core materials.

6.6 Conclusion

This chapter presents a novel hybrid metaheuristic optimization technique termed as Aquila-Grasshopper-Optimization. The application of this hybrid metaheuristic optimization technique is elucidated to study the influence of core material and core trench on the performance of SI-PMSM. Six structurally different topologies of models are designed, out of which three models have low carbon silicon steel, M19-29G, as core material and rest three have a non-grain oriented fully processed electrical steel, M400-50A as core material. The meta-models for core-losses in terms of motor geometry parameters are developed using 36 FEM experiments and surrogate modelling technique.

The performance of proposed novel AGO technique is tested for 23 Benchmark functions and further implemented for the formulated core loss minimization problem. It is inferred that by optimizing motor geometry at design stage, not only core losses are reduced but the overall torque performance of the motor is improved. It is observed that usage of non-grain oriented fully processed electrical steel in stator and rotor core of electric motor is one of the measures to improve the efficiency of SI-PMSM motor. Use of M400-50A in stator and rotor core results not only in achieving reduction in core losses but also enhances the torque producing capability of the motor as compared to the usage of M19-29G.

It is established that appropriately designed trench cuts can be employed in stator and rotor structure without affecting the magnetic flux density for electric vehicle applications, where light weight and high-performance motors are preferred. The trench cuts are employed in Model III, Model IV, Model V and Model VI. It is observed that by providing trench cuts in models, the weight of the motor is reduced and power density is improved.

In addition, the model performance is investigated under deviation in parameter values using sensitivity analysis. The results show that Model with non-grain oriented electrical steel is less sensitive to perturbations in parameters value.

Chapter 7

Thermal Modelling of PMSM for Fault Diagnosis

7.1 General

Heat dissipation is observed in all energy conversion devices. Thermal supervision is an important feature of electric machine because it is one of the essential factors which defines operating range and overloading capacity of the machine [264-266]. The design methodologies of electric machines have matured during last decades. This leads to their usage in various industrial applications. However, overheating is still observed in machines due to inaccurate handling and abrupt faults.

This chapter presents the thermal analysis of designed and optimised PMSM models using Lumped Parameter Thermal Network technique. The LPTN models of both motors, PMSM-1 and PMSM-2, are designed. The change in the temperature in different parts of the motor under different operating conditions are computed using the designed LPTN models.

The LPTN models are utilized to carry out the fault diagnosis in the motor. To identify which part of the motor is faulty, statistical technique called Linear Discriminant Analysis (LDA) is used. Different nodes in LPTN are treated as differentiable classes (or groups). FEM analysis is used for evaluating the loss information in motor parts (nodes). The change in temperature is computed for different operating conditions and the corresponding discriminant functions are obtained for each class feature. For an unknown change in temperature at a particular operating condition, the specific classes are identified to diagnose the faulty part in the motor.

7.2 LPTN Structure

The fundamental rule for the construction of LPTN is to establish an equivalent electric circuit of the given electrical system, which is the SI-PMSM in this research work. Every part of the motor is represented by a node in the circuit. The mutual connection between two nodes takes place using thermal resistance between the corresponding nodes. Heat flow occurs through these resistances in LPTN models.

For a system having n_t nodes, the conductance matrix, $\boldsymbol{G}$, is expressed as given in equation (7.1). The power loss infused in each node is represented as a corresponding loss vector, $\boldsymbol{Pl}$, which is given in equation (7.2). The temperature vector, $\boldsymbol{\vartheta}$, given by equation (7.3) represents

the change in temperature with respect to the ambient working temperature of the system. The temperature of each node is computed by using (7.4).

$$\boldsymbol{G} = \begin{bmatrix} \sum_{i_t=1}^{n_t} \frac{1}{R_{1,i_t}} & \frac{-1}{R_{1,2}} & \cdots & \frac{-1}{R_{1,n_t}} \\ \frac{-1}{R_{2,1}} & \sum_{i_t=1}^{n_t} \frac{1}{R_{2,i_t}} & \cdots & \frac{-1}{R_{2,n_t}} \\ \cdots & \cdots & & \cdots \\ \frac{-1}{R_{n_t,1}} & \frac{-1}{R_{n_t,2}} & \cdots & \sum_{i_t=1}^{n_t} \frac{1}{R_{n_t,n_t}} \end{bmatrix} \tag{7.1}$$

$$\boldsymbol{Pl} = \begin{bmatrix} Pl_1 \\ Pl_2 \\ \cdots \\ Pl_{n_t} \end{bmatrix} \tag{7.2}$$

$$\boldsymbol{\vartheta} = \begin{bmatrix} \vartheta_1 \\ \vartheta_2 \\ \cdots \\ \vartheta_{n_t} \end{bmatrix} \tag{7.3}$$

$$\boldsymbol{\vartheta} = \boldsymbol{G^{-1}Pl} \tag{7.4}$$

7.2.1 Node Configuration

For the construction of LPTN structure, the optimal values of motor dimensions are used, which is presented in Table 7.1. The different materials used in analysis of models and their corresponding properties are shown in Table 7.2. The material properties are considered at ambient temperature. The various symbols used are pictorially shown in Fig. 7.1 for better clarity.

Table 7.1

Machine Dimensions (subscript 1 in the symbols indicates designation for PMSM-1 and subscript 2 in the symbols indicates designation for PMSM-2)

Parameters	**PMSM-1**	**PMSM-2**	**Parameters**	**PMSM-1**	**PMSM-2**
Poles,	6	14	Outer rotor radius (4_1 or 4_2)	33 mm	60 mm
Slots	9	36	Air gap length	0.8 mm	0.8 mm
Stack length	50 mm	150 mm	Stator inner radius (12_1 or 12_2)	33.8 mm	60.8 mm
Shaft Diameter	24 mm	28 mm	Inner radius of 1st tooth segment (9_1 or 9_2)	33.8 mm	60.5 mm
Magnet embrace angle (8_1 or 8_2)	52.9^0	21.8^0	Inner radius of 2nd tooth segment (10_1 or 10_{2a} & 10_{2b})	34.8 mm	62 mm & 62.2 mm

Parameters	PMSM-1	PMSM-2	Parameters	PMSM-1	PMSM-2
Magnet radial thickness ($4_1 - 6_1$ or $4_2 - 6_2$)	5.7 mm	8 mm	Inner radius of 3rd tooth segment (11_1 or 11_2)	49 mm	77.1 mm
Magnet inset side width (5_1 or 5_2)	3 mm	2 mm	Slot angle at 1st tooth segment (1_1or 1_2)	3.7^0	7.1^0
Magnet inner radius (9_1or 9_2)	27.3 mm	52 mm	Slot angle at 2nd tooth segment (2_1or 2_2)	3.7^0	5.3^0
Magnet outer radius (4_1 or 4_2)	33 mm	60 mm	Slot angle at 3rd tooth segment (3_1or 3_2)	20^0	4^0
Magnet pole eccentricity	3.8 mm	2 mm	Slot fill factor	0.45	0.45
Rotor symmetry section angle (7_1 or 7_2)	60^0	25.7^0	Stator outer radius	55 mm	100 mm
Conductor inner radius (12_1 or 12_2)	35 mm	62.18 mm	Conductor outer radius (13_1 or 13_2)	48 mm	76 mm

Table 7.2

Material used in the Motor and their Thermal Conductivities

Machine Part	Materials	Thermal Conductivity (w/mk) at 25° c
Rotor core	M400-50A	28
Stator core	M400-50A	28
Windings	Copper	401
Magnets	NdFeB	9

The concept of designing LPTN models is to develop a model for paths of heat flow occurring in the motor and thermal resistances associated to it. The axial flow of heat path mainly considers flow of heat from rotor node to the outer casing node. This research work aims to study the thermal performance of the motor at the design stage. At design stage, the basic model consists of stator, rotor, windings, magnets. Thus, the outer casing frame are not included for thermal study. The radial flow of heat path consists of mainly stator node, rotor node, winding node, tooth node, air gap node and yoke node; and has been considered here for developing LPTN models. The node configurations of both models are presented in Fig. 7.2. The node in the form of square, are dependent on radius as well as the angular position of the machine part whereas the node in the form of circle, depends only on radius of location of that machine part.

For example, the node in air gap is indicated by a circle as it is presumed that the temperature distribution is uniform at that particular radius. On the other hand, the magnet node is indicated by a square. It represents the temperature at particular angular position of magnet in the motor, i.e., at the middle of the magnet at that particular radius.

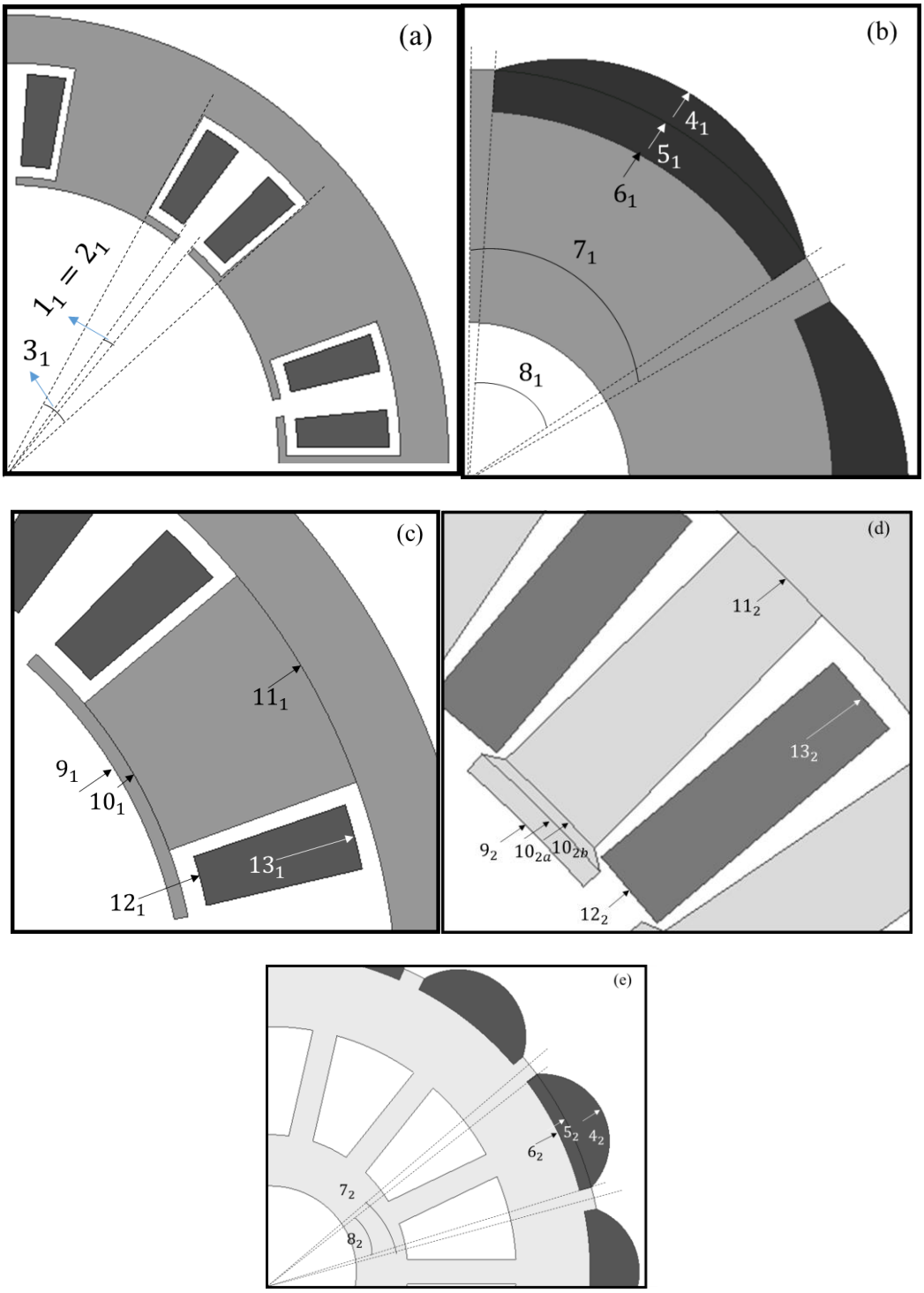

Fig. 7.1 Important Angles and Radii: (a) Stator of PMSM-1, (b) Rotor of PMSM-1, (c) Stator Tooth and Conductor of PMSM-1, (d) Stator Tooth and Conductor of PMSM-2, (e) Rotor of PMSM-2

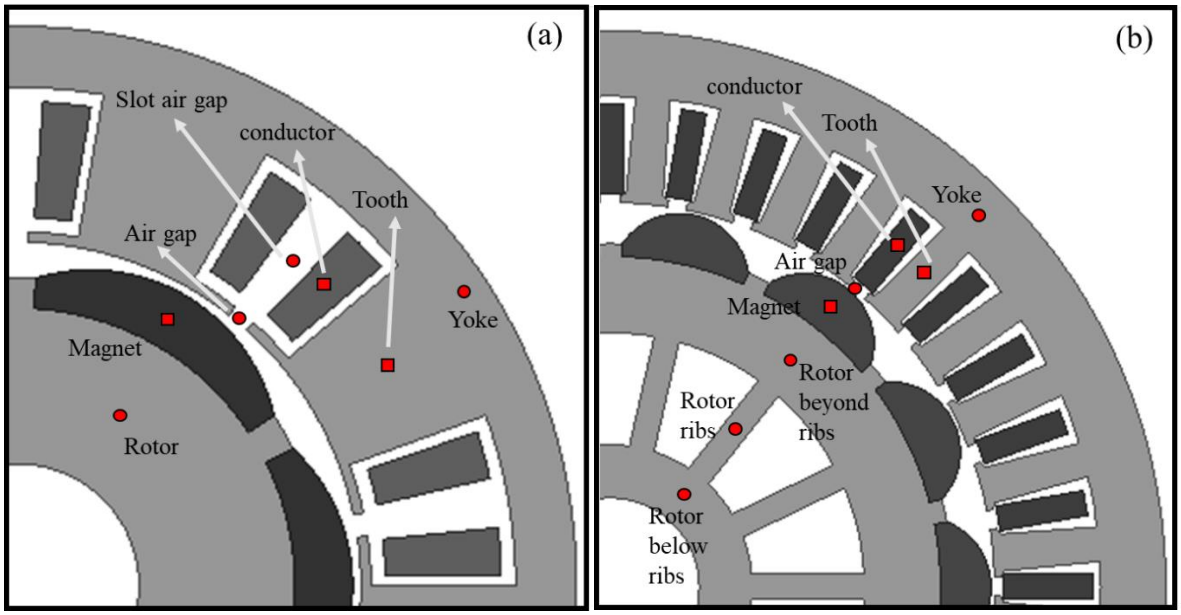

Fig. 7.2 Node Placement for designing LPTN Model : (a) PMSM-1, (b) PMSM-2

7.2.2 Computation of Conductance Matrices

This section elucidates the computing the thermal resistances between the nodes. For the computation of thermal resistance between node, various parts of the model structure are divided into different segments, each representing simple geometrical shapes. The segmentation performed in each part of the models are represented in Fig. 7.3. Then, each part of the structure is analysed and necessary assumptions are recorded to compute the corresponding thermal resistances associated with it.

For LPTN modelling, the air surrounding the area around the magnets is assumed to be having infinite thermal resistance. The slot openings are generally not addressed [267]. For the thermal investigation of motors, as a part of this research work, thermal resistances associated with air gap is considered infinite as the thermal conductivity of air is low. The thermal expansion phenomena related to metals and the variation in thermal conductivity with respect to temperature change is also ignored. It is because this information purely depends upon macroscopic parameters such as entropy, pressure, volume etc. At steady state, the macroscopic parameters do not alter with time. The thermal models, here, are developed at steady state condition. Hence, such variations are not considered in this investigation.

It is observed from Fig. 7.3 that the basic geometrical shapes are rectangular, hexahedrons, disk-shaped hollow cylinder or angular segment of hollow cylinder, as presented in Fig. 7.4. If thermal conductivity, λ, is known for a particular object, its thermal resistance is computed using

appropriate mathematical expression. The thermal resistance of a rectangular object is given by (7.5):

$$R_r = \frac{L_r}{\lambda A_r} \tag{7.5}$$

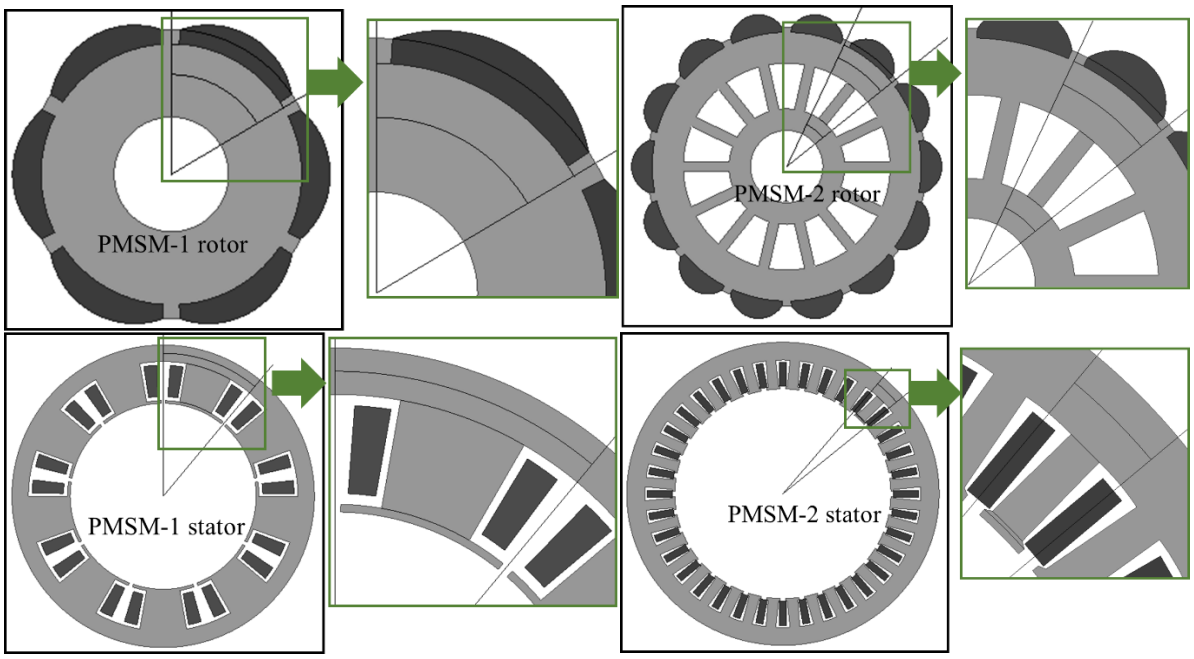

Fig. 7.3 Segmentation Performed in PMSM Models for Computation of Thermal Resistance

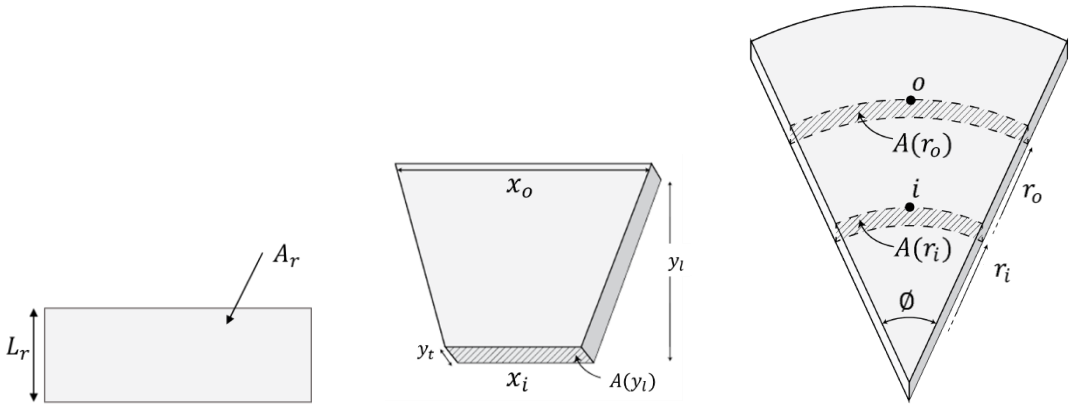

(a) (b) (c)

Fig.7.4 (a) Rectangular Object (b) Hexahedron (c) A Segment or Disk-shape of a Hollow Cylinder

The thermal resistance of a hexahedron is given as:

$$R_h = y_l \frac{\ln\left(\frac{x_o}{x_i}\right)}{y_t \lambda (x_o - x_i)} \tag{7.6}$$

Where y_t is the thickness, λ is thermal conductivity, x_i is inner width, x_o is outer width and y_l is the length of hexahedron.

The thermal resistance for disk-shaped hollow cylinder is computed using (7.7).

$$R_{hd} = \frac{ln\left(\frac{r_o}{r_i}\right)}{2\pi l_d \lambda} \tag{7.7}$$

Where variables r_i and r_o are inner and outer radii of such object. The computation of thermal resistance for a segment of angle ϕ at the centre is performed using :

$$R_{hs} = \frac{2\pi}{\phi} \frac{ln\left(\frac{r_o}{r_i}\right)}{2\pi l_s \lambda} \tag{7.8}$$

The design of LPTN model makes use of modelling symmetries present in the models. Around the perimeter of a cylindrical machine, the flow of heat is symmetrical in general. That means it is not recommended to put a node in each stator tooth. It is because the modelling symmetries can be used to scale thermal resistance of such part of the motor in order to obtain overall equivalent thermal resistance for that part of the machine. For example, if there are 'sm' symmetrical heat flow paths, ('sm' is symmetry factor), the effective thermal resistance, associated to a particular part of motor, is only '$1/sm$' times of the thermal resistance associated to the corresponding single element. Hence, for different parts of the rotor, the symmetry factor is the number of poles of that model and for different parts of the stator, the symmetry factor is the number of teeth or slots. The LPTN models for PMSM-1 and PMSM-2 are presented in Figs. 7.5(a) and 7.5(b) respectively. Air coolant is considered for developing LPTN models.

The conductance matrices for PMSM-1 and PMSM-2 are computed using thermal resistances between each node using (7.1). Since the nodes in LPTN models are placed in the middle of a particular part of the structure, it means only half distance is covered in the thermal resistance computation. Such two parts are in parallel for path of heat flow and hence, heat flow gets split up between them. In such cases, the thermal resistances are divided by 2. And in case of a node representing a fraction of machine, the corresponding thermal resistances are scaled by its symmetry factor.

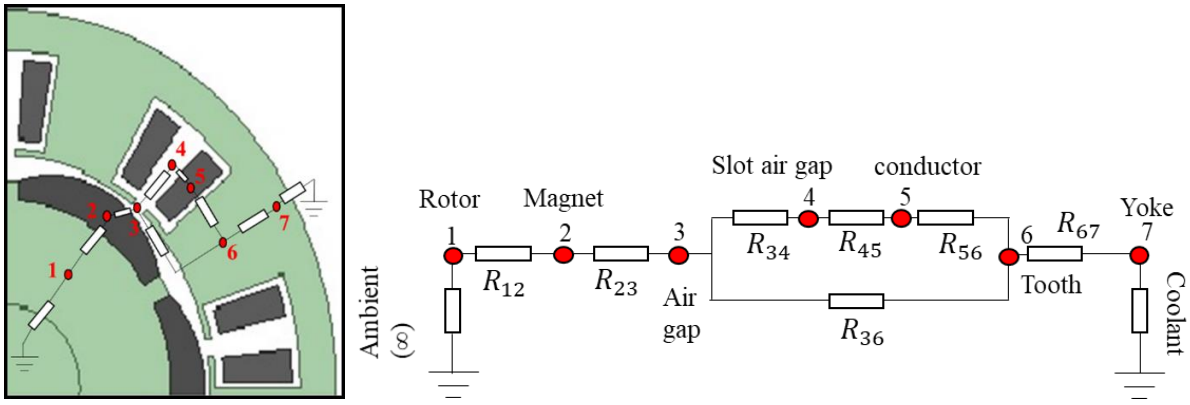

(i) (ii)

(a)

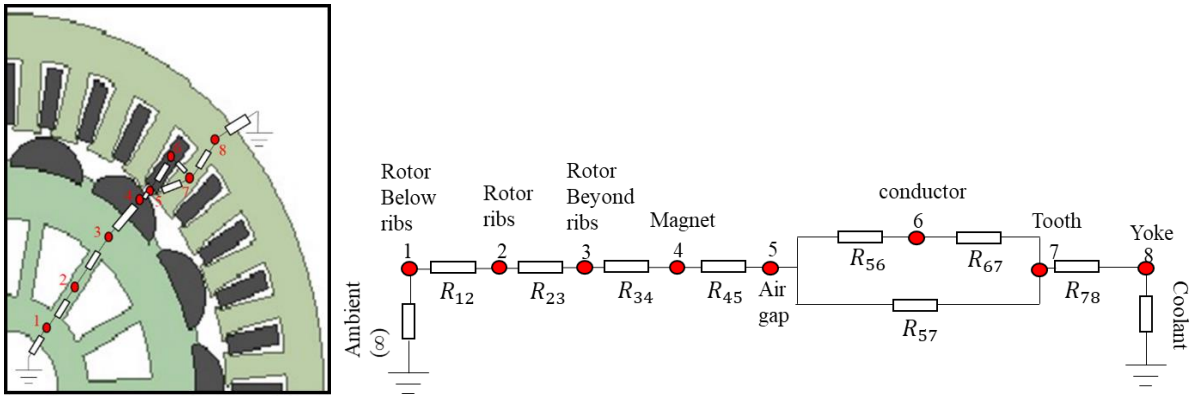

(i) (ii)

(b)

Fig. 7.5 LPTN based Thermal Modelling;

(a)(i) Node Placement in PMSM-1, (a)(ii) LPTN Model of PMSM-1;

(b) (i) Node Placement in PMSM-2, (b)(ii) LPTN Model of PMSM-2. (R_{pq} = thermal resistance between p^{th} and q^{th} nodes)

For computing vector $\boldsymbol{\vartheta}$ at a particular operating condition, the loss vector $\boldsymbol{Pl}$ is required, which is computed using FEM analysis. Simulations are performed, using ANSYS Maxwell, to calculate losses in each part, by setting eddy effects in the optimized models. The temperature of coolant is set to be constant at ambient temperature. The contact resistances are neglected for simplifying the analysis. The corresponding conductance matrices obtained for PMSM-1 and PMSM-2 are presented by (7.9) and (7.10) respectively.

$$G = \begin{bmatrix} 90.51 & -36.456 & -54.054 & 0 & 0 & 0 & 0 \\ -36.456 & 148.959 & 0 & -0.673 & 0 & 0 & 0 \\ -54.054 & 0 & 74.544 & 0 & -502.51 & -22.346 & 0 \\ 0 & -111.982 & -20.49 & 1.010 & -0.337 & 0 & 0 \\ 0 & -0.521 & 0 & -0.337 & 502.847 & 0 & 0 \\ 0 & 0 & 0 & 0 & 0 & 172.783 & -150.437 \\ 0 & 0 & 0 & 0 & 0 & -150.437 & 3756.639 \end{bmatrix} \quad (7.9)$$

$$G = \begin{bmatrix} 163.372 & -50.3778 & 0 & 0 & 0 & 0 & 0 & 0 \\ -50.3778 & 110.98 & -60.606 & 0 & 0 & 0 & 0 & 0 \\ 0 & -60.606 & 262.626 & 0 & 0 & 0 & 0 & 0 \\ 0 & 0 & -202.02 & -2.739 & -2.916 & 0 & 0 & 0 \\ 0 & 0 & 0 & -2.739 & 2047.867 & -1893.957 & -151.171 & 0 \\ 0 & 0 & 0 & 0 & -2.916 & -1893.57 & 1896.87 & 0 \\ 0 & 0 & 0 & 0 & -151.171 & 0 & 575.532 & -424.36 \\ 0 & 0 & 0 & 0 & 0 & 0 & -424.36 & 17552.76 \end{bmatrix} \quad (7.10)$$

7.3 Fault Diagnosis using LPTN

Fault diagnosis has evolved as an important practice for design engineers to analyse fault tolerance capability and ensuring reliability of the motor design. The usage of LPTN models for fault diagnosis in the overall motor geometry design is presented in this section. In LPTN modelling, equation (7.3) gives the rise in temperature at different nodes of the thermal model. To operate motor within the safe thermal limits of various parts, the change in temperature of different parts of the motor is required to be noted and observed at different operating conditions. For detecting the change in temperature, power loss analysis in various parts of the motor is performed. The practice of comparing the loss spectrum for unhealthy and healthy cases is not one of the accurate ways to figure which power component contributes the most comprehensive information to diagnose the fault and/or distinguish among the faults. Hence, the change is temperature of the nodes are chosen as features for analysis through classifier. Thus, to identify the faulty part of the motor, Linear Discriminant Analysis (LDA) methodology is used. The classification of faults is validated by implementing it for the two developed SI-PMSM models: PMSM-1 and PMSM-2.

For fault diagnosis, the models are analysed for two operating conditions: full load and 50% of full load operation. The different nodes in LPTN are treated as differentiable classes (or groups). The FEM analysis is used for obtaining the loss information in motor parts (nodes). The change in temperature is computed using the LPTN models, developed in previous section. In LDA, discriminant functions are obtained for each class feature. For particular unknown change in temperature data, the specific class can be identified to diagnose the faulty part in the motor.

7.3.1 LDA Classification w.r.t. Temperature Change

For implementation of LDA, initially various samples are recorded at different operating conditions of the models. For each class vector, t_q, the mean corrected vector, t_q^o, is computed by subtracting global mean vector, μ_g, from vector, t_q. Then, covariance matrix for each class, c_q, having S_q no. of samples is computed using (7.11)

$$c_q = \frac{(t_q^o)^T t_q^o}{S_q} \tag{7.11}$$

The overall covariance matrix is computed for each entry (r_C, s_C) using (7.12)

$$C_v(r_C, s_C) = \frac{1}{S}\sum_{q=1}^{t_q} S_q \, c_q(r_C, s_C) \tag{7.12}$$

Where S are overall total samples. Variables r_C and s_C denote the response no and sample no respectively. The discriminant function for each class is computed using (7.13).

$$f_q^{LD} = \mu_q {C_v}^{-1} t_\gamma^T - \frac{1}{2}\mu_q {C_v}^{-1} \mu_q^T + \ln(pr_q) \tag{7.13}$$

Where μ_q is the mean vector of each class, t_γ is γ^{th} object to be identified, $pr_q = \frac{S_q}{S}$ is the prior probability vector for each class. The particular object or unknown sample of temperature data is assigned to a particular class that has the maximum value of LD function [268]. For instance, a vector sample q is assigned to class or group φ, if and only if (7.14) satisfies:

$$f_\varphi(t_\gamma) \geq f_\gamma(t_\gamma) \; \forall \; \varphi \neq \gamma \tag{7.14}$$

7.3.2 Results and Discussions

For PMSM-1, the sample region contains 70 samples that belong to seven classes. For each class, 10 sample data are computed for speeds variation from 2100 rpm to 3000 rpm with a step of 100 rpm. Similarly, change in temperature along with the power loss analysis is performed for PMSM-2. Each class contains ten samples for speed variations from 2100 rpm to 3000 rpm in steps of 100 rpm.

The change in temperature vector, $\boldsymbol{\vartheta}$, for PMSM-1 and PMSM-2, observed for corresponding speed variation at full and 50 % full load condition are shown in Table 7.3 and Table 7.4 respectively. The corresponding discriminant functions are also shown for each class (node). Thereafter, for any unknown sample of temperature change data, the value of these LD functions is computed. The unknown sample belongs to that class or node which has the maximum value of LD function. For validation of accurateness of this method, that temperature change data is

collected whose class (node) is already known. For this, the model is run at different speeds. By comparing the result using analytical analysis and LDA classification, it is found that the appropriate classification has been performed by the proposed methodology. The corresponding change in temperature data and its classification results for PMSM-1 and PMSM-2 are shown in Table 7.5 and Table 7.6 respectively. The results obtained are validated through comparison with the results obtained through FEA analysis. It is found that the proposed method is capable of identifying the correct classification of faulty part in the motor for both the optimised models developed for PMSM-1 and PMSM-2.

Table 7.3

Change in Temperature Vector, $\boldsymbol{\vartheta}$ for corresponding Speed Variation of PMSM-1

Classes of Faults	**Samples for Temperature Change (^oC)**		**Mean vector μ_q ; q=class**	**Discriminant functions**
	Full Load	**50% Full Load**		
Class 1 (rotor)	[0.28; 1.00 ; … ; 1.05; 0.13]	[0.90; 0.08; … ; 0.08; 0.37]	[0.199 0.092]	$f_1^{LD} = \mu_1 {C_v}^{-1} t_\gamma^T - \frac{1}{2}\mu_1 {C_v}^{-1} \mu_1^T + \ln(pr_1)$
Class 2 (magnet)	[0.85; 0.62; … ; 0.29; 0.69]	[0.25; 0.07; … ; 0.47; 0.95]	[0.062 0.317]	$f_2^{LD} = \mu_2 {C_v}^{-1} t_\gamma^T - \frac{1}{2}\mu_2 {C_v}^{-1} \mu_1^T + \ln(pr_2)$
Class 3 (air gap)	[0.42; 0.10; … ; 0.09; 0.03]	[0.30; 0.49; … ; 0.24; 0.27]	[0.024 0.073]	$f_3^{LD} = \mu_3 {C_v}^{-1} t_\gamma^T - \frac{1}{2}\mu_3 {C_v}^{-1} \mu_3^T + \ln(pr_3)$
Class 4 (slot air gap)	[0.58; 0.34; … ; 0.25; 0.16]	[0.57; 0.25; … ; 0.06; 0.08]	[0.117 0.015]	$f_4^{LD} = \mu_4 {C_v}^{-1} t_\gamma^T - \frac{1}{2}\mu_4 {C_v}^{-1} \mu_4^T + \ln(pr_4)$
Class 5 (conductor)	[0.01; 0.06; … ; 0.19; 0.49]	[0.62; 1.28; … ;-1.26; 1.16]	[0.151 0.473]	$f_5^{LD} = \mu_5 {C_v}^{-1} t_\gamma^T - \frac{1}{2}\mu_5 {C_v}^{-1} \mu_5^T + \ln(pr_5)$
Class 6 (tooth)	[0.78; 0.13; … ; 0.33; 0.07]	[0.98; 1.36; … ; 0.19; 2.49]	[0.377 0.943]	$f_6^{LD} = \mu_6 {C_v}^{-1} t_\gamma^T - \frac{1}{2}\mu_6 {C_v}^{-1} \mu_6^T + \ln(pr_6)$
Class 7 (yoke)	[0.29; 0.32; … ; 0.43; 0.06]	[0.90; 0.68; … ; 6.45; 0.34]	[0.527 1.739]	$f_7^{LD} = \mu_7 {C_v}^{-1} t_\gamma^T - \frac{1}{2}\mu_7 {C_v}^{-1} \mu_7^T + \ln(pr_7)$

Table 7.4

Change in Temperature Vector, $\boldsymbol{\vartheta}$ for corresponding Speed Variation of PMSM-2

Classes of Faults	**Samples for Temperature Change (^oC)**		**Mean vector μ_q ; q=class**	**Discriminant functions**
	Full Load	**50% Full Load**		
Class 1 (rotor below ribs)	[2.28; 1.00 ; … ; 1.15; 1.13]	[1.90; 1.08; … ; 2.32; 1.33]	[1.173 1.042]	$f_1^{LD} = \mu_1 {C_v}^{-1} t_\gamma^T - \frac{1}{2}\mu_1 {C_v}^{-1} \mu_1^T + \ln(pr_1)$
Class 2 (rotor ribs)	[1.85; 1.62; … ; 1.29; 1.69]	[1.25; 2.37; … ; 1.47; 0.93]	[1.162 1.313]	$f_2^{LD} = \mu_2 {C_v}^{-1} t_\gamma^T - \frac{1}{2}\mu_2 {C_v}^{-1} \mu_2^T + \ln(pr_2)$
Class 3 (rotor beyond ribs)	[1.42; 1.18; … ; 1.09; 2.03]	[3.30; 1.49; … ; 1.24; 2.27]	[1.024 2.071]	$f_3^{LD} = \mu_3 {C_v}^{-1} t_\gamma^T - \frac{1}{2}\mu_3 {C_v}^{-1} \mu_3^T + \ln(pr_3)$
Class 4 (magnet)	[2.58; 1.84; … ; 1.15; 1.16]	[1.57; 1.25; … ; 1.06; 3.08]	[1.415 1.915]	$f_4^{LD} = \mu_4 {C_v}^{-1} t_\gamma^T - \frac{1}{2}\mu_4 {C_v}^{-1} \mu_4^T + \ln(pr_4)$

Classes of Faults	Samples for Temperature Change (^oC)		Mean vector μ_q ; q=class	Discriminant functions
	Full Load	50% Full Load		
Class 5 (air gap)	[1.01; 1.45; … ; 1.19; 2.49]	[1.69; 1.28; … ;1.26; 1.16]	[1.131 1.73]	$f_5^{LD} = \mu_5 {C_v}^{-1} t_\gamma^T - \frac{1}{2}\mu_5 {C_v}^{-1} \mu_5^T + \ln(pr_5)$
Class 6 (conductor)	[1.78; 1.91; … ; 2.62; 1.17]	[1.38; 1.31; … ; 2.19; 1.32]	[1.397 1.943]	$f_6^{LD} = \mu_6 {C_v}^{-1} t_\gamma^T - \frac{1}{2}\mu_6 {C_v}^{-1} \mu_6^T + \ln(pr_6)$
Class 7 (tooth)	[1.29; 1.32; … ; 1.48; 1.19]	[1.90; 1.68; … ; 1.43; 3.34]	[1.827 1.791]	$f_7^{LD} = \mu_7 {C_v}^{-1} t_\gamma^T - \frac{1}{2}\mu_7 {C_v}^{-1} \mu_7^T + \ln(pr_7)$
Class 8 (yoke)	[1.46; 1.62; … ; 1.52; 1.01]	[1.42; 1.64; … ; 1.45; 2.14]	[1.401 1.392]	$f_8^{LD} = \mu_8 {C_v}^{-1} t_\gamma^T - \frac{1}{2}\mu_8 {C_v}^{-1} \mu_8^T + \ln(pr_8)$

Table 7.5

Analysis of LDA Classification w.r.t. Temperature Change in PMSM-1; (Here t_γ represents a vector containing two temperature change values; one value at full load and second value at 50 % full load)

t_γ (γ^{th} object to be identified)	f_1^{LD}	f_2^{LD}	f_3^{LD}	f_4^{LD}	f_5^{LD}	f_6^{LD}	f_7^{LD}	Class No. using Analytical Classification	Class No. using LDA Classification
[0.73 0.22]	**59.78**	56.34	54.92	55.67	53.01	58.23	58.11	1	1
[0.01 0.05]	14.61	13.01	13.98	**15.91**	13.57	14.78	14.90	4	4
[0.19 0.56]	24.81	22.83	**26.91**	25.59	21.65	23.91	25.09	3	3
[0.85 0.45]	42.69	**44.91**	43.85	41.77	40.98	42.74	43.80	2	2
[0.01 1.41]	38.91	35.67	35.10	37.57	36.90	33.79	**39.41**	7	7
[1.03 0.23]	41.99	42.17	41.78	40.09	**43.17**	42.59	41.04	5	5
[0.85 1.08]	51.90	52.01	53.21	51.89	54.99	55.23	53.11	6	6

Table 7.6

Analysis of LDA Classification w.r.t. Temperature Change in PMSM-2; (Here t_γ represents a vector containing two temperature change values; one value at full load and second value at 50 % full load)

t_γ (γ^{th} object to be identified)	f_1^{LD}	f_2^{LD}	f_3^{LD}	f_4^{LD}	f_5^{LD}	f_6^{LD}	f_7^{LD}	f_8^{LD}	Class No. using Analytical Classification	Class No. using LDA Classification
[1.01 2.16]	24.61	23.22	23.98	**26.17**	23.27	24.17	24.18	25.91	4	4
[1.85 3.45]	61.69	**64.29**	63.86	61.37	63.98	62.74	62.81	61.99	2	2
[2.01 1.41]	36.91	35.63	32.16	32.57	37.15	33.79	**38.29**	34.91	7	7
[1.19 2.56]	44.81	42.83	**47.29**	45.59	44.65	43.91	45.09	46.82	3	3
[1.92 3.11]	60.19	65.34	63.54	63.21	60.32	64.38	63.28	**66.54**	8	8
[1.85 1.08]	51.90	52.01	53.21	51.89	54.99	**55.23**	53.11	52.49	6	6
[1.73 1.22]	**59.78**	56.34	51.92	55.58	50.01	48.26	48.61	50.33	1	1
[2.03 1.23]	61.99	64.17	61.78	60.07	**68.13**	62.59	61.04	62.59	5	5

7.4 Conclusion

This chapter presents the thermal modelling of PMSM models using LPTN technique. The nodal configurations of the developed optimised models for PMSM-1 and PMSM-2 are presented, where each node represents a part of the motor. For computing thermal resistances between these nodes, the motor geometries are divided into segments that have recognizable shapes. Thus, the conductance matrices are formed for both models. For computing change in temperature at each node, the loss vector is computed using FEM analysis.

The developed LPTN models are utilized for performing fault diagnosis in the developed optimised SI-PMSM Models. For this, the statistical approach of LDA is implemented. The linear discriminant (LD) functions for each class or node of LPTN models are computed in terms of the unknown temperature data. This is achieved by collecting various samples of temperature data at different values of speeds from 2100 rpm to 3000 rpm with step variations of 100 rpm. The motors are operated at full load and 50 % of full load condition.

For fault diagnosis, if any temperature vector is needed to be classified into a particular class (or node of LPTN), the value of LD functions is computed for each class using this temperature vector. The class, having the maximum value for that particular temperature vector, is found to be containing that sample of temperature vector. Or, in other words, the temperature vector belongs to that node of LPTN model, for which the maximum value of LD function is obtained. The results obtained from analytical classification is compared with those obtained from LDA classification. It is observed that proposed LDA classification is 100 % effective for fault diagnosis.

Chapter 8

Conclusion and Future Scope of Works

8.1 General

The EV industry is picking pace across the globe. The PMSM, due to its compact size, light weight and reliable operational characteristics, showcase its capability in multiple areas of EV application. The design stage of motor provides a good opportunity to improve its performance thereby reducing the operational cost. Depending upon the application, the design objectives are to be explicitly defined as a part of efficient design management. It is an established fact that variation in the GP of motor impacts the overall electromagnetic performance of motor. Therefore, the selection of appropriate GP and electro-mechanical parameters of motor at the design stage is of utmost importance. In addition, appropriate design optimization techniques should also be utilised for optimising the motor performance in accordance with the design objective. It is essential to reduce the design complexity using appropriate techniques. Surrogacy is an efficient technique to define the design objectives in the terms of input design parameters of motor. For design optimization, the surrogate models of various performance parameters are utilized as objective functions. MH techniques are applied to obtain optimized GPs of the motor.

8.2 Conclusion

This research work explores the modelling and analysis of two powertrains (a) one used in conventional ICE based powertrain, which use the spark ignition type of generic engine and (b) another power train used in EVs. The conventional powertrain is modelled in Simulink and the information obtained from the dynamic analysis of ICE powertrain is set as the benchmark parameters for evaluating the performance of electric powertrain. Key vehicle performance parameters like maximum speed attained and acceleration achieved using conventional ICE have been considered for setting the benchmark. Based on the set benchmark, the simulation model of the EVPT is developed using SI-PMSM with FOC as well as SVPWM control strategies. The developed simulation models of the EVPT are tested and analysed under various operating conditions including traction and braking modes of operation of vehicle. The designed controllers show fast response to load and speed perturbations and the proposed powertrain model is found suitable for EV application.

Two major uses of motor in EV application include use as compressor motor in environment conditioning system and use as traction motor. Accordingly, process cycle for the design and development of two SI-PMSMs, one a smaller sized compressor motor used in the environment conditioning system (PMSM-1) and the second a larger traction motor used in the drive system (PMSM-2) of EVs, having different ratings and configurations are discussed. The process includes the design and development of a preliminary model of the motor and its testing to ascertain suitability for the intended applications as stated above. The designs of the preliminary models are then optimised for better torque response and reduction of losses. In addition, sensitivity analysis of the designed models is also carried out. Thermal analysis of the optimised motor design is carried out using LPTN technique and utilised for fault diagnosis.

For the design and development of the preliminary models of PMSM-1 and PMSM-2, the motor configurations, GP and material properties for initial designs are discussed. FEM analysis of preliminary designs is carried out to verify the appropriateness of the designed models. The torque performance, back-emf at low-speed operation, flux linkage and mesh plots show accurate electromagnetic behaviour of the models. To obtain better electromagnetic performance of the developed preliminary models, variation in GP is carried out. It is found that even a small change of around 1 mm in various design parameters shows noticeable variation in electromagnetic performance of the motor. If GP of models are repeatedly changed, the task of redesigning and re-analysing the altered models becomes time consuming. To overcome this limitation, meta-models of various output characteristic parameters are designed using RSM scheme. Various experiments are performed to obtain FEM results with respect to variations of design parameters. Using the DOEs, the necessary β coefficients of RSM are obtained for corresponding output parameters through LSM technique. The verification of meta-models is carried out using RMSE test. The test results show that the meta-models are appropriately formulated.

The implementation of a novel ITM&GA mechanism for the development and performance analysis of an optimized model of PMSM-1, proposed to be used for compressor application in EVs, is enumerated. The improvement in torque characteristic of the motor helps in better compression and suction operations of the refrigerant in electric compressors of air conditioning systems of EVs. With increase in vehicle speed, electric compressors have to produce steady output power with less fuel consumption to maintain a good COP. For this prognosis, the motor geometry is optimized by performing 18 experiments in Phase I and then undergoing the surrogacy stage which further assists 100 experiments (generations) in genetic algorithms in

Phase II of the proposed ITM&GA optimization technique. The performance of initial model of PMSM-1 is compared with the model obtained by TTM and proposed ITM&GA techniques. It is observed that application of ITM&GA yields more reduction in cogging torque, torque ripples, THD and more improvement in torque characteristics as compared to TTM. By comparing the optimal model performance using TTM and ITM&GA, it is concluded that ITM&GA method improves motor performance of PMSM-1 substantially as compared to that obtained by TTM.

In addition, a novel hybrid metaheuristic optimization technique termed as Aquila-Grasshopper-Optimization is presented. The application of this hybrid metaheuristic optimization technique is elucidated to study the influence of core material and core trench on the performance of PMSM-2, which is intended to be used for traction application in EVs. Six structurally different topologies of models are designed, out of which three models have a low carbon silicon steel, M19-29G, as core material and rest three have a non-grain oriented fully processed electrical steel, M400-50A as core material. The meta-models for core-losses in terms of motor geometry parameters are developed using 36 FEM experiments and surrogate modelling technique. The performance of proposed novel AGO technique is tested for 23 Benchmark Functions and further implemented for the formulated core loss minimization problem. It is observed that usage of non-grain oriented fully processed electrical steel in stator and rotor core of electric motor improves the efficiency of SI-PMSM motor. Use of M400-50A in stator and rotor core results not only in achieving reduction in core losses but also enhances the torque producing capability of the motor as compared to the usage of M19-29G. It is inferred that by optimizing motor geometry at design stage, not only core losses are reduced but the overall torque performance of the motor is also improved.

It is observed that incorporating appropriately designed trench cuts in models reduces weight of the motor and improves power density. For applications where light weight and high-performance motors are preferred, appropriately designed trench cuts can be employed in stator and rotor structure without affecting the magnetic flux density. The performance of the optimized model of PMSM-2 is also investigated under deviation in parameter values using sensitivity analysis. The optimised Model with non-grain oriented electrical steel is less sensitive to perturbations in parameters value.

To validate the robustness of the designs of the developed SI-PMSMs, thermal modelling of PMSM models is done using LPTN technique. The nodal configuration of the developed optimised models for PMSM-1 and PMSM-2 are presented, where each node represents a part

of the motor. For computing thermal resistances between these nodes, the motor geometries are divided into segments that have recognizable shapes. Accordingly, conductance matrices are formed for both the models. Change in temperature at each node is estimated using the loss vector, computed using FEM analysis. The developed LPTN models are utilized for performing fault diagnosis in the optimised SI-PMSM models. For this, the statistical approach of LDA is implemented. The linear discriminant functions for each class or node of LPTN models are computed in terms of unknown temperature data. This is achieved by collecting various samples of temperature data at different values of speeds from 2100 rpm to 3000 rpm with a step variation of 100 rpm. The motors are operated at full load and 50% of full load condition. The results obtained from analytical classification is compared with those obtained from LDA classification and it is observed that proposed LDA classification is effective for fault diagnosis.

8.3 Scope of Future Work

Through this research work, the defined objectives are achieved successfully. However, the research work can further be expanded by using multi-objective functions for efficiency optimization of motor. Multi-objective design optimization is altogether a vast area of research in which the Pareto optimal solution is to be utilised to satisfy multiple conditions at the same time. Further, the thermal modelling of motor models can be performed by performing the division of geometry into complex structures. And the thermal models can be exploited for more research application areas other than fault diagnosis.

Appendix A: Laboratory Testing of EVPT System using Test Bench Emulator

In this Appendix, the technical details of different components of emulator system are presented. In addition, the control circuitry developed for applying sensor-less control using field-oriented control technique is also discussed.

A.1 EVPT Test Bench Emulator

In the proposed emulator system, a 3 Hp, 380 V Compage PMSM is coupled with pulley, wheels and 1.68 Hp, 380 V Compage PM synchronous generator. The PMSM acts as the traction device, extended motor shafts and pulley system acts as transmission unit and gear system for EVPT system respectively, as shown in Fig. A.1. Table A.1 presents the specifications of various components of EVPT system.

A.2 Belt Pulley Transmission System in EVPT Emulator

The simple belt-pulley drive system is utilized in the emulator system. It is performing the job of transmission unit in the system. The schematic diagram of belt-pulley transmission system is shown in Fig. A.2.

The vehicle and wheel speed can be derived as function of motor speed provided the parameters of transmission system are known. It is assumed that zero slip is present in mechanical parts of the system, wheels have same radius and vehicle is moving in straight line. Therefore, left wheel rotational speed (ω_{wl}) and right wheel rotational speed (ω_{wr}) will be equal, given by (A.1).

$$\omega_{wl} = \omega_{wr} = \omega_w \tag{A.1}$$

Where ω_w is wheel rotational speed in rad/s. Vehicle and wheel moves in linear direction together due to which linear speed of vehicle is same as that of wheel. Thus, if we compute linear speed of wheel, we obtain the speed of vehicle, given by (A.2).

$$v_{wl} = v_{wr} = v_w = v_v \tag{A.2}$$

Where v_{wl} and v_{wr} are left and right wheel linear speed respectively. The variables v_w and v_v are linear speed of wheel and vehicle respectively. For the belt-pulley system, the pulley ratio is defined by (A.3).

$$p_r = \frac{r_{dn}}{r_{dr}} \tag{A.3}$$

The rotational speeds of driver pulley (of radius r_{dr}) and driven pulley (of radius r_{dn}) are related to the pulley ratio as (A.4).

$$\frac{\omega_{dr}}{\omega_{dn}} = \frac{r_{dn}}{r_{dr}} = p_r \quad \text{(A.4)}$$

Where ω_{dr} and ω_{dn} represents rotational speeds of driver and driven pulley respectively.

Since the driver pulley is connected to the traction motor through the motor shaft, the driver pulley rotational speed will be equal to motor rotational speed, ω_m, given by (A.5).

$$\omega_{dr} = \omega_m \quad \text{(A.5)}$$

Now the corresponding pulley ratio will reduce the wheel speed. So the wheel rotational speed is given as (A.6):

$$\omega_w = \frac{\omega_{dn}}{p_r} \quad \text{(A.6)}$$

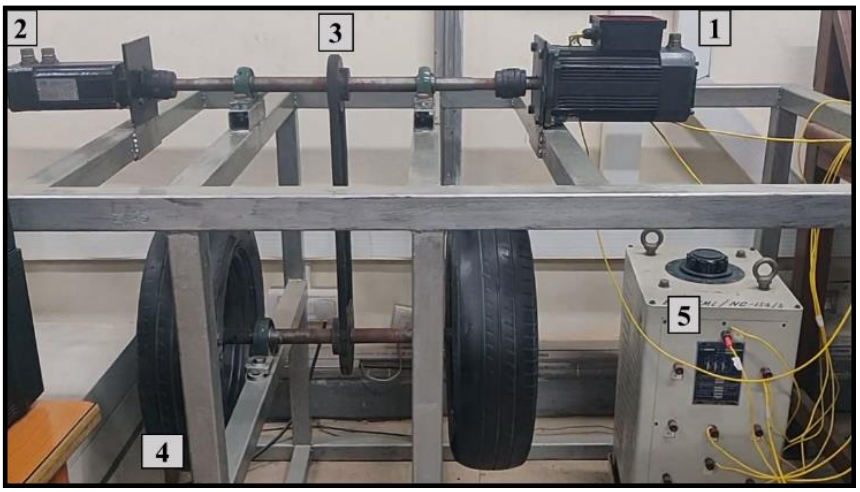

Fig. A.1 EVPT Test Bench Emulator System consisting of 1: PMSM, 2: PMSG, 3: Belt-pulley system, 4: Wheel, 5: Three phase Autotransformer

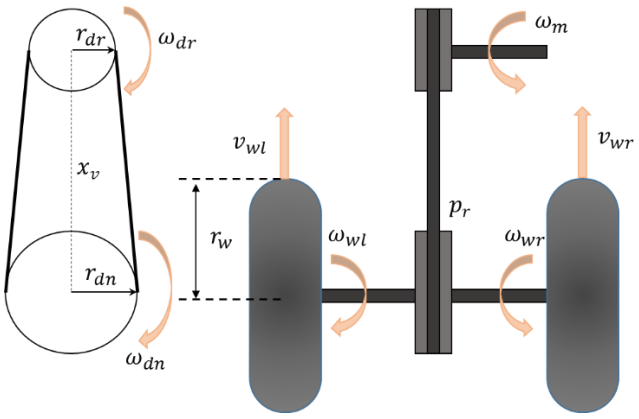

Legend

r_{dr}	: driver pulley radius in m
r_{dn}	: driven pulley radius in m
x_v	: vertical distance between pulleys in m
ω_{dr}	: driver pulley rotational speed in rad/s
ω_{dn}	: driven pulley rotational speed in rad/s
ω_m	: motor rotational speed in rad/s
ω_{wl}	: left wheel rotational speed in rad/s
ω_{wr}	: right wheel rotational speed in rad/s
v_{wl}	: left wheel linear speed in m/s
v_{wr}	: right wheel linear speed in m/s
p_r	: pulley ratio
r_w	: wheel radius in m

Fig. A.2. Schematic Representation of PT Transmission System

The linear speed of wheel, v_w, in m/s is given as (A.7):

$$v_w = \omega_w \times r_w \quad \text{(A.7)}$$

By the combination of equations (A.4), (A.5), (A.6), (A.7), the vehicle or wheel linear speed is obtained in m/s as (A.8):

$$v_v = v_w = N_m \times \frac{\pi}{30} \times \frac{1}{{p_r}^2} \times r_w \quad \text{(A.8)}$$

Where N_m is rotational speed of motor in rpm.

So the vehicle (V_v) or wheel (V_w) linear speed in km/h is calculated as (A.9):

$$V_v = V_w = \frac{3.6\, N_m\, \pi\, r_w}{30\ {p_r}^2} \quad \text{(A.9)}$$

This derived equation helps to monitor the vehicle/wheel speed during emulator speed testing.

Table A.1

Emulator System Specifications

Motor Specifications			
Power	2.28 kW	Field intensity	3.035 x 10^{-3} Nm-sec
Voltage	380 V	Moment of inertia	1.5x10^{-3} kg-m^2
Torque	24 Nm	Magnetic flux	0.1194 V-sec
Poles	6	Line resistance	2.8 Ω
Phases	3	Line inductance	26 mH
Vehicle Specifications			
Wheel Mass	1100 kg	Wheel velocity threshold	0.05 m/s
Frontal Area	3 m^2	Wheel radius	0.25 m
Drag Coefficient	0.4	Rolling radius	0.3 m
Load capacity	1600 kg	Driven to drive pulley ratio	1.5

A.3 Test Bench Control Set up

Three phase supply is applied to the three-phase inverter system. IGBT modules, SKM75GB12T4 are used for providing fast switching using the PWM pulses generated using the C code written in the IDE tool called Kinetis Design Studio (KDS), which is the test software for Freescale microcontroller unit (MCU). TWR-KV46F150M MCU is used for implementing control of the drivetrain. The Specifications of MCU is given in Table A.2. To operate the MCU, control circuitry is needed for limiting the three phase currents and DC bus rectified voltage under the range of 0-3.3 V. LEM 55P current sensors are used to sense the stator input currents to the motor which is operated by supplying $\pm$15V. The DC regulated supply is provided using 2231A-30-3 Triple Channel Keithley DC power supply. The schematic diagram of control circuitry is presented in Fig. A.3. The test bench developed for the EVPT emulator system is shown in Fig. A.4.

A.4 Sensor-less Field Oriented Control of EVPT system

The motor parameters vary with the dynamics of the vehicle which makes the calculation of motor quantities quite difficult. So, for simplifying calculation part, dynamic model of motor is developed in the synchronously rotating frame. Clarke's and Park's transformations are applied to convert three phase to two phase quantities in stationary and rotating reference frames respectively. The stator voltages, V_d and V_q in direct and quadrature axes are given by (A.10) and (A.11) respectively. The stator fluxes, $\lambda_d$and $\lambda_q$in two orthogonal axes are given by (A.12) and (A.13) respectively.

Table A.2

TWR-KV46F150M Microcontroller Specifications

Features	**Value**
KV46F256VLL15 Processor	150 MHz ARM Cortex M4+ core
Memory	256 KB flash, 32 KB SRAM
Timing and control	18 channels Flex Timer modules (FTM), four 32 bit periodic interrupt timer (PTT)
Mixed signal channels	Two 12 bit ADC
Connectivity	Two UARTs (RS232), SPI and I^2C module
System power	5 V from USB or power jack J516
Debug Interface	2x10 pin ARM Cortex JTAG connector
Analog inputs	Four thermistors RT1-RT4 (10kΩ), operating temperature: $-20^oC\ to\ 90^oC$

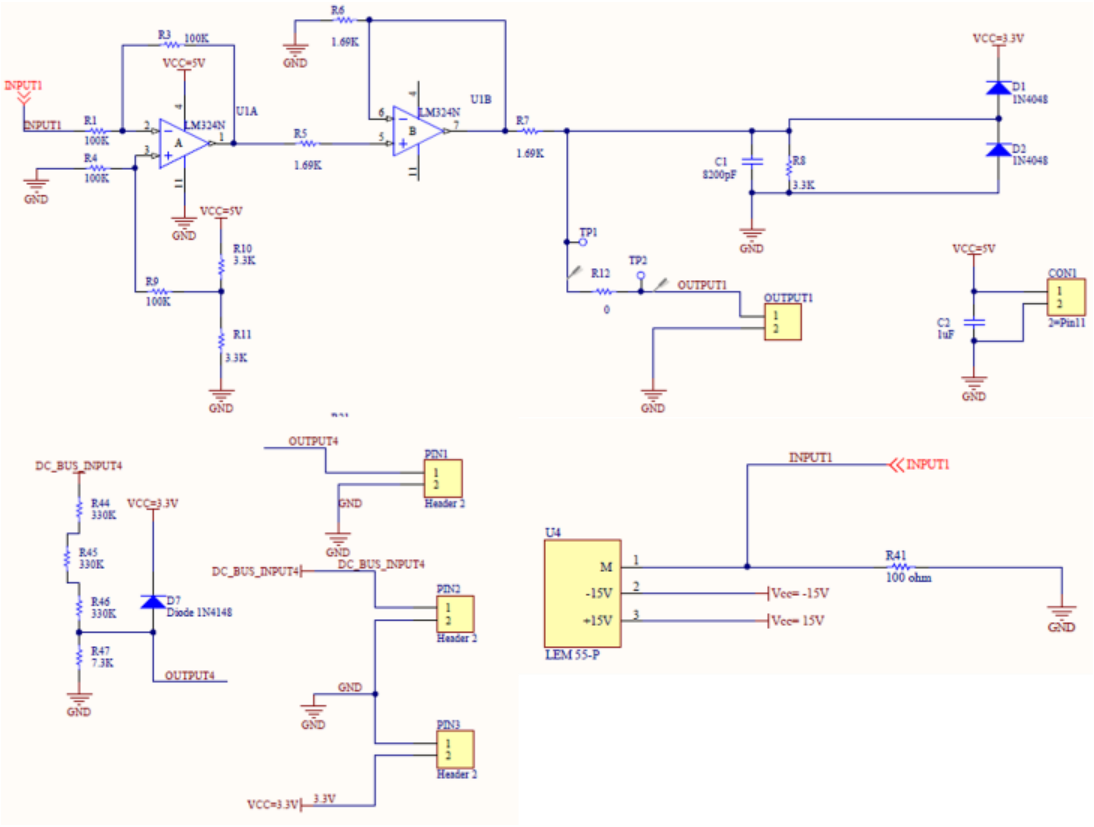

Fig. A.3 Schematic Diagram of Control Circuitry

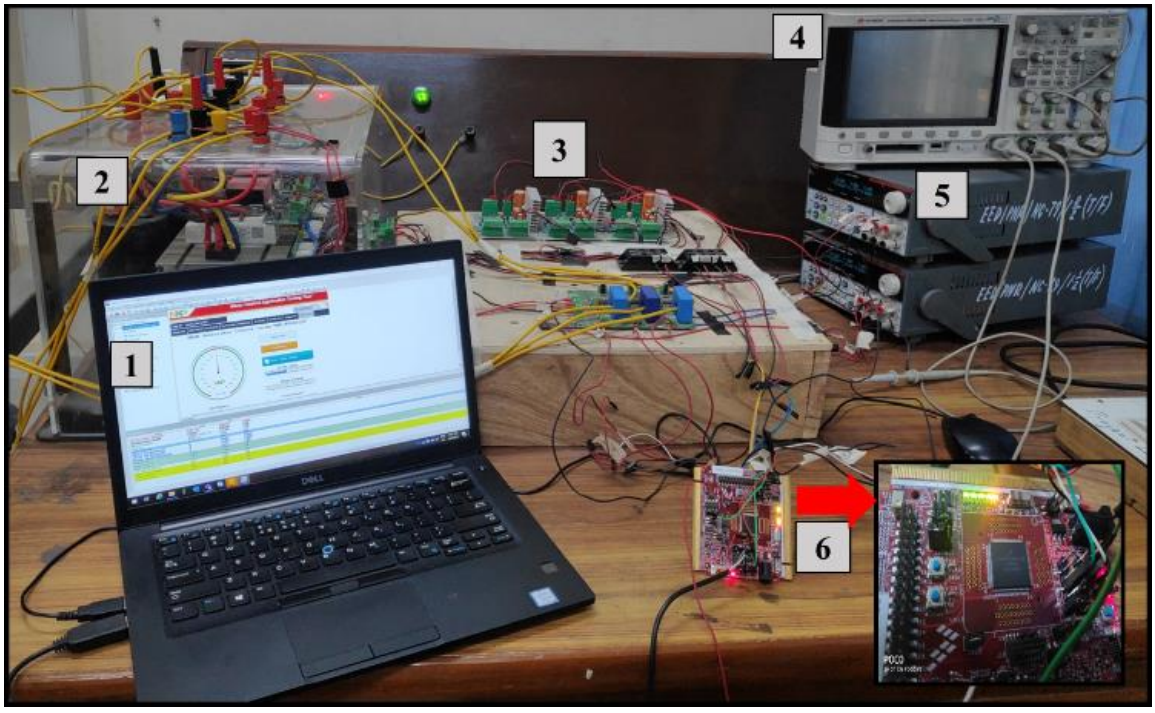

Fig. A.4 The Test Bench Set Up consisting of 1: Human Machine Interface, 2: Three Phase Inverter, 3: Control Circuitry, 4: DSO, 5: Regulated DC Supply, 6: MCU

$$V_d = R_s I_d + \frac{d}{dt}\lambda_d - \omega_r \lambda_q \tag{A.10}$$

$$V_q = R_s I_q + \frac{d}{dt}\lambda_q + \omega_r \lambda_d \tag{A.11}$$

$$\lambda_q = L_q\, I_q \tag{A.12}$$

$$\lambda_d = L_d I_d + \lambda_m \tag{A.13}$$

Where λ_m is the flux produced by PMs, R_s is stator resistance, ω_r is rotor speed, L_q, L_d, I_q, I_d are quadrature and direct axes inductances and currents respectively. The electromagnetic torque, T_{em} developed by PMSM is given by (A.14):

$$T_{em} = \frac{3}{2}P\left(\lambda_d I_q - \lambda_q I_d\right) = \frac{3}{2}P\left(\lambda_m I_q + (L_d - L_q) I_q I_d\right) \tag{A.14}$$

The mechanical equation of torque for motor having load torque T_l is given by (A.15):

$$T_{em} = \frac{J_m}{P}\frac{d}{dt}(\omega_r) + \frac{B_m}{P}\omega_r + T_l \tag{A.15}$$

In FOC technique, the torque and flux producing components of the stator currents are decoupled to control them independently using conventional PI controllers. In sensor-less control, the motor control is analysed by shifting the perspective from stator to rotor. A new position and speed estimator block is added to calculate the possible rotor position and speed respectively. The detailed block diagram to implement sensor-less control of PMSM is presented in Fig. A.5.

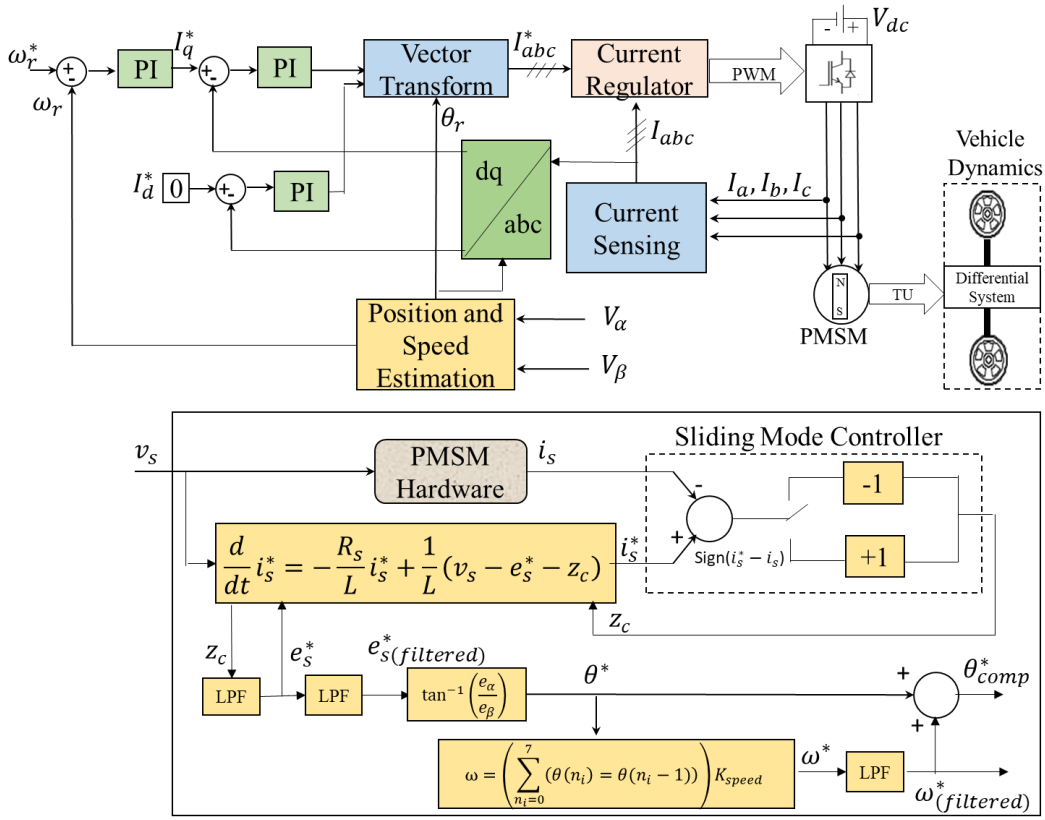

Fig. A.5 Schematic Diagram for Sensor-less FOC of EVPT

Two terms in (A.14) are called 'Magnetic torque', produced by permanent magnets along with q axis current I_q and 'Reluctance torque', produced due to interaction of direct and quadrature axes currents respectively. Reluctance torque operation is helpful in flux weakening region of the torque speed curve beyond base speed of the motor which is a crucial affair for operating traction motor. Whereas magnetic torque component is utilized in field-oriented control in which direct axis stator current I_d is maintained equal to zero and I_q component of stator current is controlled to regulate the speed of powertrain system. Sensor-less control strategy is based upon the back emf estimation using electrical model of PMSM in simplified form. By observing per phase PMSM electrical model (Fig. A.6), the phase resistance, phase inductance and back emf of the motor follow the mathematical relationship given by (A.16). This equation is simplified to obtain digital interpretation of phase current ((A.17) - (A.19)).

$$v_s = Ri_s + L\frac{d}{dt}i_s + e_s \tag{A.16}$$

$$\frac{d}{dt}i_s = -\frac{R}{L}i_s + \frac{1}{L}(v_s - e_s) \tag{A.17}$$

$$\frac{i_s(z+1)-i_s(z)}{T_{sp}} = -\frac{R}{L}i_s(z) + \frac{1}{L}(v_s(z) - e_s(z)) \tag{A.18}$$

$$i_s(z+1) = \left(1 - T_{sp}\frac{R}{L}\right)i_s(z) + \frac{T_{sp}}{L}(v_s(z) - e_s(z)) \tag{A.19}$$

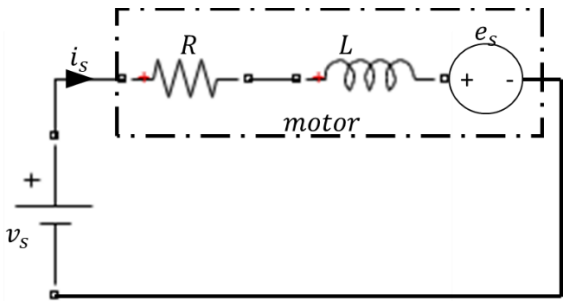

Fig. A.6 Simplified per phase Electrical Model of PMSM

Where $i_s(z+1)$ is the present sample current vector, $i_s(z)$ is previous sample current vector, $v_s(z)$ is previous sample voltage vector, $e_s(z)$ is previous sample back emf vector and T_{sp} is the sampling period. The position and speed estimator works by observing the measured current from motor hardware and estimated current from digitized motor model. The Sliding Mode Controller generates an output voltage correction factor voltage (z_c) on the basis of the sign of the error between measured and estimated currents. The correction factor voltage z_c is filtered to obtain back emf which is updated over every control cycle. Vector components of back emf (e_α, e_β) are used to estimate theta. By the cause of filtering action applied during theta

estimation, theta has to be compensated which depends on the speed of the motor. This compensation is performed by first calculating motor speed by sampling method and then filtering it to obtain the amount of compensation. The outputs obtained from the position and speed estimator block are estimated theta and motor speed.

A.5 Results and Discussions

The analysis of the results obtained from the simulation studies of the model and developed laboratory emulator system are presented herein.

Simulink Model

A MATLAB/Simulink model of EVPT system is developed and analysed under different operating conditions of the vehicle. The designed model is presented in Fig. A.7 consists of vehicle body connected via transmission and differential system, which is used for transferring mechanical energy in the powertrain system. The performance of implemented controller is tested by running Simulink model for four different cases; constant speed, variable speed, ramped speed and braking modes of operation.

a) Constant Speed Operation:

By setting constant reference speed of 100 rad/s, the speed tracking capability of the system is analysed under load torque variation. Gain constants of the controller are chosen as: K_p =1000 and $K_I = 5$ respectively. The initial values of all estimated parameters are assumed to be zero. The load disturbance of 15 Nm is applied at t=1.5 s. It is observed that initially vehicle runs at 70 km/h steadily and the vehicle accelerates (@ 5.5 m/s2) at the instant of load variation as the controller generates the required q-axis current, i_q to control drive speed thereby tracking the load variation accurately. Stator reference currents, torque, motor and vehicle speed plots are shown in Fig. A.8.

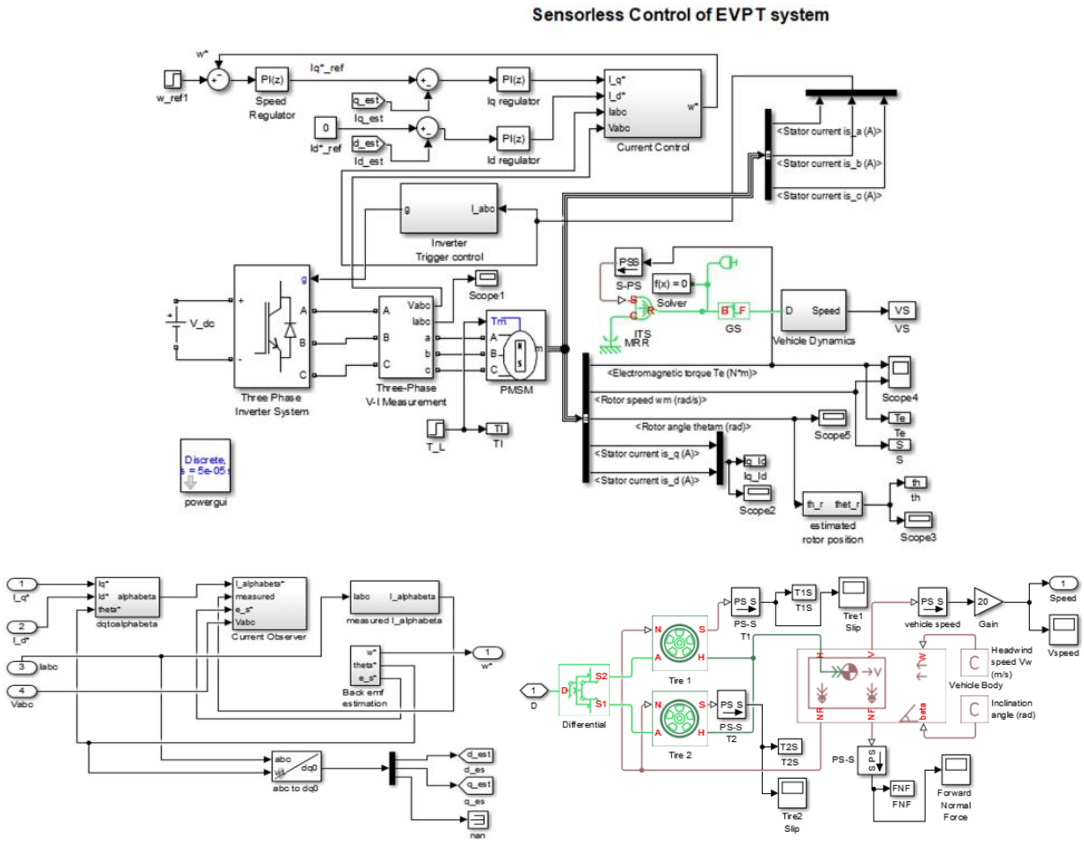

Fig. A.7 MATLAB/Simulink Model of the EVPT

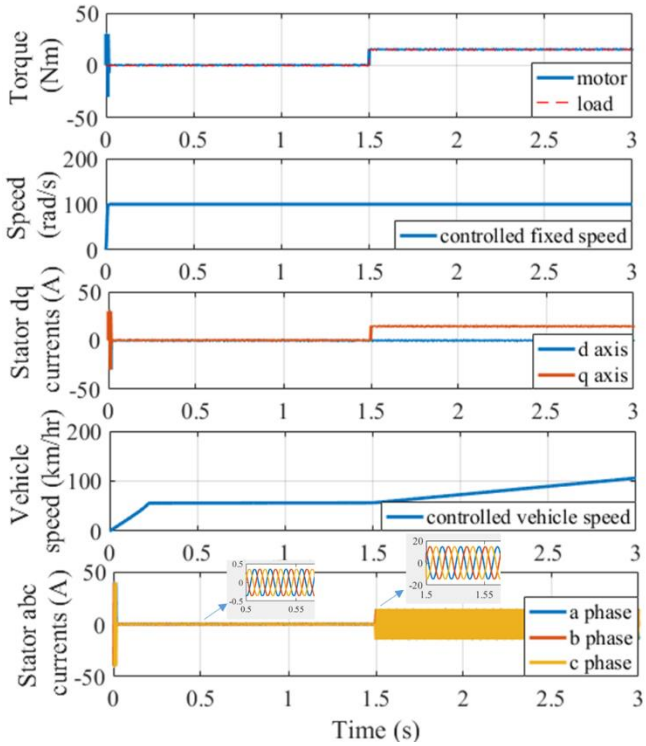

Fig. A.8 Simulink Model Response for Fixed Speed Profile with Variable Load

b) Variable Speed Operation:

The motor is started from rest. A change of speed command from 0 rad/s to 150 rad/s is given to the system at t = 1s. Thereafter, a load disturbance of 10 Nm is given to the system at t = 2s. The vehicle accelerates *@ 33.3 m/s*^{2} at speed command and *@ 6.9 m/s*^{2} at load command. Simulation result plots for motor and vehicle speed, torque and current are shown in Fig. A.9.

c) Ramped Speed Operation:

When the model performance is tested with an increasing reference speed with acceleration of 1 rad/s2 input, it is observed that vehicle starts with a speed of 40 km/h and then runs at steady speed until a load disturbance of 10 Nm at t = 1 s. Thereafter, vehicle accelerates at 4.16 m/s2. The speed regulation performed by controller to the EVPT system is shown in Fig. A.10.

The above mentioned three case studies report the behaviour of EVPT system for traction mode of vehicle.

d) Braking Mode of Operation:

For testing the braking mode, the load is varied at t =1 s from 10 Nm to 0 Nm and the speed command is given to the system from 150 rad/s to 0 rad/s at t = 2 s. The vehicle runs initially at 80 km/h and is observed to be decelerating at 16.6 m/s2 at the instant of braking and reaches to 0 km/h at 2.29 s (Fig. A.11).

This study shows that field control is easy to implement and can be effectively used to regulate the necessary vehicle speed.

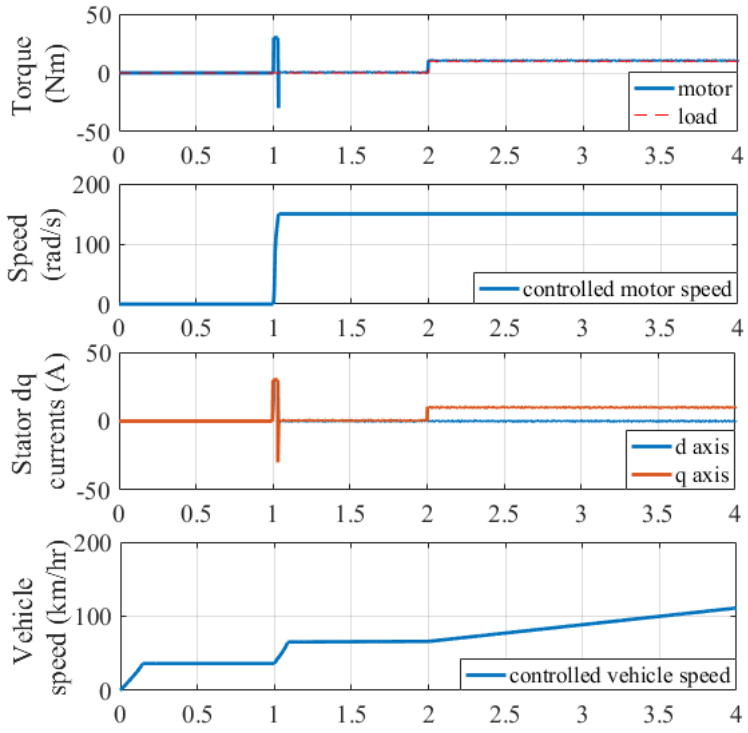

Fig. A.9 Simulink Model Response for Step Variable Speed and Load Profile

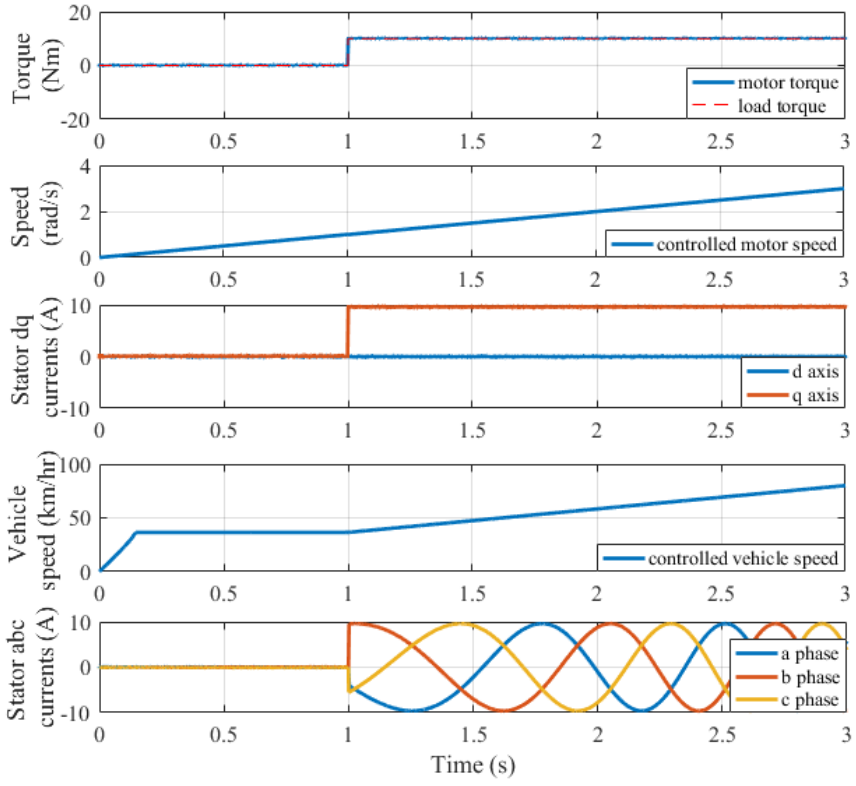

Fig. A.10 Simulink Model Response for Increasing Speed Profile with Variable Loading

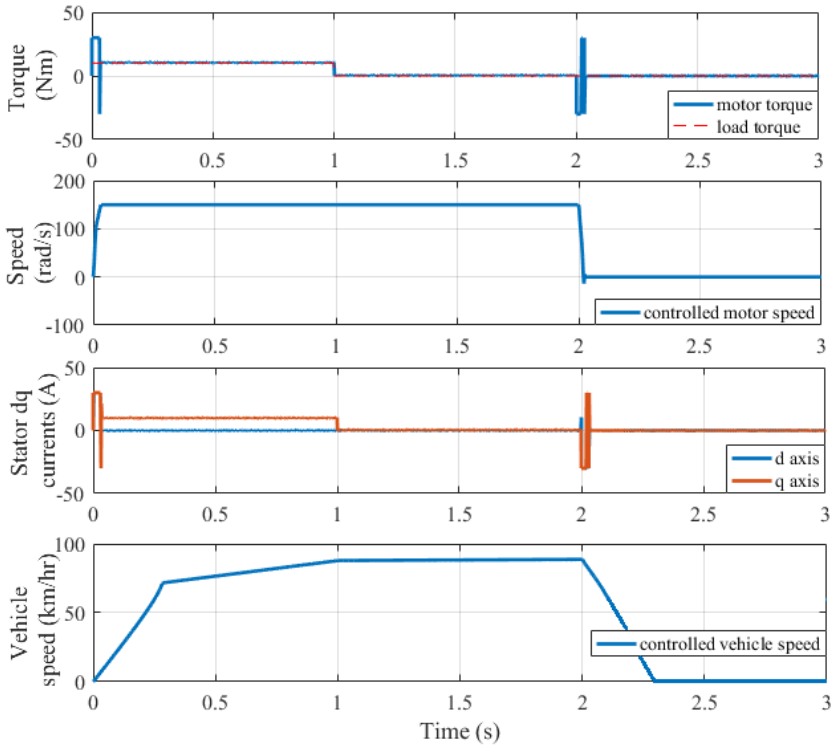

Fig. A.11 Simulink Model Response for Decreasing Speed Profile

EVPT Emulator Analysis

The emulator is supplied with 290 V, 3φ voltage using 18.28 kVA, 415 V, 3 φ variable autotransformer. The rectified DC voltage is given as input to the MCU unit. This is because the sensor-less control operation requires initial minimum speed to obtain estimated back emf value. At first, FreeMASTER executes the start-up subroutine to provide the initial jerk/ramp to the motor by energizing stator windings with suitable estimated rotor position angle. The communication for this control operation is performed by FreeMASTER through the USB interface. FOC regulates I_d and I_q accordingly during the whole process. Then as the motor accelerates, the required d and q axis currents are generated accordingly. The motor is tested for different modes of operation as described below:

a) Start-up Mode

Initially, 50 V DC supply is given to the MCU to perform start up process to estimate the possible rotor position. The ramps are provided at the interval of 1.4 s to establish the alignment of the rotor with the rotating flux linkage. The wheels attain maximum of 69.9 rpm initially. Thereafter, the d and q axes currents are generated to get the desired initial speed ramp and torque. Response of EVPT system during start up process is shown in Fig. A.12.

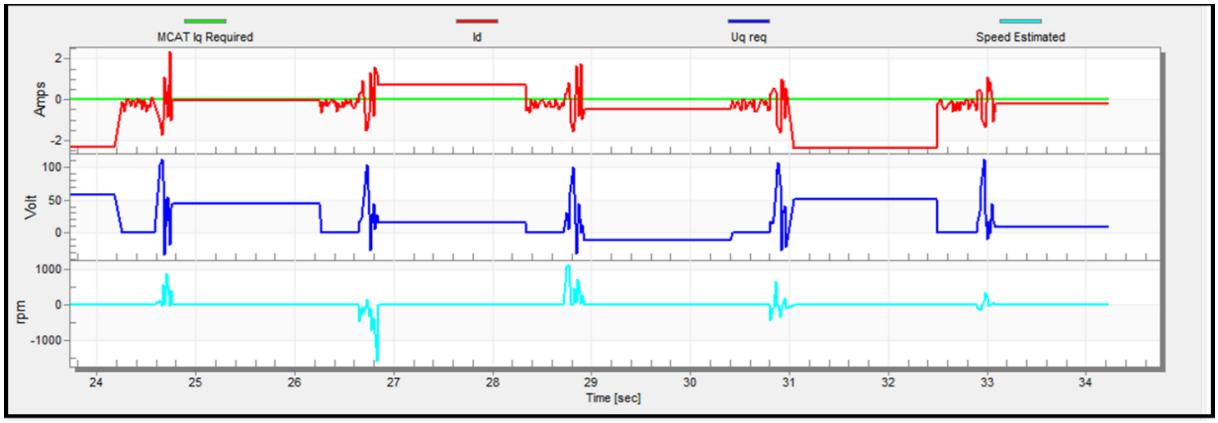

(a)

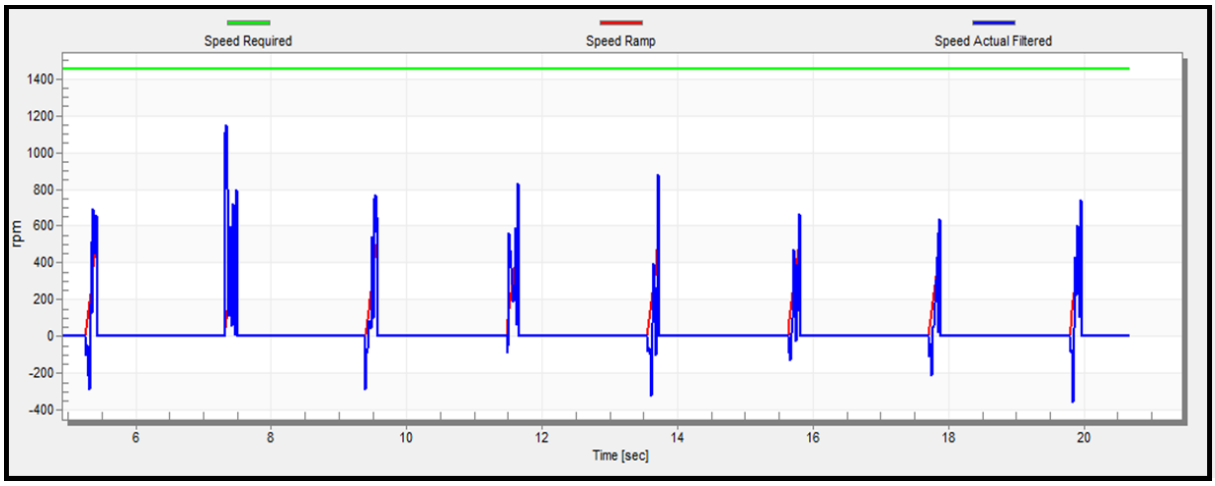

(b)

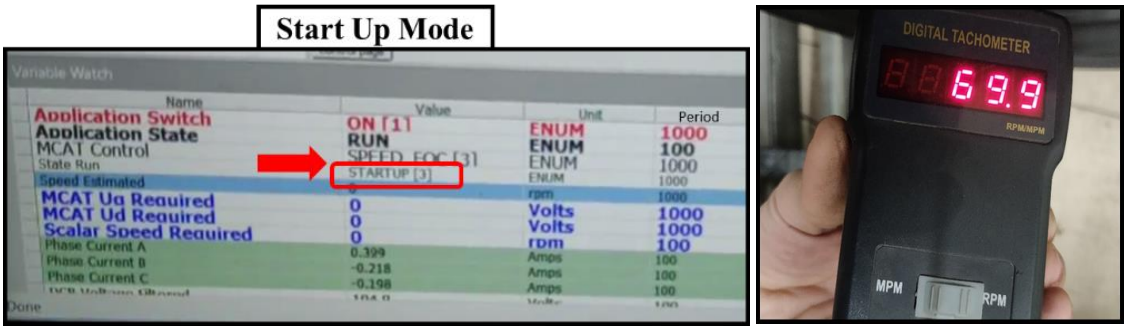

(c)

Fig. A.12 Response of EVPT during Start-up Mode, (a) Speed, Uq, d and q axes plots, (b) Speed response of EVPT, (c) FreeMASTER 2.0 Variable Watch Window and tachometer reading for start-up

b) Freewheeling Mode of Operation

Freewheel or rolling mode is a mode of operation in which vehicle PT system performs the apparent check of currently effective driving speed. The current and speed response during freewheel operation are shown in Fig. A.13. At the end of start-up and freewheel mode, the software switches the logic to sensor-less closed loop control. Based on different speed commands given to the motor, the estimated and measured values of wheel or vehicle speeds

are recorded in Table A.3. It can be seen that the error between estimated and measured speeds is ~0.05% which verifies the feasibility of belt-pulley system transmission system used in the emulator system.

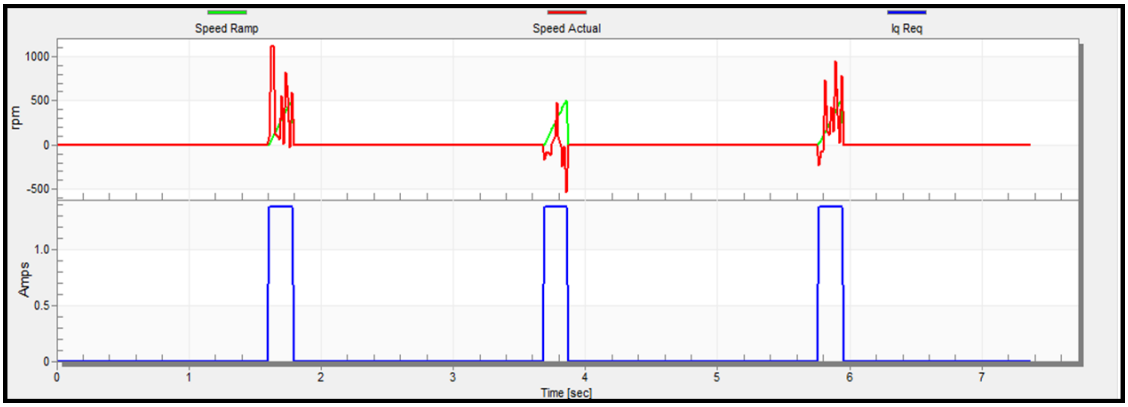

(a)

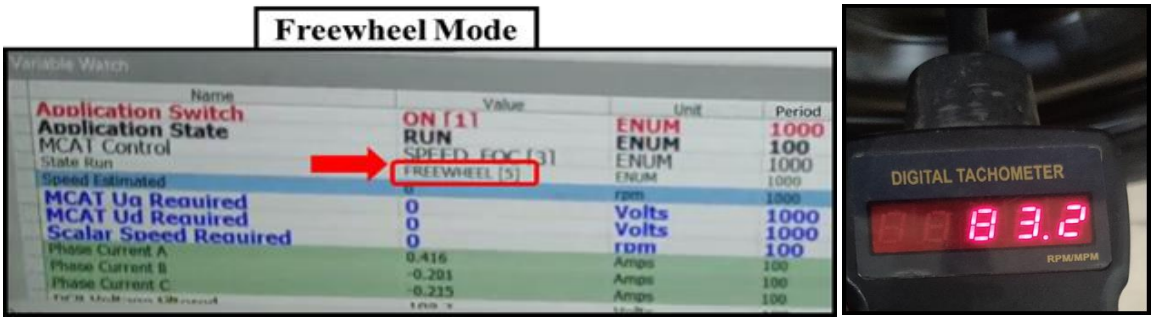

(b)

Fig. A.13 Response of EVPT during Freewheeling Mode of Operation, (a) Current and Speed Responses of the motor, (b) FreeMASTER 2.0 Variable Watch Window and Tachometer Reading for Freewheel Process

Table A.3

Spin Mode Test Along with Belt-Pulley System at Different Speeds of Motor

Speed command to motor (rpm)	**Estimated angular speed of wheel (rpm)**	**Measured angular speed of wheel using Tachometer (rpm)**	**Linear speed of vehicle using equation (A.9) (km/h)**
93	41.3	39.1	3.89
293	130.2	129.6	12.27
814	361.7	360.2	34.09
1020	453.3	452.9	42.72
1456	647.1	646.0	60.98
1870	831.1	829.5	78.33

c) Acceleration Mode

When speed of the motor is changed from 0 rpm to 700 rpm, the desired q axis current is generated, enough to make the motor reach its required speed with acceleration of 104.7 rad/s^2 as shown in Fig. A.14. The phase currents in stator winding are shown in Fig. A.15.

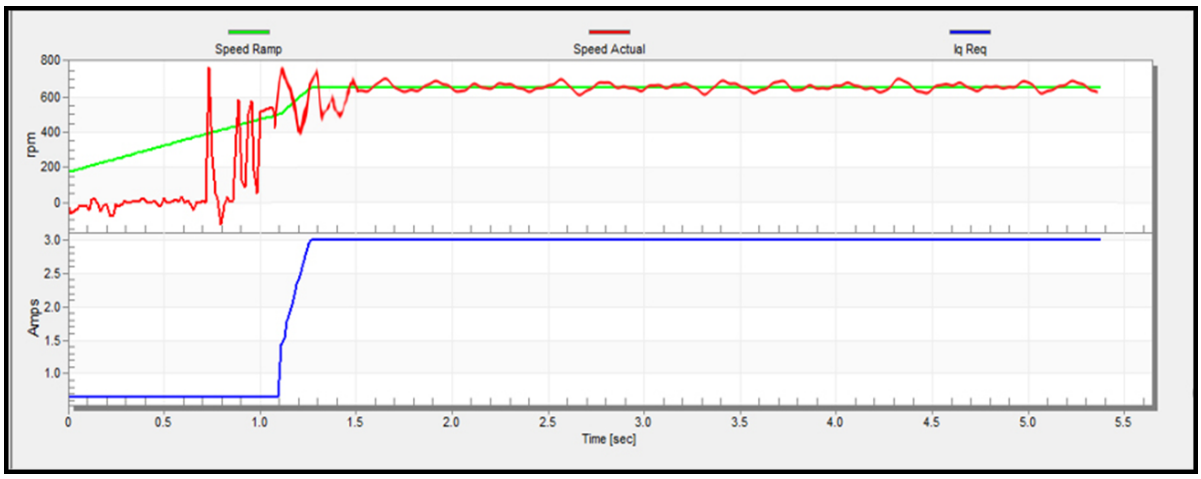

Fig. A.14 Response of EVPT during Acceleration (0 rpm to 700 rpm)

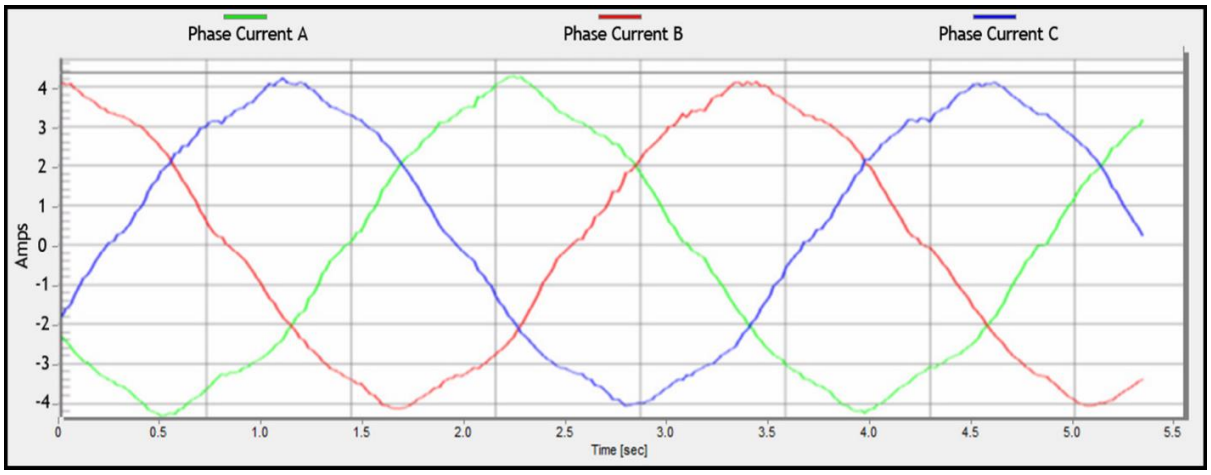

Fig. A.15 Steady State Phase Current Waveforms in Motor

d) Braking Mode of Operation

The motor is given command at t = 1 s to stop to test the braking response of the motor. The speed trace of the motor during braking from 780 rpm to 0 rpm is shown in Fig. A.16 (deceleration @ 81.68 rad/s2). The comparison of measured and estimated rotor position during sensor-less FOC implementation on EVPT system is shown in Fig. A.17.

e) Drive Cycle Test

To predict the future driving patterns for various vehicle applications and reducing the road test expense, the technique of simple drive cycle test is applied to the emulator system. For this,

NEDC is designed and fed as input command to the system as shown in Fig. A.18. The speed response of the power train system for the drive cycle is shown in Fig. A.19.

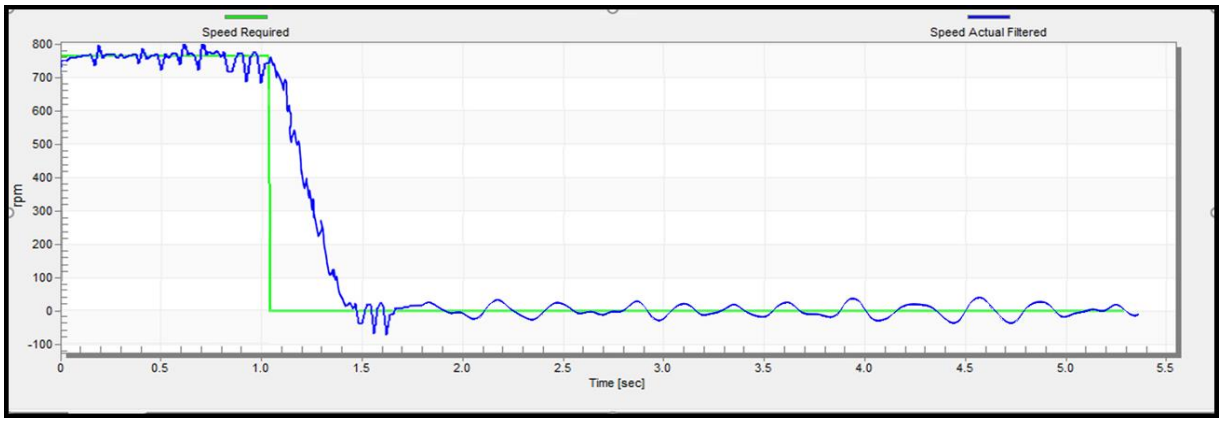

Fig. A.16 Response of EVPT during Braking (780 rpm to 0 rpm)

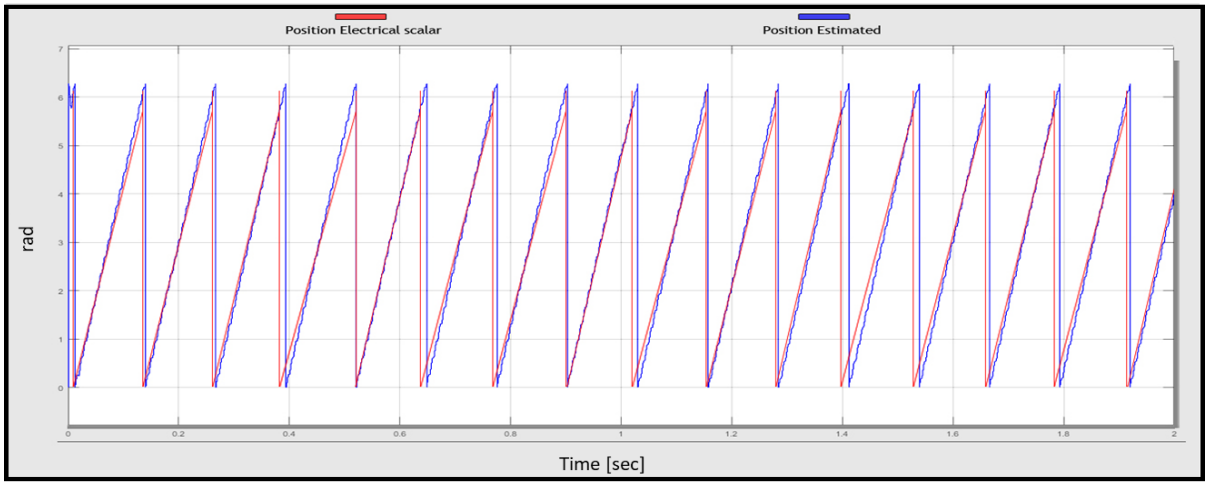

Fig. A.17 Comparison of Measured and Estimated Rotor Position

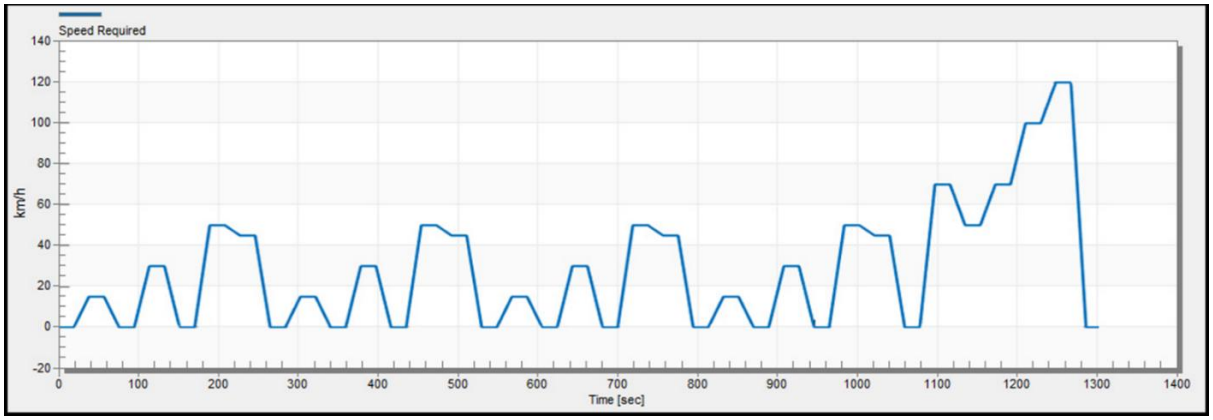

Fig. A.18 Drive Cycle for Vehicle Test

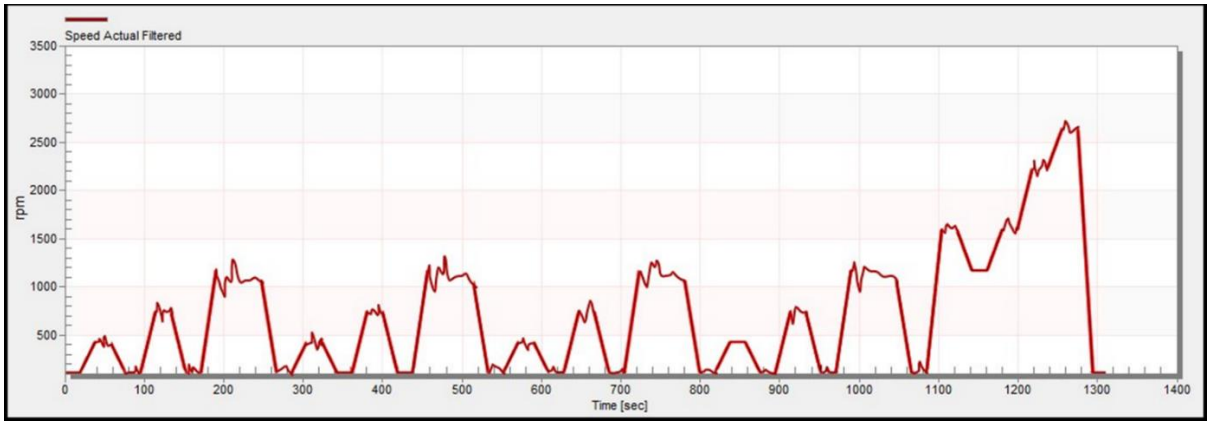

Fig. A.19 Speed Response of the EVPT for the Drive Cycle Test

Appendix B: Advantages of Motor Geometry Selection

In SI-PMSM, if thickness of magnets and pole embrace are too low, they lose their necessary contribution in producing rotating magnetic flux. Being a 14-pole motor, the upper limit of magnetic pole embrace is chosen in accordance to the rotor outer surface peripheral length for surface inset type PMSM, so that space between the magnets can be utilized for flux linkage and thereby reducing the flux leakage. An electric motor with small stack length produces lower torque during high-speed operation. Even though higher stack length results in higher torque, the torque reduces swiftly with increase in speed. Hence, stack length has to be optimum under considered constraints. Constraints for three design parameters are: 3mm $\leq$ A $\leq$ 8 mm, 0.65 $\leq$ B $\leq$ 0.85, 150mm $\leq$ C $\leq$ 170mm. Lower limits and upper limits of all three parameters are considered to obtain least core loss with optimum torque and reduced weight.

The magnetic pole eccentricity is chosen as 2 mm to mitigate the torque ripple [263] and thickness of magnet is measured from the centre of the pole periphery. Selection of rotor geometry provides the advantage of decrease in motor weight and core loss along with the reduction in torque ripples. For proving this, Model II with optimized geometry is analysed with two designs of rotors: Rotor A having pole eccentricity equal to 0 mm and Rotor B having pole eccentricity equal to 2 mm. Fig. B.1 illustrates the comparison and percentage of reduction in core loss, torque ripple and weight of the motor by employing the proposed design of the rotor in surface inset PMSM-2.

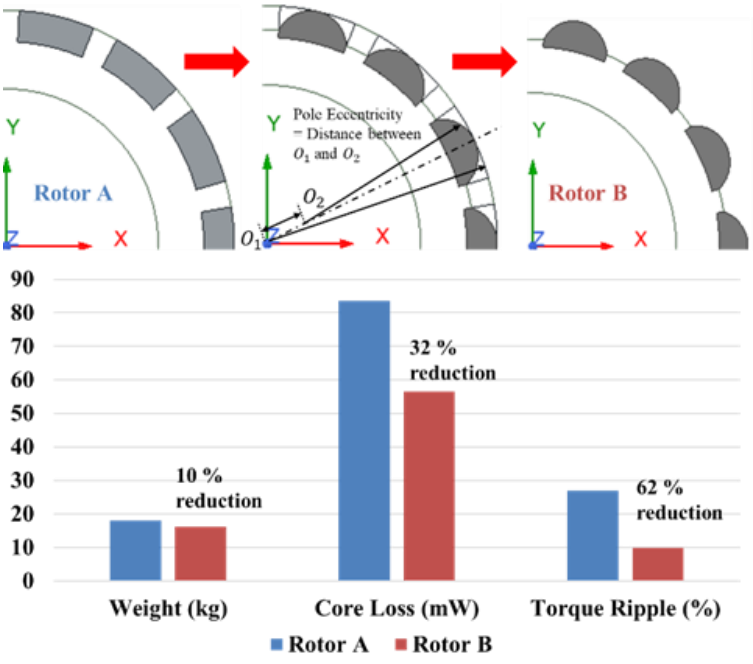

Fig. B.1 Effect of Change in Rotor Geometry (Pole Eccentricity)

REFERENCES

[1] M Zeraoulia, M H Benbouzid and D Diallo, "Electric Motor Drive Selection issues for HEV propulsion systems: A comparative study", *IEEE Trans. Vehicular Technology*, pp. 1756-1764, Nov. 2006.

[2] Farzad R Salmasi, "Control Strategies for Hybrid Electric Vehicles: Evolution, classification, Comparison and Future Trends", *IEEE Trans. Vehicular Technology*, pp.2393-2404, Sept. 2007.

[3] J D Santiago, H Bernhoff, B Ekergard, "Electrical Motor Drivelines in commercial all-electric vehicles: A Review", *IEEE Trans. Vehicular Technology*, pp. 475-484, Feb. 2012.

[4] Ramya, K C & Janarthanan, Geetha & Sridevi, A. & Rai, Rajakumar and Shirley, D., "Analysis of the Different Types of Electric Motors Used in Electric Vehicles", *E-Mobility*, pp.43-57, 10.1007/978-3-030-85424-9_3, Jan. 2022.

[5] Hashemnia, Mohammad Naser & Asaei, Behzad., "Comparative study of using different electric motors in the electric vehicles", *18th International Conference on Electrical Machines, ICEM*, pp. 1 – 5, 10.1109/ICELMACH.2008.4800157, Oct. 2008.

[6] Berry. Irene Michelle, "The Effects of Driving Style and Vehicle Performance on the Real-World Fuel Consumption of U.S. Light-Duty Vehicles", *MS Thesis, Massachusetts Institute of Technology*, 2010.

[7] Prathamesh Joshi and Prof. A.S. Ugale, "Overview of transmission system for the electric vehicle", *International Research Journal of Engineering and Technology (IRJET)*, Vol. 7, pp. 1-4, June 2020.

[8] J. Lee, "Structural design optimization of electric motors to improve torque performance", *Doctor of Philosophy Thesis, University of Michigan*, 2010.

[9] Tounsi, Souhir, Naourez, Benhadj, Neji, Rafik and Sellami, F. "Optimization of electric motor design parameters maximizing the autonomy of electric vehicles", *International Review of Electrical Engineering*, Vol. 2, pp. 118-126, Jan 2007.

[10] Cai, W., Wu, X., Zhou, M., Liang, Y. and Wang, Y., "Review and Development of Electric Motor Systems and Electric Powertrains for New Energy Vehicles", Automotive Innovation, Vol. 4, pp. 3–22, https://doi.org/10.1007/s42154-021-00139-z, Feb. 2021.

[11] S. Sidda, "A Study on Industrial Motor Drives Comparison and Applications of PMSM and BLDC Motor Drives", *International Conference on Energy, Communication, Data Analytics and Soft Computing, ICECDS*, 10.1109/ICECDS.2017.8390224, August 2017.

[12] Barve Nikita Rajendra, Kishor V Bhadhane, Avhad Nikita Vijay and Yadav Prashant Ramsingar, "Overview of Electric Drive Motors Use in Electric Vehicles", *International Journal for Modern Trends in Science and Technology*, Vol. 06, Issue 04, pp. 308-314, April 2020.

[13] Z. Yang, F. Shang and I. P. Brown, "Comparative Study of Interior Permanent Magnet, Induction, and Switched Reluctance Motor Drives for EV and HEV Applications", *IEEE Transactions on Transportation Electrification*, Vol. 1, pp. 245-253, Oct. 2015.

[14] Hekmati, A., Sadeghi Mahalli, I., Siamaki, M., "A Survey on Permanent Magnet Synchronous Machines: Recent Applications and Trends", *Electromechanical Energy Conversion Systems*, 1(3), pp. 42-50. doi: 10.30503/eecs.2020.251768.1015, 2021.

[15] S. Sakunthala, R. Kiranmayi and P. N. Mandadi, "A study on industrial motor drives: Comparison and applications of PMSM and BLDC motor drives," *International Conference on Energy, Communication, Data Analytics and Soft Computing (ICECDS)*, pp. 537-540, doi: 10.1109/ICECDS.2017.8390224, 2017.

[16] Heidari, H.; Rassõlkin, A.; Kallaste, A.; Vaimann, T.; Andriushchenko, E.; Belahcen, A.; Lukichev, D.V. "A Review of Synchronous Reluctance Motor-Drive Advancements", *Sustainability*, Vol. 13, pp. 729, https://doi.org/10.3390/su13020729, 2021.

[17] D. Fodorean, L. Idoumghar, M. B. Evilliers, P. Minciunescu, and C. Irimia, "Hybrid Differential Evolution Algorithm Employed for the Optimum Design of a High-Speed PMSM Used for EV Propulsion," *IEEE Transactions On Industrial Electronics,* Vol. 64, No. 12, pp. 9824-9832, Dec. 2017.

[18] T. Nakata, M. Sanada, S. Morimoto, and Y. Inoue, "Automatic Design of IPMSMs Using a Genetic Algorithm Combined with the Coarse-Mesh FEM for Enlarging the High-Efficiency Operation Area", *IEEE Transactions On Industrial Electronics*, Vol. 64, No. 12, pp. 9721-9728, Dec. 2017.

[19] Arora, A. S. and Gurmeet S., "Review of design and performance of permanent magnet synchronous motor", *International Journal of Industrial Electronics and Electrical Engineering*, Vol. 3, No. 10, pp. 20-26, Oct. 2015.

[20] Qu, Yang, Li, Yin-Sheng, Sotelo, and Ma. "A Novel Surface Inset Permanent Magnet Synchronous Motor for Electric Vehicles", *Symmetry*, Vol. 12, No. 179, 10.3390/sym12010179, Jan. 2020.

[21] Srirekha A, and Bashetty K., "Infinite to finite: An overview of finite element analysis", *Indian Journal of Dental Research*, Vol. 21, No. 3, pp. 425-432, Sep, 2010.

[22] Szabó, B. and Babuška, I., "Finite Element Analysis: Method, Verification and Validation", 2021.

[23] Martyanov A.S., and Neustroyev N.I., "Analysis of electromechanical systems using ANSYS Maxwell", *Alternative Energy and Ecology (ISJAEE),* Vol. 19, pp. 47-52, 2014.

[24] Mark A. Austin, "Engineering Programming in MATLAB : A Primer", Feb. 2000.

[25] Cao, Wenping, Bukhari, Syed and Aarniovuori, L., "Review of Electrical Motor Drives for Electric Vehicle Applications", *Mehran University Research Journal of Engineering and Technology,* Vol. 38, pp. 525-540, 10.22581/muet1982.1903.01, 2019.

[26] Bharadwaj, N. V., Chandrasekhar, P., and Sivakumar, M., "Induction motor design analysis for electric vehicle application", *INTERNATIONAL CONFERENCE ON MULTIFUNCTIONAL MATERIALS (ICMM),* doi:10.1063/5.0019486, 2020.

[27] Ruuskanen, Vesa, Nerg, Janne, Parviainen, A., Rilla, Marko and Pyrhönen, J., "A Design and Drive-Cycle Based Analysis of Direct-Driven Permanent Magnet Synchronous Machine for a Small Urban Use Electric Vehicle," *16th European Conference on Power Electronics and Applications, EPE-ECCE Europe,* 10.1109/EPE.2014.6910915, 2014.

[28] L. Dang, N. Bernard, N. Bracikowski, G. Berthiau, "Design optimization with flux-weakening of High-Speed PMSM for electrical vehicle considering the driving cycle", *IEEE Transactions on Industrial Applications*, 10.1109/TIE.2017.2726962, July 2017.

[29] Donaghy-Spargo, C. M., "Synchronous reluctance motor technology: opportunities, challenges and future direction", *Engineering & technology reference.* pp. 1-15, May 2016.

[30] Zhiming Gao, and Tim J. LaClair, "Electric and Conventional Vehicle Performance over Eco driving cycles: Energy Benefits and Component Loss", *International Battery, Hybrid and Fuel Cell Electric Vehicle Symposium, 32nd Electric Vehicle Symposium (EVS32) Lyon, France,* May 2019.

[31] Wu, Guang, Zhang, Xing and Dong, Zuomin, "Powertrain architectures of electrified vehicles: Review, classification and comparison", *Journal of the Franklin Institute,* Vol. 352, 10.1016/j.jfranklin.2014.04.018, Jan. 2014.

[32] L. Ting-ting, T. Yu, W. Gang, and W. Shu-mao, “Simulation of PMSM Vector Control System Based on Matlab/Simulink”, *International Conference on Measuring Technology and Mechatronics Automation*, Vol. 2, pp. 343-346, DOI 10.1109/ICMTMA.2009.117, 2009.

[33] X. Zhang, K. Yan and W. Zhang, "Composite Vector Model Predictive Control With Time-Varying Control Period for PMSM Drives," in *IEEE Transactions on Transportation Electrification*, vol. 7, no. 3, pp. 1415-1426, Sept. 2021, doi: 10.1109/TTE.2020.3047898.

[34] S. Sakunthala, R. Kiranmayi and P. N. Mandadi, "A Review on Speed Control of Permanent Magnet Synchronous Motor Drive Using Different Control Techniques," *2018 International Conference on Power, Energy, Control and Transmission Systems (ICPECTS)*, 2018, pp. 97-102, doi: 10.1109/ICPECTS.2018.8521574.

[35] J. Xia, Z. Li, D. Yu, Y. Guo and X. Zhang, "Robust Speed and Current Control With Parametric Adaptation for Surface-Mounted PMSM Considering System Perturbations," in *IEEE Journal of Emerging and Selected Topics in Power Electronics*, vol. 9, no. 3, pp. 2807-2817, June 2021, doi: 10.1109/JESTPE.2020.3015288.

[36] M. Wang, D. Sun, W. Ke and H. Nian, "A Universal Lookup Table-Based Direct Torque Control for OW-PMSM Drives," in *IEEE Transactions on Power Electronics*, vol. 36, no. 6, pp. 6188-6191, June 2021, doi: 10.1109/TPEL.2020.3037202.

[37] D. Majchrzak and P. Siwek, "Comparison of FOC and DTC methods for a Matrix Converter-fed permanent magnet synchronous motor," *2017 22nd International Conference on Methods and Models in Automation and Robotics (MMAR)*, 2017, pp. 525-530, doi: 10.1109/MMAR.2017.8046883.

[38] F. Aymen and S. Lassâad, "A new adaptive high speed control algorithm used for a FOC or a DTC PMSM drive strategies," *IECON 2012 - 38th Annual Conference on IEEE Industrial Electronics Society*, 2012, pp. 4472-4476, doi: 10.1109/IECON.2012.6389465.

[39] M. Aguirre, C. Calleja, A. Lopez-de-Heredia, J. Poza, A. Aranburu and T. Nieva, "FOC and DTC comparison in PMSM for railway traction application," *Proceedings of the 2011 14th European Conference on Power Electronics and Applications*, 2011, pp. 1-10.

[40] O. Lehmann, N. K. Nguyen, J. Schuster and J. Roth-Stielow, "Optimized sensorless DTC of PMSM for electric vehicles by using a switching command synchronized evaluation at standstill and low speed," *2015 9th International Conference on Power Electronics and ECCE Asia (ICPE-ECCE Asia)*, 2015, pp. 1386-1393, doi: 10.1109/ICPE.2015.7167960.

[41] Z. Wang, J. Chen, M. Cheng and K. T. Chau, "Field-Oriented Control and Direct Torque Control for Paralleled VSIs Fed PMSM Drives with Variable Switching Frequencies," in *IEEE Transactions on Power Electronics*, vol. 31, no. 3, pp. 2417-2428, March 2016, doi: 10.1109/TPEL.2015.2437893.

[42] I. Shchur and Y. Biletskyi, "Energetic Microscopic Representation (EMR) and Passivity-Based Control of Multi-Input Systems with Non-Linear Coupled Dynamics (PMSM control example)," *2020 IEEE Problems of Automated Electrodrive. Theory and Practice (PAEP)*, 2020, pp. 1-6, doi: 10.1109/PAEP49887.2020.9240793.

[43] Song Chi, “Position-sensorless control of permanent magnet synchronous machines over wide speed range”, Doctorate of Philosophy Thesis, Ohio State University, 2007.

[44] Hasegawa, M., and K. Matsui, “Position sensorless control for interior permanent magnet synchronous motor using adaptive flux observer with inductance identification,” I*ET electric power applications*, Vol. 3, No. 3, pp. 209-217, 2009.

[45] Lu, Kaiyuan, Xiao Lei, and Frede Blaabjerg, "Artificial inductance concept to compensate nonlinear inductance effects in the back EMF-based sensorless control method for PMSM,” *IEEE Transactions on Energy Conversion*, Vol. 28, No. 3, pp. 593-600, 2013.

[46] Piippo, Antti, Marko Hinkkanen, and Jorma Luomi, "Sensorless control of PMSM drives using a combination of voltage model and HF signal injection", *IEEE Industry Applications Conference, 39th IAS Annual Meeting.* Vol. 2., 2004.

[47] Zhao, Yue, et al., "An extended flux model-based rotor position estimator for sensorless control of salient-pole permanent-magnet synchronous machines," *IEEE Transactions on Power Electronics,* Vol. 30, No. 8, pp. 4412-4422, 2014.

[48] Qiu, Albert, Bin Wu, and Hassan Kojori, "Sensorless control of permanent magnet synchronous motor using extended Kalman filter", *Canadian Conference on Electrical and Computer Engineering, (IEEE Cat. No. 04CH37513)*, Vol. 3, 2004.

[49] Wang, Zheng, et al., "Position sensorless control of interleaved CSI fed PMSM drive with extended Kalman filter", *IEEE Transactions on Magnetics,* Vol. 48, No. 11, pp. 3688-3691, 2012.

[50] Zhu, Guchuan, et al., "A nonlinear state observer for the sensorless control of a permanent-magnet AC machine", *IEEE Transactions on Industrial Electronics,* Vol. 48, No. 6, pp. 1098-1108, 2001.

[51] Ge, Yang, Lihui Yang, and Xikui Ma, "Sensorless control of PMSM using generalized extended state observer and adaptive resistance estimation", *IET Electric Power Applications*, Vol. 14, No. 11, pp. 2062-2073, 2020.

[52] Apte, Aishwarya, et al., "Disturbance-observer-based sensorless control of PMSM using integral state feedback controller." *IEEE Transactions on Power Electronics*, Vol. 35, No. 6, pp. 6082-6090, 2019.

[53] Jiacai, Huang, et al., "Sensorless vector control of PMSM using sliding mode observer and fractional-order phase-locked loop", *Proceedings of the 31st Chinese Control Conference, IEEE,* 2012.

[54] Anwer, Abbas Mahmood Oghor, Fuad Alhaj Omar, and Ahmet Afsin Kulaksiz, "Design of a fuzzy logic-based MPPT controller for a PV system employing sensorless control of MRAS-based PMSM", *International Journal of Control, Automation and Systems*, Vol. 18, No. 11, pp. 2788-2797, 2020.

[55] Abd Samat, Ahmad Asri, et al., "Comparison between Takagi Sugeno FIS and PI Controller: An Adaptation Scheme of MRAS for Speed Sensorless Control of PMSM", *Applied Mechanics and Materials*, Vol. 785, Trans Tech Publications Ltd, 2015.

[56] Saihi, L., and A. Boutera, "Robust sensorless sliding mode control of PMSM with MRAS and Luenberger extended observer", *8th International Conference on Modelling, Identification and Control (ICMIC). IEEE,* 2016.

[57] Kivanc, Omer Cihan, and Salih Baris Ozturk, "Sensorless PMSM drive based on stator feedforward voltage estimation improved with MRAS multi-parameter estimation", *IEEE/ASME Transactions on Mechatronics*, Vol. 23, No. 3, pp. 1326-1337, 2018.

[58] Fan, Shicai, et al., "A hybrid speed sensorless control strategy for PMSM based on MRAS and fuzzy control", *Proceedings of the 7th International Power Electronics and Motion Control Conference, IEEE,* Vol. 4, 2012.

[59] Cao, Yongjuan, Qiang Li, and Li Yu, "A Software for Design and Analysis of PMSM Based on ANSYS", *2009 First International Conference on Information Science and Engineering. IEEE*, 2009.

[60] Baranski, Mariusz, Wojciech Szelag, and Wieslaw Lyskawinski, "Experimental and simulation studies of partial demagnetization process of permanent magnets in electric motors", *IEEE Transactions on Energy Conversion*, Vol. 36, No. 4, pp. 3137-3145, 2021.

[61] Sheela, A., Suresh, M., Shankar, V. G., Panchal, H., Priya, V., Atshaya, M., and Dharaskar, S., "FEA based analysis and design of PMSM for electric vehicle applications using magnet software", *International Journal of Ambient Energy*, pp. 1-6, 2020.

[62] Siecoban, R., Martiş, R., Martiş, C., Husar, C., Coadălată, L., and Irimia, C., "Multiphysics design, analysis and optimisation platform of PMSM for automotive applications", *International Conference and Exposition on Electrical and Power Engineering (EPE), IEEE,* pp. 251-25, Oct. 2016.

[63] Gu, L., "A Comparison of Polynomial Based Regression Models in Vehicle Safety Analysis", *ASME Design Engineering Technical Conferences - Design Automation Conference, ASME*, Pittsburgh, PA, DAC-21063, Sep. 2001.

[64] Koch, P. N., Simpson, T. W., Allen, J. K. and Mistree, F., "Statistical approximations for multidisciplinary design optimization: The Problem of Size", *Journal of Aircraft*, Vol. 36, No. 1, pp. 275-286, 1991.

[65] Barthelemy, J. F. M. and Haftka, R., "Approximation concepts for optimal structural design: a review," *Structural Optimization*, Vol. 5, pp. 129-144, 1993.

[66] Haftka, R. T., Scott, E. P. and Cruz, J. R., "Optimization and experiments: a survey," *Applied Mechanics Review*, Vol. 51, No. 7, pp. 435-448, 1998.

[67] Simpson, T. W., Peplinski, J., Koch, P. N. and Allen, J. K., "Metamodels for computer-based engineering design: survey and recommendations," *Engineering with Computers*, Vol. 17, No. 2, pp. 129-150, 2001.

[68] Ullman, D. G., "Toward the ideal mechanical engineering design support system," *Research in Engineering Design*, Vol. 13, pp. 55-64, 2002.

[69] Koehler, J. R. and Owen, A., "Computer Experiments," *Handbook of Statistics, Elsevier Science, New York*, pp. 261-308, 1996.

[70] Taguchi, G., Yokoyama, Y. and Wu, Y., "Taguchi Methods: Design of Experiments," *American Supplier Institute,* Allen Park, Michigan, 1993.

[71] Owen, A., "Orthogonal Arrays for Computer Experiments, Integration, and Visualization," *Statistica Sinica*, Vol. 2, pp. 439-452, 1992.

[72] Hedayat, A. S., Sloane, N. J. A. and Stufken, J., "Orthogonal Arrays: Theory and Applications," *Springer, New York*, 1999.

[73] Kalagnanam, J. R. and Diwekar, U. M., "An Efficient Sampling Technique for Off-Line Quality Control," *Technometrics,* Vol. 39, No. 3, pp. 308-319, 1997.

[74] Meckesheimer, M., Booker, A. J., Barton, R. R. and Simpson, T. W., "Computationally inexpensive metamodel assessment strategies," *AIAA Journal,* Vol. 40, No. 10, pp. 2053-2060, 2002.

[75] Fang, K. T., Lin, D. K. J., Winker, P. and Zhang, Y., "Uniform Design: Theory and Application," *Technometrics*, Vol. 39, No. 3, pp. 237-248, 2000.

[76] McKay, M. D., Bechman, R. J. and Conover, W. J., "A Comparison of Three Methods for selecting values of input variables in the analysis of output from a Computer Code," *Technometrics,* Vol. 21, No. 2, pp. 239-245, 1979.

[77] Iman, R. L. and Conover, W. J., "Small Sensitivity Analysis Techniques for Computer Models with an application to risk assessment," *Communication Statistics - Theory and Methods*, Vol. 9, No. 17, pp. 1749-1842, 1980.

[78] Tang, B., "Orthogonal Array-based Latin Hypercubes," *Journal of American Statistical Association,* Vol. 88, No. 424, pp. 1392-1397, 1993.

[79] Park, J. S., "Optimal Latin-hypercube Designs for Computer Experiments," Journal of Statistical Planning Inference, Vol. 39, pp. 95-111, 1994.

[80] Ye, K. Q., Li, W. and Sudjianto, A., "Algorithmic Construction of Optimal Symmetric Latin Hypercube designs," *Journal of Statistical Planning and Inferences*, Vol. 90, pp. 145-159, 2000.

[81] Sacks, J., B., S. S. and Welch, W. J., "Designs for Computer Experiments," *Technometrics,* Vol. 31, No. 1, pp. 41-47, 1989.

[82] Papadrakakis, M., Lagaros, M. and Tsompanakis, Y., "Structural Optimization Using Evolution Strategies and Neural Networks," *Computer Methods in Applied Mechanics and Engineering,* Vol. 156, No. 1-4, pp. 309-333, 1998.

[83] Dyn, N., Levin, D. and Rippa, S., "Numerical procedures for surface fitting of scattered data by Radial Basis Functions," *SIAM Journal of Scientific and Statistical Computing,* Vol. 7, No. 2, pp. 639-659, 1986.

[84] Fang, H. and Horstemeyer, M. F., "Global response approximation with Radial Basis Functions," *Journal of Engineering Optimization,* Vol. 38, No. 4, pp. 407-424, 2006.

[85] Friedman, J. H., "Multivariate adaptive regressive splines," *The Annals of Statistics,* Vol. 19, No. 1, pp. 1-67, 1991.

[86] De Boor, C. and Ron, A., "On multivariate polynomial interpolation," *Constructive Approximation,* Vol. 6, pp. 287-302, 1990.

[87] Montgomery, D., "Design and Analysis of Experiments," *John Wiley and Sons, New York,* 1991.

[88] Wong, P. C. and Bergeron, R. D., "30 Years of Multidimensional Multivariate Visualization," *Scientific Visualization - Overviews, Methodologies and Techniques, IEEE Computer Society Press, Los Alamitos, CA,* pp. 3-33, 1997.

[89] Keim, D. A. and Kriegel, H. P., "Visualization techniques for mining large databases: a comparison," *IEEE Transactions on Knowledge and Data Engineering,* Vol. 8, No. 6, pp. 923-938, 1996.

[90] Winer, E. H. and Bloebaum, C. L., "Development of Visual Design Steering as an Aid in Large-scale Multidisciplinary Design Optimization. Part I: Method Development," *Structural and Multidisciplinary Optimization,* Vol. 23, No. 6, 412-424, 2002.

[91] Winer, E. H. and Bloebaum, C. L., "Development of Visual Design Steering as an Aid in Large-scale Multidisciplinary Design Optimization. Part II: Method Validation," *Structural and Multidisciplinary Optimization,* Vol. 23, No. 6, pp. 425 – 435, 2002.

[92] Eddy, J. and Lewis, K. E., "Visualization of Multi-Dimensional Design and Optimization Data Using Cloud Visualization," *ASME 2002 Design Engineering Technical Conference and Computers and Information in Engineering Conference,* Montreal, Canada, DETC2002/DAC-34130, Sep. 2002.

[93] Ligetti, C., Simpson, T. W., Frecker, M., Barton, R. R. and Stump, G., "Assessing the Impact of Graphical Design Interfaces on Design Efficiency and Effectiveness," *Transactions of the ASME, Journal of Computing and Information Science in Engineering,* Vol. 3, No. 2, pp. 144-154, 2003.

[94] Box, G. E. P. and Draper, N. R., "Evolutionary Operation: A Statistical Method for Process Management," *John Wiley & Sons, Inc., New York,* 1969.

[95] Welch, W. J., Buck, R. J., Sacks, J., Wynn, H. P., Mitchell, T. J. and Morris, M. D., "Screening, Predicting, and Computer Experiments," *Technometrics,* Vol. 34, No. 1, pp. 15-25, 1992.

[96] Balabanov, V. O., Giunta, A. A., Golovidov, O., Grossman, B., Mason, W. H. and Watson, L. T., "Reasonable design space approach to response surface approximation," *Journal of Aircraft,* Vol. 36, No. 1, pp. 308-315, 1999.

[97] Chen, W., Allen, J. K., Schrage, D. P. and Mistree, F., "Statistical experimentation methods for achieving affordable concurrent systems design," *AIAA Journal,* Vol. 35, No. 5, pp. 893-900, 1997.

[98] Toropov, V., van Keulen, F., Markine, V. and de Doer, H., "Refinements in the multi-point approximation method to reduce the effects of noisy structural responses," *6th*

AIAA/USAF/NASA/ISSMO Symposium on Multidisciplinary Analysis and Optimization, AIAA-96-4087-CP, Vol. 2, Sep. 1996.

[99] Alexandrov, N., Dennis, J. E. J., Lewis, R. M. and Torczon, V., "A trust region framework for managing the use of approximation models in optimization," *Structural Optimization,* Vol. 15, No. 1, pp. 16-23, 1998.

[100] Rodríguez, J. F., Renaud, J. E. and Watson, L. T., "Trust Region Augmented Lagrangian Methods for Sequential Response Surface Approximation and Optimization," *Transactions of ASME, Journal of Mechanical Design,* Vol. 120, pp. 58-66, 1998.

[101] Renaud, J. E. and Gabriele, G. A., "Approximation in Non-hierarchical System Optimization," *AIAA Journal,* Vol. 32, pp. 198-205, 1994.

[102] Li, B., Shiu, B.-w. and Lau, K.-j., "Fixture configuration design for sheet metal laser welding with a two-stage Response Surface Methodology," *ASME 2001 Design Engineering Technical Conferences and Computers and Information in Engineering Conference, ASME, Pittsburgh, Pennsylvania, USA,* DETC2001/DAC-21096, Sep. 2001.

[103] Dennis, J. E. and Torczon, V., "Managing Approximation Models in Optimization," *Multidisciplinary Design Optimization: State of the Art, Society for Industrial and Applied Mathematics,* Philadelphia, 1996.

[104] Osio, I. G. and Amon, C. H., "An Engineering Design Methodology with Multistage Bayesian Surrogates and Optimal Sampling", *Research in Engineering Design,* Vol. 8, No. 4, pp. 189-206, 1996.

[105] Schonlau, M. S., Welch, W. J. and Jones, D. R., "Global Versus Local Search in Constrained Optimization of Computer Models," *New Development and Applications in Experimental Design, Institute of Mathematical Statistics,* pp. 11-25, 1998.

[106] Wang, G. G., "Adaptive Response Surface Method Using Inherited Latin Hypercube Design Points," *Transactions of ASME, Journal of Mechanical Design,* Vol. 125, pp. 210-220, 2003.

[107] Wang, G. G. and Simpson, T. W., "Fuzzy Clustering Based Hierarchical Metamodeling for Space Reduction and Design Optimization," *Journal of Engineering Optimization,* Vol. 36, No. 3, pp. 313-335, 2004.

[108] Wang, L., Shan, S. and Wang, G. G., "Mode-Pursuing Sampling Method for Global Optimization on Expensive Black-box Functions," *Journal of Engineering Optimization,* Vol. 36, No. 4, pp. 419-438, 2004.

[109] F. Glover, "Future paths for integer programming and links to artificial intelligence," *Computers & Operations Research,* Vol. 13, No. 5, pp. 533–549, 1986.

[110] C. Blum, A. Roli, "Metaheuristics in combinatorial optimization: overview and conceptual comparison," *ACM Computing Surveys (CSUR),* Vol. 35, No. 3, pp. 268–308, 2003.

[111] M. A. Basset, L. A. Fatah and A. K. Sangaiah, "Metaheuristic Algorithms: A Comprehensive Review", *Computational Intelligence for Multimedia Big Data on the Cloud with Engineering Applications, Elsevier,* DOI: 10.1016/B978-0-12-813314-9.00010-4, pp. 185-224, 2018.

[112] I. Rechenberg, "Evolution Strategy: Optimization of Technical Systems by Means of Biological Evolution," *Fromman-Holzboog, Stuttgart,* Vol. 104, 1973.

[113] Fogel, L. J., Owens, A. J., and Walsh, M. J., "Artificial intelligence through simulated evolution", *John Wiley & Sons,* 1966.

[114] J.R. Koza, "Genetic Programming: A Paradigm for Genetically Breeding Populations of Computer Programs to Solve Problems," *Stanford University, Department of Computer Science, Stanford, CA,* 1990.

[115] J.R. Sampson, "Adaptation in natural and artificial systems," *John h. Holland,* 1976.

[116] L.N. De Castro, J. Timmis, "Artificial Immune Systems: A New Computational Intelligence Approach," *Springer Science & Business Media*, 2002.

[117] M. Dorigo, "Optimization, Learning and Natural Algorithms," *Ph.D. Thesis, Politecnico di Milano, Italy*, 1992.

[118] R. Eberhart, J. Kennedy, "A new optimizer using particle swarm theory," *Proceedings of the Sixth International Symposium on Micro Machine and Human Science, IEEE*, pp. 39–43, 1995.

[119] L.N. De Castro, "Immune, swarm, and evolutionary algorithms. Part I: basic models," *Proceedings of the 9th International Conference on Neural Information Processing, IEEE, ICONIP*, Vol. 3, pp. 1464-1468, 2002.

[120] L.N. de Castro, "Immune, swarm, and evolutionary algorithms. Part II: philosophical comparisons," *Proceedings of the 9th International Conference on Neural Information Processing, IEEE, ICONIP*, Vol. 3, pp. 1469–1473, 2002.

[121] A.Y. Lam, V.O. Li, "Chemical-reaction-inspired metaheuristic for optimization," *IEEE Transactions on Evolutionary Computation*, Vol. 14, No. 3, pp. 381–399, 2010.

[122] D.T. Connolly, "An improved annealing scheme for the qap", *European Journal of Operational Research*, Vol. 46, No. 1, pp. 93–100, 1990.

[123] É. Taillard, "Robust taboo search for the quadratic assignment problem," *Parallel Computing*, Vol. 17, No. 4–5, pp. 443–455, 1991.

[124] E. Taillard, F, "Ant: fast ant system", *Handbook of Applied Optimization*, 2002.

[125] M. Abdechiri, M.R. Meybodi, H. Bahrami, Gases brownian motion optimization: an algorithm for optimization (GBMO), Applied Soft Computing 13 (5) (2013) 2932–2946.

[126] F. Lardeux, F. Saubion, J.-K. Hao, "GASAT: a genetic local search algorithm for the satisfiability problem," *Evolutionary Computation*, Vol. 14, No. 2, pp. 223–253, 2006.

[127] L. Yingbiao, "A genetic algorithm based on adapting clause weights," *Chinese Journal of Computer*, Vol. 7, No. 2, pp. 20–32, 2005.

[128] Z.W. Geem, J.H. Kim, G. Loganathan, "A new heuristic optimization algorithm: harmony search," *Simulation*, Vol. 76, No. 2, pp. 60–68, 2001.

[129] A. Milad, "Harmony search algorithm: strengths and weaknesses," *Journal of Computer Engineering and Information Technology*, Vol. 2, No. 1, pp. 1-7, 2013.

[130] O. Abdel-Raouf, and M.A.-B. Metwally, "A survey of harmony search algorithm," *International Journal of Computer Applications*, Vol. 70, No. 28, 2013.

[131] R.A. Mora-Gutiérrez, J. Ramírez-Rodríguez, and E.A. Rincón-García, "An optimization algorithm inspired by musical composition," *Artificial Intelligence Review*, Vol. 41, No. 3, pp. 301–315, 2014.

[132] R.A. Mora-Gutiérrez, J. Ramírez-Rodríguez, E.A. Rincón-García, A. Ponsich, and O. Herrera, "An optimization algorithm inspired by social creativity systems," *Computing*, Vol. 94, No. 11, pp. 887–914, 2012.

[133] M. Mahdavi, M. Fesanghary, E. Damangir, "An improved harmony search algorithm for solving optimization problems," *Applied Mathematics and Computation*, Vol. 188, No. 2, pp. 1567–1579, 2007.

[134] M.G. Omran, M. Mahdavi, "Global-best harmony search," *Applied Mathematics and Computation*, Vol. 198, No. 2, pp. 643–656, 2008.

[135] Q.-K. Pan, P.N. Suganthan, M.F. Tasgetiren, J.J. Liang, "A self-adaptive global best harmony search algorithm for continuous optimization problems," *Applied Mathematics and Computation*, Vol. 216, No. 3, pp. 830–848, 2010.

[136] S.A. Salem, "BOA: a novel optimization algorithm," *International Conference on Engineering and Technology (ICET), IEEE*, pp. 1–5, 2012.

[137] M. Dorigo, V. Maniezzo, A. Colorni, "Ant system: optimization by a colony of cooperating agents," *IEEE Transactions on Systems, Man, and Cybernetics, Part B (Cybernetics)*, Vol. 26, No. 1, pp. 29–41, 1996.

[138] S. Mirjalili, "SCA: a sine cosine algorithm for solving optimization problems," *Knowledge-Based Systems*, Vol. 96, pp. 120–133, 2016.

[139] X.-S. Yang, "Flower pollination algorithm for global optimization," *UCNC, Springer*, pp. 240–249, 2012.

[140] X. Yang, "Firefly algorithm, in: Nature-Inspired Metaheuristic Algorithms," *Luniver Press* (Chapter 8).

[141] N. Metropolis, A.W. Rosenbluth, M.N. Rosenbluth, A.H. Teller, and E. Teller, "Equation of state calculations by fast computing machines," *The Journal of Chemical Physics,* Vol. 21, No. 6, pp. 1087–1092, 1953.

[142] S. Kirkpatrick, C.D. Gelatt, M.P. Vecchi, "Optimization by simulated annealing," *Science,* Vol. 220, No. 4598, pp. 671–680, 1983.

[143] P.J. van Laarhoven, and E.H. Aarts, "Performance of the simulated annealing algorithm," *Simulated Annealing: Theory and Applications*, Springer, pp. 77–98, 1987.

[144] M. Nieto-Vesperinas, F. Fuentes, and R. Navarro, "Performance of a simulated-annealing algorithm for phase retrieval," *JOSA*, Vol. 5, No. 1, pp. 30–38, 1988.

[145] C.R. Reeves, "Modern Heuristic Techniques for Combinatorial Problems," *John Wiley & Sons*, Inc., 1993.

[146] X. Gu, "The Behavior of Simulated Annealing in Stochastic Optimization," *Iowa State University*, 2008.

[147] E. Rashedi, H. Nezamabadi-Pour, and S. Saryazdi, "GSA: a gravitational search algorithm," *Information Sciences*, Vol. 179, No. 13, pp. 2232–2248, 2009.

[148] H. Nezamabadi-Pour, and F. Barani, "Gravitational search algorithm: concepts, variants, and operators," *Handbook of Research on Modern Optimization Algorithms and Applications in Engineering and Economics, IGI Global*, pp. 700–750, 2016.

[149] S.M. Abdulhamid, M.S.A. Latiff, S.H.H. Madni, and O. Oluwafemi, "A survey of league championship algorithm: prospects and challenges," arXiv preprint arXiv:1603.09728.

[150] R.V. Rao, V.J. Savsani, and D. Vakharia, "Teaching–learning-based optimization: a novel method for constrained mechanical design optimization problems," *Computer-Aided Design,* Vol. 43, No. 3, pp. 303–315, 2011.

[151] E. Mezura-Montes, and C.A.C. Coello, "A simple multi-membered evolution strategy to solve constrained optimization problems," *IEEE Transactions on Evolutionary Computation,* Vol. 9, No. 1, pp. 1–17, 2005.

[152] R.L. Becerra, and C.A.C. Coello, "Cultured differential evolution for constrained optimization," *Computer Methods in Applied Mechanics and Engineering,* Vol. 195, No. 33, pp. 4303–4322, 2006.

[153] A.E. Muñoz Zavala, A.H. Aguirre, E.R. Villa, and Diharce, "Constrained optimization via particle evolutionary swarm optimization algorithm (peso)," *Proceedings of the 7th Annual Conference on Genetic and Evolutionary Computation*, ACM, pp. 209–216, 2005.

[154] F.-z. Huang, L. Wang, and Q. He, "An effective co-evolutionary differential evolution for constrained optimization," *Applied Mathematics and Computation*, Vol. 186, No. 1, pp. 340–356, 2007.

[155] F. Glover, and C. McMillan, "The general employee scheduling problem: An integration of MS and AI," *Computers & Operations Research,* Vol. 13, No. 5, pp. 563–573, 1986.

[156] F. Glover, and E. Taillard, "A user's guide to tabu search," *Annals of Operations Research,* Vol. 41, No. 1, pp. 1–28, 1993.

[157] F. Glover, "Tabu Search Fundamentals and Uses," *Graduate School of Business, University of Colorado, Boulder,* 1995.

[158] M.M. Cangalovic, V. Kovacevic-Vujcic, L. Ivanovic, M. Drazic, and M. Asic, "Tabu search: a brief survey and some real-life applications," *Yugoslav Journal of Operations Research,* Vol. 6, No. 1, pp. 5–18, 1996.

[159] S. Hanafi, "On the convergence of tabu search," *Journal of Heuristics,* Vol. 7, No. 1, pp. 47–58, 2001.

[160] M. Mastrolilli, and L.M. Gambardella, "Maximum satisfiability: how good are tabu search and plateau moves in the worst-case", *European Journal of Operational Research,* Vol. 166, No. 1, pp. 63–76, 2005.

[161] J. Brownlee, "Clever Algorithms: Nature-Inspired Programming" *Recipes, Jason Brownlee,* 2011.

[162] P. Hansen, and N. Mladenovi´c, "Variable neighborhood search: principles and applications," *European Journal of Operational Research,* Vol. 130, No. 3, pp. 449–467, 2001.

[163] É.D. Taillard, and S. Voss, "Popmusic—partial optimization metaheuristic under special intensification conditions," *Essays and Surveys in Metaheuristics, Springer,* pp. 613–629, 2002.

[164] P. Shaw, "Using constraint programming and local search methods to solve vehicle routing problems," *International Conference on Principles and Practice of Constraint Programming, Springer,* pp. 417–431, 1998.

[165] R. Bent, and P. Van Hentenryck, "Spatial, temporal, and hybrid decompositions for large-scale vehicle routing with time windows," *CP,* Vol. 6308, pp. 99–113, 2010.

[166] B. Alatas, "Chaotic harmony search algorithms," *Applied Mathematics and Computation,* Vol. 216, No. 9, pp. 2687–2699, 2010.

[167] H. Bingol, and B. Alatas, "Chaotic league championship algorithms," Arabian Journal for Science and Engineering, Vol 41, No. 12, pp. 5123–5147, 2016.

[168] H.A. Hefny, and S.S. Azab, "Chaotic particle swarm optimization," *7th International Conference on Informatics and Systems (INFOS), IEEE,* pp. 1–8, 2010.

[169] P. Snaselova, and F. Zboril, "Genetic algorithm using theory of chaos," *Procedia Computer Science,* Vol. 51, pp. 316–325, 2015.

[170] T. Cai, F. Pan, and J. Chen, "Adaptive particle swarm optimization algorithm," *Fifth World Congress on Intelligent Control and Automation,* WCICA, IEEE, Vol. 3, pp. 2245–2247, 2004.

[171] S.Walton, O. Hassan, K. Morgan, and M. Brown, "Modified cuckoo search: a new gradient free optimisation algorithm," *Chaos, Solitons & Fractals,* Vol. 44. , No. 9, pp. 710–718, 2011.

[172] H. Aguiar e Oliveira, L. Ingber, A. Petraglia, M.R. Petraglia, and M.A.S. Machado, "Stochastic Global Optimization and Its Applications with Fuzzy Adaptive Simulated Annealing," *Springer Publishing Company, Incorporated,* 2012.

[173] T. Stützle, and H.H. Hoos, "Max–min ant system," *Future Generation Computer Systems,* Vol. 16, No. 8, pp. 889–914, 2000.

[174] V. Kumar, D. Kumar, and J.K. Chhabra, "Improved grey wolf algorithm for optimization problems," *International Symposium on "Fusion of Science & Technology",* pp. 18–22, 2016.

[175] X.-S. Yang, S. Deb, and S. Fong, "Accelerated particle swarm optimization and support vector machine for business optimization and applications," *Networked Digital Technologies*, pp. 53–66, 2011.

[176] M. Lohokare, B. Panigrahi, S. Pattanaik, S. Devi, and A. Mohapatra, "Optimal load dispatch using accelerated biogeography based optimization," *Joint International Conference on Power Electronics, Drives and Energy Systems (PEDES) & 2010 Power India, IEEE*, pp. 1–5, 2010.

[177] M.N.M. Salleh, and K. Hussain, "Accelerated mine blast algorithm for anfis training for solving classification problems," *International Journal of Software Engineering and Its Applications*, Vol. 10, No. 6, pp. 161–168, 2016.

[178] A. Ozkis, and A. Babalik, "Accelerated abc (a-abc) algorithm for continuous optimization problems," *Lecture Notes on Software Engineering*, Vol. 1, No. 3, pp. 262, 2013.

[179] H. Wang, S. Rahnamayan, H. Sun, and M.G. Omran, "Gaussian bare-bones differential evolution," *IEEE Transactions on Cybernetics*, Vol. 43, No. 2, pp. 634–647, 2013.

[180] S.M. Farahani, A. Abshouri, B. Nasiri, and M.Meybodi, "A gaussian firefly algorithm," *International Journal of Machine Learning and Computing*, Vol. 1, No. 5, pp. 448, 2011.

[181] J. Kennedy, "Bare bones particle swarms," *Proceedings of the 2003 IEEE Swarm Intelligence Symposium, SIS'03, IEEE*, pp. 80–87, 2003.

[182] F. Zou, L.Wang, X. Hei, D. Chen, Q. Jiang, and H. Li, "Bare-bones teaching-learning-based optimization," *The Scientific World Journal*, 2014.

[183] G.R. Raidl, "A unified view on hybrid metaheuristics," *Hybrid Metaheuristics*, Vol. 4030, pp. 1–12, 2006.

[184] C. Blum, and A. Roli, "Hybrid metaheuristics: an introduction," *Hybrid Metaheuristics, Springer*, pp. 1–30, 2008.

[185] M. Ehrgott, and X. Gandibleux, "Hybrid metaheuristics for multi-objective combinatorial optimization," *Hybrid Metaheuristics, Springer*, pp. 221–259, 2008.

[186] C. Blum, J. Puchinger, G. Raidl, and A. Roli, "A brief survey on hybrid metaheuristics," *Proceedings of BIOMA*, pp. 3–18, 2010.

[187] D. Binu, M. Selvi, and A. George, "MKF-Cuckoo: hybridization of cuckoo search and multiple kernel-based fuzzy c-means algorithm," *AASRI Procedia*, Vol. 4, pp. 243–249, 2013.

[188] X.-S. Yang, and S. Deb, "Cuckoo search via Lévy flights," *World Congress on Nature & Biologically Inspired Computing, NaBIC 2009, IEEE*, pp. 210–214, 2009.

[189] L. Chen, C.P. Chen, and M. Lu, "A multiple-kernel fuzzy c-means algorithm for image segmentation," *IEEE Transactions on Systems, Man, and Cybernetics, Part B (Cybernetics)*, Vol. 41, No. 5, pp. 1263–1274, 2011.

[190] L.-Y. Tseng, and S.-C. Liang, "A hybrid metaheuristic for the quadratic assignment problem," *Computational Optimization and Applications*, Vol. 34, No. 1, pp. 85–113, 2006.

[191] E. Nabil, "A modified flower pollination algorithm for global optimization," *Expert Systems with Applications*, Vol. 57, pp. 192–203, 2016.

[192] S.A.-F. Sayed, E. Nabil, and A. Badr, "A binary clonal flower pollination algorithm for feature selection," *Pattern Recognition Letters*, Vol. 77, pp. 21–27, 2016.

[193] T.G. Crainic, and M. Toulouse, "Parallel metaheuristics," *Fleet Management and Logistics, Springer*, pp. 205–251, 1998.

[194] H. Narasimhan, "Parallel artificial bee colony (pabc) algorithm," *World Congress on Nature & Biologically Inspired Computing, NaBIC, IEEE*, pp. 306–311, 2009.

[195] G. Luque, and E. Alba, "Parallel Genetic Algorithms: Theory and Real World Applications," *Springer*, Vol. 367, 2011.

[196] C.C. Ribeiro, and I. Rosseti, "Efficient parallel cooperative implementations of grasp heuristics," *Parallel Computing*, Vol. 33, No. 1, pp. 21–35, 2007.

[197] P. Cowling, G. Kendall, and E. Soubeiga, "A hyper-heuristic approach to scheduling a sales summit," *International Conference on the Practice and Theory of Automated Timetabling, Springer*, pp. 176–190, 2000.

[198] E.K. Burke, M. Gendreau, M. Hyde, G. Kendall, G. Ochoa, E. Özcan, and R. Qu, "Hyper-heuristics: a survey of the state of the art," *Journal of the Operational Research Society*, Vol. 64, No. 12, pp. 1695–1724, 2013.

[199] V.V. de Melo, and W. Banzhaf, "Drone squadron optimization: a novel self-adaptive algorithm for global numerical optimization," *Neural Computing and Applications*, pp. 1–28, 2017.

[200] J.P. Papa, G.H. Rosa, D. Rodrigues, and X.-S. Yang, "Libopt: an open-source platform for fast prototyping soft optimization techniques," arXiv preprint arXiv:1704.05174.

[201] Jawad Faiz, B M Ebrahimi, Bilal A and Hamid A: "Finite Element Transient Analysis of Induction motors under mixed eccentricity fault", *IEEE Trans. on Magnetics*, Vol.44, No.1, Sep. 2008.

[202] Elias K Strangas, Abdullah A. and Hassan K. Khalil: "Speed Control of Permanent Magnet Synchronous Motor with uncertain parameters and unknown disturbances", *IEEE Trans. on Control System Technology*, pp.1-8, June 2020.

[203] A. Boglietti, A. Cavagnino, D. Staton, M. Shanel, M. Mueller and C. Mejuto, "Evolution and Modern approaches for thermal analysis of electrical machines", *IEEE Trans. on Industrial electronics*, Vol. 56, pp. 871-881, Mar. 2009.

[204] A. Boglietti, A. Cavagnino and D. A. Staton, "Thermal analysis of TEFC induction motors", *38th IAS Annual Meeting on Conference Record of the Industry Applications Conference*, Vol. 2, pp. 849-856, Oct. 2003, doi: 10.1109/IAS.2003.1257630.

[205] Staton, Dave, D. Hawkins, and M. Popescu, "Thermal Behavior of Electrical Motors–An Analytical Approach", *INDUCTICA Technical Conference Program, CWIEME, Berlin*, pp. 5-7, May 2009.

[206] Z. Xiaochen, L. Weili, C. Shukang, C. Junci and Z. Chunbo, "Thermal analysis of solid rotor in PMSM used for EV", *IEEE Vehicle Power and Propulsion Conference*, pp. 1637-1642, Sep., 2009, doi: 10.1109/VPPC.2009.5289644.

[207] T. D. Kefalas and A. G. Kladas, "Finite element transient thermal analysis of PMSM for aerospace applications", *XXth International Conference on Electrical Machines*, pp. 2566-2572, Sep. 2012, doi: 10.1109/ICElMach.2012.6350246.

[208] W. Tong, R. Sun, C. Zhang, S. Wu and R. Tang, "Loss and Thermal Analysis of a High-Speed Surface-Mounted PMSM with Amorphous Metal Stator Core and Titanium Alloy Rotor Sleeve", *IEEE Trans. on Magnetics*, Vol. 55, pp. 1-4, June 2019, doi: 10.1109/TMAG.2019.2897141.

[209] D. Staton, A. Boglietti and A. Cavagnino, "Solving the more difficult aspects of electric motor thermal analysis in small and medium size industrial induction motors", *IEEE Transactions on Energy Conversion*, Vol. 20, pp. 620-628, Sept. 2005, doi: 10.1109/TEC.2005.847979.

[210] Eguren I., Almandoz G., Egea A., Elorza L. and Urdangarin A., "Development of a Thermal Analysis Tool for Linear Machines", *Applied Sciences*, Vol. 11, pp. 1-19, June 2021, doi: 10.3390/app11135818.

[211] Rehman Z. and Seong K., "Three-D Numerical Thermal Analysis of Electric Motor with Cooling Jacket", *Energies, MDPI*, Vol. 11, pp. 1-15, Jan. 2018, doi: 10.3390/en11010092.

[212] Xie Y, Guo J, Chen P and Li Z., "Coupled Fluid-Thermal Analysis for Induction Motors with Broken Bars Operating under the Rated Load", *Energies, MDPI*, Vol. 11, pp. 1-24, August 2018, doi: 10.3390/en11082024.

[213] Y. Gai, Y. C. Chong, H. Adam, X. Deng, M. Popescu and J. Goss, "Thermal Analysis of an Oil-Cooled Shaft for a 30000 r/min Automotive Traction Motor", *IEEE Trans. on Industry Applications*, Vol. 56, pp. 6053-6061, Dec. 2020, doi: 10.1109/TIA.2020.3025745.

[214] A. Adouni and A. J. Marques Cardoso, "Thermal Analysis of Synchronous Reluctance Machines – A Review", *Electric Power Components and Systems*, Vol. 47, pp. 471-485, Mar. 2019, doi: 10.1080/15325008.2019.1602688.

[215] D. Diallo, M.E.H. Benbouzid and M. Zeraoila, "Electric motor drive selection issues for HEV propulsion systems: a comparative study", *IEEE Trans. Vehicular Technology*, Vol. 55, pp. 1756-1764, Nov. 2006.

[216] Hossein Dadkhah, "Global Collaboration and role of OEM and suppliers in making of successful Electric Vehicles", *IEEE Transportation Electrification conference and expo*, pp. 1-1, 2015.

[217] G. H. Gelb and B. Berman, "Propulsion systems for electric cars", *IEEE Trans. Vehicular Technology*, Vol. 23, pp. 61-72, Aug. 1974.

[218] D.Q. Dang, N. Thi-Thuy Vu, H. Ho Choi and J.W. Jung, "Speed control system design and experimentation for interior PMSM drives", *International Journal of Electronics, Taylor and Francis*, Vol. 102, pp. 865-875, July 2014.

[219] J.W.G. Turner, and S.W. Bredda, "Spark Ignition Engine", *Internal Combustion Engines: Performance, Fuel Economy and Emissions: IMechE, London*, Nov. 2013.

[220] T. Thiringer and E.A. Grunditz, "Performance analysis of current BEVs based on comprehensive review of specifications", *IEEE Trans. Transportation Electrification*, Vol. 2, pp. 270-289, May 2016.

[221] Erkin Dincmen and Bilin A. Guvenc, "A control strategy for parallel hybrid electric vehicles based on extremum seeking", *International Journal of Vehicle Mechanics and Mobility, Taylor and Francis*, Vol. 50, pp. 207-215, June 2011.

[222] C. Sourkounis and Philip Dost, "On influence of Non Deterministic Modulation schemes on a drivetrain system with a PMSM within an Electric Vehicle", *IEEE Trans Industry Applications*, Vol. 52, pp. 3388-3397, Feb. 2016.

[223] E. A. Grunditz and T. Thiringer, "Performance analysis of current BEVs based on a comprehensive review of specifications", IEEE Transactions on Transportation Electrification, Vol. 2, No. 3, pp. 270-290, Sep. 2016.

[224] E. A. Grunditz, "Design and Assessment of Battery Electric Vehicle Powertrain, with Respect to Performance, Energy Consumption and Electric Motor Thermal Capability", *Doctorate of Philosophy Thesis, Chalmers University of Technology*, Sweden, 2016.

[225] A T A Salim, I Yuwono, W Pribadi, N Romandoni, L Yuwana, R Rosallino, S A Putri, and T M Alqoriah, "The Performance Characteristics of Electric Motors with Variation of Load In Application in Two-Wheeled Vehicles", *Journal of Physics: Conference series, IOP publishing*, Vol. 1845, 2021.

[226] D.Q. Dang, N. Thi-Thuy Vu, H. Ho Choi and J.W. Jung, "Speed control system design and experimentation for interior PMSM drives", *International Journal of Electronics, Taylor and Francis*, Vol. 102, pp. 865-875, July 2014.

[227] M.O. Badawy, T. Husain and Y. Sozer, "Integrated control of and IPM motor drive and a novel hybrid energy storage system for electric vehicles", *IEEE Trans. Industry Applications*, Vol. 53, pp. 5810-5819, Aug. 2017.

[228] C. Rossi, D. Pontara, M. Bertoldi and D. Casadei, "Management of Multi-drive powertrain for full electric vehicle in degraded operating conditions", *IEEE Vehicle Power and Propulsion Conference*, pp. 1-6, Dec. 2017.

[229] Nicorici, Andreea-Madalina, Szabo, Lorand and Martis, Claudia, "Design and Analysis of a Permanent Magnet Synchronous Machine used in Automotive Applications", *IEEE International Conference on Environment and Electrical Engineering and IEEE Industrial and Commercial Power Systems Europe, (EEEIC / I&CPS Europe)*, pp. 1-6, 10.1109/EEEIC.2019.8783826, June 2019.

[230] C. Lu, S. Ferrari, and G. Pellegrino, "Two Design Procedures for PM Synchronous Machines for Electric Powertrains", *IEEE Transactions on Transportation Electrification*, Vol. 3, No. 1, pp. 98-107, Mar. 2017.

[231] V. Ruuskanen, J. Nerg, J. Pyrhönen, S. Ruotsalainen, and R. Kennel, "Drive Cycle Analysis of a Permanent-Magnet Traction Motor Based on Magnetostatic Finite-Element Analysis", *IEEE Transactions on Vehicular Technology*, Vol. 64, No. 3, pp. 1249-1253, Mar. 2015.

[232] W. Q. Chu and Z. Q. Zhu, "Average torque separation in permanent magnet synchronous machines using frozen permeability," *IEEE Transactions on Magnetics*, Vol. 49, No. 3, pp. 1202–1210, Mar. 2013.

[233] M. Popescu, D. M. Ionel, T. J. E. Miller, S. J. Dellinger, and M. I. McGilp, "Improved finite element computations of torque in brushless permanent magnet motors," *IEE Proceeding on Electric Power Applications*, Vol. 152, No. 2, pp. 271–276, Mar. 2005.

[234] M. Ibrahim and P. Pillay, "Aligning the Reluctance and Magnet Torque in Permanent Magnet Synchronous Motors for Improved Performance," *IEEE Energy Conversion Congress and Exposition (ECCE)*, pp. 2286-2291, doi: 10.1109/ECCE.2018.8558276, Sep. 2018.

[235] S. Ogasawasa and H. Akagi, "Rotor position estimation based on magnetic saliency of an IPM motor-realization of a wide-speed range from zero to the rated speed," *Conference Record of 1998 IEEE Industry Applications Conference. Thirty-Third IAS Annual Meeting (Cat. No.98CH36242)*, Vol. 1, pp. 460-466, doi: 10.1109/IAS.1998.732343, Oct. 1998.

[236] M. Miyamasu and K. Akatsu, "An approach to generate high reluctance torque in an inset-type PMSM by square current excitation," *IEEE International Conference on Power and Energy (PECon)*, pp. 440-445, doi: 10.1109/PECon.2012.6450253, Dec. 2012.

[237] Wang, S., and Wook, S., "Design optimization and experimental verification of permanent magnet synchronous motor used in electric compressors in electric vehicles", *Applied Science*, Vol. 10, pp. 1–16, May 2020.

[238] S. Fang, H. Liu, H. Wang, H. Yang and H. Lin, "High Power Density PMSM with lightweight structure and high-performance soft magnetic alloy core," *IEEE Transactions on Applied Superconductivity*, Art no. 0602805, doi: 10.1109/TASC.2019.2891630, Vol. 29, No. 2, pp. 1-5, March 2019.

[239] Z. Zhang, H. Ma, A. Wang and C. Yang, "Study on circle-annulus meshing methods using ANSYS software and its application in motor electromagnetic field analysis," *International Conference on Electrical and Control Engineering*, pp. 403-406, doi: 10.1109/ICECENG.2011.6057029, Sep. 2011.

[240] Qian, Z., Seepersad, C. C., Joseph, V. R., Allen, J. K., and Jeff Wu, C. F., "Building surrogate models based on detailed and approximate simulations," *Journal of Mechanical Design*, Vol. 128, No. 4, pp. 668-677, July 2006.

[241] A. J. Keane, I. Voutchkov, "Robust design optimization using surrogate models," *Journal of Computational Design and Engineering*, Vol. 7, No. 1, pp. 44–55, https://doi.org/10.1093/jcde/qwaa005, Feb. 2020.

[242] M. A. Bezerra, R. E. Santelli, E. P. Oliveira, L. S. Villar, L. A. Escaleira, "Response surface methodology (RSM) as a tool for optimization in analytical chemistry," *Talanta,* Vol. 76, No. 5, pp. 965-977, Sep. 2008.

[243] Draper, N. Richard, and F. Pukelsheim. "An overview of design of experiments," *Statistical Papers,* Vol. 37, No. 1, pp. 1-32, Mar. 1996.

[244] J. A. Ghani, H. Jamaluddin, M. A. Rahman and B. Md. Deros, "Philosophy of Taguchi Approach and Method in Design of Experiment", *Asian Journal of Scientific Research,* Vol. 6, pp 27-37, 2013.

[245] S. Zossak, P. Sovicka, M. Sumega, P. Rafajdus, "Evaluating Low Speed Limit of Back-EMF Observer for Permanent Magnet Synchronous Motor," *Transportation Research Procedia,* Vol. 40, pp. 610-615, 2019.

[246] Wang, S., and Wook, S., "Design optimization and experimental verification of permanent magnet synchronous motor used in electric compressors in electric vehicles," *Applied Science,* Vol. 10, pp. 1–16, 2020.

[247] Chen, J., D. Wang, L. Wu X. Zheng, F. Birnkammer, and D. Gerling, "Influence of temperature on magnetic properties silicon steel laminations", *AIP Advances,* Vol. 7, 2017.

[248] Gomaa, A., "Performance characteristics of automotive air conditioning system with refrigerant R134a and its alternatives", International Journal of Energy and Power Engineering, Vol. 4, pp. 168–177, Jan. 2015.

[249] Feng, Y., and Zhang, C., "Core loss analysis of interior permanent magnet synchronous machines under SVPWM excitation with considering saturation," *Energies,* Vol. 10, pp. 005–006, 2017.

[250] Koo, M.-M., Kim, J.-M., Kim, C.-W., Ahn, J.-H., Hong, K., and Jang-Young, C., "Core loss analysis of permanent magnet synchronous generator with slot-less Stator", *IEEE Transactions on Applied Superconductivity,* Vol. 28, No. 3, pp. 1–4, 2018.

[251] Guo, Y., Jianguo, Z., Lu, H., Lin, Z., and Li, Y., "Core loss calculation for soft magnetic composite electrical machines", *IEEE Transactions on Magnetics,* Vol. 48, No. 11, pp. 3112–3114, 2012.

[252] Yao, A., Odawara, S., Sugimoto, T., and Fujisaki, K., "Core loss properties of a motor with Nano crystalline Rotor and Stator cores under inverter excitation," *IEEE Transactions on Magnetics,* Vol. 54, No. 11, pp. 1–5, 2018.

[253] Okamoto, S., Denis, N., Kato, Y., Ieki, M., and Fujisaki, K., "Core loss reduction of an interior PMSM using amorphous stator core," *IEEE Transactions on Industrial Applications,* Vol. 52, No. 3, pp. 2261–2266, 2016.

[254] Mohamed, E.E., "Electromagnetic performance of partitioned stator PM machines with dual C-core/E-core topologies," *International Middle East Power System Conference (MEPCON),* 2017.

[255] Huang, Y., Dong, J., Zhu, J., and Guo, Y., "Core loss modeling for permanent magnet motor based on flux variation locus and finite element method", *IEEE Transactions on Magnetics,* Vol. 48, pp. 1023–1026, 2012.

[256] Gordon, R.S., and Liu, X., "Core losses in Permanent magnet motors," *IEEE Transactions on Magnetics,* Vol. 26, pp. 1653–1655, 1990.

[257] Laith, A., Dalia, Y., Abd, E., Ahmed, A.E., Mohammed, A., Amir, and H.G., "Aquila Optimizer: a novel meta heuristic optimization algorithm", *Computers and Industrial Engineering,* Vol. 157, pp. 1–59, July 2021.

[258] Shahrzad, S., Seyedali, M., and Andrew, L., "Grasshopper optimization algorithm: theory and application," *Advances in Engineering Software,* Vol. 105, pp. 30–47, 2017.

[259] Juan, C., Pavlos, S., Eduardo, C., and Rafael, E., "Core lamination selection for distribution transformers based on sensitivity analysis," *Electrical Engineering*, Vol. 95, pp. 33–42, 2013.

[260] Laith, A., Daibat, A., "A comprehensive survey of the grasshopper optimization algorithm: results, variants and applications," *Neural Computing and Application*, Vol. 32, pp. 15533–15556, 2020.

[261] Faiz, J., Ebrahimi, B.M., Bilal, A., and Hamid, A., "Finite element transient analysis of induction motors under mixed eccentricity fault", *IEEE Transactions on Magnetics*, Vol. 44, No. 1, pp. 66–74, 2008.

[262] Strangas, E.K., Abdullah, A., Khalil, and H. K., "Speed Control of Permanent Magnet Synchronous Motor with uncertain parameters and unknown disturbances," *IEEE Transactions on Control System Technology*, pp. 1–8, 2020.

[263] Zhao, J., Li, B., Liu, X., Li, X., and Chen, Z., "Research on the torque and back emf performance of a high speed PMSM used for flywheel energy storage," *Energies*, Vol. 8, pp. 2877–2880, 2015.

[264] A. Boglietti, A. Cavagnino, D. Staton, M. Shanel, M. Mueller and C. Mejuto, "Evolution and Modern approaches for thermal analysis of electrical machines", *IEEE Trans. on Industrial electronics*, Vol. 56, pp. 871-881, Mar. 2009.

[265] A. Boglietti, A. Cavagnino and D. A. Staton, "Thermal analysis of TEFC induction motors", *38th IAS Annual Meeting on Conference Record of the Industry Applications Conference*, Vol. 2, pp. 849-856, Oct. 2003, doi: 10.1109/IAS.2003.1257630.

[266] Staton, Dave, D. Hawkins, and M. Popescu, "Thermal Behaviour of Electrical Motors–An Analytical Approach", *INDUCTICA Technical Conference Program, CWIEME, Berlin*, pp. 5-7, May 2009.

[267] B. Andersson, "Lumped Parameter Thermal Modelling of Electric Machines, Analysis of an Interior Permanent Magnet Synchronous Machine for Vehicle Applications," *Master of Science Thesis, Chalmers university of technology, Goteborg, Sweden*, 2013.

[268] T. Y. Young and T. W., "Calvert, Classification, Estimation and Pattern Recognition," *American Elsevier Publishing Co., Inc.*, 1974.

PUBLICATIONS

The list of publications in journals including those presented and published in proceedings of Conferences out of this research work are given below:

Journals (SCI/SCIE):

1. M. Verma, M. Sreejeth, M. Singh, "Application of hybrid metaheuristic technique to study influence of core material and core trench on performance of Surface Inset PMSM", *Arabian Journal of Science and Engineering, Springer*, Impact Factor: 2.334, Vol. 47, pp. 3037-3053, 21914281, 10.1007/s13369-021-06017-4, Aug, 2021.
1. M. Verma, M. Singh, M. Sreejeth, "Integrated Taguchi method assisted polynomial Metamodeling & Genetic Algorithm based optimization of Surface Inset Permanent Synchronous Motor for performance improvement", *IET Electrical Systems in Transportation, IET/Wiley*, Impact Factor: 2.268, Vol. 12, pp. 26-35, 20429738, 10.1049/els2.12035, Sep, 2021.
1. M. Verma, M. Sreejeth, M. Singh, T. S. Babu, H. H. Alhelou, "Chaotic mapping based advanced Aquila Optimizer with single stage evolutionary algorithm", *IEEE Access*, Impact Factor: 3.476, (In-press), 2022.

International/National Conferences:

1. M. Verma, M. Sreejeth, M. Singh, "Performance Evaluation of conventional and electric powertrain", 8^{th} *IEEE India International Conference on Power Electronics (IICPE), MNIT Jaipur, Rajasthan,* ISSN978-1-5386-4996-1, 10.1109/IICPE.2018.8709429, Dec, 2018.
2. M. Verma, M. Sreejeth, M. Singh, "Implementation and Analysis of field Control on Electric Vehicle Power Train System Employing PMSM as Traction Device", $\mathbf{2^{nd}}$ *IEEE International Conference on Power Electronics, Intelligent Control and Energy Systems (ICPEICES), DTU, Delhi*, ISSN978-1-5386-6625-8, 10.1109/ICPEICES.2018.8897480, Oct, 2018.
3. M. Verma, M. Sreejeth, M. Singh, "Case Study for Surface Inset Permanent Magnet synchronous Motor via Finite Element Analysis", $\mathbf{3^{rd}}$ *International Online Conference on Emerging Trends in Multi-Disciplinary Research (ETMDR), Rajasthan, India,* ISSN978-93-5593-524-3, Jan, 2022.
4. M. Verma, M. Sreejeth, M. Singh, "Fault Diagnosis via thermal modelling of Surface Inset PMSM", 4^{th} *International Conference on Recent Trends in Multi-Disciplinary Research (ICRTMDR), IFERP, Maldives,* ISSN978-93-92105-26-5, Dec, 2021.
5. M. Verma, M. Sreejeth, M. Singh, "Implementation, Analysis and Emulation of electric vehicle powertrain system with sensor-less field controlled PMSM drive", 7^{th} *International Congress on Information and Communication Technology (ICICT), London, UK*, Feb, 2022.

Book Chapter(s):

1. M. Verma, M. Sreejeth, M. Singh, "Total Quality Management of research articles in electrical engineering", in Book, entitled, "Six Sigma and Quality Management", *IntechOpen Ltd, England, Wales No. 11086078,* (In-press), 2022.
2. S. Ranjan, M. Verma, M. Singh, M. Sreejeth, "Intelligent Control for PMSM drivetrain", in Book entitled, "Intelligent Control for Modern Transportation Systems", *Publisher: CRC Press, Taylor and Francis Group,* (Accepted), 2022.